Present and past biogeochemical functioning of the benthic ecosystem of the West Gironde Mud Patch (Bay of Biscay) : remineralization, recycling and burial processes of C and associated elements (O2, N, Mn, Fe, P, S)

Nicolas Dubosq

université de BORDEAUX

THÈSE PRÉSENTÉE

POUR OBTENIR LE GRADE DE

DOCTEUR DE

L'UNIVERSITÉ DE BORDEAUX

ÉCOLE DOCTORALE SCIENCES ET ENVIRONNEMENTS

SPECIALITÉ : Biogéochimie et écosystèmes

Par Nicolas DUBOSQ

Fonctionnement biogéochimique actuel et passé de l'écosystème benthique de la Vasière Ouest Gironde (golfe de Gascogne) : processus de reminéralisation, recyclage et stockage du C et des éléments associés (O_2, N, Mn, Fe, P, S)

Sous la direction de : Sabine Schmidt

Soutenue le 27 novembre 2023

Membres du jury :

M. ANSCHUTZ, Pierre	Professeur, Université de Bordeaux	Président du jury
M. GRENZ, Christian	Directeur de recherche, CNRS	Rapporteur
M. RADAKOVITCH, Olivier	Chercheur, IRSN	Rapporteur
Mme MOURET, Aurélia	Maîtresse de conférences, Université d'Angers	Examinatrice
Mme SCHMIDT, Sabine	Directrice de recherche, CNRS	Directrice de thèse
M. DEFLANDRE, Bruno	Maître de conférences, Université de Bordeaux	Co-encadrant (Invité)

Fonctionnement biogéochimique actuel et passé de l'écosystème benthique de la Vasière Ouest Gironde (golfe de Gascogne) : processus de reminéralisation, recyclage et stockage du C et des éléments associés (O_2, N, Mn, Fe, P, S)

Résumé

Afin d'améliorer la compréhension du fonctionnement biogéochimique des marges continentales sous l'influence de grands fleuves (RiOMars pour *River-dominated Ocean Margins*), la Vasière Ouest Gironde (VOG) a été prise comme un modèle de système tempéré non-deltaïque soumis à un fort hydrodynamisme. La réalisation de mesures *in situ* et l'analyse d'échantillons prélevés au cours de huit campagnes océanographiques réalisées à différentes saisons entre 2016 et 2021 ont permis de caractériser son fonctionnement biogéochimique de l'échelle saisonnière à pluriséculaire. Les résultats montrent qu'en zone proximale (i.e., < 42.5 m), l'important hydrodynamisme entraine une instabilité sédimentaire avec des dépôts superficiels sablo-vaseux transitoires (< 10 cm) recouvrant des vases reliques. Cela induit un régime diagénétique en deux couches, une moderne et une relique, présentant des fonctionnements biogéochimiques différents. Dans les sédiments modernes superficiels, la matière organique est reminéralisée par respiration aérobie et par des processus de dégradation suboxiques. Au contraire, la réduction des sulfates est le processus de reminéralisation dominant dans les vases reliques. De plus, des mesures de plusieurs phases dissoutes et particulaires ont mis en évidence un fonctionnement différent des cycles biogéochimiques du fer et du soufre entre les vases reliques et les sédiments du reste de la VOG. Dans la zone distale, où la sédimentation est plus continue, la séquence diagénétique se dilate progressivement vers le large, probablement en relation avec la diminution de la labilité de la matière organique et l'augmentation de la bioturbation. Les mesures saisonnières ont notamment mis en évidence une variation de l'intensité de la respiration aérobie en réponse à des évènements saisonniers tels que l'efflorescence printanière et les désoxygénations de l'eau de fond. A l'échelle pluri-décennale, plus de la moitié du carbone organique déposé dans la zone distale est séquestré dans les sédiments avec un taux d'enfouissement maximum de 45 gC m^{-2} an^{-1}. Les charges en carbone organique du sédiment montrent, qu'à l'échelle pluriséculaire, ce stockage est moins efficace et principalement lié à la taille des particules déposées. A cette échelle de temps, la reminéralisation de la matière organique est limitée par sa labilité et sa biodisponibilité. Les résultats ont également mis en évidence que la VOG est un puits via la précipitation de minéraux authigènes (P, S, Fe, Si) et l'adsorption sur les particules sédimentaires (C, Fe, Mn). Ce travail a finalement montré qu'en raison de sa nature non-deltaïque la VOG présente un fonctionnement biogéochimique différent de celui des RiOMars de haute énergie déjà étudiés, ce qui suggère qu'elle pourrait correspondre à un nouveau modèle de RiOMars.

Mots-clés : cycles biogéochimiques, reminéralisation, carbone organique, océan côtier, vasière, golfe de Gascogne, diagenèse précoce

UMR CNRS 5805 EPOC
Environnements et Paléoenvironnements Océaniques et Continentaux
Allée Geoffroy Saint Hilaire – CS 50023 – 33615 Pessac Cedex - France

Present and past biogeochemical functioning of the benthic ecosystem of the West Gironde Mud Patch (Bay of Biscay): remineralization, recycling and burial processes of C and associated elements (O_2, N, Mn, Fe, P, S)

Abstract

In order to improve the understanding of the biogeochemical functioning of River-dominated Ocean Margins (RiOMars), the West Gironde Mud Patch (WGMP) was used as a model of a temperate non-deltaic system subjected to a high hydrodynamics. Measurements and sampling, carried out during eight cruises in different seasons between 2016 and 2021, allowed to characterize its biogeochemical functioning from seasonal to multi-century scales. Results showed that in the proximal area (i.e., < 42.5 m), the high hydrodynamics results in a sediment instability with a surface layer of transient sandy muds (< 10 cm) overlying relic muddy sediments. This induces a digenetic regime divided into two layers, a modern and a relic, having distinct biogeochemical functioning. In the superficial modern layer, organic matter is remineralized through aerobic respiration and suboxic degradation processes. Conversely, sulfate reduction is the main remineralization process occurring in relic deposits. Moreover, measurements of several particulate and dissolved compounds highlighted that the cycles of iron and sulfur differ between relic sediments and the rest of the WGMP. In the distal area, where a more continuous sedimentation occurs, the diagenetic sequence gradually expands seaward, likely due a decrease in organic matter lability and an increase in bioturbation. Seasonal measurements highlighted that aerobic respiration rates vary in response to seasonal events such as the spring blooms and bottom water deoxygenation. On a multi-decennial scale, more than half of the organic carbon deposited in the distal area is buried in sediments with a maximum burial rate of 45 gC m^{-2} y^{-1}. The organic carbon load of the sediments shows that, this burial is less efficient on a multi-century scale and is mainly related to the grain-size of deposited particles. On this time scale, organic matter remineralization is limited by its lability and bioavailability. Results also highlighted that the WGMP is a sink through the precipitation of authigenic minerals (P, S, Fe, Si) and the adsorption on particles (C, Fe, Mn). Finally, this work has shown that, due to its non-deltaic nature, the biogeochemical functioning of the WGMP differs from that of previously studied high-energy RiOMars, suggesting that it could represent a new RiOMars model.

Keywords: biogeochemical cycles, remineralization, organic carbon, coastal ocean, mudflat, Bay of Biscay, early diagenesis

UMR CNRS 5805 EPOC
Environnements et Paléoenvironnements Océaniques et Continentaux
Allée Geoffroy Saint Hilaire – CS 50023 – 33615 Pessac Cedex - France

Financements

Ce travail de thèse a pu être réalisé grâce à une bourse doctorale du Ministère de l'Enseignement Supérieur, de la Recherche et de l'Innovation. Il a bénéficié de financements par les projets (1) JERICO-NEXT (Programme de Recherche et d'Innovation Horizon 2020 de l'Union Européenne), (2) VOG (LEFE – CYBER et EC2CO) et (3) MAGMA (Laboratoire d'excellence COTE (ANR-10-LABX-45), Conseil Régional de Nouvelle Aquitaine et Office Français de la Biodiversité). Les missions océanographiques réalisées au cours de cette thèse ont été financées par la Flotte Océanographique Française.

Remerciements

Maintenant que j'arrive à la fin de cette thèse, je la vois comme une aventure au cours de laquelle j'ai croisé de nombreuses personnes sans lesquelles elle n'aurait sans doute pas été la même.

Je tiens à commencer par remercier Sabine Schmidt et Bruno Deflandre pour m'avoir proposé ce sujet de thèse, accompagné et soutenu au cours de ces quatre années. Nos nombreuses discussions et le temps que vous m'avez accordé m'ont permis d'apprendre, d'avancer et de me remotiver quand cela a été nécessaire.

Je remercie également la direction et l'ensemble des membres de l'UMR EPOC pour m'avoir accueilli au laboratoire ainsi que Christian Grenz, Olivier Radakovitch, Pierre Anschutz et Aurélia Mouret pour avoir accepté de faire partie de mon jury de thèse. Je vous remercie particulièrement pour vos retours sur mon mémoire et pour les discussions très enrichissantes que nous avons eues lors de ma soutenance.

Je tiens à remercier l'ensemble des membres des projets JERICONext, VOG et MAGMA avec lesquels j'ai eu l'occasion (et la chance) de travailler. J'ai une pensée particulière pour celles et ceux avec qui j'ai embarqué sur le Côte de la Manche et ai partagé des moments aussi bien magnifiques que difficiles lorsque la mer nous malmenait ! Ces missions et l'ensemble de ce travail n'auraient bien sûr pas été possibles sans les équipages du navire, que je remercie chaleureusement et grâce à qui nous avons pu avoir de très beaux jeux de données.

Je remercie également Antoine Grémare et Bastien Lamarque pour m'avoir appris de nombreuses notions de statistiques et d'écologie ainsi que pour nos journées de travail et nos discussions sur les traitements statistiques. Je remercie Sylvain Rigaud pour m'avoir accueilli plusieurs fois à Nîmes et initié à PHREEQC lors de nos journées au port de la Rochelle. Merci également à Joël pour le traitement des données satellites. Antoine et Sylvain, je vous remercie à nouveau ainsi qu'Edouard pour avoir accepté de faire partie de mon comité de suivi de thèse et m'avoir aidé à réfléchir sur ce grand jeu de données.

De nombreuses mesures présentées dans ce manuscrit n'auraient pas été réalisées sans le soutien technique duquel j'ai bénéficié. C'est pourquoi je tiens à remercier l'ensemble des personnes qui ont participé à l'acquisition de ces données et tout particulièrement Martin, Marie-Ange, Nathalie, Dominique, Céline et Marie-Claire avec qui j'ai passé de nombreuses heures dans les labos.

Je tiens également à remercier les stagiaires que j'ai encadré, avec qui j'ai travaillé ou qui m'ont simplement permis d'avoir de la compagnie dans ce grand bureau du B18. Je pense notamment

à Anaïs, Emeline, Arthuro, Margot, Jason, John et Samnath. Merci à vous pour votre travail, nos discussions et votre bonne humeur.

Comme une thèse ce n'est pas uniquement de la recherche, je voulais également remercier l'équipe pédagogique de l'UF STE au sein de laquelle j'ai pu faire mes premiers pas d'enseignant. J'ai vraiment adoré cette expérience. J'ai également une pensée particulière pour la promo 2021 de l'Ecole d'été AMME et notamment pour la Team 4 ! Vous m'avez permis de prendre un grand bol d'oxygène à un moment où j'en avais besoin.

Ce travail n'aurait sans doute pas abouti sans les moments de décompression et de déconnexion passés avec mes parents et mes amis. J'ai une pensée particulière pour Guéwen, Fred, Kevin Thomas, Morgane, Julien, Antho et Pauline. Un grand merci plein d'émotions pour vous ! Un grand merci également à la team roller de l'école de patinage du SAM, vous avez m'avez permis de me vider la tête tous les mardis soir au cours de cette dernière année ! Mes nombreuses (et parfois impressionnantes) chutes ne m'ont pas empêché de finir d'écrire !

Enfin et bien évidement, un énorme merci à Chloé (et Arwen), pour m'avoir soutenu, motivé, boosté, supporté et avoir écouté mes plaintes pendant ces quatre années de thèse ! Ton soutien quotidien et constant m'a permis d'arriver au bout de ce travail.

Table des matières

INTRODUCTION GÉNÉRALE 1

CHAPITRE 1: ETAT DE L'ART ET STRATÉGIE DE L'ÉTUDE 6

1. Etat de l'art sur la Vasière Ouest Gironde 7

1.1 Localisation géographique et contexte global 7
1.2 Formation de la Vasière Ouest Gironde 8
1.3 Structuration et fonctionnement sédimentaire actuel 9
1.4 Structuration et fonctionnement biogéochimique et écologique 10

2. Stratégie de l'étude 11

2.1 Structuration spatiale des descripteurs de la matière organique et de la macrofaune benthique 13
2.2 Structuration et fonctionnement biogéochimique de la Vasière Ouest Gironde de l'échelle saisonnière à pluriséculaire 14

CHAPITRE 2: CONTEXTE HYDRO-SÉDIMENTAIRE ET VARIABILITÉ SPATIOTEMPORELLE DES DESCRIPTEURS DE LA MATIÈRE ORGANIQUE ET DE LA MACROFAUNE BENTHIQUE DANS LA VASIÈRE OUEST GIRONDE 17

PARTIE A - PREMIERES OBSERVATIONS DE DESOXYGENATIONS SAISONNIERES DES EAUX DE FOND AU LARGE DE L'ESTUAIRE DE LA GIRONDE (GOLFE DE GASCOGNE, ATLANTIQUE NORD EST) 19

Résumé 20

1. Introduction 21

2. Material and methods 22

2.1 Field measurements 22
2.2 Satellite and Gironde flow data 22

3. Results 23

3.1 Gironde flow and satellite data 23
3.2 Temperature and salinity 25
3.3 Dissolved oxygen, pH, Chl-*a* and turbidity 27

4. Discussion 27

4.1 Structuring of the water column from seasonal to inter-annual scales 27
4.2 Probable causes of deoxygenations 28
4.3 Potential futures responses to global warming 30
4.4 The need to establish a long-term *in situ* monitoring of the WGMP 31

5. Conclusions 32

PARTIE B - PREMIERE ESTIMATION DE L'ENFOUISSEMENT DU CARBONE ORGANIQUE DANS LA VASIERE OUEST GIRONDE (GOLFE DE GASCOGNE) 34

Résumé 35

1. Introduction 36

2. Material and methods 37

2.1 Study site 37
2.2 Sampling 38
2.3 Physical characteristics of sediments 38
2.4 Radionuclide analysis 39
2.5 Particulate organic carbon 39

2.6 Statistical treatment 40
3. Results 40
3.1 Physical characteristics of sediments and sedimentary structures 40
3.2 ^{210}Pb profiles in interface sediments 42
3.3 Sedimentary organic carbon 43
4. Discussion 45
4.1 Sedimentation in the WGMP 45
4.2 Quantitative assessment of OC burial rates in the WGMP 47
4.3 Qualitative comparison of OC burial efficiency: direct use of OC content and SA 49
4.4 Comparison with other continental shelves 51
5. Conclusion 52
PARTIE C - VARIATIONS SPATIOTEMPORELLES DES DESCRIPTEURS DE LA MATIERE ORGANIQUE ET DE LA MACROFAUNE BENTHIQUE 54
1. Structuration spatiale des caractéristiques du sédiment de surface et de l'activité de la macrofaune benthique 55
2. Dynamique spatiale et temporelle des caractéristiques du sédiment de surface et de la composition de la macrofaune benthique 56
POINTS CLES DU CHAPITRE 2 59
CHAPITRE 3: STRUCTURATION ET FONCTIONNEMENT BIOGÉOCHIMIQUE DE LA VASIÈRE OUEST GIRONDE À L'ÉCHELLE SAISONNIÈRE ET IMPLICATIONS POUR L'ÉCOSYSTÈME 60
1. Introduction 61
2. Material and methods 61
2.1 Pore waters analyses 61
2.2 Solid phase analyses 62
2.3 Oxygen and nutrient fluxes at the sediment-water interface 63
2.3.1 Oxygen and nutrient fluxes measured by cores incubations 63
2.3.2 Vertical distributions of dissolved oxygen in sediments and calculations of diffusive oxygen uptakes 64
2.4 Data treatments 65
3. Results and discussion 65
Part A – Structuration and biogeochemical functioning of the West Gironde Mud Patch 65
3.1 Organic matter remineralization and secondary diagenetic processes 65
3.2 Differential functioning of early diagenesis: relic vs modern sediments 72
3.3 Does the WGMP has a biogeochemical functioning like the others RiOMars? 78
Part B – Implications of the biogeochemical functioning of the WGMP on the ecosystem 79
3.4 Organic carbon remineralization rates by the different degradation pathways 79
3.4.1 Spatial structuration of organic carbon remineralization rates 79
3.4.2 Seasonal dynamic of organic carbon remineralization rates 82
3.4.3 Factors controlling the variability of organic carbon remineralization rates by aerobic respiration 82
3.5 Total organic carbon remineralization rates and efficiencies in the WGMP 85
3.6 Consequences of the biogeochemical functioning of the WGMP 88
3.6.1 Sediment oxygen consumption: a key factor controlling the bottom water deoxygenation in the WGMP? 88

3.6.2 The WGMP sediment: a major source of nitrogenous nutrients for the continental shelf off the Gironde? ... 90
4. Conclusion ... 90

POINTS CLES DU CHAPITRE 3 ... 92

CHAPITRE 4: PROCESSUS DE DIAGENÈSE PRÉCOCE À L'ÉCHELLE PLURISÉCULAIRE DANS UN SYSTÈME DE MARGE CONTINENTALE TEMPÉRÉE SOUS L'INFLUENCE D'UN GRAND FLEUVE (LA VASIÈRE OUEST GIRONDE, GOLFE DE GASCOGNE) ... 93

Résumé ... 94
1. Introduction ... 95
2. Material and methods ... 96
2.1 Study site ... 96
2.2 Sampling ... 97
2.3 Physical characteristics of sediments ... 98
2.4 Radiocarbon ages and ^{210}Pb ... 98
2.5 Pore waters analyses ... 99
2.6 Solid phase analyses ... 100
2.7 Data treatments ... 101
3. Results ... 102
3.1 Physical characteristics of sediments and organic compounds ... 102
3.2 Pore waters composition ... 104
3.3 Inorganic particulate compounds ... 105
4. Discussion ... 107
4.1 Structuration of the sedimentary record and origin of organic matter ... 107
4.2 Organic matter recycling and burial: influence of organic matter reactivity and bioavailability ... 109
4.3 Burial of elements on a multi-century scale ... 111
4.3.1 Formation of authigenic minerals ... 111
4.3.2 Burial of particulate iron and manganese oxyhydroxydes : implications for the sequestration of phosphorus and metallic contaminants ... 115
5. Conclusion ... 116

POINTS CLES DU CHAPITRE 4 ... 118

SYNTHÈSE ET PERSPECTIVES ... 119

1. Structuration et fonctionnement biogéochimique de la Vasière Ouest Gironde de l'échelle saisonnière à pluridécennale ... 120
2. Fonctionnement biogéochimique de la Vasière Ouest Gironde de l'échelle pluridécennale à pluriséculaire ... 123
3. La Vasière Ouest Gironde : un nouveau modèle de RiOMar? ... 123
4. Perspectives ... 125

RÉFÉRENCES ... 127

ANNEXE 1 ... 156

ANNEXE 2 ... 200

ANNEXE 3 ... 237

ANNEXE 4 ... 242

Introduction générale

A l'échelle mondiale, le flux de carbone organique particulaire exporté des rivières à l'océan est estimé entre 120 et 240 Tg an^{-1} (Cai, 2011; Li et al., 2017; Ludwig et al., 1996; Luo et al., 2022). Cependant, moins de 20% de ce matériel atteint les zones profondes de l'océan (Burdige, 2005). Ainsi, ces particules se déposent principalement au niveau des marges continentales qui sont des environnements de transition entre le domaine continental et l'océan profond (Burdige, 2005; Foucault et al., 2014; McKee et al., 2004). Jusqu'à 90% du carbone organique enfoui dans l'océan l'est au niveau des marges continentales (Hedges and Keil, 1995) mais on estime également que 55 à 80% du flux de carbone organique continental y est reminéralisé (Blair and Aller, 2012; Burdige, 2005). Ces zones de transition sont donc des « hot spots » pour le stockage et le recyclage de la matière organique (Bianchi et al., 2018) et apparaissent comme des environnements clés pour la compréhension du cycle biogéochimique du carbone et des éléments qui lui sont associés (e.g., azote, phosphore, oxygène).

Les marges continentales soumises à l'influence de grands fleuves (i.e., RiOMars pour *River-dominated Ocean Margins*) ont un impact majeur sur ces cycles biogéochimiques. Dans ces systèmes, les processus biogéochimiques sont largement influencés par les apports particulaires et dissous des fleuves (McKee et al., 2004). En raison de ces apports, les RiOMars ont des taux de production primaire, de sédimentation, et d'enfouissement du carbone organique parmi les plus importants des environnements océaniques (McKee et al., 2004). De plus, ce sont des zones où la reminéralisation de la matière organique labile mais également de la matière organique plus réfractaire est particulièrement efficace (Aller, 1998; Blair and Aller, 2012). Blair and Aller (2012) ont proposé une classification des RiOMars en trois catégories à partir des caractéristiques de la matière organique sédimentaire et des conditions environnementales qui contrôlent l'efficacité de sa préservation dans les sédiments :

- Les RiOMars de type 1 regroupent des systèmes de haute énergie dans lesquels les sédiments sont fréquemment remis en suspension dans une colonne d'eau bien oxygénée. Ces remises en suspension prolongent le temps d'exposition de la matière organique à l'oxygène dissous, soumettent les sédiments à des alternances de conditions oxiques et anoxiques et entrainent un mélange de matière organique labile et plus réfractaire induisant un *priming effect*[1] (Bianchi, 2011; Blair and Aller, 2012; Zhu et al., 2016). Ces différents processus favorisent la reminéralisation de la matière organique marine mais également terrigène, pourtant plus réfractaire. Cela conduit à une faible préservation de la matière organique et par conséquent à un intense recyclage des nutriments. En raison de cette importante

[1] Augmentation des taux de reminéralisation de composés organiques « réfractaires » en réponse à un apport de composés organiques plus « labiles ». Bianchi (2011)

reminéralisation de la matière organique, ces systèmes ont été qualifiés « d'incinérateurs ». Le delta de l'Amazone est souvent présenté comme site modèle de ce type d'environnements (Aller, 1998; Aller et al., 1996). On peut également citer le plateau de la mer de Chine orientale influencé par le fleuve Yangtze (Yao et al., 2014; Zhu et al., 2016) ou encore le delta du Mississippi (Corbett et al., 2004).

- Les RiOMars de type 2 correspondent à des environnements de faible énergie avec d'importants taux d'accumulation de sédiments comme le prodelta du Rhône (Pastor et al., 2011a) ou encore l'éventail sédimentaire du Bengale (Galy et al., 2007) également qualifié d'éventail du Ganges-Brahmapoutre (Blair and Aller, 2012). Les importants taux de sédimentation mesurés dans ces systèmes conduisent à une importante préservation de la matière organique.

- Les RiOMars de type 3 regroupent des marges continentales principalement actives influencées par des rivières de montagne. Elles sont caractérisées par des apports sédimentaires épisodiques liés à des évènements de tempêtes et par une matière organique sédimentaire peu réactive. Dans ces environnements, le temps d'exposition de la matière organique à l'oxygène dissous est relativement faible ce qui limite sa dégradation. Ainsi, malgré des taux de sédimentation moyens, ces RiOMars ont des taux de préservation du carbone organique parmi les plus élevés des environnements océaniques. Le plateau continental californien notamment influencé par le fleuve Eel en est un exemple (Blair et al., 2004; Leithold et al., 2005).

Cette classification permet une compréhension globale du fonctionnement biogéochimique des RiOMars et plus spécifiquement de leur capacité à stocker et recycler le carbone organique. Elle distingue notamment les RiOMars de type 1, caractérisés par un intense recyclage de la matière organique, des types 2 et 3 où sa préservation est efficace. Toutefois, la compréhension de la structuration et du fonctionnement biogéochimique des RiOMars est souvent difficile en raison de leur importante hétérogénéité spatiale. Ces systèmes peuvent d'ailleurs être subdivisés en plusieurs sous-environnements caractérisés par des fonctionnements biogéochimiques différents (McKee et al., 2004). Par exemple, les RiOMars de type 1 sont typiquement constitués d'une zone proximale avec des vases mobiles et d'une zone plus au large, moins soumise à l'hydrodynamisme, où les taux de sédimentation et de bioturbation sont plus importants (Aller, 2004). Dans ces systèmes, la matière organique est intensément reminéralisée dans la zone de vases mobiles puis exportée dans la zone plus au large où elle est enfouie. Ainsi, les taux de reminéralisation et de séquestration de la matière organique peuvent varier entre les différents sous-environnements constitutifs d'un RiOMar (McKee et al., 2004).

Bien que cette classification donne une vision globale du fonctionnement de ces environnements, elle est avant tout basée sur des systèmes tropicaux et subtropicaux. En effet, le prodelta du Rhône (type 2) est le seul système tempéré présent dans cette classification. De plus, les RiOMars de type 1 incluent uniquement des systèmes avec des apports sédimentaires supérieurs à 100 Mt an^{-1} (Walsh and Nittrouer, 2009) et connectés à l'embouchure du fleuve. En effet, au niveau du delta de l'Amazon, du delta du Mississippi et de la ceinture de vase de la mer de Chine orientale, les sédiments vaseux commencent à se déposer aux alentours de 10 m de profondeur voire à des bathymétries inférieures (Aller et al., 1986; Corbett et al., 2004; Nittrouer et al., 1983; Yao et al., 2014).

Dans ce contexte, la Vasière Ouest Gironde (VOG) apparait comme un RiOMar original par rapport à ceux intégrés dans cette classification. En effet, c'est un système sédimentaire tempéré, soumis à un fort hydrodynamisme et sous l'influence d'un estuaire avec un flux de sédiments modéré (~ 1.5 Mt an^{-1} ; Jouanneau et al., 1999). De plus, contrairement aux RiOMars de haute énergie inclus dans la classification de Blair and Aller (2012), la VOG est déconnectée de l'embouchure du fleuve qui l'alimente en sédiments avec une limite supérieure vers 30 m de profondeur (Lesueur et al., 2002). Ces particularités par rapport aux RiOMars de type 1 déjà étudiés en font un site original dont l'étude pourrait permettre d'améliorer la compréhension du fonctionnement des RiOMars soumis à un fort hydrodynamisme. En dépit de l'originalité de ce système, le fonctionnement biogéochimique de la VOG a été peu étudié. Jusqu'à présent, les travaux qui y ont été menés ont principalement porté sur son fonctionnement sédimentaire (Jouanneau et al., 1989; Lesueur et al., 1991, 1996, 2001, 2002; Parra et al., 1999; Weber et al., 1991). Les deux seules études biogéochimiques s'intéressant à ce système (i.e., Massé et al., 2016; Relexans et al., 1992) ont porté sur un trop faible nombre de paramètres et de stations pour définir correctement sa structuration spatiale et son fonctionnement biogéochimique.

C'est dans ce contexte que s'inscrit cette thèse dont l'objectif général consiste à caractériser le fonctionnement biogéochimique de la VOG de l'échelle saisonnière à pluriséculaire. Plus spécifiquement, ce travail vise à :

- Estimer la capacité de la VOG à stocker le carbone organique à partir de la quantification du taux d'enfouissement du carbone organique et de l'estimation de l'efficacité de ce stockage.
- Caractériser qualitativement et quantitativement les processus de reminéralisation du carbone organique sédimentaire sur des échelles saisonnières à interannuelles.
- Définir les facteurs contrôlant la variabilité spatiale et temporelle des processus de reminéralisation du carbone organique de l'échelle saisonnière à interannuelle.

- Caractériser les processus diagénétiques dans les sédiments de la VOG de l'échelle pluridécennale à pluriséculaire. Plus spécifiquement, il s'agit (1) d'étudier les processus de recyclage du carbone organique ainsi que leurs facteurs de contrôle et de (2) définir le devenir des éléments impliqués dans les processus de la diagenèse précoce (i.e., Mn, Fe, P, S, Ca, Si) sur ces échelles de temps.
- Comparer la structuration et le fonctionnement biogéochimique de la VOG avec d'autres systèmes de marges continentales, notamment les RiOMars de type 1.

Afin de répondre à ces objectifs ce manuscrit est divisé en quatre chapitres. Il commence par une synthèse des connaissances actuelles sur la formation et le fonctionnement sédimentaire, biogéochimique et écologique de la VOG (**Chapitre 1**). La stratégie d'échantillonnage mise en place pour répondre aux objectifs de cette thèse est ensuite exposée **(Chapitre 1)**. Avant de s'intéresser aux processus biogéochimiques ayant lieu dans le compartiment benthique, il était nécessaire de préciser le contexte dans lequel ils se produisent. Ainsi, le **Chapitre 2** s'attache à définir le contexte hydrologique et sédimentaire ainsi que la structuration spatiale et la variabilité saisonnière des descripteurs de la matière organique. Le fonctionnement biogéochimique de la VOG est ensuite caractérisé à l'échelle saisonnière et comparé à celui d'autres RiOMars, notamment de type 1 (**Chapitre 3**). La seconde partie de ce chapitre se focalise plus spécifiquement sur la capacité de la VOG à recycler le carbone organique. Enfin, les processus de diagenèse précoce dans les sédiments de la VOG sont caractérisés sur des échelles pluridécennales à pluriséculaires (**Chapitre 4**).

Chapitre 1 :

Etat de l’art et stratégie de l’étude

1. Etat de l'art sur la Vasière Ouest Gironde

1.1 Localisation géographique et contexte global

La Vasière Ouest Gironde (VOG) est localisée sur le plateau continental du golfe de Gascogne qui s'étend de la côte nord de l'Espagne jusqu'à la pointe bretonne (**Figure 1.1** ; Borja et al., 2019). Dans cet environnement tempéré, l'hydrodynamisme est dominé par les tempêtes et les fortes houles dont les amplitudes maximales sont de l'ordre de 9 à 15 m à l'échelle décennale (Cirac et al., 2000) et jusqu'à 25 m à l'échelle centennale (Jouanneau et al., 1989). Cet important hydrodynamisme influence les processus sédimentaires sur le plateau continental, notamment via la remise en suspension des sédiments lors des tempêtes (Cirac et al., 2000; Jouanneau et al., 1989; Lesueur et al., 2001, 2002). Les dépôts superficiels de ce plateau continental sont principalement sableux. Cependant, on y observe également la présence de plusieurs systèmes sédimentaires vaseux comme la Grande Vasière, la Vasière Ouest Gironde et la Vasière Basque (**Figure 1.1** ; Allen and Castaing, 1977; Jouanneau et al., 1999; Lesueur et al., 2002). Etant donné que les vases sont classiquement plus riches en matière organique que les sables (Mayer, 1994a), ces systèmes constituent des zones préférentielles d'accumulation de matière organique et sont donc de potentiels « hot spots » pour sa reminéralisation et séquestration (Bianchi et al., 2018).

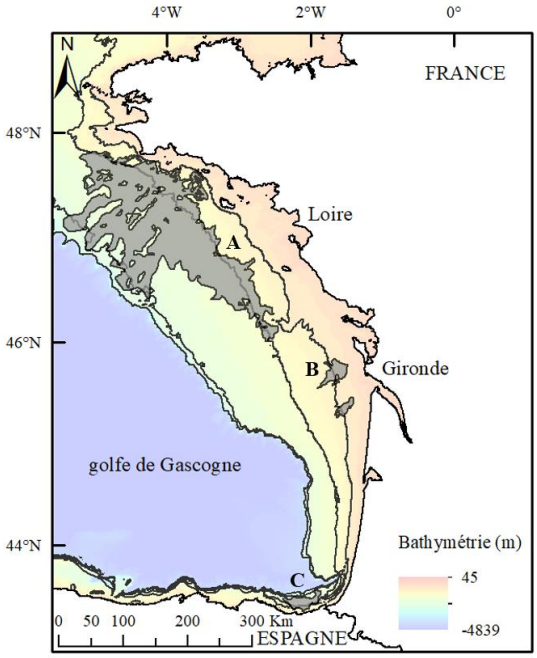

Figure 1.1 : Carte du golfe de Gascogne avec la localisation des vasières du plateau continental (zones grises) dont la Grande Vasière (**A**), la Vasière Ouest Gironde (**B**) et la Vasière Basque (**C**).

La VOG est une vasière subtidale localisée entre 30 et 75 m de profondeur. Elle se situe à environ 40 km de l'embouchure de l'estuaire de la Gironde qui constitue sa principale source

de sédiments (**Figure 1.1** ; Parra et al., 1999; Weber et al., 1991). Cette influence de l'estuaire de la Gironde ainsi que l'important hydrodynamisme local suggèrent que la VOG pourrait appartenir aux RiOMars de type 1 de la classification de Blair and Aller (2012).

1.2 Formation de la Vasière Ouest Gironde

La mise en place de la VOG a fait l'objet de plusieurs hypothèses depuis les années 1950. La première étude s'intéressant à la formation des vasières du golfe de Gascogne suggère qu'elles sont le résultat de dépôts de sédiments fins en période de bas niveau marin dans des étangs, lacs, lagunes et anciens estuaires (Berthois and Le Calvez, 1959). Ces auteurs suggèrent qu'une transgression marine aurait causé la remobilisation et l'étalement de ces dépôts permettant ainsi le comblement de vallées fluviatiles. Cependant, ils ne précisent pas la chronologie des périodes de dépôts et de remobilisation. De plus, ils n'excluent pas une sédimentation actuelle dans certaines parties de ces vasières. Cette hypothèse de mise en place de la VOG est qualifiée d'« hypothèse paléogéographique ». Elle a été soutenue par plusieurs études menées au cours des années 1970. Le premier élément ayant appuyé cette hypothèse est la datation de débris coquillers prélevés à la base des sédiments vaseux d'une carotte échantillonnée dans la VOG vers 50 m de profondeur. L'âge de ces débris, estimé à 10 050 ± 150 ans B.P. (*Before Present*), a soutenu l'hypothèse d'une mise en place de la VOG dans une zone littorale, à proximité de l'embouchure de l'estuaire de la Gironde, lors d'une période de bas niveau marin (Feral, 1970). Des travaux sédimentologiques et micropaléontologiques effectués à la même période indiquent qu'elle se serait formée dans un environnement lagunaire, connecté à l'estuaire de la Gironde et à la mer, qui serait progressivement devenu marin en raison de la transgression marine de l'Holocène (Carbonel et al., 1975; Moyes, 1974; Pujos, 1976; Vigneaux et al., 1971).

Quelques années après ces travaux, une seconde hypothèse sur la mise en place de la VOG a été développée par Castaing (1981). L'auteur suggère que la formation de ce corps sédimentaire aurait débuté vers 7 000 ans B.P. et résulterait du transport de particules fines depuis l'estuaire de la Gironde et le Pertuis de Maumusson jusqu'à des zones où les turbulences deviennent suffisamment faibles pour permettre leur dépôt. Cette hypothèse a été qualifiée d'« hypothèse dynamique » (Castaing, 1981; Lesueur, 1992).

Le prélèvement de carottes longues (> 2 m) à différentes profondeurs dans la VOG entre 1987 et 1991 a permis la réalisation de nouvelles datations et de nouvelles études palynologiques et sédimentologiques (Lesueur et al., 1991, 1996, 2002). Tout d'abord, des datations au carbone 14 de débris coquillers présents dans le substrat sableux (~ 2000 ans B.P) ont mis en évidence que la VOG était plus récente que ce qui avait été suggéré par les travaux

antérieurs. L'étude des assemblages palynologiques dans les sédiments vaseux confirme un âge inférieur à 1500 ans B.P. (Lesueur et al., 1991). Cependant, bien que le début de la sédimentation vaseuse soit estimé à cette période, la majorité des dépôts aurait vraisemblablement eu lieu au cours des derniers cinq à six siècles (Lesueur et al., 1996). Ces nouvelles datations réfutent l'« hypothèse paléogéographique » de mise en place de la VOG et affinent l'« hypothèse dynamique », en précisant notamment la chronologie des dépôts et les facteurs ayant influencé la mise en place de la VOG. Ces travaux ont montré que sa formation serait liée à la fois (1) au remplissage de l'estuaire de la Gironde ayant induit une augmentation de l'export de sédiments vers le plateau continental, (2) à des changements morphologiques de l'estuaire de la Gironde, (3) à des variations climatiques telles que le « Petit Age Glaciaire » (4) ainsi qu'aux activités humaines dans le bassin versant de la Gironde (e.g., agriculture, déforestation). Cependant, étant donné la simultanéité de ces forçages, leur influence respective sur la mise en place de la VOG est difficile à déterminer (Lesueur et al., 1996).

1.3 Structuration et fonctionnement sédimentaire actuel

La VOG est principalement alimentée en particules fines (i.e., silts et argiles) par l'estuaire de la Gironde (Parra et al., 1999; Weber et al., 1991) avec des apports plus importants en période de crue (Constantin et al., 2018; Lesueur et al., 2002). Entre novembre et avril, la présence d'un front thermo-halin localisé vers 100 m de profondeur empêche le transfert des particules sédimentaires provenant de l'estuaire de la Gironde vers le talus continental (Castaing et al., 1999). Ce blocage de l'export des particules vers le large au moment où les apports sédimentaires fluviaux sont les plus importants favorise l'accumulation de sédiments dans les vasières du plateau continental (i.e., la Vasière Ouest Gironde, la Grande Vasière ; Castaing et al., 1999; Lesueur et al., 2002). En plus de ces apports fluviaux, la VOG est alimentée par la sédimentation de particules biogéniques produites dans la colonne d'eau et par des apports de sable du plateau continental adjacent remobilisé lors des tempêtes (Lesueur et al., 2002; Weber et al., 1991). Cependant, l'influence de ces différentes sources n'est pas homogène sur l'ensemble de la vasière.

A partir de l'étude de carottes sédimentaires et de données géophysiques, Lesueur et al. (2002) ont proposé une synthèse de la structuration et du fonctionnement sédimentaire de la VOG (**Figure 1.2**). Ce travail a notamment permis de différencier la partie proximale de la vasière de sa partie distale. La partie proximale (< 40 m de profondeur) est caractérisée par la présence de vases reliques peu bioturbées surmontées de dépôts sableux transitoires apportés du plateau continental adjacent lors des tempêtes. Dans cette zone, les dépôts vaseux sont uniquement saisonniers et remobilisés lors d'évènements de fort hydrodynamisme (Jouanneau et al., 1989; Lesueur et al., 2001). A l'inverse, la partie distale (40 – 70 m de profondeur) est

moins soumise à l'hydrodynamisme et caractérisée par la présence de dépôts de vase récents fortement bioturbés (Jouanneau et al., 1989; Lesueur et al., 2001, 2002). La diminution de l'hydrodynamisme avec l'augmentation de la profondeur influence également l'enregistrement sédimentaire, constitué d'une succession de séquences sédimentaires élémentaires rythmiques typiques de tempêtes (Lesueur et al., 1991, 1996, 2002; Lesueur and Tastet, 1994). L'étude de la fréquence de ces séquences élémentaires indique une récurrence des évènements de fort hydrodynamisme tous les 20 ans en zone proximale et tous les 80 ans en zone distale (Lesueur et al., 2002). Ces estimations correspondent à des fréquences minimales car les séquences élémentaires ont pu être détruites par les tempêtes suivantes ou la bioturbation (Lesueur et al., 2002). De plus, elles ne sont basées que sur les évènements assez énergétiques pour laisser une trace durable dans l'enregistrement sédimentaire. Cependant, les tempêtes entraineraient une remobilisation des sédiments de surface de la VOG de 8 à 140 jours par an selon leur profondeur (Lesueur et al., 1991).

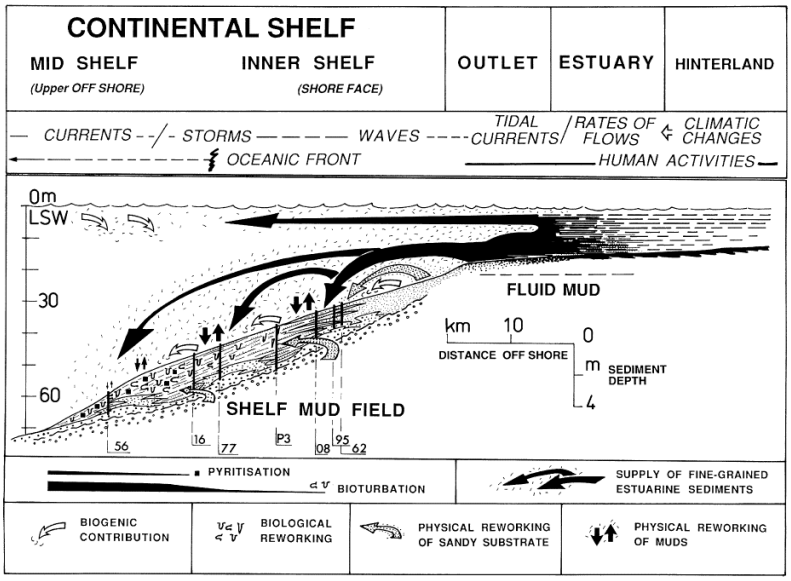

Figure 1.2 : Synthèse des processus sédimentaires responsables de l'accumulation de particules fines dans les vasières du plateau continental Aquitain au large de l'estuaire de la Gironde. D'après Lesueur et al. 2002.

1.4 Structuration et fonctionnement biogéochimique et écologique

La structuration et le fonctionnement biogéochimique et écologique de la VOG n'ont fait l'objet que de deux études basées sur trois stations réparties sur des transects côte - large (i.e., Massé et al., 2016; Relexans et al., 1992). Ces travaux ont montré que les teneurs en carbone organique du sédiment de surface (0 – 1 cm) augmentent vers le large et sont inversement corrélées à la granulométrie. Les teneurs en pigments (i.e., chlorophylle-*a* et phéophytine-*a*) des sédiments de surface sont également plus élevées dans les zones centrales et distales que dans la partie proximale de la vasière. Cependant, la labilité de la matière organique diminue

vers le large mais de façon non significative (Relexans et al., 1992). La réalisation de dix campagnes d'échantillonnage à différentes périodes de l'année entre 1985 et 1988 a mis en évidence que les caractéristiques de la matière organique des sédiments de surface ne varient pas de façon marquée sur des échelles saisonnières et interannuelles (Relexans et al., 1992). La seule exception est la chlorophylle-*a* dont les teneurs étaient plus élevées en été mais de façon non significative. Cette absence de dynamique saisonnière pourrait être en partie liée à la résolution choisie pour l'échantillonnage (0 – 1 cm). En effet, des mesures effectuées sur la tranche 0 – 1 mm ont montré que les teneurs en carbone organique particulaire variaient saisonnièrement sur le premier millimètre mais pas sur le premier centimètre de sédiments (Relexans et al., 1992).

Concernant la macrofaune benthique (faune > 1mm), Massé et al. (2016) ont mis en évidence une diminution des abondances (i.e., nombre d'individus par m²) et de la richesse spécifique (i.e., nombre d'espèces par station) vers le large. Cette étude a également montré une variation de la composition de la macrofaune benthique entre la partie proximale et les zones centrales et distales de la vasière. Cette variation entraine notamment un changement des processus de bioturbation. En zone proximale, les organismes bioturbateurs sont principalement des ophiures qui remanient seulement les premiers centimètres de sédiments. Au contraire dans les zones centrales et distales, les organismes bioturbateurs sont principalement des polychètes constructeurs de terriers dont les activités impactent les sédiments sur une épaisseur plus importante. Cela est cohérent avec les études sédimentologiques qui avaient observé davantage de traces de bioturbation dans les carottes prélevées dans la zone distale de la VOG (Jouanneau et al., 1989; Lesueur et al., 1991, 2002). Ces variations spatiales des caractéristiques et de la composition de la macrofaune benthique ont été attribuées à des variations de la disponibilité des composés organiques et de l'hydrodynamisme (Massé et al., 2016).

2. Stratégie de l'étude

Les études antérieures ont montré l'existence de variations spatiales des descripteurs de la matière organique et de la macrofaune benthique. Cependant, la mise en évidence de ces gradients est basée sur l'échantillonnage d'uniquement trois stations. De plus, la dynamique temporelle de l'ensemble des paramètres mesurés n'a pas pu être caractérisée. Enfin, les processus de reminéralisation de la matière organique ainsi que le stockage du carbone et des éléments associés n'ont pas été abordés par ces travaux. La stratégie d'échantillonnage mise en place dans le cadre des projets JERICO-NEXT, VOG et MAGMA visait à combler ces manques afin d'améliorer notamment la compréhension de la structuration et du fonctionnement biogéochimique de la VOG de l'échelle saisonnière à pluriséculaire.

Table 1.1 : Synthèse des paramètres mesurés dans le cadre des missions océanographiques réalisées dans la VOG entre 2016 et 2021. Seules les variables inclues dans ce travail de thèse sont représentées. Les croix indiquent que l'ensemble des échantillons prélevés ont été analysés pour un paramètre donné. Si ce n'est pas le cas, les niveaux ou le nombre d'échantillons analysés ou manquant sont indiqués. Les cases grises indiquent que le paramètre n'a pas été mesuré dans le cadre de la mission.

			Mission d'échantillonnage synoptique	Missions saisonnières						Mission "Kullenberg"
Périodes			Juin 2018	Octobre 2016	Août 2017	Janv. - Fév. 2018	Avril 2018	Avril 2021	Octobre 2021	Juillet 2019
Missions			JERICObent-5	JERICObent-1	JERICObent-2	JERICObent-3*	JERICObent-4	MAGMA-1*	MAGMA-2*	JERICObent-7*
Stations échantillonnées			32 stations	1 - 2 - 3 - 8 - 4 - 6 - 7 - 9 - 9i	1 - 2 - 3 - 8 - 4 - 7 - 9	1 - 2 - 3 - 4	1 - 2 - 3 - 8 - 4	1 - 2 - 10 - 3 - 8 - 4 - 4K	1 - 2 - 10 - 3 - 8 - 4	3 - 4
Paramètres mesurés										
Caractéristiques de la colonne d'eau*				T, S, O_2, Chl-*a*	T, S, O_2, Chl-*a*	T, S, O_2, Chl-*a* , turbidité	T, S, Chl-*a* , O_2, turbidité	T, S, O_2	T, S, O_2, pH, turbidité	T, S, O_2, Chl-*a* , turbidité
Sédiment - phase particulaire	Caractéristiques physiques du sédiment	Granulométrie [a]	0 - 1 cm	x	x	x	x	x	x	x
		Porosité*	0 - 1 cm	x	x	x	x	x	x	x
		Surface spécifique*,[b]	0 - 1 cm	x	x	x	x	x	x	x
		SCOPIX - Photos de carottes sédimentaires [c]	x	x	x	x	x	uniquement sur les nouvelles stations		x
	Caractéristiques de la matière organique	Carbone organique*,[b]	0 - 1 cm	x	x	x	x	x**	x**	x
		Azote total*,[b]	0 - 1 cm	x	x	x	x	x**	x**	x
		Acides aminés totaux et disponibles	0 - 1 cm, 11 st.	0 - 1 cm	0 - 1 cm	0 - 1 cm	0 - 1 cm	0 - 1 cm**	0 - 1 cm**	19 éch. (st. 3 - 3K)
		Pigments*,[b]	0 - 1 cm, 31 st.	x	x	x	x	x**	0 - 1 cm**	x
		$\delta^{13}C$; $\delta^{15}N$ [d,e]	0 - 1 cm	0 - 1 cm	0 - 1 cm	0 - 1 cm	0 - 1 cm	0 - 1 cm	0 - 1 cm	37 éch. répartis sur les quatre carottes
	Composés inorganiques	Fe et Mn réductibles et acide-soluble et P associé*		x**	x	x	x	x**	x**	x
		Sulfures particulaires (AVS - CRS)						AVS uniquement**	AVS sur 6 st. CRS sur 3 st.**	x
		Radioéléments ($^{210}Pb_{xs}$) [f]		x	x	x	x	x	x	x
		Datations au ^{14}C [g]								11 mesures
Sédiments - phase dissoute	pH*			x	x	x	x	x	x	x
	Potentiel redox								x	
	Sels nutritifs (NO_3^-, NO_2^-, NH_4^+, $Si_{(d)}$)*,[b]			x	x	x	x	x	x	x
	Carbone inorganique dissous*			x	x	x	x	x	x	x
	Carbone organique dissous[b]			x	x	x	x	x	x	x
	Fe, Mn et P inorganique disssous*			x	x	x	x	x**	x**	x
	Sulfures*			x				x**	x**	x
	Méthane*			x	x					x
	Eléments majeurs (SO_4^{2-}, Cl^-, Na^+, K^+, Mg^{2+}, Ca^{2+})*			x	x	x	x	x**	x**	x
	Eléments traces métalliques [h]							x**	x**	
Flux	Profils d'O_2 à l'interface eau-sédiment et flux diffusifs associés*			*ex situ*	*in situ*	*in situ*	*in situ*	*in situ* **	*in situ* **	*ex situ*
	Flux totaux d'oxygène et de sels nutritifs à l'interface eau-sédiment*				x	x	x	x	x	
Faune benthique	Abondance ; Biomasse ; Richesse spécifique [i]			x	x	x	x	x	x	
Traces d'activités de la faune (SPI)	Qualification et quantification des traces d'activités biologiques		x**	x	x	x	x	pas de mesures aux st. 8 et 10	x	

* missions et analyses auxquelles j'ai participées ; ** implication de stagiaires

Plateformes techniques support :

[a]Plateforme technique "Granulométrie et Lithopréparation" (GraL, UMR 5805 EPOC)

[b]Plateforme technique "Biogéochimie Aquatique" (UMR 5805 EPOC)

[c]Plateforme technique "Analyse des Carottes Sédimentaires" (PACS, UMR 5805 EPOC)

[d]Plateforme de Spectrométrie Isotopique (UMR 7266 LIENSs)

[e]Plateforme Analytique de Chimie des Environnements Marins (PACEM, UMR 7294 MIO)

[f]Spectrométrie Gamma (Sabine Schmidt, UMR 5805 EPOC)

[g]Laboratoire de Mesure du Carbone 14 (LMC14, UMR 8212 LSCE ; demande ARTEMIS, Frédérique Eynaud)

[h]Plateforme technique "Analyse des Elements en Traces dans l'Environnement et Isotopes" (AETE-ISO, UMS 3282 OREME)

[i]Plateforme technique "Biodiversité" (UMR 5805 EPOC)

Les paramètres mesurés dans le cadre des missions océanographiques décrites ci-dessous et inclus dans ce travail sont synthétisés dans la ***Table 1.1****. L'acquisition de ces nombreux paramètres a été permise grâce au soutien de plusieurs plateformes analytiques de l'UMR 5805 EPOC mais également grâce à des plateformes extérieures (****Table 1.1****). Parmi les paramètres utilisés dans le cadre de cette thèse, j'ai traité l'ensemble des données permettant de caractériser la colonne d'eau et ai réalisé, pour la phase solide, la plupart des mesures de porosité, carbone organique, carbone et azote total, pigments, fer, manganèse et phosphore. Pour la phase dissoute, j'ai réalisé la plupart des mesures de carbone inorganique, fer, manganèse et phosphore dissous, sulfures et éléments majeurs. J'ai également participé aux mesures de pH, de sels nutritifs et de méthane bien que je n'ai pas réalisé la majorité des analyses. Enfin, j'ai traité la plupart des profils d'oxygène dissous à l'interface eau-sédiment et ai participé aux mesures de flux totaux d'oxygène et de sels nutritifs. J'ai également participé à quatre des neuf missions océanographiques présentées dans ce travail. Ma première participation a eu lieu dans le cadre de mon stage de master 1 (janvier – février 2018) et les trois autres dans le cadre de ma thèse (juillet 2019, avril et octobre 2021).*

2.1 Structuration spatiale des descripteurs de la matière organique et de la macrofaune benthique

Etant donné que les caractéristiques de la matière organique et de la macrofaune benthique peuvent influencer les processus biogéochimiques dans les sédiments, il était nécessaire de mieux définir la structuration spatiale de ces paramètres. Pour cela, 32 stations réparties sur l'ensemble de la VOG ont été échantillonnées en juin 2018 lors d'une mission océanographique sur le N/O « Côtes de la Manche » (**Figure 1.3**, Schmidt and Deflandre, 2018). Dans la **Table 1.1**, cette mission est qualifiée de « mission d'échantillonnage synoptique ».

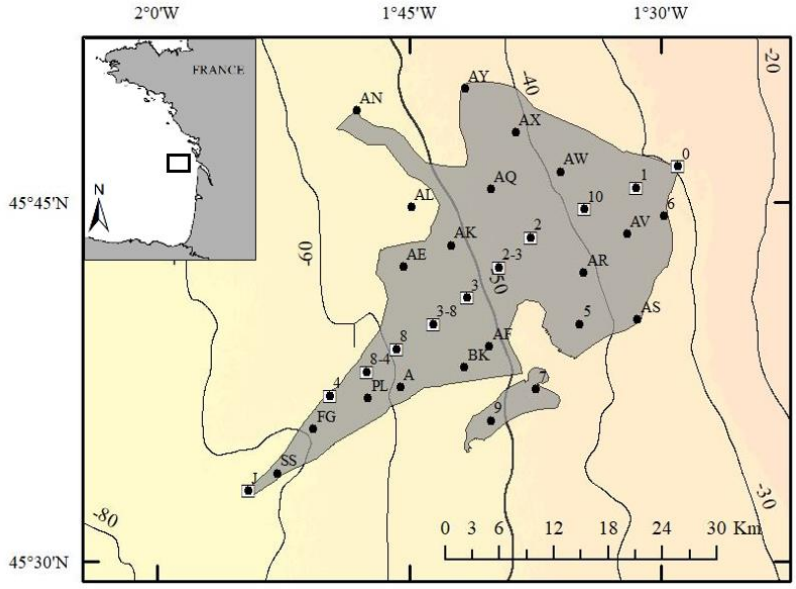

Figure 1.3 : Carte de la Vasière Ouest Gironde avec la localisation des 32 stations échantillonnées dans la VOG en juin 2018 (ronds noirs). Les carrés blancs représentent les stations pour lesquelles des mesures d'acides aminés ont été réalisées.

A chaque station, une carotte sédimentaire a été prélevée à l'aide d'un carottier monotube UWITEC®. Le premier centimètre de sédiment a été échantillonné et séparé en deux sous-échantillons qui ont été immédiatement congelés. Ces échantillons ont été analysés pour la granulométrie, la surface spécifique et les caractéristiques de la matière organique (teneurs en carbone organique, en chlorophylle-*a* et en phéophytine-*a*, $\delta^{13}C$ du carbone organique ; **Table 1.1**). Les acides aminés totaux (THAA, *Total Hydrolysable Amino Acids*) et disponibles (EHAA, *Enzymatically Hydrolyzable Amino Acids*) ont été analysés à 11 stations réparties sur un transect côte - large bathymétrique (**Figure 1.3**). Les méthodes d'analyse de ces paramètres sont décrites en détails dans Lamarque et al., (2021) (**Annexe 1**). La caractérisation de l'activité de la macrofaune benthique, réalisée à partir des images d'un profileur d'images sédimentaires (Ocean Imaging System®) équipé d'un appareil photo Nikon® D7100, faisait partie des travaux de thèse de Bastien Lamarque (Lamarque, 2022). Une synthèse de ces travaux est succinctement présentée dans le chapitre 2 en raison de l'influence de la macrofaune benthique sur les processus biogéochimiques.

2.2 Structuration et fonctionnement biogéochimique de la Vasière Ouest Gironde de l'échelle saisonnière à pluriséculaire

Afin de caractériser la structuration et le fonctionnement biogéochimique de la VOG sur des échelles saisonnières à pluridécennales, six missions océanographiques sur le N/O « Côtes de la Manche » ont été réalisées à différentes saisons entre 2016 et 2021 (Deflandre, 2016; Deflandre et al., 2021). Les sites d'études sont répartis sur deux transects côte - large bathymétriques (**Figure 1.4A**). A chaque mission, entre 4 et 9 stations ont été échantillonnées en fonction des conditions météorologiques qui se sont souvent avérées défavorables (**Table 1.1**). Afin de préciser le contexte hydrologique au moment de l'échantillonnage de chaque station, plusieurs paramètres de la colonne d'eau ont été mesurés (**Table 1.1**). A partir de 2018, un jour par mission a été consacré à la réalisation de ces mesures sur 12 stations réparties sur un transect bathymétrique (**Figure 1.4A**). A chaque station les distributions verticales d'oxygène dissous à l'interface eau-sédiment ont été mesurées *in situ* à l'aide d'un profileur de microélectrodes, excepté en octobre 2016 où ces mesures ont été réalisées *ex situ* en raison d'un problème technique. Ces profils d'oxygène dissous ont permis de quantifier la profondeur de pénétration de l'oxygène ainsi que les flux diffusifs d'oxygène à l'interface eau-sédiment. Jusqu'à 12 carottes de sédiment non perturbées ont été prélevées à l'aide d'un carottier multitube de type MC6 *Oktopus GmbH*. Quatre carottes ont été incubées à l'obscurité et à température de l'eau de fond pour mesurer les flux d'oxygène totaux et de nutriments (nitrates, ammonium) à l'interface eau-sédiment. Une carotte a été découpée pour la détermination du Plomb 210 en excès dont les profils permettent d'estimer des taux de sédimentation (SAR) et

d'accumulation de masse (MAR). En octobre 2021, des mesures de potentiel redox du sédiment ont été réalisées sur cette carotte. Une carotte a été découpée sous atmosphère inerte (N_2) pour la mesure des caractéristiques physiques du sédiment, de la composition de la fraction dissoute et de plusieurs paramètres de la fraction solide (carbone organique, azote total, isotopie de la matière organique, fer, manganèse et phosphore particulaires). Un échantillon de chaque tranche de sédiment a été immédiatement congelé pour réaliser les mesures sur la phase solide. Le sédiment restant a été centrifugé à température *in situ* sous atmosphère inerte (N_2) afin de récupérer les eaux porales qui ont été conditionnées (i.e., acidifiées, stockées au frigidaire ou au congélateur) selon les analyses à réaliser. Une autre carotte a été consacrée aux mesures de carbone organique (et inorganique pour avril et octobre 2021) dissous. Enfin, trois carottes ont été découpées pour l'analyses des teneurs en pigments (chlorophylle-*a* et phéophytine-*a*) et en acides aminés totaux et disponibles. Ces échantillons ont été rapidement congelés afin d'éviter la dégradation des pigments. Une carotte supplémentaire a été échantillonnée pour la mesure des concentrations en méthane en octobre 2016 et août 2017 ainsi que pour déterminer les teneurs en sulfures particulaires (i.e., AVS pour *Acid Volatile Sulfides* et CRS pour *Chromium Reducible Sulfides*) en avril et octobre 2021. Les méthodes d'analyse des phases particulaires et dissoutes des sédiments sont décrites dans les chapitres où ces données sont discutées.

A chaque station, trois bennes Hamon ont été prélevées pour la caractérisation de la macrofaune benthique (abondance et biomasse spécifiques, richesse spécifique). Le traitement de ces données sur la période 2016 – 2018 faisait partie des travaux de thèse de Bastien Lamarque (Lamarque, 2022).

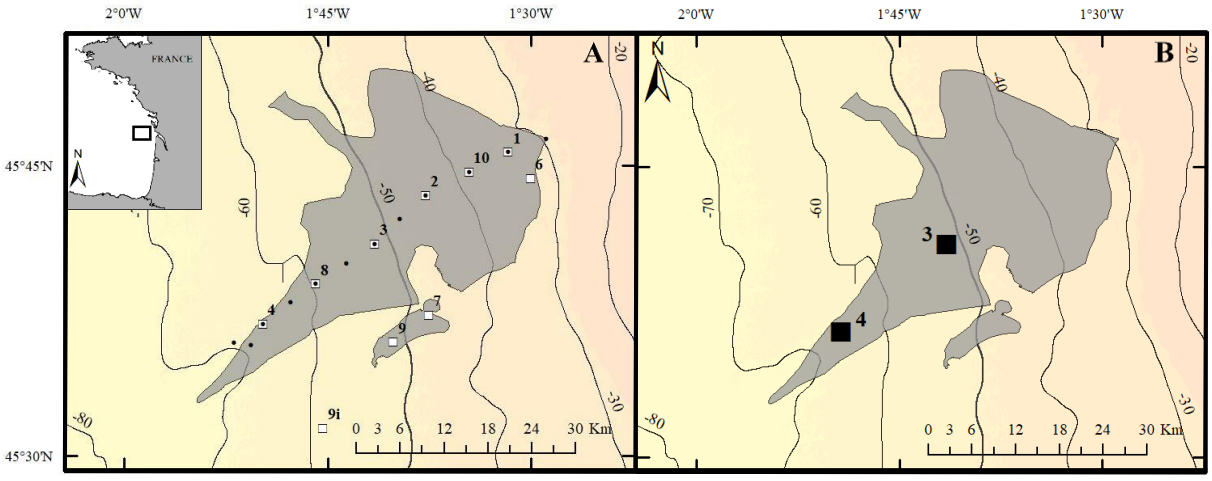

Figure 1.4 : Carte de la Vasière Ouest Gironde avec (**A**) la localisation des stations échantillonnées saisonnièrement de 2016 à 2021 (carrés blancs) et des stations de mesure des paramètres physicochimiques de la colonne d'eau (ronds noirs) et (**B**) la localisation des stations de prélèvement de carottes d'interface et Kullenberg pour la caractérisation du fonctionnement biogéochimique de la VOG de l'échelle pluridécennale à pluriséculaire.

Afin de caractériser le fonctionnement biogéochimique de la VOG de l'échelle pluridécennale à pluriséculaire, des carottes de sédiment d'environ 3 m ont été prélevées dans les parties centrales et distales de la vasière à l'aide d'un carottier Kullenberg lors d'une mission océanographique réalisée en juillet 2019 sur le N/O « Côte de la Manche » (**Figure 1.4B** ; Deflandre, 2019). En raison de la destruction de l'interface eau-sédiment par le carottier Kullenberg, des carottes d'interface ont également été prélevées avec un carottier monotube UWITEC®. Ces carottes ont été découpées sous atmosphère inerte (N_2). Chaque tranche de sédiment a été échantillonnée pour la mesure (1) des concentrations en méthane, (2) des teneurs en sulfures particulaires, (3) des teneurs en pigments et (4) des autres caractéristiques de la phase solide (**Table 1.1**). Le reste des sédiments a été centrifugé sous atmosphère interne (N_2) et à température *in situ* afin de récupérer les eaux porales qui ont été conditionnées en fonction des analyses à réaliser. Les distributions verticales de l'oxygène dissous à l'interface eau-sédiment ont été déterminées sur une carotte sédimentaire d'interface non perturbée à l'aide de microélectrodes à oxygène de type Clark (Revsbech, 1989). Le protocole d'échantillonnage et les méthodes d'analyse des différents paramètres mesurés dans le cadre de cette mission sont décrits en détails dans le Chapitre 4.

Chapitre 2

Contexte hydro-sédimentaire et variabilité spatiotemporelle des descripteurs de la matière organique et de la macrofaune benthique dans la Vasière Ouest Gironde

Ce chapitre est divisé en trois parties décrivant différents aspects du contexte de cette étude.

La **première partie** s'attache à définir le contexte hydrologique de la Vasière Ouest Gironde. Les résultats sont présentés sous la forme d'un article scientifique :

Dubosq, N., Schmidt, S, Sudre, J., Rigaud, S., Lamarque, B., Danilo, M., Grémare, A., Deflandre, B. (2022) *First observations of seasonal bottom water deoxygenations off the Gironde estuary (Bay of Biscay, North East Atlantic). Frontiers in Marine Science*. 9:1006453. doi: 10.3389/fmars.2022.1006453

La **deuxième partie** est consacrée à la caractérisation de la sédimentation aux stations échantillonnées en octobre 2016 ainsi qu'à l'estimation de leur capacité à stocker le carbone organique à l'échelle pluridécennale. Les résultats sont présentés sous la forme d'un article scientifique:

Dubosq, N., Schmidt, S., Walsh, J.P., Grémare, A., Gillet, H., Lebleu, P., Poirier, D., Perello, M.-C., Lamarque, B., Deflandre, B., 2021. *A first assessment of organic carbon burial in the West Gironde Mud Patch (Bay of Biscay). Continental Shelf Research* 221, 104419. https://doi.org/10.1016/j.csr.2021.104419

La **troisième partie** porte sur la structuration spatiale et la variabilité saisonnière des caractéristiques du sédiment de surface et des descripteurs de la macrofaune benthique. Elle présente une brève synthèse des deux articles suivants enrichie de données acquises lors des missions océanographiques d'avril et octobre 2021. Ces articles sont respectivement disponibles en Annexe 1 et Annexe 2.

Lamarque, B., Deflandre, B., Galindo Dalto, A., Schmidt, S., Romero-Ramirez, A., Garabetian, F., Dubosq, N., Diaz, M., Grasso, F., Sottolichio, A., et al. (2021). *Spatial Distributions of Surface Sedimentary Organics and Sediment Profile Image Characteristics in a High-Energy Temperate Marine RiOMar: The West Gironde Mud Patch. Journal of Marine Science and Engineering*, 242. doi: 10.3390/jmse9030242.

Lamarque, B., Deflandre, B., Schmidt, S., Bernard, G., Dubosq, N., Diaz, M., et al. (2022). *Spatiotemporal dynamics of surface sediment characteristics and benthic macrofauna compositions in a temperate high-energy River-dominated Ocean Margin. Continental Shelf Research* 247, 104833. doi: 10.1016/j.csr.2022.104833.

Partie A - Premières observations de désoxygénations saisonnières des eaux de fond au large de l'estuaire de la Gironde (golfe de Gascogne, Atlantique Nord Est)

Dubosq N.[1], Schmidt S.[2], Sudre J.[3], Rigaud S.[4], Lamarque B.[1], Danilo M.[1], Grémare A.[1], Deflandre B.[1]

[1] Univ. Bordeaux, CNRS, Bordeaux INP, EPOC, UMR 5805, F-33600 Pessac, France

[2] CNRS, Univ. Bordeaux, Bordeaux INP, EPOC, UMR 5805, F-33600 Pessac, France

[3] CNRS, UAR CPST, F-83507 La Seyne sur mer, France

[4] Université de Nîmes, EA 7352 CHROME, F-30021 Nîmes, France

Article publié en 2022 dans la revue *Frontiers in Marine Science*

Résumé

Bien qu'elles ne soient pas systématiquement considérées comme des zones de minimum d'oxygène, les marges continentales sous l'influence de grands fleuves sont sensibles aux désoxygénations. Par exemple, le plateau continental au large de l'estuaire de la Gironde, dans le golfe de Gascogne, n'avait pas encore été étudié dans cette perspective alors que des simulations récentes suggèrent que cette zone pourrait avoir subi des désoxygénations au cours des dernières décennies. Afin de combler cette lacune, des profils de température, de salinité et d'oxygène dissous ont été réalisés dans la colonne d'eau du plateau continental du golfe de Gascogne au large de la Gironde au cours de sept missions océanographiques menées à différentes saisons entre 2016 et 2021. Des profils de turbidité, chlorophylle-*a* et pH ont également été mesurés au cours de certaines de ces missions. En hiver, la colonne d'eau est légèrement stratifiée en raison des importants débits de la Gironde. Ensuite, une stratification thermique est présente du printemps à l'automne. De la même manière, l'oxygène dissous montre une dynamique saisonnière avec une colonne d'eau bien oxygénée en hiver, une sursaturation en oxygène dissous dans les 20 premiers mètres de la colonne d'eau lors de l'efflorescence printanière et enfin une diminution progressive des concentrations en oxygène dissous dans l'eau de fond jusqu'à atteindre un minimum en automne. La plus faible saturation en oxygène observée à cette période a été de 45% (octobre 2016). Ces désoxygénations s'expliquent par la mise en place d'une stratification saisonnière qui isole les eaux de fond du printemps à l'automne. Elles sont probablement accentuées par l'advection d'eaux désoxygénées depuis le nord du golfe de Gascogne et la sédimentation de matière organique produite dans les eaux de surface par la production primaire. Une meilleure compréhension de ces processus dans le contexte de changement global actuel nécessite sans aucun doute une meilleure documentation de la dynamique de l'oxygène dissous à travers la mise en place d'un suivi *in* situ, continu et sur le long-terme.

Mots clés: désoxygénation, plateau continental, évolution saisonnière, stratification, golfe de Gascogne, oxygène dissous

1. Introduction

Worldwide the number of oceanic areas affected by hypoxia, as well as the frequency and the spatial and temporal extents of this phenomenon, are increasing (Breitburg et al., 2018; Oschlies et al., 2018; Wakelin et al., 2020). This trend is more pronounced in coastal regions (Breitburg et al., 2018; Gilbert et al., 2010) and constitutes a rising threat for ecosystems. Indeed, many impacts (e.g. migrations, local extinctions, population and individual size decrease) up to food web perturbations have been observed (Breitburg et al., 2018; Fennel and Testa, 2019; Levin, 2018; Roman et al., 2019). Despite these potential effects on ecosystems supporting fisheries, the consequences of climate changes on dissolved oxygen (DO) in the coastal ocean are still poorly documented (Wakelin et al., 2020).

Although not systematically considered as Oxygen Minimum Zones, River-dominated Ocean Margins (RiOMar) are vulnerable to DO depletions due to riverine nutrient inputs. Indeed, they can promote excess phytoplankton production inducing a DO consumption for their degradation (Breitburg et al., 2018; Cai et al., 2011; Diaz and Rosenberg, 2008; Testa and Kemp, 2011; Wang et al., 2021). A recent simulation suggested that several areas of the North-West European continental shelves, including the Bay of Biscay, a wide inlet of the North Atlantic Ocean, would be vulnerable to deoxygenation (Ciavatta et al., 2016). The shelf off the Loire and Gironde, the main rivers flowing into the Bay of Biscay (**Figure 2.1A**), is estimated to experience relatively frequent deoxygenations over recent decades. Moreover, an ecological model applied to the French Atlantic shelf also simulated hypoxia south from the Gironde but the authors themselves considered this result “too severe and unrealistic” (Ménesguen et al., 2019). In fact, the only reported anoxia episode along the French shelf of the Bay of Biscay has been registered in July 1982 in its northernmost sector, off the smaller and eutrophicated Vilaine river (**Figure 2.1A**, Rossignol-Strick, 1985). Following this event, a high frequency monitoring of the Vilaine Bay revealed recurrent deoxygenations and even hypoxia in bottom waters (Ratmaya et al., 2022; Retho et al., 2020). The lack of such *in situ* data in the southern sector of the Bay of Biscay precludes confirming the occurrence of deoxygenation suggested by the models.

The continental shelf off the Gironde is subjected to strong hydrodynamics, and is thus mainly composed of sands and gravels but also of several mud patches (Lesueur et al., 2002). Among them, the West Gironde Mud Patch (WGMP) is a well-defined sedimentary area located about 40 km off the Gironde and comprised between 30 and 75 m depth (**Figure 2.1B**). The WGMP is of particular interest due to its economic importance for common sole (*Solea solea*) and Norway lobster (*Nephrops norvegicus*) fishing but also for its biological activity (Lamarque et al., 2021) and its capability to store carbon (Dubosq et al., 2021). Its sedimentary functioning

is studied since the 1990's and its benthic ecological structuration was recently defined (Dubosq et al., 2021; Fontanier et al., 2022; Lamarque et al., 2021; Lesueur et al., 1991, 2002). However, there was still no information on DO in the WGMP water column. The present study aims to fill this gap by presenting the first measurements of DO and ancillary data (temperature, salinity, chlorophyll-*a*, turbidity, pH) in the water column along a cross-shelf transect covering the WGMP. This gives a first insight of the DO dynamics in this RiOMar, from seasonal to inter-annual scales, and its controlling factors.

2. Material and methods

2.1 Field measurements

Seven cruises were performed from 2016 to 2021 on the R/V "Côtes de la Manche" to investigate the biogeochemical and ecological functioning of the benthic ecosystem of the WGMP (Deflandre, 2016; Deflandre et al., 2021). Even if these cruises were mainly dedicated to sediments, depth profiles of DO, temperature and salinity were performed in the water column at each sampling station (**Figure 2.1B**, **Table 8.1 – Annex 3**). Following the observation of unexpected low bottom DO concentrations during the first cruise, the strategy was completed from 2018 by a day per cruise (except in July 2019) dedicated to the achievement of cross-shelf transects from station 0 to W or 12 (**Figure 2.1B**).

Additional parameters were measured more occasionally: pH (October 2021), chlorophyll-*a* (October 2016, August 2017, January and April 2018, July 2019) and turbidity (January and April 2018, July 2019, October 2021). Depth profiles were acquired using inter-calibrated sensors: a CTD SeaBird SBE-19plus, autonomous sensors (STPS, SDOT, STBD, *NKE Instrumentation*) and a WiMo Plus multiparameter probe (*NKE Instrumentation*, October 2021). Profile resolutions varied from two to five measurements by meter depending on the response time of each sensor. Turbidity sensors were inter-calibrated using formazin, allowing to provide turbidity data in Formazin Nephelometric Units (FNU). Water density was calculated from temperature, salinity and depth using the seawater state equation (Pond and Pickard, 2007). The significance of the correlations between salinity above the halocline at each site and daily river flows and between DO concentrations and pH was assessed using a Spearman's rank correlation coefficient (software SigmaPlot 14).

2.2 Satellite and Gironde flow data

The NASA Aqua/MODIS data (4 km resolution, NASA Ocean Color, https://oceancolor.gsfc.nasa.gov/) were used to replace *in situ* measurements in the annual cycles of sea surface temperatures (SST) and biological production. SST and surface

chlorophyll-*a* (Chl-*a*) concentrations were extracted for the proximal (longitudinal and latitudinal limits: 1°28.80'W to 1°37.50'W; 45°47.50'N to 45°40.00'N) and distal (1°42.50'W to 1°50.00'W; 45°42.50'N to 45°35.00'N) areas of the WGMP from the 01/01/2016 to the 12/31/2021 (**Figure 2.1B**). Each area consisted in 25 pixels whose values were averaged. For the entire period, 2189 pictures were available for SST and 2192 for surface Chl-*a* concentrations. However, some of them contained no or very little data due to cloud cover. Only pictures with at least 11 pixels per area were retained to calculate mean values. Outliers, with no data in the three previous or following days to confirm the value, were excluded. Monthly-averages of surface Chl-*a* concentrations were calculated to reduce the day-to-day variability and better identify trends.

The Gironde fluvial discharge corresponds to the sum of those of its two main tributaries, the Garonne and Dordogne rivers, whose measuring gauging stations are at Tonneins and Lamonzie Saint Martin, respectively. Data were extracted from the data portal *hydro.eaufrance.fr*.

3. Results

3.1 Gironde flow and satellite data

For the period 2016 to 2021, the daily Gironde flow ranged from 117 (August 2019) to 7900 $m^3 s^{-1}$ (February 2021) with a mean of 762 $m^3 s^{-1}$ (**Figure 2.1C**). It is slightly higher than the average over the period 2008 – 2021 (745 $m^3 s^{-1}$, *hydro.eaufrance.fr*). The lowest flows were recorded in summer and the highest in winter and spring. The intensity and duration of the high flow period presented a large inter-annual variability. For example, daily flows were above mean from January to June 2018, whereas it only happened for a few weeks in 2019. SST also showed a well-defined seasonal cycle (**Figure 2.1C**) with warmer waters in summer (> 20°C) and colder in winter (< 11°C). The inter-annual variability of SST was mainly reflected in a variation of the period during which extreme values were reached. For example, the lowest temperature was measured at the end of February in 2018 but in mid-January in 2021.

Surface Chl-*a* concentrations are an indicator of the net primary production. Monthly averages varied from 0.6 to 5.6 µg L^{-1} with higher values in the proximal than in the distal area (**Figure 2.1C, Table 8.2 – Annex 3**). They were at their highest in late winter and spring, and then decreased to a minimum in summer. A slight increase occurred in autumn. Interestingly, longer and more intense blooms periods were observed during the years with longer high flow periods (i.e., 2016, 2018 and 2020, **Figure 2.1C**).

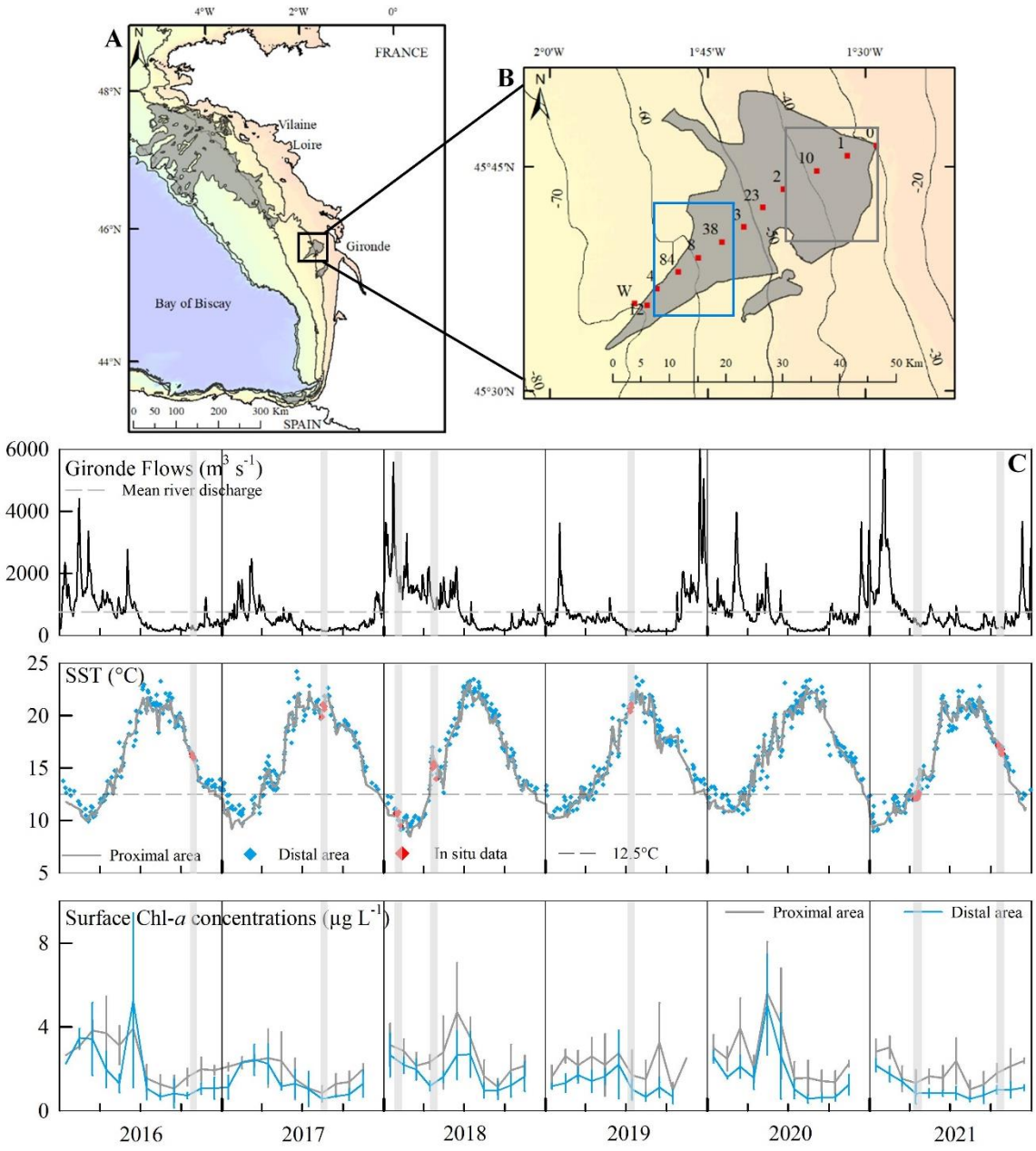

Figure 2.1: (A) The Bay of Biscay with the locations of mud patches (gray areas) and of the two main rivers, **(B)** map of the WGMP showing the locations of sampling stations (red squares) and the areas of satellite data extractions (rectangles). **(C)** Hydrological context: Gironde flows, Sea Surface Temperatures and monthly averages of surface Chl-*a* concentrations in the distal and proximal areas from the 01/01/2016 to the 12/31/2021. Gray lines indicate sampling periods.

Satellite data allowed defining the hydrological context of each cruise. The winter cruise took place during a high flow and cold period. Not surprisingly, the summer cruises correspond to the warmest and driest (the lowest river flows) period. River flows and temperatures showed the highest variability in spring and autumn. However, the two autumnal cruises presented rather similar characteristics: a surface temperature around 16 - 17°C, a slight increase in flows rate with autumnal rains, and a moderate net primary production in surface waters. On the

contrary, the two spring cruises had contrasting hydrological contexts: Gironde flows were still high in April 2018, combined with relatively high Chl-*a* levels whereas they were below the mean in April 2021.

3.2 Temperature and salinity

Based on temperature and salinity profiles, the water column can be divided into two layers (**Figure 2.2**, **Figure 8.1 – Annex 3**). Whatever the season, bottom water salinities were quite constant with values between 34.8 and 35.4. The same pattern was observed for temperatures in the central and distal areas with values from 11.5 to 12.5°C, excepted for the cruise of August 2017 during which bottom waters were slightly warmer (between 12.8 and 13.5°C). In contrast, surface temperatures and salinities varied seasonally, partly due to freshwater inputs from the Gironde as previously described by Puillat et al. (2004).

In winter 2018, surface waters were colder and fresher (mean salinity between 30 and 32) than bottom waters (**Figure 8.1 – Annex 3**) due to the Gironde plume spread, inducing a haline stratification. After the period of the highest flows, usually observed in winter (**Figure 2.1C)**, flows decreased and the associated haline stratification weakened until to become negligible, as observed on salinity profiles in August 2017 and October 2016 where the salinity difference between surface and bottom waters was less than 0.5 (**Figure 8.1 – Annex 3**). The intensity of the spring haline stratification varied depending on years due to the variability of river flows. Indeed, the difference in flows rates resulted in lower surface salinities and a more pronounced haline stratification in April 2018 compared to April 2021 (**Figure 2.2**).

Along with the decrease in river flows and associated haline stratification, the warming of surface waters in spring induced the establishment of a thermocline, the timing of which is variable. For example, temperatures decreased with depth from 15°C to 11.6°C in April 2018 while they were rather constant along the depth profile in April 2021 (about 12.5°C, **Figure 2.2**). The thermal stratification was particularly marked in August 2017 with a temperature decrease from 21°C to 13.5°C (**S Figure 8.1 – Annex 3**). During the two autumnal cruises, a thermocline was still present but shallower in 2016 than in 2021. The thermocline depth was highly variable from cruise to cruise, from about 15 m (April 2018) to 30 m (October 2021) in the central WGMP (i.e., station 3, **Figure 2.2**). Temperature and salinity as well as the seasonal variability of the thermal stratification are consistent with previous hydrological studies at the scale of the Bay of Biscay continental shelf (Koutsikopoulos and Le Cann, 1996; Puillat et al., 2004; Vincent and Kurc, 1969).

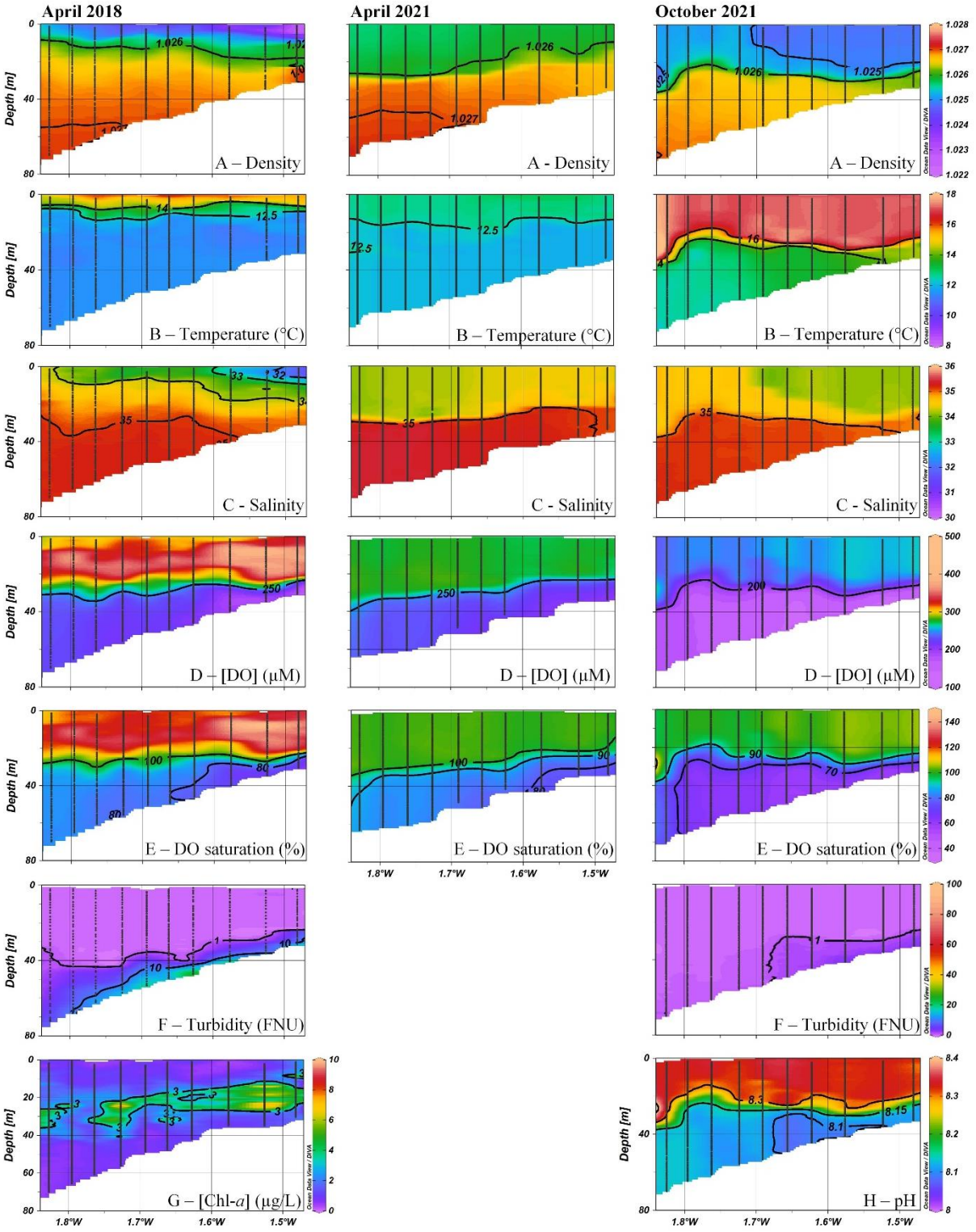

Figure 2.2: Transects (10 sites, from station 0 to 4) of density, temperature, salinity, dissolved oxygen (DO) concentrations and saturations, turbidity, Chl-*a* (April 2018) and pH (October 2021) in the water column of the West Gironde Mud Patch against longitude at three different periods (i.e., April 2018 and 2021 and October 2021). Profiles were interpolated with the software *Ocean Data View*. Gray dots represent the measurements points.

3.3 Dissolved oxygen, pH, Chl-*a* and turbidity

Dissolved oxygen concentrations in the water column were highly contrasted between cruises and seasons with values ranging from 121 to 414 µM. In January 2018, the whole water column was well-oxygenated (**Figure 2.3**, **Figure 8.1 – Annex 3**) due to water mixing related to winter storminess. However, in spite of this apparent homogeneity, a minimum of 90% DO saturation was observed in proximal bottom waters. From spring to autumn, the first 20 to 30 meters were also well-oxygenated (**Figure 2.2**), and even oversaturated in April 2018 up to 147%. This was related to a spring bloom as highlighted by satellite-derived data and depth profiles of Chl-*a* concentrations (**Figures 2.1C** and **2.2**). On the contrary, bottom waters were DO under-saturated over the whole WGMP. These depletions were relatively weak in April 2018 and 2021 with DO saturations always above 70% but more intense in October 2016, July 2019, and October 2021 with minimum saturations of 45, 53 and 59%, respectively (**Figure 2.3**). These depletions were more pronounced in the proximal area.

Turbidity varied from negligible values to 90 FNU, highlighting the presence of a benthic nepheloid layer (**Figure 2.2**, **Figure 8.1 – Annex 3**). This layer was more marked in the proximal area and varied seasonally with higher turbidity in January and April 2018 (values up to 90 and 26 FNU, respectively) than in July 2019 (< 2 FNU) and October 2021 (< 11 FNU). These results are consistent with a previous study of the distribution of suspended sediments on the Bay of Biscay continental shelf (Castaing et al., 1999).

The pH profiles measured in October 2021 showed rather constant values around 8.3 in the first 20 meters, followed by a decrease in depth below 8.15, slightly more pronounced in the proximal area (**Figure 2.2**).

4. Discussion

4.1 Structuring of the water column from seasonal to inter-annual scales

Both salinity and temperature control the water column stratification. However, they are considered separately because their respective contributions to stratification are difficult to define with density alone. As bottom water temperatures and salinities were quite constant regardless of season, surface values were used to infer the intensities of thermal and haline stratifications. The steady level of bottom temperatures is consistent with previous studies that identified a water mass characterized by a constant temperature of around 12°C, “the Cold Pool”, extending from Brittany to the mouth of the Gironde (Koutsikopoulos and Le Cann, 1996; Puillat et al., 2004; Vincent and Kurc, 1969). In fact, this value is of the order of magnitude of the bottom temperatures measured in the central and distal WGMP. Considering

that the bottom temperatures of the central area (i.e., station 3) varied between 11.6 and 12.5°C (except in August 2017), we defined 12.5°C as the surface temperature threshold above which thermal stratification occurs. SST records and temperature profiles support a classical annual pattern with the gradual establishment of a thermocline, the precise timing of which is variable (**Figures 2.1C**, **2.2** and **2.3)**. After its establishment, the thermal stratification intensifies until reaching a maximum in summer, and then progressively decreases in autumn although it is still present (**Figures 2.1C** and **2.3**). Finally, the thermocline inversion in winter indicates its complete disappearance. A significant correlation ($p<0.01$) between the mean salinity above the halocline and Gironde daily flows indicates that the flows control the establishment of the haline stratification. An annual pattern of the water column structuration over the shelf off the Gironde can therefore be inferred. First, a haline stratification is well established in winter. It then decreases due to decreasing flows while a thermal stratification is gradually established in spring. It intensifies until summer, and decreases in autumn until its complete removal. During the period of the thermocline disappearance, flows rates increase and a haline stratification is established again. However, this stratification varies due to contrasted flows: it was almost absent in October 2016 and slightly higher in 2021 (**Figure 2.1C**, **Figure 8.1 – Annex 3**).

4.2 Probable causes of deoxygenations

Dissolved oxygen measurements highlighted substantial deoxygenation of the bottom waters of the WGMP, down to a DO saturation of 45%, in July 2019, October 2016 and 2021. This was very surprising for such an environment subjected to strong hydrodynamics that control its sedimentological and ecological structuration (Dubosq et al., 2021; Lamarque et al., 2021; Lesueur et al., 2002). These DO depletions are related to the establishment of a thermal stratification from spring to autumn (**Figure 2.3**). The isolation of bottom waters from the atmosphere limits DO renewal by preventing mixing with well-oxygenated surface waters. In the isolated waters, DO is consumed by several processes, i.e., bacterial degradation of organic matter, respiration of organisms, consumption by sediment, that have gradually led to the observed depletions. It is interesting to note that the maximum DO depletion does not coincide with the maximum intensity of the thermal stratification (**Figure 2.4**). In fact, deoxygenations are more pronounced when the duration of the stratification (number of days with SST > 12.5°C) is longer (**Figure 2.4**). The stratification duration, and thus the residence time of bottom waters, therefore have a major influence on the intensity of deoxygenation. This is consistent with previous observations in other RiOMar systems such as the East China Sea (Wang et al., 2021) and the Gulf of Mexico (Rabouille et al., 2008).

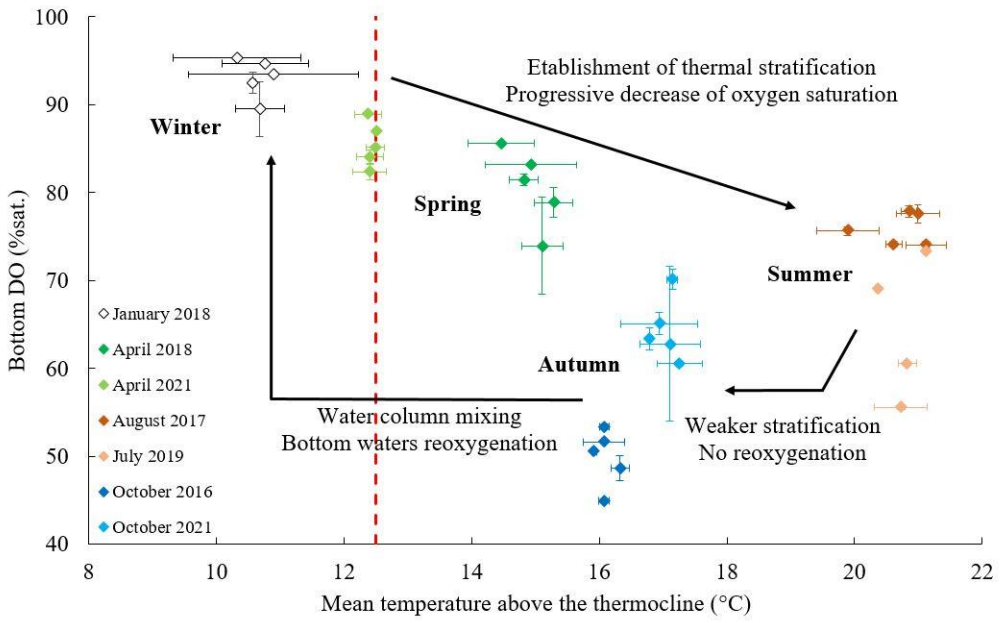

Figure 2.3: Mean dissolved oxygen (DO) saturation in bottom waters (based on the 5 meters above the bottom) against the mean temperature above the thermocline for each cruise and stations 1, 2, 3, 8 and 4. When several profiles were available, DO saturations and temperatures of the several profiles were averaged. The red dash line represents the threshold of 12.5°C above which the thermal stratification occurs.

The bottom deoxygenation is most likely amplified by the input of organic matter from local primary production. Indeed, the higher DO depletion in autumn 2016 compared to 2021 may be due to the higher primary production of surface waters in 2016 (**Figure 2.1C**), whose sedimentation induced a higher DO consumption in the underlying waters for its degradation. The pH measurements in October 2021 revealed a positive correlation between pH and DO ($r=0.903$, $p<0.001$, **Figure 8.2 – Annex 3**). This indicates that aerobic respiration, which consumes oxygen and produces carbon dioxide, is the main process inducing the observed deoxygenation. Such a relationship between DO and pH was commonly observed in other oceanic environments (Cai et al., 2011; Mucci et al., 2011; Steckbauer et al., 2020; Yang et al., 2021; Zhai et al., 2019).

Primary production off the Gironde estuary is partly controlled by nutrient inputs and by winter haline stratification due to high river flows (Labry et al., 2001). The inter-annual variability of river flows therefore partly controls that of the primary production, resulting in higher surface Chl–*a* concentrations in years with longer periods of high flow. The higher surface Chl-*a* concentrations in the proximal than distal WGMP (**Figure 2.1C**) support this hypothesis, suggesting that Gironde flows indirectly influence the intensity of deoxygenation. However, the rivers of the northern Bay of Biscay, the Loire and the Vilaine, are also likely to influence the waters off the Gironde, although they are more remote. A recent study based on tritium signatures of the Loire and the Gironde rivers suggested a significant input of water

from the Loire off the Gironde in summer and autumn (Oms, 2019). As recurrent summer hypoxia occur in the lower Loire estuary (Schmidt et al., 2019) and the Vilaine Bay (Ratmaya et al., 2022; Retho et al., 2020), the southward spreading of these oxygen-depleted waters may reinforce the deoxygenation off the Gironde. In contrast, the Gironde does likely not exacerbate deoxygenations by supplying deoxygenated waters to the shelf as seasonal hypoxia is episodic and limited to the upper estuary (Lanoux et al., 2013; Schmidt et al., 2019).

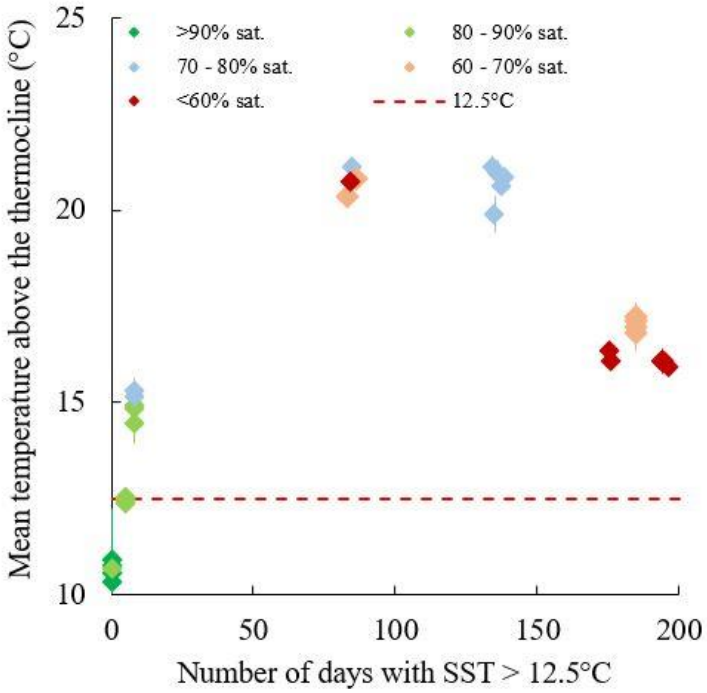

Figure 2.4: Relationships of the mean temperature above the thermocline, the duration of the thermal stratification (number of days with SST > 12.5°C) and the dissolved oxygen saturations of bottom waters in the water column of the continental shelf off the Gironde for each cruise and stations 1, 2, 3, 8 and 4. Dissolved oxygen saturations were average over the 5 meters above the bottom.

4.3 Potential futures responses to global warming

Simulations of the evolution of European continental shelves until 2100 predict that waters of the Bay of Biscay will become fresher and warmer due to global warming (Wakelin et al., 2020). The salinity decrease is an indirect effect of climate changes related to a modification of hydrological cycles and of an increase in river flows (Gröger et al., 2013; Wakelin et al., 2020). This will result in an increase of the intensity and duration of the stratification. Simultaneously, the net primary production is expected to decrease on the Bay of Biscay continental shelf. These changes will result in an estimate decrease of bottom water DO concentrations of 10.9 ± 2.8 µM between the periods 1980 – 2009 and 2070 – 2090 (Wakelin et al., 2020), mainly related to a decrease of DO solubility induced by temperature and salinity changes. Variations in stratification or net primary production only have a significant effect on annual minimums of

DO concentrations. However, this effect is low compared to that of solubility (-1.3 ± 3.1 against -8.8 ± 2.2 µM, respectively).

These results are quite surprising because our data highlights that the duration of the stratification is one of the main factors controlling the deoxygenation (**Figure 2.4**). Therefore one would have expected that the increase in the duration of stratification would reinforce deoxygenation. One explanation could be that the authors have grouped the impacts of stratification and primary production under the term "ecosystem effect". Thus, although stratification enhanced deoxygenation, it also limits the supply of recycled nutrients from bottom to surface waters and thus reduces primary production and the DO consumption for its degradation (Wakelin et al., 2020). However, the impact of climate changes on riverine freshwater and nutrient inputs was not included in the simulation while nutrient loads and primary production can widely influence deoxygenations (Li et al., 2016). The relative effects of stratification and river flow on primary production must therefore be assessed to better estimate their respective impact on the future deoxygenations. At last, as the continental shelf off the Gironde is influenced by water advection from the north of the Bay of Biscay (Oms, 2019), it is possible that future changes of hypoxia intensities in the lower Loire estuary and the Vilaine Bay impact the deoxygenation.

4.4 The need to establish a long-term *in situ* monitoring of the WGMP

This study highlighted that summer and autumnal deoxygenation occurs on the continental shelf off the Gironde. This seems to be mainly related to a thermal stratification from spring to autumn inducing an isolation of the bottom waters that are progressively depleted in DO. The intensity of deoxygenation appears to be influenced by the duration of the stratification, the intensity of primary production, which is itself partly controlled by the duration of the high flow period, and by a probable advection of deoxygenated waters from the north of the Bay of Biscay. However, these hypotheses need to be reinforced. DO variability depends on several factors (e.g. consumption by respiration; physical transport; production by photosynthesis ;Fennel and Testa, 2019) and is affected by different temporal cycles (e.g. daily and tidal, seasonal, decadal climatic cycles; Gilbert et al., 2010). Thus, more severe deoxygenations probably occur, but only episodically, as observed in the Gironde estuary (Schmidt et al., 2019). Furthermore, due to the multiple factors influencing the DO dynamics, it is difficult to predict its long-term evolution merely based on these first results. To better document the DO variability on large spatial and temporal scales, satellite data are a powerful tool (Kim et al., 2017). However as such data must be validated with *in situ* measurements (Kim et al., 2020; Triana and Wahyudi, 2021), an *in situ* monitoring must first be performed. The implementation of such a long-term and continuous monitoring would allow to characterize the

duration and intensity of deoxygenation events and their controlling factors. These measurements coupled to satellite data would finally allow improving model outputs to anticipate the system evolution in response to climate changes and its impacts on ecosystems and fisheries. Indeed, as the common sole presents a reduced activity when DO saturations drops below 40% (Van den Thillart et al., 1994), an exacerbation of deoxygenation could question the long-term presence of this commercial species, affecting the local economy.

Considering that deoxygenation is observed throughout the whole WGMP and that the influence of the Gironde flow decreases seaward, we recommend monitoring only a single site close to the mud patch center. The site should be chosen on the basis of recent bathymetry maps and avoiding known trawling areas. Because such a dynamic area is challenging to instrument due to winter storminess, swells and currents, one recommendation would be to ensure at least a monitoring of DO, temperature, salinity and pressure in the bottom waters in order to document the occurrences, durations and intensities of deoxygenations. However, if possible, it would be ideal to perform these measurements also in surface waters to better characterize the temporal variability of the water column. In that case, the addition of chlorophyll-*a*, pH and pCO_2 sensors would allow to precise the influence of primary production on deoxygenations and to document the pH dynamics, closely related to that of DO.

5. Conclusions

This work enables to document for the first time the DO dynamics and its controlling factors on seasonal to inter-annual scales in the water column of the continental shelf off the Gironde. Results validate the occurrence of bottom water deoxygenations that were suggested by models (Ciavatta et al., 2016; Wakelin et al., 2020). Although deoxygenation has already been reported in RiOMars (Cai et al., 2011; Fennel and Testa, 2019; Rabouille et al., 2008; Wang et al., 2021), this was quite surprising that a thermal stratification can isolate bottom waters and trigger deoxygenation in such an energetic environment. If the stratification seems to be the main factor inducing these deoxygenations, they are potentially reinforced by inputs of organic matter from local production and by the advection deoxygenated water from the northern Bay of Biscay. This work enables us to alert about the deoxygenation issues in this ecosystem of a great economic interest in a context of global warming, the potential effects of which being still uncertain. A better understanding of DO dynamics undoubtedly requires the establishment of a long-term and continuous *in situ* monitoring.

Author contribution

BD and AG conceived the projects and performed funding acquisition. SS conceived of the presented idea. ND, BD, SS, BL, SR and MD performed *in situ* measurements and data qualification; ND, SS and BD analyzed data. JS extracted and analyzed satellite data. ND wrote the manuscript with support from SS and BD. All co-authors commented on and approved the final manuscript.

Conflict of Interest

The authors declare that the research was conducted in the absence of any commercial or financial relationships that could be construed as a potential conflict of interest.

Funding

This work was supported by: (1) the JERICO-NEXT project (European Union's Horizon 2020 Research and Innovation program under grant agreement no. 654410), (2) the LEFE-EC2CO VOG project), and (3) the MAGMA project cofounded by the COTE Cluster of Excellence (ANR-10-LABX-45), the Nouvelle-Aquitaine Regional Council, and the French Biodiversity Agency. Cruises were funded by the French Oceanographic Fleet. Doctoral fellowships were provided to N. Dubosq and B. Lamarque by the french Ministry of Higher Education, Research and Innovation.

Acknowledgments

We sincerely acknowledge the captains and crews of the R/V “Côtes de la Manche” (CNRS-INSU) for their great help during the cruises.

Data Availability Statement

The complete dataset of dissolved oxygen and ancillary parameters acquired during the 7 cruises between 2016 and 2021 in the water column of the West Gironde Mud Patch is freely available on the SEANOE data repository at : https://www.seanoe.org/data/00783/89508 ; DOI: 10.17882/89508

Partie B - Première estimation de l'enfouissement du carbone organique dans la Vasière Ouest Gironde (golfe de Gascogne)

Dubosq N.[1], Schmidt S.[2], Walsh J.P.[3], Grémare A.[1], Gillet H.[1], Lebleu P.[1], Poirier D.[1], Perello M-C.[1], Lamarque B.[1], Deflandre B.[1]

[1] Univ. Bordeaux, CNRS, Bordeaux INP, EPOC, UMR 5805, F-33600 Pessac, France

[2] CNRS, Univ. Bordeaux, Bordeaux INP, EPOC, UMR 5805, F-33600 Pessac, France

[3] Coastal Resources Center, University of Rhode Island, Kingstom, RI 02881, USA

Article publié en 2021 dans la revue *Continental Shelf Research*

Résumé

Plusieurs vasières de milieu de plateau sont présentes sur le plateau continental du golfe de Gascogne dont La Grande Vasière au nord, la Vasière Ouest Gironde au large de l'estuaire de la Gironde et la vasière Basque à proximité de la côte espagnole. En général, ces dépôts sont de quelques mètres d'épaisseur et recouvrent un substrat plus grossier. Actuellement, des interrogations subsistent concernant leur capacité à stocker les sédiments fins et le carbone. Cette étude s'intéresse à la sédimentation dans la Vasière Ouest Gironde dans l'objectif de réaliser une première estimation des taux d'enfouissement du carbone organique dans ce système. Des carottes sédimentaires d'interface ont été prélevées à neuf stations le long de deux transects bathymétriques en octobre – novembre 2016. Des radiographies aux rayons X et des analyses granulométriques ont été utilisées pour caractériser les structures sédimentaires. Des profils de $^{210}Pb_{xs}$ ont été mesurés afin de calculer des taux de sédimentation et d'accumulation de masse. Les structures sédimentaires indiquent des apports sableux épisodiques surmontant des dépôts plus anciens dans la zone proximale et une sédimentation assez régulière aux stations localisées plus au large. Dans la zone central – externe du transect nord, un taux de sédimentation maximum (0.47 cm yr^{-1}) suggère la présence d'un dépocentre. Les taux de sédimentation mesurés sur le transect sud étaient plus faibles (<0.3 cm y^{-1}), à l'exception de deux stations où les apports sédimentaires semblent massifs mais sporadiques. Les taux d'enfouissement du carbone organique augmentent vers le large jusqu'à un maximum de 45 gC m^{-2} y^{-1}. Afin d'évaluer la charge en carbone organique des sédiments indépendamment des variations granulométriques, les teneurs en carbone organique (OC) ont été normalisées à la surface spécifique (SA). Une comparaison qualitative de l'efficacité d'enfouissement du carbone organique aux différentes stations basée sur le ratio OC/SA a mis en évidence trois groupes de sites avec des efficacités d'enfouissement respectivement faibles, moyennes et relativement élevées. Ces différentes efficacités d'enfouissement sont probablement dues à des variations des environnements sédimentaires et des conditions de dépôts liées à des variations de l'hydrodynamisme local et de la profondeur. Ce travail met en évidence le contrôle probable de l'intensité de l'hydrodynamisme et des apports sédimentaires sur la quantité de carbone organique stockée dans les sédiments de la Vasière Ouest Gironde.

Mots clés: taux d'accumulation de sédiments, enfouissement du carbone organique, Vasière Ouest Gironde, golfe de Gascogne, plateau continental

1. Introduction

Organic carbon storage in marine sediments is recognized as a long-term sink for atmospheric carbon dioxide (Berner, 1990, 1982). Understanding the ocean carbon cycle and quantifying carbon storage in the oceans are therefore crucial for improving future climate scenarios (Blair and Aller, 2012; Burdige, 2007; Keil, 2017; Muller-Karger, 2005; Włodarska-Kowalczuk et al., 2019). With about 90% of the modern organic carbon preservation occurring in Rivers-dominated Ocean Margins (RiOMars) systems (Hedges and Keil, 1995; McKee et al., 2004), special attention should be paid to these areas. Although three types of RiOMars have been defined by Blair and Aller (2012), it can be difficult to understand the nature of an individual system because of high spatial and temporal variability (McKee et al., 2004). Owing to these variabilities, each RiOMar can be divided in several sub-environments where major organic carbon (OC) preservation controlling factors may be different (McKee et al., 2004). Moreover, most studies of RiOMars have focused on tropical systems whose results are difficult to translate to higher latitudes (Yao et al., 2014; Zhu et al., 2016). This explains why, in spite of numerous studies on RiOMars (e.g. Aller, 1998; Aller et al., 1996, 1986; Aller and Blair, 2006; Blair and Aller, 2012; Deng et al., 2006; Kuzyk et al., 2017; McKee et al., 2004; Pastor et al., 2018, 2011; Yao et al., 2014; Zhu et al., 2013 and references therein), mechanisms controlling OC preservation in these environments as well as their carbon burial capabilities are not yet fully understood and quantified.

On the Northeast Atlantic margin, the Bay of Biscay continental shelf extends over more than 1000 km, from the Celtic to the North Iberian margins (Borja et al., 2019; Bourillet et al., 2006; Schmidt et al., 2014). Surface shelf sediments are mainly sand. However on the shelf lie also several mid-shelf mud belts and patches including (1) “La Grande Vasière” to the north, (2) the West Gironde Mud Patch off the Gironde estuary and (3) the Basque Mud Patch in front of San Sebastian and Bayonne (**Figure 2.5** ; Allen and Castaing, 1977; Jouanneau et al., 2008, 1999; Lesueur et al., 2002). Overall they are of several meters thick and cover coarser substrate (Jouanneau et al., 1989, 1999; Lesueur et al., 2001, 2002). Mud belts and patches are found on many continental shelves around the world. Typically, they are bounded by dynamic sands on their landward side and are the result of river-derived sediment deposition in areas of lower hydrodynamics (i.e., where waves and currents are more reduced on the seabed; McCave, 1972; Walsh and Nittrouer, 2009). Indeed, their mid-shelf location is directly related to the fact that higher-energy conditions at shallower depth closer to the coast preclude fine sediment accumulation (Dias et al., 2002; McCave, 1972; Walsh and Nittrouer, 2009). These areas are important for biogeochemical transformations and are known organic carbon sinks (McKee et al., 2004).

The West Gironde Mud Patch is particularly interesting because it is under the influence of the Gironde estuary which is the major source of fine sediments for the Bay of Biscay continental shelf (Constantin et al., 2018; Jouanneau et al., 1989, 1999; Lesueur et al., 1991, 1996, 2002; Weber et al., 1991). Studies led in 1990's have rather well defined its sedimentary functioning and suggested a control of sedimentation and resuspension processes by hydrodynamics (Jouanneau et al., 1989; Lesueur et al., 1991, 2002). Only few studies have focused on the WGMP biogeochemistry and ecology (i.e., Massé et al., 2016; Relexans et al., 1992), and have performed too few measurements to characterize its sedimentological, biogeochemical and ecological functioning. This explains why the capability of the WGMP to store OC has not yet been estimated. The present study aims therefore to characterize sedimentation intensity and preferential areas of sediment accumulation in the WGMP to conduct a first estimate of OC burial rates and efficiencies along two cross-shelf bathymetric transects.

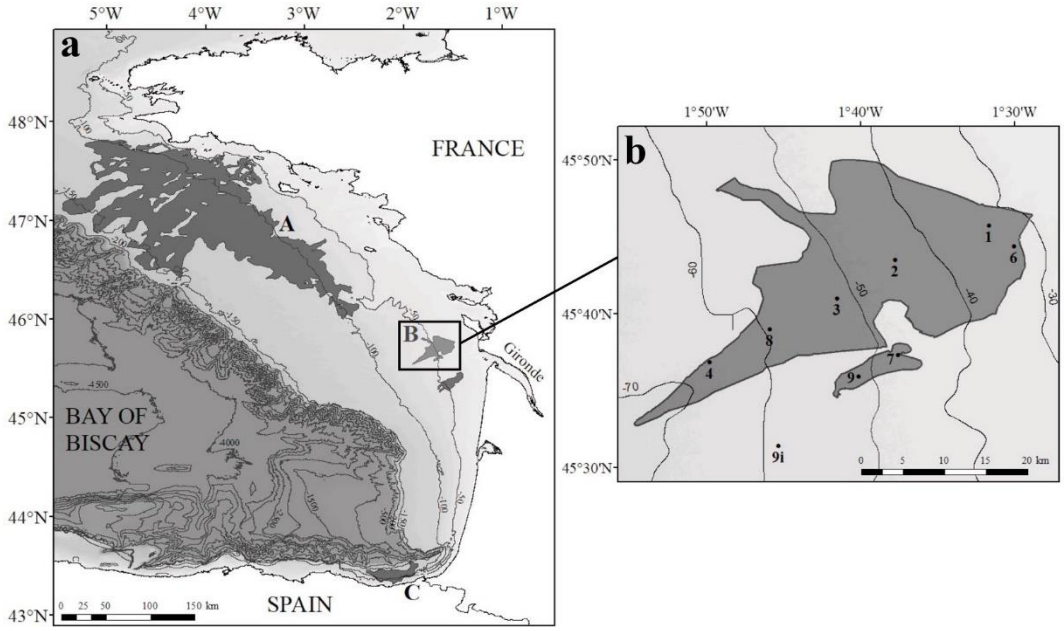

Figure 2.5: (**a**) Map of the Bay of Biscay continental shelf with the locations of mud belts and patches: A - La Grande Vasière, B - The Gironde Mud Patches, and C - The Basque Mud Patch. (**b**) Map of the WGMP showing the location of sampling stations (black circles). The synoptic map of the West Gironde Mud Patch has been determined during the JERICOBENT-5-TH cruise (Gillet and Deflandre, 2018).

2. Material and methods

2.1 Study site

Formed during the Holocene by filling a depression interpreted as a paleo-valley (Lesueur et al., 1996, 2002), the West Gironde Mud Patch is a silty clay sedimentary patch located in the Bay of Biscay, about 40 km seaward of the Gironde estuary mouth. It lies between 30 and 75 m

depth with a surface of about 420 km² (Jouanneau et al., 1989; Lesueur et al., 1991; Massé et al., 2016). The WGMP is influenced by Gironde inputs (Constantin et al., 2018; Jouanneau et al., 1989; Lesueur et al., 2002), which are the highest during river floods (Constantin et al., 2018; Lesueur et al., 2002). On a historical scale, climatic fluctuations (e.g., the "Little Ice Age") and anthropogenic activities like deforestation during the medieval period or estuary management since the XIXth century (e.g. dredging, channel hardening) seem to have modified sediment transport processes and therefore the amount of sediments exported to the shelf (Lesueur et al., 1996, 2002). Sediments are transported from the estuary to the WGMP in a benthic nepheloid layer and believed to be deposited in its deeper part (Weber et al., 1991). During their sedimentation, estuarine particles are mixed with biogenic material (e.g. diatoms) produced in the water column (Weber et al., 1991). In the proximal WGMP, sandy inputs from the adjacent continental shelf can be mixed with silt and clay sediments during storm events (Lesueur et al., 2002; Weber et al., 1991).

2.2 Sampling

The JERICOBENT-1 cruise took place in October - November 2016 on the R/V *Côtes de la Manche* (Deflandre, 2016). Undisturbed sediment cores were collected using a MC6 *Octopus GmbH* multicorer on two transects (**Figure 2.5**). The northern transect includes five stations (1, 2, 3, 8 and 4), and the southern one has four stations (6, 7, 9 and 9i). At each site, three cores were used to characterize sedimentation. A sediment core (core A) was carefully extruded for radioisotope measurements, every 0.5 cm from the top core to 4 cm and every 1 cm below until the core bottom. A second core (core B) was sliced for organic carbon content and sediment surface area measurements every 0.5 cm over the first centimeter, every 1 cm until 5 cm then every 2 cm until 21 cm and every 5 cm below. All the samples were immediately frozen aboard the ship and kept in the freezer until analysis. An additional sediment core was preserved for X-ray imaging (core C), which was performed within a few days after sampling. Due to the thinness of the mud, station 9i was only sampled for radioisotope measurements before repositioning the vessel.

2.3 Physical characteristics of sediments

Radiographical images, which provide a continuous record of sedimentary structures, were performed on a longitudinal section of the preserved sediment core using an X-ray imaging system (SCOPIX). Images recorded were converted in 8 bits to bring out sedimentary structures at high resolution (Lofi and Werber, 2001). Dry bulk density (DBD) was calculated on core A by comparing sediment weight before and after drying at 60°C according to the following expression: $DBD = (1-(V_w/(V_w+V_s))*\rho$ with V_w and V_s respectively volumes of water and

particles in the sample and ρ, particle density (i.e., 2.65 g cm^{-3}). Sediment grain-size was measured on cores A and B using a Malvern Mastersizer 2000 laser diffraction particle size analyzer. The grain-size distributions being unimodal with the exception of three samples within sandy layers (i.e. cores B, St. 1: 0.5-1 cm, 1-1.5 cm; St. 4: 20-22 cm), median grain-size (D50) and sand content were used as grain-size descriptors.

2.4 Radionuclide analysis

The sedimentation framework was determined based on ^{210}Pb. ^{210}Pb ($T_{1/2}$ = 22.3 years) is a naturally-occurring radionuclide continuously delivered by atmospheric fallout and *in situ* production. This ^{210}Pb, readily scavenged by the particulate phase in the water column and deposited at the seabed by sedimentation, is referred to as ^{210}Pb in excess ($^{210}Pb_{xs}$) of that found within sediment due to the decay of its parent isotope, ^{226}Ra. Radionuclide activities (^{210}Pb, ^{226}Ra) were measured using a high-efficiency, broad energy gamma detector equipped with a Cryo-Cycle II (Mirion). The γ detector is calibrated using IAEA certified materials (RGU-1). Errors on activities are based on standard deviation counting statistics. Excess ^{210}Pb activities were calculated by subtracting the activity supported by its parent, ^{226}Ra, from the total ^{210}Pb activity in the sediment. Sediment layers were measured downcore until reaching negligible $^{210}Pb_{xs}$ activities or the bottom of the core. Sediment and mass accumulation rates (SAR and MAR, respectively) were calculated below the mixed layers from the slope of the $^{210}Pb_{xs}$ profiles against depth and cumulative mass, respectively, using the CF:CS (constant flux and constant sedimentation) model.

It must be noted that ^{137}Cs could be also detected during the same counting sessions. The occurrence of ^{137}Cs ($T_{1/2}$ = 30 years), an artificial radionuclide, is primarily the result of the nuclear weapon test fallout in the early 1960s. In coastal sediments, its detection is an indicator of sediment deposited since 1950. ^{137}Cs activities present low to negligible activities in WGMP sediments, and are not presented in this work. Data (radionuclides, grain-size, dry bulk density) are openly available in a public repository that issues datasets with DOIs (Schmidt, 2020).

2.5 Particulate organic carbon

OC content was measured on freeze-dried pre-weighed sediments using a LECO CS 200. In order to remove carbonates before analysis, an aliquot of about 100 mg was acidified with HCl 2 M and dried at 50°C (Cauwet et al., 1990; Etcheber et al., 1999). Sample was then introduced into a furnace where particulate OC combustion produced carbon dioxide which was quantitatively dosed by infrared absorption (Etcheber et al., 1999). The reproducibility of replicated analyses was better than 5%.

Organic carbon contents were normalized to surface area of sediments (SA, expressed in m^2 g^{-1}) to minimize variations strictly due to grain-size changes (Hedges and Keil, 1995; Mayer, 1994a). A subsample of freeze-dried sediments was first homogenized and degassed overnight at 150°C. SA was then assessed using a Gemini® VII Surface Area Analyzer (2390a model; Micromeritics®) by a multi-point BET method (Aller and Blair, 2006; Mayer, 1994a).

2.6 Statistical treatment

The significance of correlations between median grain-size and surface area of the sediments and between surface area and organic carbon content was assessed using a Spearman's rank correlation coefficient. These analyses were run with the software SigmaPlot version 14.

3. Results

3.1 Physical characteristics of sediments and sedimentary structures

Sedimentary environments vary in the WGMP. Indeed, although sediments are mainly silt and clay with a median grain-size of 15 - 20 µm, some peripheral stations (i.e., 1, 6 and 7) have deposits of varying silty and sandy sediments (**Figure 2.6**). At these sites, median grain-size is higher than 20 µm in some layers of higher sand content (> 6%, **Figure 2.6**). Moreover, the base of these layers is characterized by an erosive contact. The two most proximal stations (i.e., 1 and 6) stand out by having a sandy layer on core top. Based on the grain-size profiles and X-ray images, the thickness of this layer varies from 1 to 4 cm at station 1 depending on cores, which indicates a high spatial variability in the proximal area. Below this surface layer, median grain-size is rather constant with depth but finer than the size measured at other sites, with values around 12 and 10 µm at stations 1 and 6, respectively. Interestingly, similar finer sediments are observed at station 9 from a depth of 17 cm. X-ray images also highlight the presence of thin sandy layers at the shallowest stations (i.e., 1, 2, 3, 6, and 7) which become less frequent with increasing depth (**Figure 2.6**).

The dry bulk density increases in depth on cores with a rather constant grain-size (e.g. stations 8 and 4, **Figure 2.6**) as usually observed in interface sediments because of sediment compaction. On the contrary, DBD profiles show variations, usually related to sandy layers, on cores 1, 2, 6, 7 and 9i. These laminae are well preserved in the proximal area (i.e., stations 1 and 6) and at station 7 compared to more distal sites (i.e., 8 and 4) where sediments are homogeneous. The station 9i, at the end of the southern transect is different from the other; it is characterized by a mud deposit of about 14 cm covering a medium sand substratum (**Figure 2.6**).

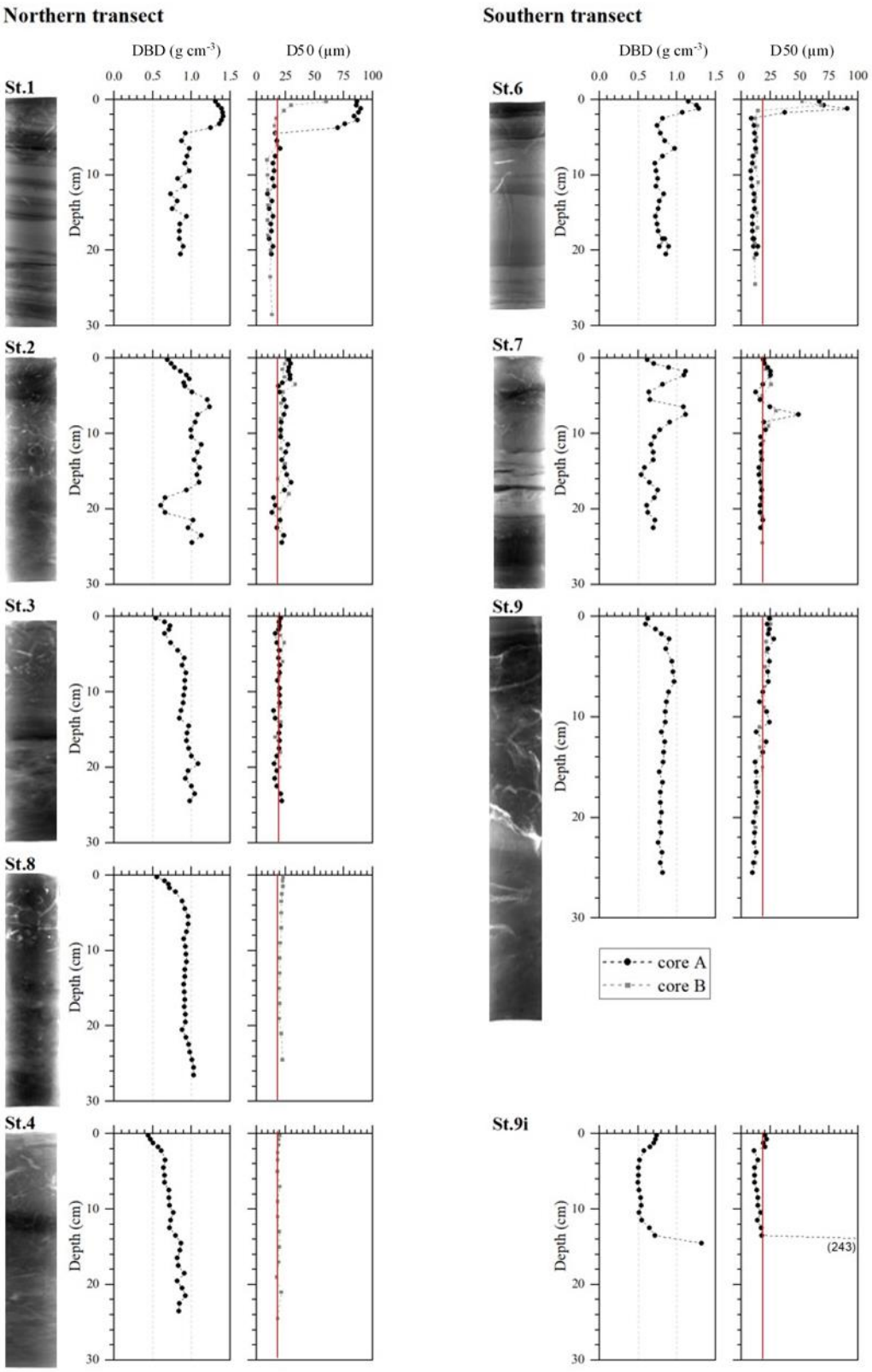

Figure 2.6: Sedimentary structures: X-ray images and profiles of dry bulk density and median grain-size with depth of cores collected along the northern (left) and southern (right) transects. The red line defines the background grain-size (~20 µm), and in some cases higher sand content is observed (>6%).

3.2 ^{210}Pb profiles in interface sediments

Along the two depth transects, surface excess ^{210}Pb ranged between 24 and 111 mBq^{-1}, increasing with depth (**Figure 2.7**). However, the small difference of depth among sites (affecting water column production) cannot account for such low activities at sites 1 and 6. Rather, the lower activities are likely due to dilution by sand. There are three types of $^{210}Pb_{xs}$ profiles. The first group corresponds to the proximal stations 1 and 6. The two most proximal stations present low surface activities, associated with sand, and a rapid activities decrease with depth to reach almost supported levels at about 10 - 15 cm. These profiles reflect rather low mean apparent sediment and mass accumulation rates, about 0.1 - 0.2 cm yr^{-1} and < 200 mg cm^{-2} yr^{-1} (**Table 2.1**). The second group includes stations 7 and 9i along the southern transect, and to a less extent station 2 in the north. The cores present evidence of heterogeneities with depth, as revealed by X-ray images, grain-size and dry bulk density (**Figure 2.6**, *see section 3.1*). Such changes in the sediment are likely to impact the $^{210}Pb_{xs}$ activities and are not related to decay. These deep penetration of $^{210}Pb_{xs}$ with depth in the sediment associated with a low activity decrease could reflect massive deposition events. The last group corresponds to cores of the WGMP outer and deepest area, on the north stations 3, 8, and 4 and on the south station 9. At these stations, $^{210}Pb_{xs}$ profiles present a surface mixed layer, followed by a penetration at depths deeper to 25 - 30 cm. The mixed layer is comprised from 3 - 4 cm at stations 3 and 8 to 8 - 9 cm at station 4, indicating an increase of its thickness with depth. Sediment and mass accumulation rates range from 0.29 to 0.47 cm yr^{-1} and 237 to 438 mg cm^{-2} yr^{-1}. Along the northern transect, the highest SARs and MARs are observed at mid-depths (around 50 m). These results are consistent with the outcome of a first investigation of the WGMP sedimentation, based on less vertically-detailed $^{210}Pb_{xs}$ profiles established on cores sampled in 1995 (Lesueur et al., 2001).

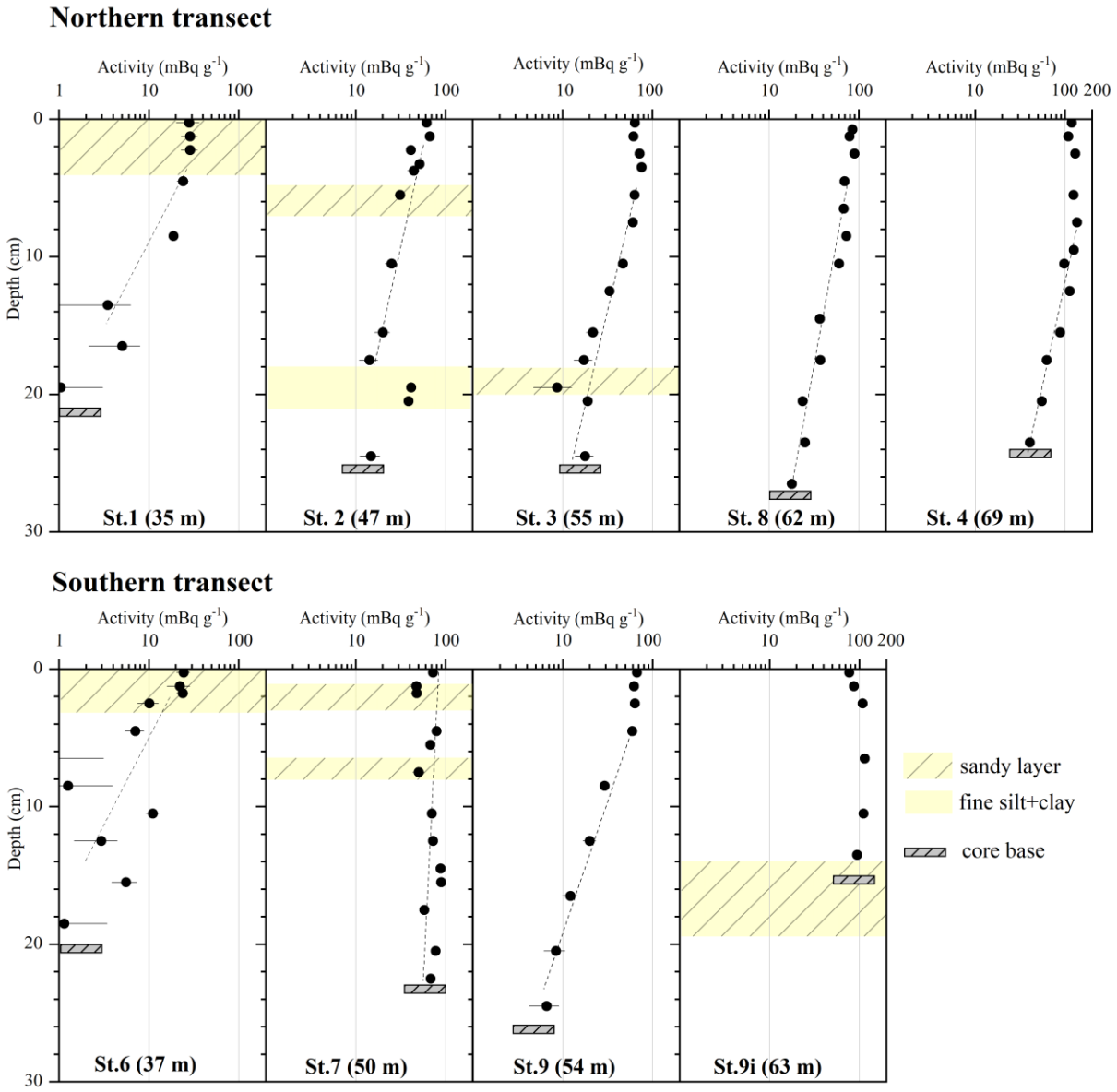

Figure 2.7: Depth profiles of $^{210}Pb_{xs}$ activity for all the sediment cores collected in the West Gironde Mud Patch in fall 2016. Next to the core label, numbers are the water depth at which the cores were collected. Errors bars correspond to 1 SD. The grey rectangle indicates the length of the core.

3.3 Sedimentary organic carbon

Surface organic carbon contents increase seaward from 0.5 to 1.5% (**Table 2.2**, **Figure 2.8**) as previously reported (Massé et al., 2016; Relexans et al., 1992). Depth OC profiles present different patterns depending on sites as reported for $^{210}Pb_{xs}$. Profiles at stations 3 and 8 present the highest values of OC at the core top which remain rather constant in the mixed layer and then decrease in depth. This pattern is different for stations 1, 2, 6 and 7 which show more erratic profiles where the lowest OC values appear to be associated with sandy layers (**Figure 2.8**). Mayer (1994a) demonstrated that the relation between OC content and grain-size is related to the adsorption of organic matter on particles, and this can be reinterpreted in terms of the

surface area of sediments. Typically, larger-sized particles such as sands have a smaller surface area than smaller-sized particles such as clays. Less organic matter is therefore adsorbed on sandy sediments than on muddy ones. These patterns are observed for the whole WGMP with significant correlations between grain-size and SA (p-value<0.01, **Figure 2.9a**) and between SA and OC content (p-value<0.01 for the two slopes, **Figure 2.9c**), indicating that the sediment OC content is at least partly controlled by the grain-size and surface area of particles.

Table 2.1: Mean bottom OC contents, sediment (SAR) and mass (MAR) accumulation rates calculated from $^{210}Pb_{xs}$ profiles and calculated OC burial rates at nine sites of the West Gironde Mud Patch. For stations 1, 6 and 9, the bottom OC values were taken at the base of modern sediments (*see **Figure 2.8***)

Transect	Stations	Lat.	Long.	Depth	Bottom OC	*n* =	SAR	MAR	OC burial rates
		°N	°W	m	%		cm yr^{-1}	mg cm^{-2} yr^{-1}	gC m^{-2} yr^{-1}
North	1	45°45'38"	1°31'41"	35	0.64 ± 0.03[a]	1	0.14 ± 0.08[b]	126 ± 73[b]	8 ± 5[b]
	2	45°43'45"	1°37'57"	47	0.66 ± 0.20	5	0.48 ± 0.09[b]	486 ± 89[b]	32 ± 16[b]
	3	45°40'58"	1°41'30"	55	0.99 ± 0.12	5	0.38 ± 0.04	361 ± 35	36 ± 8
	8	45°38'55"	1°45'48"	62	1.02 ± 0.02	5	0.47 ± 0.05	438 ± 47	45 ± 6
	4	45°36'50"	1°49'47"	69	1.30 ± 0.04	4	0.41 ± 0.07	338 ± 56	44 ± 9
South	6	45°44'22"	1°30'2"	37	0.42 ± 0.27	2	0.22 ± 0.13[b]	172 ± 102[b]	7 ± 9[b]
	7	45°37'17"	1°37'34"	50	1.41 ± 0.19	6	0.97 ± 0.20[c]	648 ± 122[c]	-
	9	45°35'54"	1°40'9"	54	1.17 ± 0.10	3	0.29 ± 0.03	237 ± 22	28 ± 5
	9i	45°31'25"	1°45'20"	63	-	-	2.83[c]	1413[c]	-

[a]analytical incertitude

[b]apparent maximum SAR, MAR and OC burial rates, presence of sandy layers

[c]indicative maximum SAR and MAR – not suitable for calculations

A classical way to minimize OC content variations strictly related to grain-size changes is to normalized OC values to particle SA (Aller and Blair, 2006; Mayer, 1994a, 1994b). An increase of OC/SA ratios in surface sediments is still observed seaward (**Figure 2.8**, **Table 2.2**). The profiles of OC/SA ratio show the highest values on cores top followed by a decrease with depth until reaching a quite constant value at cores bottom. Interestingly, a sharp change of the OC/SA ratio is observed on profiles of stations 1, 6 and 9 under which they are quite constant (**Figure 2.8**), suggesting the presence of two distinct vertical horizons in the sediment columns. These deposits stand out from most sediments of the WGMP by a lower median grain-size and a higher SA (**Figure 2.9**). Besides, we observed during slicing that these sediments were visually different, i.e. darker and much stickier. These changes can be related to a variation of sediments in term of sources or ages. From these observations, we interpret the sedimentary columns of cores 1, 6 and 9 as (1) a top part where modern deposition occurs and (2) a bottom part corresponding to old sediments (**Figure 2.8**). In the rest of the text, the two parts of these cores are respectively qualified as “modern” and “relic” deposits.

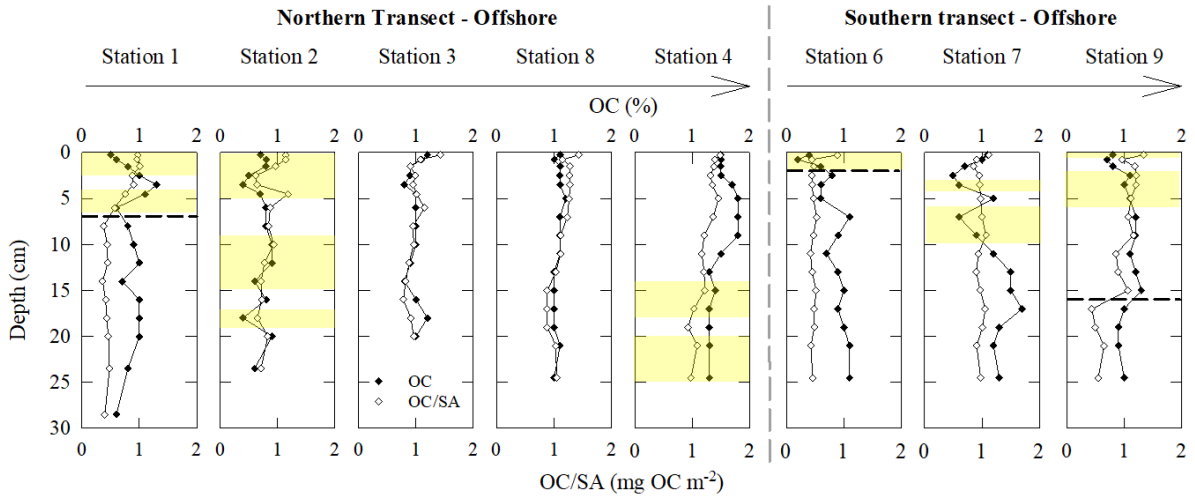

Figure 2.8: Vertical distributions of OC content (%) and OC/SA ratio (mgOC m^{-2}) in sediment cores collected in the West Gironde Mud Patch. The yellow stripes indicate the position of noticeable sandy layers. Dashed lines represent the limit between modern and relic deposits.

The OC/SA ratios at the base of modern sediments vary by more than twice depending on stations and increase with bathymetry with values of 0.5 - 0.6 mgOC m^{-2} at stations 1 and 6, 0.6-0.9 mgOC m^{-2} at station 2, and about 1.0 mgOC m^{-2} at the other (**Figure 2.8**, **Table 2.2**). Relic sediments at stations 1, 6 and 9 show quite similar OC/SA ratios of 0.42 ± 0.04, 0.47 ± 0.04 and 0.53 ± 0.09 mgOC m^{-2}, respectively (**Figure 2.8**).

4. Discussion

The sedimentary functioning of the WGMP was first investigated in the late 80s but its capability to store organic carbon on a multi-decennial scale remains still unknown. A prerequisite of establishing estimates of organic carbon burial rates and efficiencies was then to update the present-day sedimentation rates of the area. The potential factors controlling the spatial changes of OC burial rates and storage efficiencies are then discussed, and the capability of the WGMP to store OC is compared to other continental shelves.

4.1 Sedimentation in the WGMP

Sedimentary structures and sedimentation rates in the WGMP suggest a zonation of sedimentary processes in several areas, which differ by hydrodynamic intensity and the constant or transient nature of deposits. The sedimentation appears to be episodic at stations 1, 6, 7 and 9i. In addition, stations 7 and 9i are characterized by massive but sporadic deposits. The sedimentary sequences of interstratified sand and silt layers observed at the most proximal stations 1 and 6 are hypothesized to be the result of alternations of fine particles inputs during

Table 2.2: Surface and bottom core OC contents (%) and OC/SA ratios (mgOC m^{-2}). *For stations 1, 6 and 9 the bottom values were taken at the base of modern sediments.

Stations (Depth)		OC content (%)		OC/SA (mgOC m^{-2})	
		Surface	Bottom	Surface	Bottom
North	1 (35m)	0.48	0.64*	0.97	0.57*
	2 (47m)	0.70	0.56	1.14	0.71
	3 (55m)	1.15	1.02	1.42	0.96
	8 (62m)	1.08	1.01	1.43	1.04
	4 (69m)	1.53	1.25	1.49	0.98
South	6 (37m)	0.36	0.61*	0.89	0.48*
	7 (50m)	1.09	1.32	1.12	0.98
	9 (54m)	0.84	1.25*	1.34	1.07*

river floods and of sand inputs from the adjacent continental shelf during storms (Jouanneau et al., 1989; Lesueur et al., 2002; Weber et al., 1991). The modern sedimentation in the proximal area is related to the surface sandy layers, silty deposits being merely seasonal and resuspended during high hydrodynamic events (Jouanneau et al., 1989; Lesueur et al., 2001), resulting in the lowest SAR reported for the WGMP (**Table 2.1**). According to literature, relic deposits observed at these sites were dated from 3000 (Jouanneau et al., 1989) to few hundred years B.P. (Lesueur et al., 2002). The deeper and central areas are likely less subjected to hydrodynamic forces (i.e., waves and currents) and thus have higher SAR and MAR (**Figure 2.10**, **Table 2.1**). $^{210}Pb_{xs}$ profiles highlight a rather continuous fine sedimentation on the deepest stations of the northern (i.e., 3, 8 and 4) and southern (i.e., 9) transects. SAR of these sites lie a maximum of 0.47 ± 0.05 cm yr^{-1} on the outer-central part of the area, suggesting the presence of a depocenter (**Table 2.1**). The station 2 seems to correspond to a transition area between the proximal and the distal part of the mud patch. It is defined by a rather constant sedimentation interspersed by episodic sandy inputs. Besides, the difference in laminae preservation among sites indicates a variation of sediment dynamic. Indeed, the laminae preservation at stations 1, 6 and 7 suggests a high frequency of resuspension/deposition events that prevent to observe biological reworking whereas completely bioturbated facies are observed at distal sites (i.e., 8 and 4). From these results, the WGMP can be divided in three sedimentary areas which can be depicted as: (1) a proximal area subjected to a high hydrodynamics with a low sediment deposition, (2) an outer-central part with a rather constant sedimentation, and (3) patches where deposits seem massive but sporadic.

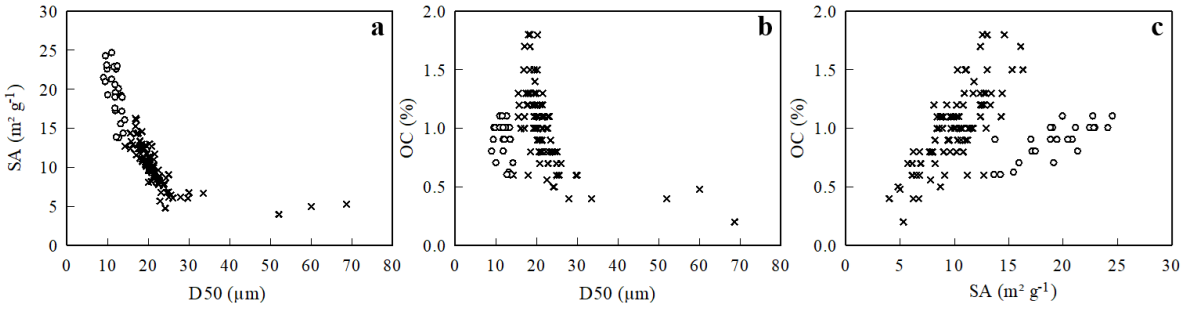

Figure 2.9: SA against median grain-size (**a**), sediment OC content against median grain-size (**b**) and SA (**c**). Cross correspond to all the sediment samples, excluding the relic sediments (white circles; stations 1, 6 and 9).

4.2 Quantitative assessment of OC burial rates in the WGMP

Sedimentation intensity and sediment OC content are known to influence OC storage in sediments (Middelburg, 2019). Therefore, the zonation of sedimentary processes in the WGMP as well as the offshore increase of surface OC content (**Figure 2.10, Table 2.2**) suggest that organic carbon burial rates vary depending on areas.

Mean organic carbon burial rates (BR) were determined by multiplying the sediment mass accumulation rate by the mean sediment OC content at the base of modern deposits (Berner, 1982; Masqué et al., 2002; Mayer, 1994a). The non-steady state of sedimentary processes at stations 7 and 9i, precluded the calculation of OC burial rates at these sites. For stations 1 and 6 where the finest fraction is likely to be resuspended during energetic events, burial rates values must be considered as maximum values for the last decades.

On the northern transect, OC burial rates increase seaward from 8 ± 5 gC m^{-2} yr^{-1} at station 1 to almost constant values of about 44 - 45 gC m^{-2} yr^{-1} at depths deeper than 60 m (**Table 2.2**, **Figure 2.10**). Indeed, despite the highest sediment OC contents at station 4, OC burial rates are equivalent at stations 4 and 8 owing to a higher MAR at station 8 (**Table 2.2**, **Figure 2.10**). This underlines that sediment accumulation intensity is a major controlling factor of organic carbon sequestration on a multi-decennial scale as already reported for other systems like the Rhône delta (Blair and Aller, 2012; Pastor et al., 2011a), the Ganges-Brahmaputra Fan (Blair and Aller, 2012), the Eel shelf (Leithold et al., 2005) and more widely for well-oxygenated marine sediments (Blair and Aller, 2012; Canfield, 1994). However, the fact that OC burial rates are lower at station 2 in spite of an important MAR indicates that burial rates also depend on OC content. It is indeed lower at this station (**Table 2.2**) due to the presence of coarser sediments. Organic carbon content at the base of modern deposits is related to (1) organic carbon inputs which are controlled by the type of sedimentation (sand versus mud) and to (2) the extent of organic matter degradation (Middelburg, 2019) whose quantification is out the

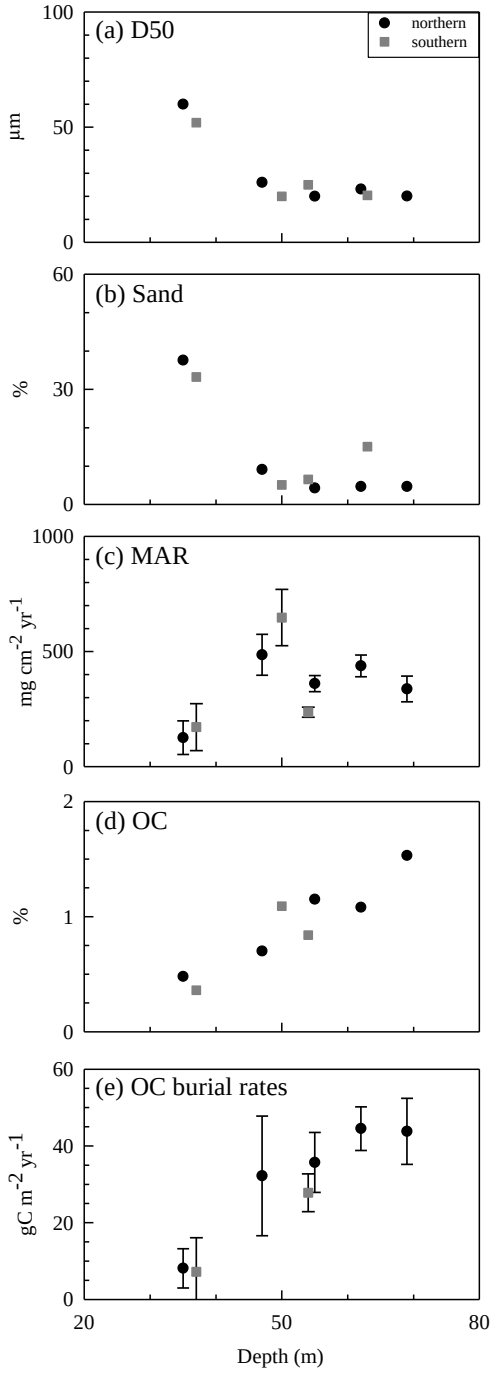

Figure 2.10: Median grain-size (a), sand (b) and organic carbon (d) contents of surface sediments, mass accumulation rates (c) and OC burial rates at multi-decennial scales (e) against water depth of stations along the northern and the southern transects of the West Gironde Mud Patch.

scope of this work. There are three sediment sources to the WGMP: (1) the Gironde estuary whose particles settle mainly in the central and distal areas, (2) a biogenic production in the water column, and (3) the adjacent continental shelf which supplies sand during energetic events (Jouanneau et al., 1989; Lesueur et al., 2002; Weber et al., 1991). On the northern transect, the decrease of surface median grain-size and sand content seaward indicates a decrease of hydrodynamic intensity with depth (**Figure 2.10**). This suggests that the type of

sedimentation, and so organic matter inputs, are controlled by the hydrodynamic intensity. Sand inputs which occur mainly in the proximal area dilute the sedimentary organic matter whereas higher OC contents are observed in the distal area where hydrodynamic intensity is lower. This clearly shows that the amount of OC stored in the WGMP is influenced by both the amount of sedimentary inputs and hydrodynamic intensity.

4.3 Qualitative comparison of OC burial efficiency: direct use of OC content and SA

The OC burial efficiency is typically assessed with the ratio of OC burial rates to inputs (Burdige, 2007). As these inputs were not quantified in this work, this quantitative approach is ruled out. Nevertheless, the OC/SA ratio allows a qualitative assessment of organic carbon burial efficiencies. Blair and Aller (2012) reported that this ratio can be used to define different types of sedimentary environments (**Figure 2.11**). Briefly areas with enhanced organic matter degradation because of frequent sediment remobilization or low sedimentation rates allowing a long oxygen exposure time are characterized by an OC/SA ratio < 0.4 mgOC m^{-2}. On the opposite, an OC/SA > 1.0 mgOC m^{-2} reflects an environment with OC inputs higher than loss through degradation (e.g. upwelling or low-oxygen areas). Intermediate values between 0.4 and 1.0 mgOC m^{-2} are observed on river-suspended particles and non-deltaic shelf. In the West Gironde Mud Patch, values of OC/SA ratios at the base of modern sediments are typical of non-deltaic continental shelves (**Table 2.2**, **Figure 2.11**), namely those which do not receive high sedimentary inputs (Blair and Aller, 2012; Mayer, 1994a). These values indicate stable organic-mineral associations which protect organic matter from microbial decomposition and result in a lower organic matter reactivity and availability for degradation (Blair and Aller, 2012). This can be due to the supply of relatively refractory organic matter from the Gironde (Etcheber et al., 2007) or to the degradation of organic matter in the sediments of the WGMP until reaching an OC/SA value from which the organic carbon is less bioavailable. The increase seaward of OC/SA ratios at the base of modern sediments indicates an increase of OC storage efficiency (**Table 2.2**, **Figure 2.11**). This is consistent with the decrease of hydrodynamic intensity which controls the extent of sediment resuspension. The higher hydrodynamic intensity at proximal sites (i.e., 1 and 6) promotes thus sediment organic matter degradation (Aller, 1998; Aller and Blair, 2006; Yao et al., 2014) and results in a low OC storage efficiency (**Table 2.2**, **Figure 2.11**). Conversely, OC storage efficiencies are the highest in the central and distal WGMP. Interestingly, in spite of higher OC burial rates at stations 8 and 4 than at station 3, the three sites seem to be equally efficient to store OC (**Figure 2.11**). Since the OC contents in surface sediments are higher at station 4, this suggests that organic matter degradation is more efficient at this station than at station 3. The discrepancy between OC burial rates and efficiencies indicates that factors controlling the amount of organic carbon stored in sediments are different

than those controlling the preservation efficiency. Therefore, if hydrodynamic intensity and the amount of sedimentary inputs control the quantity of sequestrated OC, the intensity of organic matter degradation may at least in part influence its storage efficiency. Regarding its efficiency to store OC, station 2 can merely be considered as "intermediate". The OC storage at station 7 appears as efficient as at the distal sites (**Figure 2.11**). This is likely due to the massive sedimentation occurring at this station which limits the degradation of organic matter. However, these deposits may be only transients. Accordingly, it is quite difficult to clearly determine from this study if this storage is efficient on a multi-decennial scale.

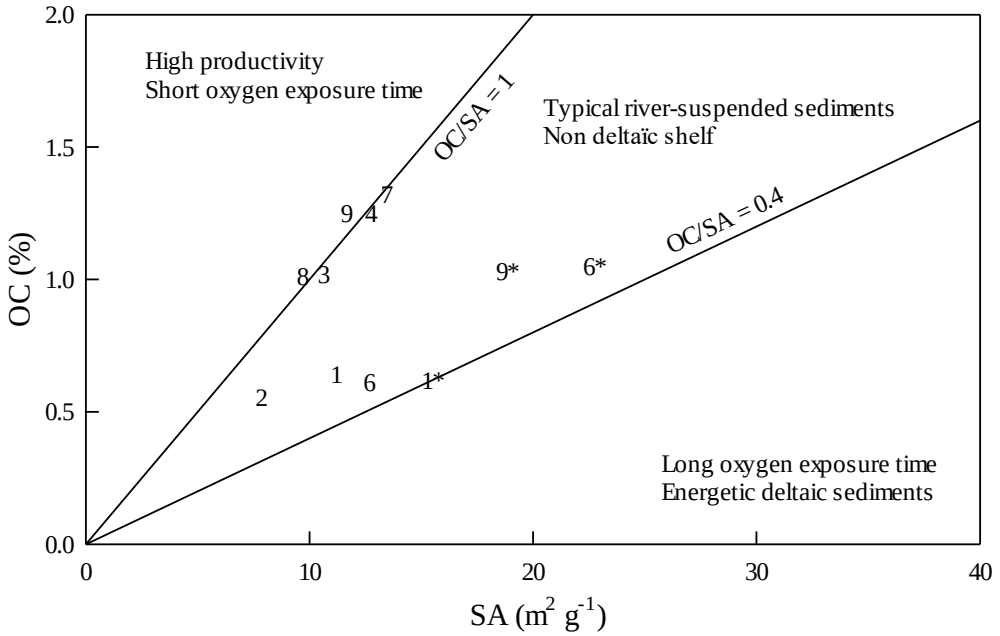

Figure 2.11: Relationship of OC contents (%) against surface area of sediments (SA; $m^2 g^{-1}$) at the base of modern and relic (*) sediments of the West Gironde Mud Patch. Adapted from Blair and Aller (2012).

Relic deposits at stations 1 and 9 present lower OC/SA ratios than modern ones (**Figures 2.8** and **2.11**). A first explanation is to consider a longer degradation duration. However, ratios of modern and relic deposits are equivalents at station 6. Low and constant OC/SA ratios (**Figure 2.8**) indicate that organic matter has been extensively degraded and reached an OC refractory background (Mayer, 1994b, 1994a). This important degradation observed at stations 1 and 6 is likely related to both degradation duration of organic matter and intense hydrodynamics in the inner WGMP.

The use of OC/SA ratios confirms a zonation of sedimentary processes in the WGMP as previously argued on the base of sedimentation characteristics (description, intensity). This could be described in terms of organic carbon storage as: (1) a proximal part characterized by a decimeter-thick modern layer with a relatively low OC storage efficiency overlying relic deposits, (2) a distal area which appears as the only efficient zone for OC storage on a multi-

decennial scale, and (3) patches represented by station 7 where apparent efficient OC storage is likely related to massive sedimentation events. These qualitative estimates of OC burial efficiencies confirm that the OC sequestration in the WGMP depends in part on the hydrodynamic intensity which controls sedimentation and resuspension processes. However, other factors like the intensity of organic matter degradation seem to influence OC storage efficiency in the central and distal WGMP.

Table 2.3: Mass accumulation rates and OC burial rates in sediments of (1) the West Gironde Mud Patch (this study) (2) the Bay of Biscay (Mouret et al., 2010), (3) the Goban Spur (Celtic margin, Van Weering et al., 1998), (4) the Iberian Margin (Van Weering et al., 2002), (5) the Gulf of Lions shelf (Accornero et al., 2003) and of (6) the Amazon deltaic shelf (Aller et al., 1996; Kuehl et al., 1986), the Bohai and Yellow Seas (Hu et al., 2016), the Zhejiang-Fujian Mud Zone (East China Sea, Sun et al., 2020), the inner Louisiana shelf (Gordon et al., 2001). The most proximal sites of the WGMP (i.e., 1 and 6) are not considered. *Average values of organic carbon burial rates.

Location	Depth	MAR	OC burial rates	References
	m	mg cm^{-2} yr^{-1}	gC m^{-2} yr^{-1}	
WGMP (Bay of Biscay)	47 - 69	237 - 486	28 - 45	This study
Bay of Biscay	550	78	7.32	Mouret et al. (2010)
Bay of Biscay	1000	36	2.52	
Bay of Biscay	1250	44	2.40	
Bay of Biscay	1500	7	0.45	
Bay of Biscay	2000	14	0.96	
Goban Spur	208	<5.8	> 0.16	Van Weering et al. (1998)
Iberian Margin	104	204.2	34.30	Van Weering et al. (2002)
Iberian Margin	123	208.9	9.00	
Iberian Margin	199	150.1	7.09	
Iberian Margin	223	157.1	5.02	
Iberian Margin	343	63.4	3.77	
Gulf of Lions	87	230	19.0	Accornero et al. (2003)
Amazon deltaic shelf	9 - 53	100 - 6900	58.3*	Aller et al. (1996), Kuehl et al. (1986)
Bohai and Yellow Seas	0 - 400	< 100 - 7000	15.3*	Hu et al. (2016)
East China Sea	45.4	200 - 700	41.2*	Sun et al. (2020)
Louisiana shelf	4 - 23	120 - 450	22.7*	Gordon et al. (2001)

4.4 Comparison with other continental shelves

On the Northeast Atlantic margin, numerous sedimentological and biogeochemical studies have been conducted (Anschutz and Chaillou, 2009; Charbonnier et al., 2019; Herman et al., 2001; Jouanneau et al., 2002; Mouret et al., 2010; Schmidt et al., 2009; van Weering et al., 2002, 1998) but only few of them have focused on the OC sequestration in sediments (Epping et al., 2002; Mouret et al., 2010; van Weering et al., 2002, 1998). Studies conducted on other

areas of the Bay of Biscay margin (Mouret et al., 2010) and on the Celtic (van Weering et al., 1998) and Iberian margins (van Weering et al., 2002), allow a comparison with organic carbon burial rates obtained in the WGMP (this work) (**Table 2.3**). There is a wide range of OC burial rates from < 0.5 gC m^{-2} yr^{-1} on the Celtic margin (van Weering et al., 1998) to 34.3 gC m^{-2} yr^{-1} on the Iberian shelf (van Weering et al., 2002). Locally, on the Bay of Biscay margin, organic carbon burial rates decrease with increasing depth, with the highest values observed for the WGMP (**Table 2.3**). These high OC burial rates are most likely due to the proximity of its main sediment source (i.e., the Gironde). Deeper on the slope, the lower organic carbon burial rates are associated with lower sedimentation rates (**Table 2.3**, Mouret et al., 2010). Besides, studies carried out on the Iberian shelf and the Celtic margin (i.e., Epping et al., 2002; van Weering et al., 2002, 1998) concluded that, as for the WGMP, variations of OC burial rates are related to variations of sedimentation intensity. These comparisons highlight that the WGMP is an area of the Northeast Atlantic margin which stores relatively high amount of organic carbon on a multi-decennial scale.

At a global oceanic scale, Blair and Aller (2012) reported and compared organic carbon burial efficiencies of many RiOMars. However quantitative estimates of OC burial rates on continental shelves, where fine sedimentation occurs, are mainly related to systems under the influence of large rivers, with average values from 15.3 gC m^{-2} yr^{-1} in the Bohai and Yellow Seas (Hu et al., 2016) to 58.3 gC m^{-2} yr^{-1} in the Amazon deltaic shelf (Aller et al., 1996) (**Table 2.3**). In addition, the spatial extent of these RiOMars (i.e., at least several thousand square kilometers) makes them important areas for organic carbon storage (Aller et al., 1996; Gordon et al., 2001; Hu et al., 2016; Qiao et al., 2017; Sun et al., 2020). Although the WGMP is one with the highest OC burial rates among the Northeast Atlantic margin systems, it cannot be considered as a major sink of organic carbon on a global oceanic scale due to its small spatial extent (i.e., 420 km²).

5. Conclusion

This study aimed to assess a first estimate of organic carbon sequestration in the West Gironde Mud Patch sediments. The amount of stored OC increases seaward with a maximum value of 45 gC m^{-2} yr^{-1}. Beyond the quantification, sedimentary structures and $^{210}Pb_{xs}$ profiles as well as a qualitative comparison of the capability of each site to store OC allow to divide the WGMP in several sedimentary sub-environments: (1) a proximal area where modern deposits are a decimeter-thick layer with a relatively low OC storage efficiency, (2) a distal part with a relatively efficient OC storage and (3) patches where OC storage seems efficient, at least temporarily.

The amount of OC sequestrated in sediments on a multi-decennial scale is mainly related to the amount of sedimentary inputs and to hydrodynamic conditions which control sedimentation intensity and nature (i.e., mud versus sand inputs). However other factors like the intensity of organic matter degradation seem to influence the efficiency of OC preservation in sediments in the central and distal areas. Further studies are therefore need to define and quantify processes which can influence this preservation in the West Gironde Mud Patch on a multi-decennial scale but also on other time scales (seasonal, inter-annual, multi-secular). At the scale of the Northeast Atlantic margin, the West Gironde Mud Patch appears efficient in storing organic carbon but its contribution to the OC storage at larger scale remains quite low because of its small surface area. Nevertheless, considering all mud patches of the Bay of Biscay continental shelf (e.g., La Grande Vasière, the Basque Mud Patch), the OC storage can be potentially significant at the North-Atlantic scale. Accordingly, it appears necessary to led further studies on these areas to define their capabilities to store organic carbon.

Declaration of competing interest

The authors declare that they have no competing financial interests or personal relationships that could have appeared to influence the work reported in this paper.

Acknowledgements

We sincerely acknowledge the captains and crews of the R/V “Côtes de la Manche” (CNRS-INSU) for their great help during the JERICOBENT-1 cruise. We also thank Rémy Synais for his work on sampling and analyses as well as François Dano for the preparation of an updated map of the WGMP during his Master 2 dissertation. This work was supported by: (1) the JERICO-NEXT project (European Union's Horizon 2020 Research and Innovation program under grant agreement no. 654410), (2) the VOG project (national program Interface LEFE-EC2CO). The cruise was funded by the French Oceanographic Fleet (DOI: 10.17600/16010400). A doctoral fellowship was provided to N. Dubosq by the french Ministry of Higher Education, Research and Innovation. We are thankful to the French Nouvelle Aquitaine Research Council (E3A Project) for co-funding both the low-background gamma detector and the microelectrode system equipped with a camera. We also thank the UMR 5805 EPOC for co-funding the Surface Area Analyzer.

Partie C - Variations spatiotemporelles des descripteurs de la matière organique et de la macrofaune benthique

Les études sédimentologiques menées depuis les années 1980 ont permis de caractériser la structuration spatiale des processus sédimentaires dans la Vasière Ouest Gironde (VOG). De leur côté, les études biogéochimiques et écologiques s'étant intéressées à la VOG ont mis en évidence des variations spatiales des descripteurs de la matière organique du sédiment de surface et de la macrofaune benthique. Cependant, le nombre de stations échantillonnées était insuffisant pour clairement définir la structuration spatiale de ces descripteurs (*voir Chapitre 1*). De plus, leur dynamique temporelle n'avait pas été caractérisée. Etant donné que ces paramètres peuvent influencer les processus biogéochimiques ayant lieu dans les sédiments, il était nécessaire de commencer par clairement définir leur dynamique spatiotemporelle. La structuration spatiale des caractéristiques des sédiments de surface et de l'activité de la macrofaune benthique a été définie par Lamarque et al. (2021) à partir des données acquises lors de la « mission d'échantillonnage synoptique » de juin 2018. La dynamique spatiotemporelle des descripteurs de la matière organique et des communautés de la macrofaune benthique a été caractérisée par Lamarque et al. (2022) à partir des données acquises entre 2016 et 2018. Une synthèse de ces travaux est présentée et complétée par les données acquises en avril et octobre 2021.

1. Structuration spatiale des caractéristiques du sédiment de surface et de l'activité de la macrofaune benthique

Cet encart est une synthèse des travaux de Lamarque et al. (2021). L'article est disponible en ***Annexe 1****.*

Les résultats obtenus dans le cadre de la mission d'échantillonnage synoptique ont permis de diviser la VOG en une zone proximale et une zone distale avec une limite aux alentours de 42.5 m de profondeur. La zone proximale est caractérisée par (1) un sédiment de surface plus grossier et moins riche en matière organique et par (2) un faible nombre de traces d'activités biologiques. Au contraire, les sédiments de la zone distale sont plus fins, plus riches en matière organique et plus bioturbés. Cependant, la labilité de la matière organique est plus faible qu'en zone proximale. Ces travaux ont également mis évidence plusieurs gradients bathymétriques au sein de la zone distale dont (1) une augmentation des teneurs en matière organique du sédiment de surface, (2) une diminution de la labilité de la matière organique végétale du sédiment de surface et (3) une augmentation de la bioturbation avec la profondeur. L'augmentation des teneurs en matière organique du sédiment de surface avec la profondeur était indépendante des variations granulométriques. Par conséquent, un tri par densité associé à des cycles de resuspension – dépôt a été suggéré pour expliquer cette augmentation. Etant donné que dans les zones côtières les processus de resuspension et l'intensité de la bioturbation sont influencés par l'hydrodynamisme et le chalutage de fond, l'influence de ces deux forçages sur la structuration spatiale des caractéristiques du sédiment de surface et l'activité de la macrofaune benthique a été déterminée. Les résultats de différentes approches statistiques ont montré que l'hydrodynamisme est le principal facteur contrôlant la structuration spatiale des caractéristiques du sédiment de surface et de l'activité de la macrofaune benthique dans la VOG.

2. Dynamique spatiale et temporelle des caractéristiques du sédiment de surface et de la composition de la macrofaune benthique

*Cet encart est une synthèse des travaux de Lamarque et al. (2022) qui incluent les données acquises lors des missions saisonnières réalisées entre 2016 et 2018. L'article est disponible en **Annexe 2**.*

Les résultats obtenus sur la période 2016 – 2018 ont confirmé la différence significative entre la partie proximale (représentée par la station 1) et distale de la VOG. Le sédiment de surface de la station 1 était plus grossier, moins riche en matière organique et en pigments que celui des stations distales (**Figure 2.12** ; **Table 2.4**). Cependant, la labilité de la matière organique, estimée avec le ratio EHAA/THAA, était plus élevée qu'en zone distale. Ces travaux ont également confirmé l'augmentation des teneurs en matière organique et la diminution de sa labilité avec la profondeur. Les seules variations saisonnières marquées des caractéristiques de la matière organique du sédiment de surface ont été observées en avril 2018. A la station 1, les teneurs en carbone organique étaient plus élevées qu'aux autres saisons en raison de la présence de sédiments superficiels plus fins à cette période. En zone distale, les teneurs en pigments étaient 2 à 4 fois plus élevées qu'aux autres saisons (**Figure 2.12** ; **Table 2.4**). Cela est directement lié au fait que la campagne d'échantillonnage ait été réalisée au cours de l'efflorescence printanière. Un modèle linéaire basé sur les distances a montré que les variations spatiales des caractéristiques du sédiment de surface sont principalement contrôlées par l'hydrodynamisme. Au contraire, leurs variations saisonnières étaient mieux corrélées aux débits de la Gironde intégrés sur 100 jours.

Les abondances de la macrofaune benthique étaient plus élevées à la station 1 et diminuaient vers le large, excepté en avril 2018 en raison de la forte abondance d'un taxon en zone distale. Au contraire, la richesse spécifique et la biomasse ne présentaient pas de tendances spatiotemporelles claires. Des analyses statistiques ont montré que la structuration spatiale de la composition de la macrofaune benthique était liée à une diminution de l'intensité de l'hydrodynamisme vers le large alors que ses variations saisonnières étaient mieux corrélées aux débits de la Gironde intégrés sur 100 jours.

Les caractéristiques du sédiment de surface (0 – 0.5 cm) prélevé à six stations en avril et octobre 2021 présentaient les mêmes tendances spatiales que celles observées sur la période 2016 – 2018 (**Figure 2.12** ; **Table 2.4**). Lors des missions océanographiques réalisées en 2021,

le transect côte-large a été complété par l'échantillonnage de la station 10, localisée en zone proximale. A cette station, le sédiment de surface était plus fin (D50 ~ 28 - 31 µm) qu'à la station 1 (D50 ~ 67 – 68 µm). Cependant, les teneurs et charges (i.e., OC/SA ratio) en carbone organique étaient proches de celles mesurées à la station 1 et plus faibles qu'aux stations de la zone distale. En octobre 2021, la labilité de la matière organique mesurée à la station 10 (EHAA/THAA ~ 41 ± 13%) était beaucoup plus élevée qu'aux autres stations (20 – 27%). Contrairement à ce qui avait été observé en avril 2018, les teneurs en pigments du sédiment de surface mesurées en avril 2021 n'étaient pas plus élevées qu'aux autres saisons (**Figure 2.12** ; **Table 2.4**). Cela est lié au fait que contrairement à la mission d'avril 2018, celle de 2021 n'a pas été réalisée lors de l'efflorescence printanière (Dubosq et al., 2022 ; *Partie A de ce chapitre*).

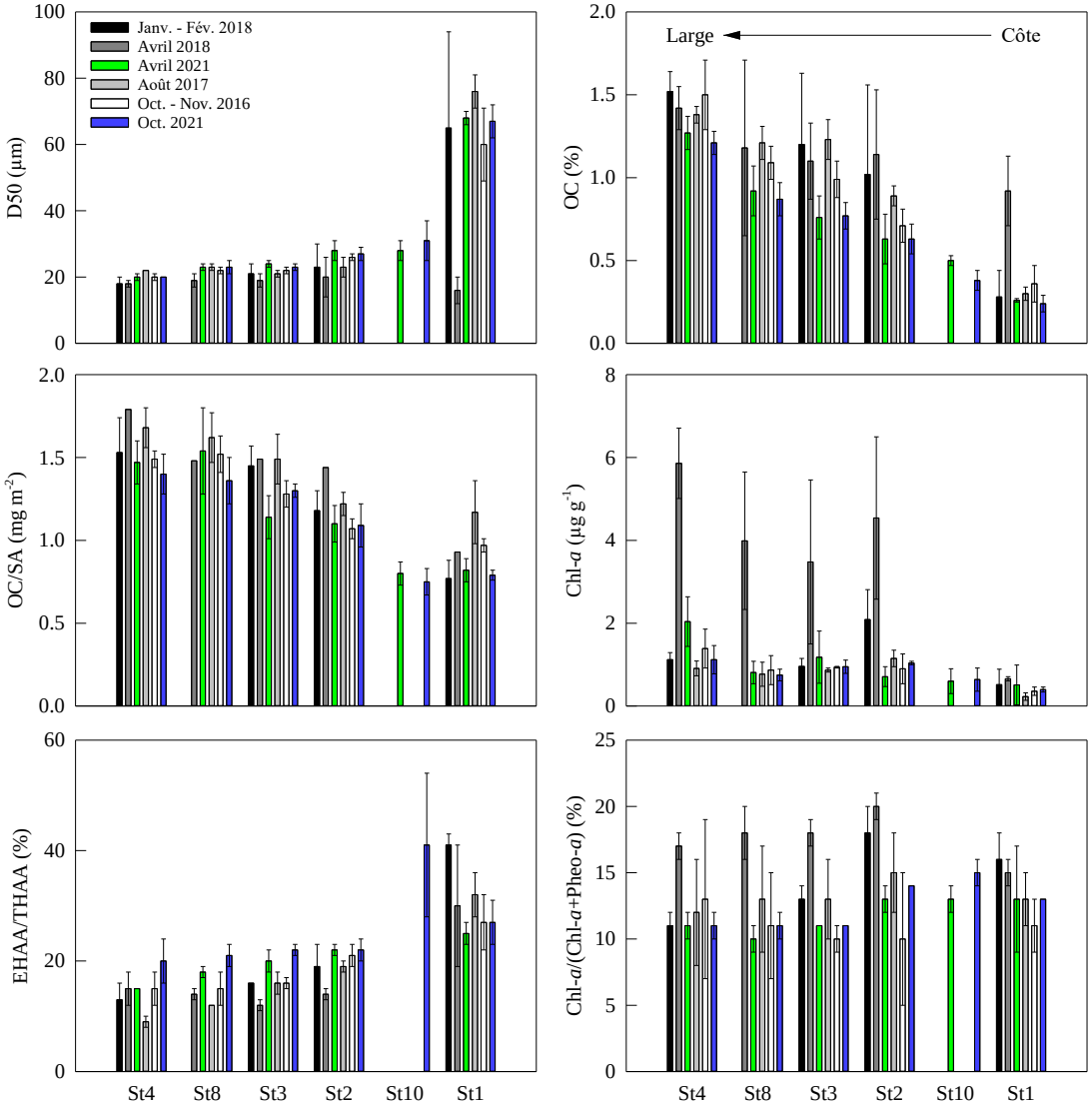

Figure 2.12 : Variations spatiales et saisonnières du D50 et des caractéristiques de la matière organique (i.e., OC, OC/SA, Chl-*a*, EHAA/THAA et Chl-*a*/(Chl-*a*+Pheo-*a*)) du sédiment de surface (0 – 0.5 cm) échantillonné dans la VOG entre 2016 et 2021, de la côte (station 1) vers le large (station 4). La figure a été réalisée à partir des données acquises entre 2016 et 2018 publiées dans Lamarque et al. (2022) et complétée par les mesures réalisées en avril (vert) et octobre (bleu) 2021.

Table 2.4 : Variations spatiales et saisonnières du D50 et des caractéristiques de la matière organique du sédiment de surface (0 – 0.5 cm) échantillonné dans la VOG au cours de six missions océanographiques réalisées entre 2016 et 2021. Les données acquises entre 2016 et 2018 sont publiées dans Lamarque et al. (2022).

Station	D50	OC	*n*=	THAA	EHAA	EHAA/THAA	*n*=	Chl-*a*	Pheo-*a*	Chl-*a*/(Chl-*a* + Pheo-*a*)	*n*=
	µm	%		µg g^{-1}	µg g^{-1}	%		µg g^{-1}	µg g^{-1}	%	
Octobre - Novembre 2016											
St1	60 ± 11	0.36 ± 0.11	4	0.69 ± 0.06	0.18 ± 0.05	27 ± 5	3	0.36 ± 0.10	2.95 ± 0.27	11 ± 2	3
St2	26 ± 1	0.71 ± 0.10	4	2.13 ± 0.13	0.44 ± 0.06	21 ± 2	3	0.90 ± 0.36	8.27 ± 1.05	10 ± 5	3
St3	22 ± 1	0.99 ± 0.11	5	2.77 ± 0.10	0.45 ± 0.02	16 ± 1	3	0.94 ± 0.02	8.39 ± 1.11	10 ± 1	3
St8	22 ± 1	1.09 ± 0.11	5	3.60 ± 0.23	0.53 ± 0.07	15 ± 3	3	0.87 ± 0.35	6.75 ± 0.37	11 ± 4	3
St4	20 ± 1	1.50 ± 0.21	5	4.49 ± 0.27	0.65 ± 0.12	15 ± 3	3	1.39 ± 0.47	9.59 ± 1.69	13 ± 6	3
Août 2017											
St1	76 ± 5	0.30 ± 0.04	6	0.51 ± 0.18	0.16 ± 0.04	32 ± 4	3	0.23 ± 0.09	1.46 ± 0.46	13 ± 2	3
St2	23 ± 3	0.89 ± 0.06	5	3.23 ± 0.29	0.61 ± 0.02	19 ± 1	3	1.15 ± 0.20	6.65 ± 0.88	15 ± 3	3
St3	21 ± 1	1.23 ± 0.12	5	3.97 ± 0.07	0.66 ± 0.10	16 ± 2	3	0.87 ± 0.05	6.07 ± 1.64	13 ± 3	3
St8	23 ± 1	1.21 ± 0.10	5	3.55 ± 0.10	0.44 ± 0.01	12 ± 0	3	0.77 ± 0.29	5.25 ± 0.57	13 ± 4	3
St4	22 ± 0	1.38 ± 0.05	5	4.10 ± 0.19	0.38 ± 0.02	9 ± 1	3	0.91 ± 0.18	6.90 ± 1.28	12 ± 4	3
Janvier - Février 2018											
St1	65 ± 29	0.28 ± 0.16	5	0.72 ± 0.32	0.29 ± 0.12	41 ± 2	3	0.52 ± 0.37	2.53 ± 1.58	16 ± 2	3
St2	23 ± 7	1.02 ± 0.54	5	3.10 ± 0.16	0.59 ± 0.14	19 ± 4	3	2.09 ± 0.72	9.61 ± 2.47	18 ± 2	3
St3	21 ± 3	1.20 ± 0.43	5	2.87 ± 0.43	0.45 ± 0.06	16 ± 0	3	0.96 ± 0.19	6.22 ± 0.63	13 ± 1	3
St4	18 ± 2	1.52 ± 0.12	5	4.32 ± 0.43	0.57 ± 0.07	13 ± 3	2	1.12 ± 0.17	9.51 ± 1.86	11 ± 1	3
Avril - Mai 2018											
St1	16 ± 4	0.92 ± 0.21	5	0.98 ± 0.51	0.26 ± 0.04	30 ± 11	3	0.66 ± 0.05	3.67 ± 0.38	15 ± 1	3
St2	20 ± 6	1.14 ± 0.39	5	3.94 ± 0.67	0.56 ± 0.07	14 ± 1	3	4.54 ± 1.96	18.16 ± 8.17	20 ± 1	3
St3	19 ± 2	1.10 ± 0.23	5	4.65 ± 1.44	0.56 ± 0.11	12 ± 1	3	3.48 ± 1.98	15.57 ± 8.18	18 ± 1	3
St8	19 ± 2	1.18 ± 0.53	5	4.36 ± 0.26	0.61 ± 0.03	14 ± 1	3	3.99 ± 1.66	18.37 ± 6.26	18 ± 2	3
St4	18 ± 1	1.42 ± 0.13	5	4.65 ± 0.49	0.72 ± 0.20	15 ± 3	3	5.86 ± 0.85	29.35 ± 2.83	17 ± 1	3
Avril 2021											
St1	68 ± 2	0.26 ± 0.01	5	1.06 ± 0.55	0.27 ± 0.16	25 ± 2	3	0.51 ± 0.48	3.02 ± 2.22	13 ± 4	3
St10	28 ± 3	0.50 ± 0.03	5	-	-	-	-	0.60 ± 0.30	3.92 ± 1.86	13 ± 1	3
St2	28 ± 3	0.63 ± 0.15	5	1.45 ± 0.21	0.32 ± 0.06	22 ± 1	2	0.71 ± 0.24	4.85 ± 1.92	13 ± 1	3
St3	24 ± 1	0.76 ± 0.13	5	2.36 ± 0.19	0.47 ± 0.01	20 ± 2	3	1.18 ± 0.63	9.10 ± 4.65	11 ± 0	3
St8	23 ± 1	0.92 ± 0.15	5	3.19 ± 0.84	0.57 ± 0.13	18 ± 1	3	0.81 ± 0.27	7.28 ± 2.72	10 ± 1	3
St4	20 ± 1	1.27 ± 0.10	5	4.74 ± 0.26	0.72 ± 0.02	15 ± 0	3	2.04 ± 0.60	17.19 ± 5.35	11 ± 1	3
Octobre 2021											
St1	67 ± 5	0.24 ± 0.05	5	0.86 ± 0.17	0.23 ± 0.01	27 ± 4	3	0.40 ± 0.06	2.61 ± 0.34	13 ± 0	2
St10	31 ± 6	0.38 ± 0.06	5	1.01 ± 0.53	0.37 ± 0.09	41 ± 13	3	0.64 ± 0.28	3.62 ± 1.24	15 ± 1	3
St2	27 ± 2	0.63 ± 0.09	5	2.08 ± 0.18	0.46 ± 0.0	22 ± 2	2	1.04 ± 0.04	6.46 ± 0.33	14 ± 0	3
St3	23 ± 1	0.77 ± 0.08	5	2.88 ± 0.30	0.63 ± 0.08	22 ± 1	3	0.95 ± 0.16	7.91 ± 1.46	11 ± 0	3
St8	23 ± 2	0.87 ± 0.10	5	2.26 ± 0.13	0.48 ± 0.04	21 ± 2	3	0.75 ± 0.14	6.13 ± 1.05	11 ± 1	3
St4	20 ± 0	1.21 ± 0.07	5	3.49 ± 0.38	0.68 ± 0.07	20 ± 4	3	1.12 ± 0.34	9.45 ± 3.49	11 ± 1	2

Points clés du Chapitre 2

- La Vasière Ouest Gironde est soumise à des désoxygénations saisonnières des eaux de fond.
- Elle peut être subdivisée en une zone proximale et une zone distale avec une limite aux alentours de 42.5 m de profondeur.
- L'hydrodynamisme contrôle la structuration spatiale (1) des processus sédimentaires et (2) des caractéristiques du sédiment de surface.
- Dans la zone proximale, la sédimentation moderne est restreinte à une couche superficielle plus grossière surmontant des sédiments reliques plus fins.
- Dans la zone distale, la sédimentation de particules fines est plutôt continue.
- Les caractéristiques du sédiment de surface varient avec la profondeur :
    - La taille médiane des sédiments diminue avec la profondeur.
    - La quantité de matière organique augmente vers le large mais sa labilité diminue.
- A l'échelle du golfe de Gascogne, la Vasière Ouest Gironde apparait plutôt efficace pour stocker le carbone organique à l'échelle pluri-décennale.
- Le stockage du carbone organique dans la Vasière Ouest Gironde à l'échelle pluri-décennale est contrôlé par l'hydrodynamisme et les apports sédimentaires.

Chapitre 3 :

Structuration et fonctionnement biogéochimique de la Vasière Ouest Gironde à l'échelle saisonnière et implications pour l'écosystème

Dubosq N.[1], Deflandre B. [1], Rigaud S. [2], Pellequer E. [1], Lamarque B. [1], Grémare A. [1], Danilo M. [1], Poirier D. [1], Cordier M-A. [3], Perello M-C. [1], Labourdette N. [3], Tenório M.[4], S. Schmidt[3]

[1] Univ. Bordeaux, CNRS, Bordeaux INP, EPOC, UMR 5805, F-33600 Pessac, France

[2] Université de Nîmes, EA 7352 CHROME, F-30021 Nîmes, France

[3] CNRS, Univ. Bordeaux, Bordeaux INP, EPOC, UMR 5805, F-33600 Pessac, France

[4] Departamento de Biologia Marinha, Instituto de Biologia, Universidade Federal do Rio de Janeiro, Rio de Janeiro CEP 21941-902, Brazil

Chapitre écrit sous une forme proche d'un article – *A soumettre*

1. Introduction

The aim of this chapter is to define the structuration and biogeochemical functioning of the West Gironde Mud Patch (WGMP) on seasonal scales. Early diagenesis processes occurring in the WGMP are first characterized and compared with those of other energetic River-dominated Ocean Margins (RiOMars). The capability of the WGMP to recycle organic carbon and the relative importance of the different remineralization processes are then discussed. At last, mass balances are performed to assess the contribution of the WGMP benthic compartment (1) to seasonal bottom water deoxygenations and (2) to nutrient inputs to the water column relative to the Gironde estuary.

This chapter is based on seasonal samplings and measurements performed on the northern transect of the WGMP in January – February 2018, April 2018 and 2021, August 2017, October 2016 and 2021 (*see Chapter 1, **Figure 1.4A***). During these cruises, from 4 to 6 stations located along a cross-shelf bathymetric transect were investigated. Details on sampling procedures are developed in the section 2.2 of the Chapter 1.

2. Material and methods

2.1 Pore waters analyses

Pore waters samples were analyzed for nitrite, nitrate and ammonium using a QuAAtro continuous segmented flow analyzer (Aminot and Kérouel, 2007). The reproducibility of measurements (better than 2%) was assessed using certified standards (*MOOS*, *NRCC*). Dissolved iron (Stookey, 1970), manganese (Charbonnier and Anschutz, 2019) and sulfides (Fonselius et al., 1999) were measured by spectrophotometry. Concentrations of major dissolved compounds (i.e., SO_4^{2-}, Cl^-, K^+, Na^+, Mg^{2+}, Ca^{2+}) were assessed by ionic chromatography (Dionex Corporation, 1986). Dissolved inorganic carbon (DIC) was measured by flow injection analysis according to Hall and Aller (1992). Concentrations of dissolved organic carbon (DOC) were measured using a high-temperature catalytic oxidation method with a Shimadzu TOC-L analyzer (Halewood et al., 2022). The reproducibility of these analyses was better than 5%. Dissolved arsenic and cobalt concentrations were analyzed in triplicate using an ICP-MS *Icap TQ* (Thermo Scientific^{TM}). Samples whose the volume was too small (i.e., < 6 mL) were first diluted with HNO_3 0.5%. pH was measured using a micro-probe just after recovering pore waters by centrifugation. Methane concentrations were measured on sediments sampled in October 2016 and August 2017 using a HP 5890A gas chromatograph. Owing to methane concentrations at a low level (< 1.2 µM) and relatively high sulfate concentrations at

core bottoms (> 20 mM), there was no more samplings for methane during the following cruises.

2.2 Solid phase analyses

The redox potential of sediments was measured onboard in October 2021 using a WTW® Multi 3630 IDS equipped with an oxidation-reduction potential sensor (ORP-T 900-P, ± 0.2 mV). Porosity of sediments was determined by comparing sediment weight before and after freeze-drying by assuming a particles density of 2.65 g cm^{-3}. Porosity was corrected for salt content using bottom water salinities (Burdige, 2006) measured using autonomous sensors (i.e., STPS and WiMo Plus multiparameter probe ; *NKE Instrumentation*). The following analyses were performed on freeze-dried sediments, excepted pigments and particulate sulfides measurements. Sediment grain-size was measured using a Malvern Mastersizer 2000 laser diffraction particle size analyzer. Surface area (SA) of sediments was assessed using a Gemini® VII Surface Area Analyzer (2390a model; Micromeritics®) by a multi-point BET method (Aller and Blair, 2006; Mayer, 1994a). Sediments were degassed overnight at 150°C prior to measurements.

Organic carbon (OC) contents were measured on crushed sediments using a LECO CS 200 (Etcheber et al., 1999) from 2016 to 2018 and then a CHN analyzer. Contents of Total and Enzymatically Hydrolysable Amino Acids (THAA and EHAA, respectively) were determined on triplicates. THAA were extracted by an acid hydrolysis (6 M HCl) during 24h at 110°C. EHAA were extracted according to the biometric method approach (Mayer et al., 1995). THAA and EHAA were then analyzed using a High-Performance Liquid Chromatography (1260 Infinity model, *Agilent*). Amino acids data are not available for the station 10 of April 2021. Contents of Chlorophyll–*a* (Chl-*a*) and Phaeophytin-*a* (Phaeo-*a*) were determined on thawed frozen sediments. Pigments were extracted overnight with 90% acetone then measured using a Perkin Elmer® LS-55 spectrofluorometer (Neveux and Lantoine, 1993). The lability of organic matter and of the vegetal biomass was assessed using the EHAA/THAA (Grémare et al., 2005) and Chl-*a*/(Chl-*a* + Phaeo-*a*) ratios, respectively.

Selective extractions were performed on 100 mg of a subsample of crushed homogenized sediments to assess particulate contents of manganese and iron (Anschutz and Deborde, 2016; Charbonnier and Anschutz, 2019; Deflandre et al., 2002). The most reactive fraction (Mn_{Asc}, Fe_{Asc}) was extracted with an ascorbate solution under shaking for 24h (Anschutz et al., 2005; Kostka and Luther, 1994). It includes amorphous manganese and iron oxyhydroxydes, which are easily reducible (Anschutz et al., 2005; Anschutz and Deborde, 2016; Kostka and Luther, 1994). The acid-soluble fraction (Mn_{HCl}, Fe_{HCl}) was extracted using a solution of 1 M HCl under

shaking for 24h. This fraction comprises that extracted with the ascorbate leaching but also more crystallized iron and manganese oxyhydroxydes, iron monosulfides, carbonates and hydrous-aluminosilicates (Kostka and Luther, 1994; Raiswell et al., 1994). Extracted iron and manganese were measured in the centrifuged and diluted (1:10) extraction solution by spectrophotometry according to the methods described previously (*see section 2.1*). The analysis of a standard (*MESS-2, NRCC*) showed a reproducibility better than 7%.

Acid Volatile Sulfides (AVS) and Chromium Reducible Sulfides (CRS) were sequentially extracted on 2 - 5 g of thawed frozen sediments in close jars under a dinitrogen atmosphere (Gagnon et al., 1995; Hsieh and Yang, 1989). AVS correspond to mackinawite and poorly crystalized greigite (Cornwell and Morse, 1987; Gagnon et al., 1995; Rickard and Morse, 2005) and CRS to sulfur associated with pyrite (Hsieh and Yang, 1989). AVS were extracted during 18h at room temperature using a 20% $SnCl_2$ solution in 9 M HCl. H_2S produced were trapped with a 20% ZnAc solution in 2 M NaOH (Gagnon et al., 1995; Hsieh and Yang, 1989). After the replacement of the trap under a dinitrogen atmosphere, CRS were extracted during 48h at room temperature using a 1 M $CrCl_2$ solution in 0.5 M HCl (Gagnon et al., 1995). Before extractions, all solutions were degassed with dinitrogen. Trapped sulfides were measured by spectrophotometry according to the method of Fonselius et al., (1999) modified to measure high concentrations of sulfides. Due to the time required to perform CRS analyses, CRS measurements were restricted to the stations 1, 10 and 4.

2.3 Oxygen and nutrient fluxes at the sediment-water interface

2.3.1 Oxygen and nutrient fluxes measured by cores incubations

Total oxygen uptakes (TOU) by the sediment and exchanges of nitrate and ammonium between the sediment and the water column were assessed by cores incubations. Immediately after sampling, four sediment cores were filled with bottom water, sealed with waterproof caps and placed in darkness at *in situ* temperature. Magnetic stirring bars fixed on the caps were used to continuously stir water overlying the sediment. Concentrations of dissolved oxygen in overlying water were monitored using micro-optodes *Pyro-Sciences*®. Incubations were stopped when these concentrations had reached ~ 75 - 80% of the initial value (Hulth et al., 1997, 1994). Concentrations of dissolved oxygen and nutrients were measured at the beginning and at the end of incubations with (1) the Winkler method (Grasshoff et al., 1983) from 2016 to 2018 and micro-optodes (*Pyro-Sciences*®) in 2021 and (2) a QuAAtro continuous segmented flow analyzer (Aminot and Kérouel, 2007), respectively. TOU and nutrient fluxes were calculated according to : $J = \frac{(Cstart - Cend) * h}{t}$ with J the flux, h the height of overlying water, Cstart and Cend the concentrations of dissolved oxygen and nutrients in overlying water at the

beginning and at the end of the incubation, t the duration of the incubation (Dalsgaard et al., 2000). Hence, a positive flux represents an uptake by sediments and conversely. Due to technical issues, core incubations could not be carried out in October 2016. At the end of incubations, the top half centimeter of each sediment core was sampled and frozen to perform additional measurements of porosity, grain-size, surface area and organic carbon content.

2.3.2 Vertical distributions of dissolved oxygen in sediments and calculations of diffusive oxygen uptakes

Depth profiles of dissolved oxygen at the sediment-water interface (SWI) were measured using an autonomous *in situ* microprofiler MP7 system (*Unisense S/A*). It was deployed between 5 and 7h at each site and was equipped with a resistivity sensor (Andrews and Bennett, 1981) for sediment surface detection and five Clark-type O_2 microelectrodes (Revsbech, 1989; OX-100 model with a tip diameter of 100 µm and a response time < 5 seconds, *Unisense S/A*). The profiling sequence was programmed to provide depth profiles of O_2 with a resolution of 100 µm from a few millimeters above the SWI to ~ 2 cm depth. Once the profile completed, sensors returned to their initial position in the overlying water and moved by about 2 cm before starting another profiling sequence. Between 4 and 18 oxygen profiles were measured depending on the site. Oxygen microelectrodes were calibrated using (1) the concentration of dissolved oxygen measured *in situ* a few cm above the SWI with an optode AADI (model 4330) and (2) the zero-O_2 concentration in the anoxic sediment. Due to technical issues with the microprofiler in October 2016, oxygen profiles were acquired *ex situ* on a sediment core maintained in *in situ* conditions using Clark-type O_2 microelectrodes and a Field Microprofiling System (FFM) coupled to a motorized micromanipulator controlled by a computer (*Unisense S/A*). Measurements were performed within 2h after core recovering.

Oxygen profiles were processed using the software ProbeFlux, a modified version of PrO_2FLUX (Deflandre and Duchêne, 2010). This software allowed defining (1) the location of the SWI characterized by a slope break in the profile and (2) the oxygen penetration depth (OPD), i.e. the depth at which dissolved oxygen concentrations became lower than the detection limit of the sensor. Diffusive oxygen uptakes (DOU) by the sediment were then computed using the numerical model PROFILE (Berg et al., 1998). This software calculates rates of dissolved oxygen consumption at steady state by fitting a model to the measured profile. For these calculations, the molecular diffusion coefficient of dissolved oxygen within the sediment (Ds) was determined as $Ds = D_0/(1+3(1-\Phi))$ with D_0, the molecular diffusion coefficient of oxygen in seawater and Φ, the mean porosity of surface sediment (0 – 0.5 cm) measured on 4 to 6 cores (Rasmussen and Jorgensen, 1992).

2.4 Data treatments

Saturation indexes of pore waters with respect to several sulfide minerals were computed based on concentrations of dissolved compounds, redox potential of sediments and pH using the software PHREEQC (Parkhurst and Appelo, 1999).

The significance of differences of remineralization rates between stations was assess using an Analysis of Variance (ANOVA) coupled to a Tukey test. The factors controlling the spatiotemporal variability of aerobic remineralization rates were define using a forward stepwise regression and a path-analysis. The path-analysis was performed using the software SmartPLS 4 (Ringle et al., 2022) while other analyses were achieved using the software SigmaPlot 14. The station 10 was not included in analyses performed to define the factors controlling the variability of aerobic remineralization rates because it was sampled at only two cruises and that some parameters were not measured (i.e., amino acids in April 2021).

3. Results and discussion

Studies on the biogeochemical functioning of high-energy RiOMars were restricted to subtropical and tropical environments. Hence, to complete the characterization of these systems, the WGMP is used as a model of a high-energy temperate RiOMar. The biogeochemical processes occurring in the WGMP are first characterized and compared to that of other energetic RiOMars. Then, the capability of the WGMP to recycle organic carbon is assessed and several mass balances are performed to estimate (1) the influence of benthic oxygen uptake on bottom water deoxygenations and (2) the contribution of the WGMP to nutrient inputs in the water column compared to the Gironde estuary.

Part A – Structuration and biogeochemical functioning of the West Gironde Mud Patch

3.1 Organic matter remineralization and secondary diagenetic processes

Biogeochemical processes occurring in the WGMP were studied between 2016 and 2021. Due to the high hydrodynamics of the area, sampling a large number of stations is challenging. In October 2021, favorable weather conditions enabled to sample a maximum of stations along a cross-shelf bathymetric transect, allowing to better characterize the spatial structuration of biogeochemical processes. Accordingly, the spatial structuration of the WGMP is first discussed based on measurements performed in October 2021 then compared with the results of other cruises.

In October 2021, the median grain-size (D50) of surface sediments decreased from 67 ± 5 µm at the station 1 to 20 ± 0 µm at the station 4 (**Table 3.1**). Organic carbon (OC) contents increased seaward from 0.24 ± 0.05 to 1.21 ± 0.07 % while the lability of organic matter, assessed with the EHAA/THAA ratio, was maximum at the station 10 (41 ± 13 %) and tended to decrease seaward. Contents of pigments were lower at the stations 1 and 10 and higher at the station 4. However, the lability of the vegetal fraction of organic matter, assessed with the Chl-*a*/(Chl-*a* + Phaeo-*a*) ratio, was maximum at the station 10 and decreased seaward (**Table 3.1**). These results are consistent with those of April 2021 (**Table 3.1**) and with measurements performed between 2016 and 2018 (Lamarque et al., 2022).

Table 3.1: Median grain-size (D50) and characteristics of organic matter of surface sediments (0 – 0.5 cm) sampled in the WGMP in April and October 2021.

Station	D50	OC	*n*=	EHAA/THAA	*n*=	Chl-*a*	Phaeo-*a*	Chl-*a*/(Chl-*a* + Phaeo-*a*)	*n*=
	µm	%		%		µg g^{-1}	µg g^{-1}	%	
April 2021									
St1	68 ± 2	0.26 ± 0.01	5	25 ± 2	3	0.51 ± 0.48	3.02 ± 2.22	13 ± 4	3
St10	28 ± 3	0.50 ± 0.03	5	-	-	0.60 ± 0.30	3.92 ± 1.86	13 ± 1	3
St2	28 ± 3	0.63 ± 0.15	5	22 ± 1	2	0.71 ± 0.24	4.85 ± 1.92	13 ± 1	3
St3	24 ± 1	0.76 ± 0.13	5	20 ± 2	3	1.18 ± 0.63	9.10 ± 4.65	11 ± 0	3
St8	23 ± 1	0.92 ± 0.15	5	18 ± 1	3	0.81 ± 0.27	7.28 ± 2.72	10 ± 1	3
St4	20 ± 1	1.27 ± 0.10	5	15 ± 0	3	2.04 ± 0.60	17.19 ± 5.35	11 ± 1	3
October 2021									
St1	67 ± 5	0.24 ± 0.05	5	27 ± 4	3	0.40 ± 0.06	2.61 ± 0.34	13 ± 0	2
St10	31 ± 6	0.38 ± 0.06	5	41 ± 13	3	0.64 ± 0.28	3.62 ± 1.24	15 ± 1	3
St2	27 ± 2	0.63 ± 0.09	5	22 ± 2	2	1.04 ± 0.04	6.46 ± 0.33	14 ± 0	3
St3	23 ± 1	0.77 ± 0.08	5	22 ± 1	3	0.95 ± 0.16	7.91 ± 1.46	11 ± 0	3
St8	23 ± 2	0.87 ± 0.10	5	21 ± 2	3	0.75 ± 0.14	6.13 ± 1.05	11 ± 1	3
St4	20 ± 0	1.21 ± 0.07	5	20 ± 4	3	1.12 ± 0.34	9.45 ± 3.49	11 ± 1	2

Measurements of dissolved and particulate compounds showed that this organic matter is degraded according to the theoretical diagenetic sequence (**Figure 3.1**; Froelich et al., 1979). Dissolved oxygen concentrations were constant in the few centimeters above sediments (i.e., between 154 and 182 µM depending on the site) then decreased sharply below the SWI (**Figure 3.1**). Mean oxygen penetration depths varied between 0.19 ± 0.09 cm and 0.52 ± 0.10 cm, which is typical of coastal areas (Aller et al., 2004; Glud, 2008; Pastor et al., 2011b). This rapid consumption of dissolved oxygen is related to remineralization of organic matter by microbial aerobic respiration and to the oxidation of reduced compounds produced in sediments diffusing toward the SWI (Glud, 2008; Jorgensen et al., 2022; Rabouille et al., 2003). Among them, the oxidation of ammonium by nitrification (i.e., production of nitrate by ammonium oxidation; Galloway, 2014) is highlighted by low ammonium concentrations at the SWI (i.e., between 0 and 19 µM) and by a maximum of nitrate concentrations in the first centimeter of sediments at

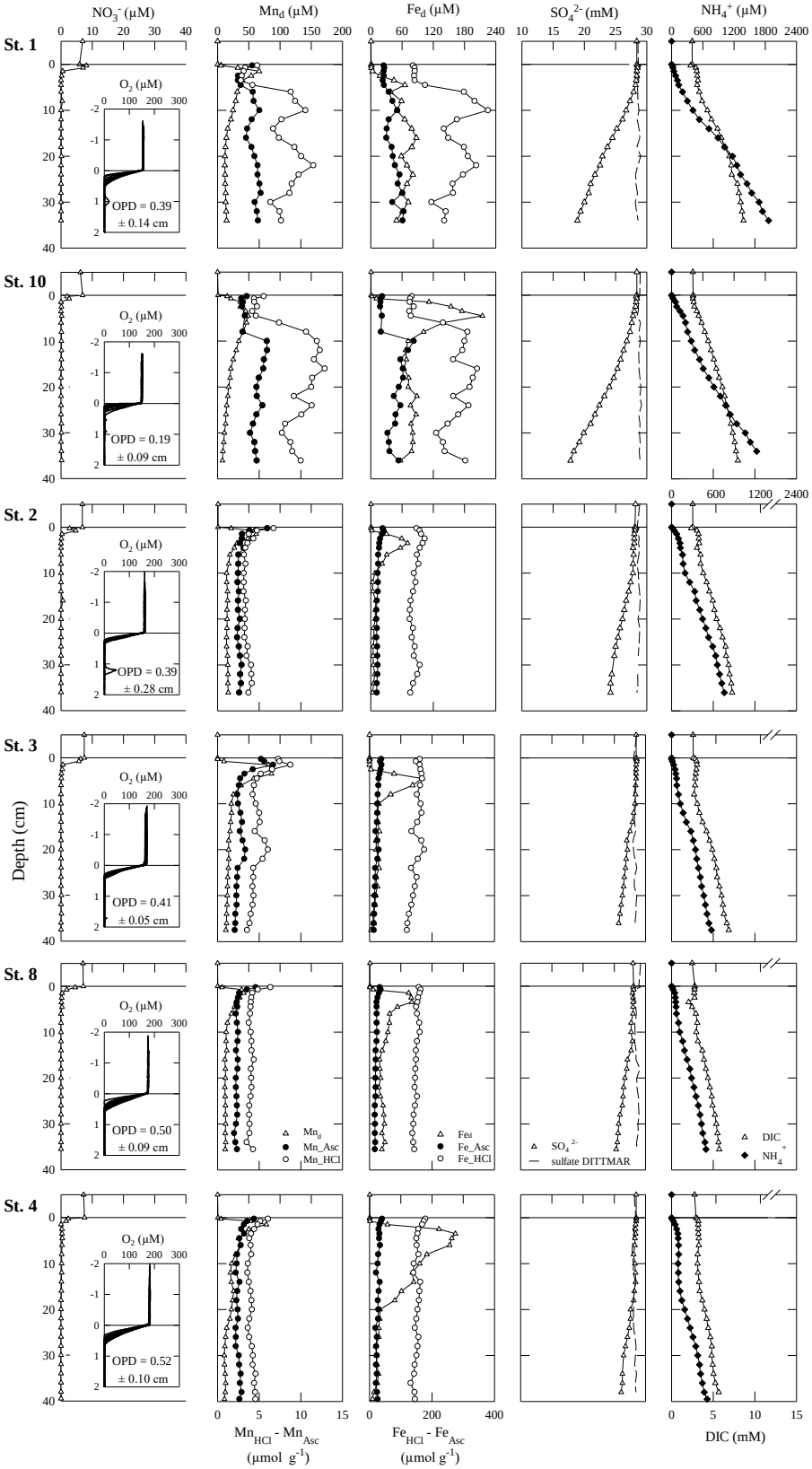

Figure 3.1: Depth profiles of dissolved oxygen (O_2), nitrate (NO_3^-), dissolved (Mn_d) and particulate ($Mn_{Asc,}$ Mn_{HCl}) manganese, dissolved (Fe_d) and particulate ($Fe_{Asc,}$ Fe_{HCl}) iron, sulfate (SO_4^{2-}), dissolved inorganic carbon (DIC) and ammonium (NH_4^+) in sediments and oxygen penetration depth (OPD) at the six stations sampled in October 2021. The dash line represents theoretical sulfate concentrations calculated from chloride concentrations using the DITTMAR ratios. Data of other cruises are available in Annex 4.

some stations (i.e., station 1 of October 2021; **Figure 3.1**). Measurements of nitrate and ammonium exchanges between the sediment and the water column by core incubations confirm the occurrence of nitrification whatever the season (**Figure 3.2**). Indeed, in average ammonium effluxes from the sediment represent only ~ 28% of the sum of nitrate plus ammonium fluxes, which indicates a relatively efficient nitrification. Interestingly, the globally higher ammonium fluxes at the station 1 suggest that nitrification would be less efficient at this site. A net flux of nitrate toward the water column implies that nitrification would be the main source of nitrate for organic matter remineralization by denitrification, which occurred in the first centimeters of sediments as indicated by the rapid nitrate consumption (**Figure 3.1** ; Burdige, 2011; Froelich et al., 1979; Hyacinthe et al., 2001).

Dissolved manganese (Mn_d) concentrations increased from ~ 0 µM at the SWI to maximums values between 20 and 95 µM at a few centimeters depth (**Figure 3.1**). These maximums occur close to the disappearance depth of nitrate. Concomitantly to build-up of Mn_d in pore waters, contents of reactive Mn oxyhydroxydes (Mn_{Asc}) progressively decreased with depth (**Figures 3.1** and **3. 3**). These decreases were clearly visible at the stations 2, 3, 8 and 4 as opposed to the stations 1 and 10. These two proximal sites are characterized by the presence of a coarser surface layer (**Figure 3.3**) overlying finer relic deposits (Dubosq et al., 2021). The presence of this coarser surface layer results in relatively low contents of Mn_{Asc} in surface sediments (**Figures 3.1** and **3.3**). This is related to the fact that amorphous Mn oxyhydroxydes are mainly associated with surfaces of particles (Poulton and Raiswell, 2005). Hence, the coarser is the sediment, the lower is the SA and so the lower are the contents of Mn oxyhydroxydes but also of Fe oxyhydroxydes, for which the same pattern is observed (**Figure 3.3**). A way to minimize variations of oxyhydroxydes contents strictly due to changes in grain-size is to normalize them with respect to sediment SA, as it is typically done for OC (Aller and Blair, 2006; Dubosq et al., 2021; Mayer, 1994a). Depth profiles of loads of reactive Mn oxyhydroxydes (i.e., Mn_{Asc}/SA) highlighted the consumption of Mn_{Asc} in surface sediments at all stations until reaching almost constant values ~ 0.2 µmol m^{-2} (**Figure 3.3**). Depth profiles of dissolved iron (Fe_d) had a shape close to that of Mn_d with a slightly deeper maximum. As for Mn, build-up of Fe_d was associated with a decrease of Fe_{Asc} sediment loads (i.e., Fe_{Asc}/SA) with depth (**Figure 3.3**). Decreases of loads of reactive Fe and Mn in the first centimeters of sediments are due to the reduction of Mn and Fe oxyhydroxydes coupled to organic matter remineralization. Mn_d and Fe_d produced by these reactions diffuse upward where they are oxidized in oxyhydroxydes. This results in (1) low concentrations of Mn_d and Fe_d and in an (2) accumulation of Mn_{Asc} and Fe_{Asc} in surface sediments (Burdige, 1993) as observed in **Figures 3.1** and **3.3**. During its upward transport by diffusion, Mn_d may be oxidized by nitrate and dissolved oxygen (Canfield et al., 1993; Hyacinthe et al., 2001). Similarly, Fe_d may be oxidized by the same compounds

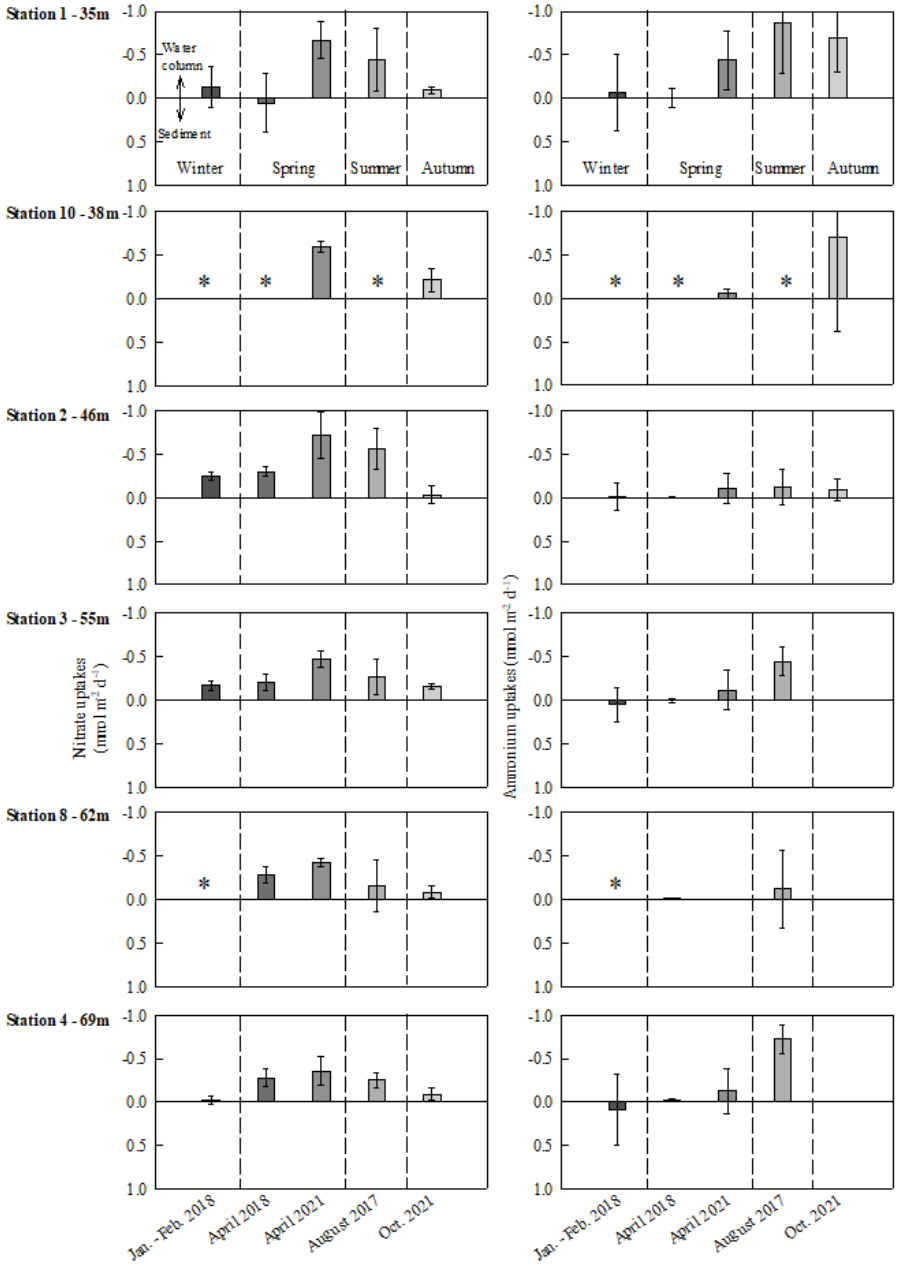

Figure 3.2: Fluxes of nitrates and ammonium at the sediment – water interface measured by cores incubations at five stations sampled in January - February 2018, April 2018 and 2021, August 2017 and October 2021. Asterisks (*) indicate that the station was not sampled during the cruise.

and by Mn oxyhydroxydes (Burdige, 1993; Canfield et al., 1993; Hyacinthe et al., 2001). On some cores, the appearance of Mn_d and Fe_d below the oxygen penetration depth (e.g., stations 1 and 3 of October 2021; **Figure 3.1**) suggests that oxygen is not always their main oxidant. A calculation based (1) on diffusive fluxes of Mn_d, Fe_d and nitrate estimated from depth profiles and on (2) stoichiometric coefficients of oxidation processes from Hyacinthe et al. (2001) shows that that up to 100% of nitrate consumed in sediments may be used to oxidize upward fluxes of Mn_d and Fe_d. This is obtained by considering that upward fluxes of Mn_d and Fe_d are solely oxidized by nitrate. Even if these compounds may be oxidized by other oxidants (e.g., dissolved oxygen) this highlights the potential important use of oxidants in processes other than organic

matter remineralization. Moreover, the oxidation of Mn_d and Fe_d by nitrate results in a production of dinitrogen (Deflandre et al., 2000; Hyacinthe et al., 2001), which may influence the nitrogen cycle by limiting the flux of regenerated nutrients to the water column. In depth, concentrations of Mn_d and Fe_d decreased until almost constant values suggesting an equilibrium with a particulate phase.

Below the maximum of Fe_d, sulfate concentrations decreased with depth, indicating the occurrence of organic matter remineralization coupled to sulfate reduction (**Figure 3.1**). However, in spite of a marked decrease of sulfate concentrations, dissolved sulfides remained close to the detection limit (~ 1 µM). Sulfate consumption was clearly more important at the stations 1 and 10 (i.e., proximal sites) than at other ones. It is most likely due to the particular sedimentary context of these sites, which induces a diagenetic regime divided in two layers with distinct biogeochemical functioning. Indeed, oxic and suboxic remineralization processes (i.e., aerobic respiration, denitrification, reduction of reactive Mn and Fe oxyhydroxydes ; Aller, 2014) appeared to be mainly restricted to surface modern deposits while sulfate reduction occurs in underlying relic sediments where sulfate is the main available oxidant for organic matter remineralization (**Figure 3.1**). At other sites, the consumption of sulfate was lower. Moreover, it tended to decrease and to start deeper seaward (**Figure 3.1**). Concomitantly to the deepening of the depth where sulfate reduction appears, we observed a widening of Fe_d peaks marking an extension of the suboxic zone. It is consistent with sediment profiles images that highlighted the seaward increase in thickness of the colored brown layer (i.e. aRPD; Lamarque et al., 2021) and reflects a depth expansion of the diagenetic sequence. This may be due to the decrease of organic matter lability seaward (**Table 3.1**; Lamarque et al., 2022, 2021) inducing a decrease in the demand for oxidants. However, it may also be related to the gradual increase in thickness of the sediment mixed layer (Dubosq et al., 2021) and to the establishment of a deeply burrowing macrofauna (Lamarque et al., 2021; Massé et al., 2016). Indeed, burrowing macrofauna may (1) inject dissolved oxygen into sediments triggering oxidation of reduced compounds such as Mn_d and Fe_d, and (2) transport particulate metallic oxyhydroxydes within the sedimentary column (Aller et al., 2001; Aller, 2014; Aller and Aller, 1998; Burdige, 2011; Jorgensen et al., 2022; Kristensen, 2000; Kristensen and Kostka, 2005). This induces an increase in the thickness of the layer enriched in metallic oxides, and in an enhancement of suboxic remineralization processes. These observations suggest that suboxic remineralization could be more important in the distal than in the proximal WGMP. Nevertheless, the accumulation of by-products of organic matter remineralization (i.e., ammonium, DIC) in pore waters decreased seaward (**Figures 3.1** and **3.2**), suggesting a decrease in remineralization intensity and tempers the potential importance of suboxic remineralization processes in the distal WGMP. However, the build-up of organic matter by-products in pore waters is a poor

proxy of the intensity of remineralization because bioirrigation may limit their accumulation due to solute exchanges with the overlying water column (Aller et al., 2001). At last, no methane was detected in these sediments (data not shown), which is consistent with the relatively high sulfate concentrations.

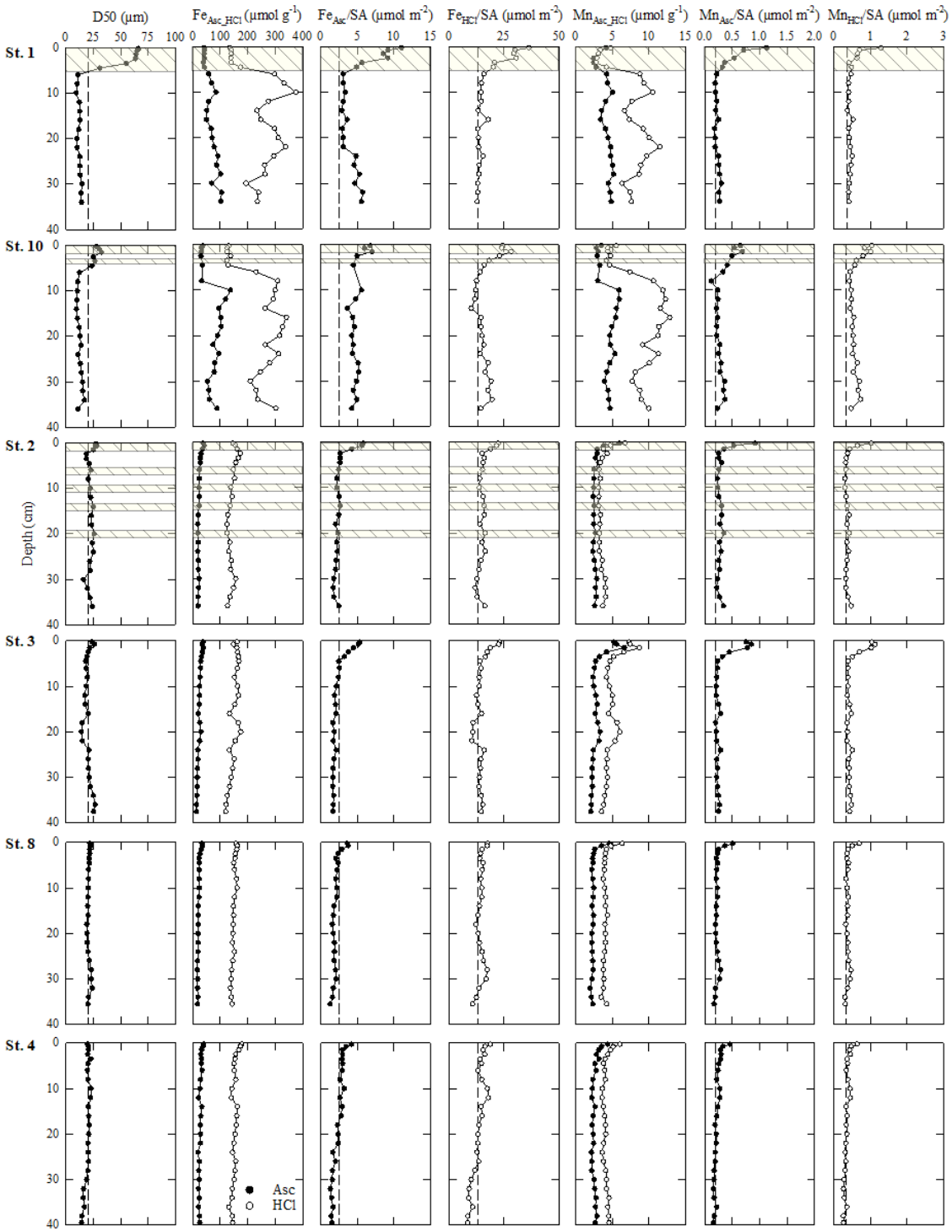

Figure 3.3: Depth profiles of median grain-size (D50), particulate iron (Fe_{Asc}, Fe_{HCl}) and manganese (Mn_{Asc}, Mn_{HCl}) contents and normalized to surface area of sediments (Fe_{Asc}/SA, Fe_{HCl}/SA, Mn_{Asc}/SA, Mn_{HCl}/SA) in sediments sampled in October 2021. Dash lines correspond to backgrounds levels (1) of D50 (~ 20 µm) and (2) of particulate iron and manganese contents normalized to SA measured in the central and distal WGMP. Yellow stripped layers represent horizons having a sand content above 10%.

Interestingly in spite of variations of remineralization pathways between stations, DIC represented more than 85% of dissolved carbon (i.e., DIC + DOC) over the whole WGMP (**Figure 3.4**). This indicates that organic matter is efficiently oxidized to inorganic compounds over the whole area (Aller and Blair, 2006; Aller et al., 2004). However, the stations 1 and 10 distinguished again by a higher relative proportion of DOC (10 - 15%) than the other sites (< 10%). This means that remineralized organic matter is almost completely oxidized in the central and distal stations while some would remain in the form of dissolved compounds in the proximal stations likely due to an accumulation of more refractory compounds (Gan et al., 2020).

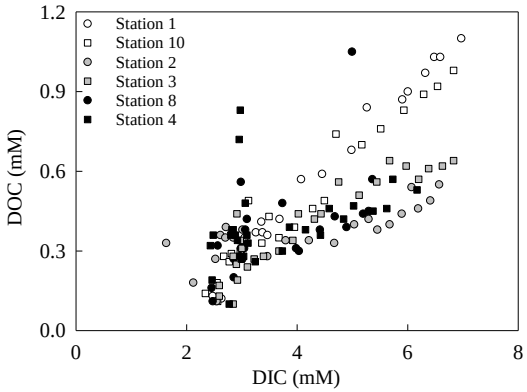

Figure 3.4: Relationship between dissolved inorganic (DIC) and organic (DOC) carbon in pore waters of sediments at the six stations sampled in October 2021.

Measurements performed during other cruises showed that depth profiles of dissolved and particulate compounds did not have marked seasonal variations (**Figure 3.5**). Hence, diagenetic processes on the first decimeters of sediments depend more on the spatial structuration than seasonal forcing.

3.2 Differential functioning of early diagenesis: relic vs modern sediments

Beyond processes of organic carbon remineralization, results highlight the occurrence of secondary reactions. As previously indicated, the decrease of Fe_d concentrations until almost constant values in depth (**Figures 3.1** and **3.5**) suggests an equilibrium of Fe_d with a particulate phase below the horizon of the reduction of iron oxyhydroxydes. However, background concentrations of Fe_d in the proximal area (~ 40 – 80 µM, stations 1 and 10) were widely higher than those of the others stations (~ 5 – 30 µM, **Figures 3.1** and **3.5**). This suggests a differential functioning of the iron cycle between relic sediments of the proximal area and the modern sediments of the distal WGMP.

At the central and distal stations, the decrease of Fe_d concentrations in depth is rather classic and suggests a precipitation with the sulfides produced during organic matter remineralization

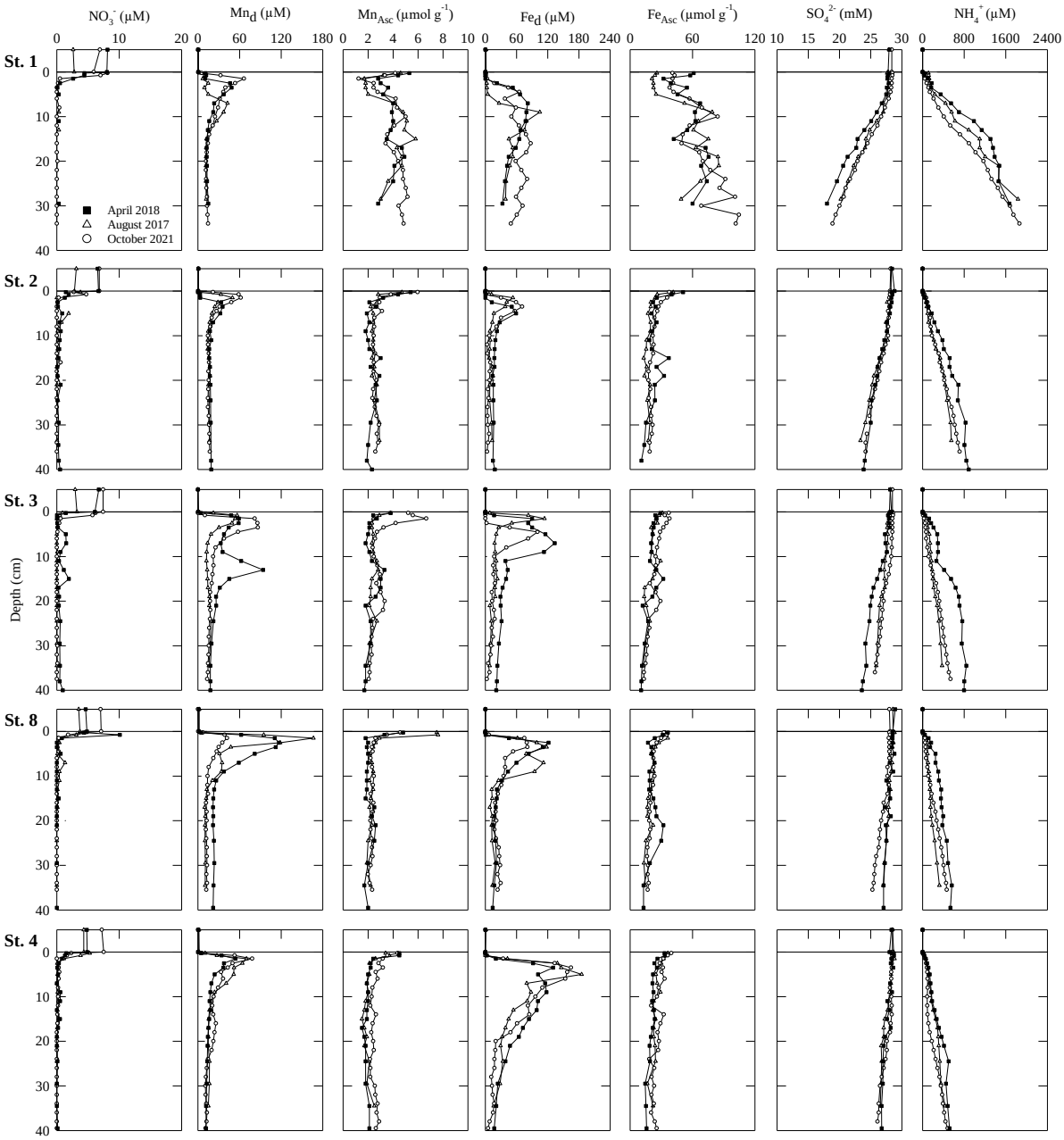

Figure 3.5: Depth profiles of nitrate (NO_3^-), dissolved manganese (Mn_d), reactive manganese oxyhydroxydes (Mn_{Asc}), dissolved iron (Fe_d), reactive iron oxyhydroxydes (Fe_{Asc}), sulfate (SO_4^{2-}), and ammonium (NH_4^+) in sediments at five stations sampled in August 2017, April 2018 and October 2021. Data of the station 10 are available in the Figure 3.1.

coupled to sulfate reduction (Burdige, 2006; Deflandre et al., 2002; Jorgensen et al., 2019; Pastor et al., 2011a). This is consistent with the low sulfide concentrations (< 1µM) and with a higher AVS content of ~ 4 - 5 µmol g^{-1} around 10 - 20 cm depth, which is the depth of the beginning of sulfate consumption (**Figures 3.5** and **3.6**). However, thermodynamic calculations show that pore waters were under-saturated with respect to greigite and mackinawite, two mineral phases included in AVS (**Figure 3.7** ; Cornwell and Morse, 1987; Rickard and Morse, 2005). This suggests that AVS likely consist in poorly crystallized phase of iron sulfides. The

decrease of AVS contents and the accumulation of CRS up to 25 - 30 µmol g^{-1} in depth indicate a conversion of AVS to pyrite (Jorgensen et al., 2019; Jorgensen, 2021 ; **Figure 3.6**). At the proximal sites (i.e., 1 and 10), AVS contents were higher with values above 5 µmol g^{-1} and increased up to 21 µmol g^{-1} (**Figure 3.6**). However in contrast to the distal stations, CRS contents were lower than 5 µmol g^{-1}, with the exception of two layers of the station 10 in October 2021 with contents up to 7.3 µmol g^{-1}. Given these relatively high contents of AVS, the higher background concentrations of Fe_d at the proximal stations was somewhat surprising. Indeed, if the diagenetic behaviors of iron and sulfur in proximal stations were similar to that in distal stations, Fe_d should also be efficiently trapped as iron sulfides. Accordingly, the higher background concentrations of Fe_d coupled to relatively high AVS but low CRS contents at the two most proximal stations suggest that the biogeochemical processes involved in the iron and sulfur cycles differ between relic and modern sediments.

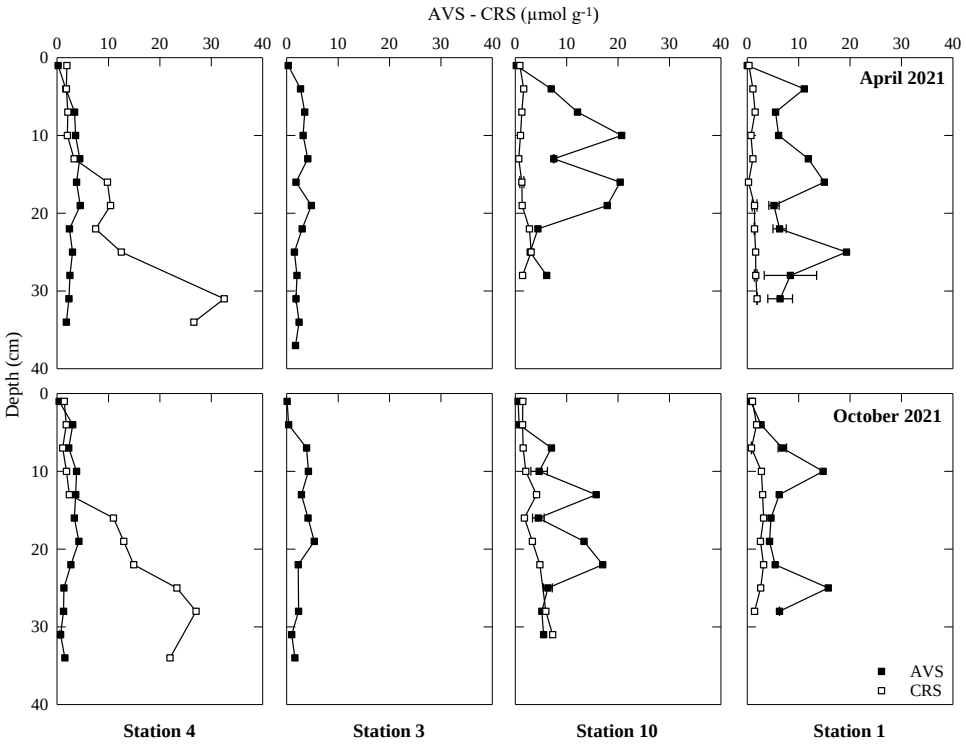

Figure 3.6 : Contents of Acid Volatile Sulfides (AVS) and Chromium Reducible Sulfides (CRS) in sediments of four stations of the WGMP sampled along a bathymetric transect in April and October 2021. CRS measurements were only performed for the stations 1, 10 and 4.

Owing to their affinities with iron oxyhydroxydes and/or sulfides, some trace metals are useful tools to clarify the diagenetic fate of iron and sulfur in marine sediments. Cobalt (Co) and arsenic (As) are particularly interesting because they both co-precipitate with iron sulfides but their affinities for oxyhydroxydes are different. Indeed, Co has a strong affinity with Mn oxyhydroxydes while As has one for Fe oxyhydroxydes on which it adsorbs (Mucci et al., 2000; Stockdale et al., 2010; Zhang et al., 2002).

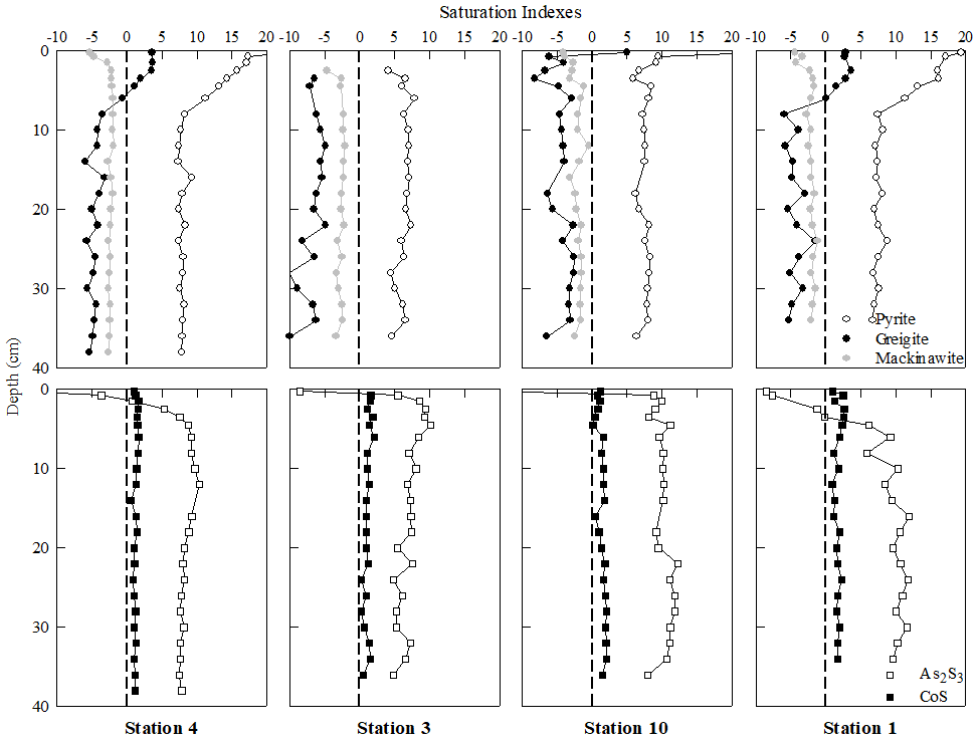

Figure 3.7: Saturation indexes of iron (greigite, mackinawite and pyrite), cobalt (CoS) and arsenic (As_2S_2) sulfide minerals in pore waters of sediments sampled at four stations of the WGMP in October 2021. Saturation indexes above zero indicate an over-saturation of pore waters with respect to the considered mineral.

At all stations, depth profiles of dissolved Co (Co_d) were similar (**Figure 3.8**). Concentrations were lower than 0.5 nM in bottom waters and gradually increased from the SWI up to a maximum between 20 and 50 nM due to the production of Co_d related to the reduction of Mn oxyhydroxydes (Stockdale et al., 2010; Zhang et al., 2002). The produced Co_d diffuses toward the SWI where it absorbs on or co-precipitates with Mn oxyhydroxydes (Stockdale et al., 2010) and downward where its concentrations decreased to constants values, which likely indicates a precipitation with sulfide minerals (Stockdale et al., 2010). This precipitation is consistent with saturation indexes of CoS comprised between 0 and 2 (**Figure 3.7**). Minerals phases controlling equilibriums with dissolved compounds tend indeed to have saturation indexes close to zero. Interestingly, concentrations of Co_d in depth were greatly higher at stations 1 and 10 (~ 10 nM) than at other sites (~ 2 nM). These differences are not related to differences of pH or redox potential, which were similar below 10 cm depth (**Figure 3.8**). Moreover, thermodynamic calculations performed with PHREEQC indicate that the speciation of Co_d did not vary between stations. Differences of Co_d concentrations below 10 cm depth between proximal and distal stations would be likely related to differential interactions with the particulate phase.

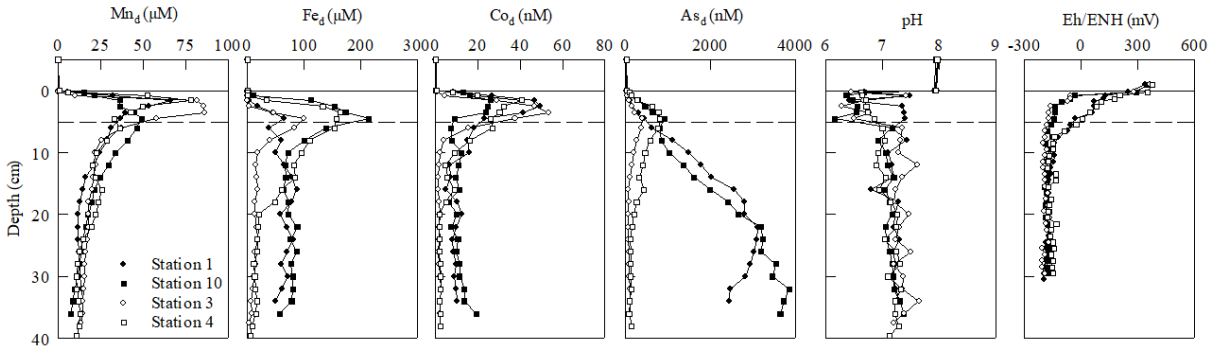

Figure 3.8: Depth profiles of dissolved manganese (Mn_d), iron (Fe_d), cobalt (Co_d) and arsenic (As_d), pH and redox potential of sediments (Eh/ENH) at four stations sampled in October 2021. The dash line represents the limit between modern and relic sediments at the stations 1 and 10.

In contrast to Co_d, depth profiles of dissolved As (As_d) were widely different between proximal and distal stations (**Figure 3.8**). In bottom waters, concentrations of As_d were low with values ~ 10 - 30 nM. At the stations 3 and 4, As_d concentrations increased from the SWI to maximum values ~ 400 and ~ 800 nM at a few centimeters depth, respectively. This build-up of As_d is related to the reduction of reactive Fe oxyhydroxydes with which As has a strong affinity (Chaillou et al., 2008; Legeleux et al., 1994; Mucci et al., 2000). In depth, concentrations of As_d decreased to constant values comprised between 60 and 120 nM, suggesting a precipitation of arsenic sulfides or a co-precipitation with iron sulfides. Thermodynamic calculations indicate that the formation of As sulfides is thermodynamically favorable (**Figure 3.7**) but saturation indexes are likely too high (i.e., between 4.8 and 10.3) for a pure phase to control the equilibrium. It is therefore most likely that As_d co-precipitates with iron sulfides. In contrast, As_d concentrations at proximal stations (i.e., 1 and 10) did not show a subsurface maximum concomitant with the Fe_d peak, but they increased progressively with depth to ~ 3 - 3.8 µM (**Figure 3.8**). These high concentrations, and the gradual accumulation of As_d with depth, indicate a production of As_d in relic sediments. Contrary to what was observed in the distal WGMP, As_d is not efficiently trapped through a co-precipitation with iron sulfides. It was quite surprising because the stations 1 and 10 present relatively high contents of AVS (**Figure 3.6**) and the highest sulfate consumption (**Figures 3.1** and **3.5**). Moreover, the precipitation of As sulfides (As_2S_3) is thermodynamically favorable with saturation indexes higher than 5.9 (**Figure 3.7**). However, these high values also indicate that it is likely not this mineral phase that controls levels of As_d in sediment pore waters. It is important to note that the highest concentrations of As_d were measured in the relic sediments of proximal sites where relatively high concentrations of Fe_d were also observed in comparison to other stations (**Figure 3.8**). As arsenic has a strong affinity with Fe oxyhydroxydes, a reduction of Fe oxyhydroxydes in relic sediments is a possible explanation for the production and accumulation of As_d in pore waters (Edenborn et al., 1986). This also explains the higher Fe_d concentrations observed at the

stations 1 and 10 in spite of the sulfate consumption and the absence of sulfide accumulation. A local production of As_d in relic deposits would explain that it is not efficiently trapped through a co-precipitation with iron sulfides as opposed to Co_d, which is solely produced in modern surface sediments and reaches relic deposits by diffusion.

Given the relatively high consumption of sulfate at the proximal stations, the reduction of iron oxyhydroxydes is most likely associated with an oxidation of sulfides produced during sulfate reduction. The higher contents of reactive iron oxyhydroxydes measured in relic sediments in comparison to the distal WGMP (**Figures 3.1** and **3.3**) likely favor this process, which induce the specific features of the iron and sulfur cycles observed in this area. Moreover, the higher values of Fe_{Asc}/SA measured in relic sediments show that this difference of oxyhydroxydes contents is not only related to grain size changes (relic deposits being finer than modern ones) but that relic sediments are enriched in Fe_{Asc}. This may be related to different origin or depositional context for these sediments in comparison to those of the rest of the WGMP.

The main by-products of sulfide oxidation by iron oxyhydroxydes are elemental sulfur (S^0) and Fe (II) (Jorgensen, 2021; Jorgensen et al., 2019; Luther et al., 1992; Taillefert et al., 2002). Fe (II) can then precipitate with dissolved sulfides to form iron sulfides (i.e., AVS ; Raiswell and Canfield, 2012). However, thermodynamic calculations show that pore waters are slightly under-saturated with respect to greigite and mackinawite (**Figure 3.7**), suggesting that a poorly crystalized sulfide mineral likely controls the equilibrium with Fe_d, as observed at the distal stations. Fe (II) produced during sulfide oxidation may also be complexed by organic ligands and then favors the reductive dissolution of Fe oxyhydroxydes. This produces complexed Fe (II) and Fe (III), the latter being able to oxidize sulfides (Luther et al., 1992; Taillefert et al., 2002). Such a reaction is interesting because complexed Fe (III) can build-up in pore waters in the absence of dissolved sulfides (Taillefert et al., 2002) and may therefore partly explain the relatively high concentrations of Fe_d measured in relic sediments of the proximal area.

Concerning the sulfur cycle, sulfides produced during sulfate reduction in relic sediments would be oxidized by iron oxyhydroxydes. This would produce Fe (II), S^0 and AVS (Jorgensen, 2021; Jorgensen et al., 2019; Raiswell and Canfield, 2012). AVS may then react with sulfides ("sulfides pathway") or polysulfides ("polysulfides pathway") to form pyrite (Jorgensen et al., 2019; Rickard and Luther, 2007). The precipitation of pyrite from the "sulfides pathway" is unlikely due to the low concentrations of sulfides. However, polysulfides are formed from S^0 and dissolved sulfides (Findlay, 2016; Rickard and Luther, 2007). Hence, the low concentrations of dissolved sulfides also limit the formation of polysulfides and so the conversion of AVS to pyrite through this pathway (Gagnon et al., 1996). Accordingly, sulfur

trapped in relic sediments is likely in the form of AVS and elemental sulfur, rather than pyrite. This is consistent with the relatively high AVS and low CRS contents in relic sediments in contrast to that measured at the station 4 (**Figure 3.6**).

3.3 Does the WGMP has a biogeochemical functioning like the others RiOMars?

In the first decimeters of the WGMP sediments, early diagenesis processes appear highly spatially structured along the cross-shelf bathymetric transect with (1) a diagenetic regime divided in two layers in the proximal area and (2) an expansion of the diagenetic sequence with increasing depth in the distal WGMP. A diagenetic regime divided in two layers with distinct biogeochemical functioning has been described at shallow depth (< 50 m) on energetic continental shelves of the Gulf of Papua and of the Amazon (Aller, 2004; Aller et al., 2008; Aller and Blair, 2006). In these environments, a suboxic mobile layer of 0.5 - 2 m thick typically overlies more consolidated sediments within which organic matter is remineralized by sulfate reduction or methane genesis (Aller and Blair, 2006). The observation of this feature typical of high-energy RiOMars in the WGMP is consistent with the high hydrodynamics of the Bay of Biscay continental shelf. Concerning the distal area, a seaward expansion of the diagenetic sequence was already observed in RiOMars like the Mississippi delta (Lin and Morse, 1991) and the Rhône prodelta (Pastor et al., 2011a). It was attributed to an increase of the distance to the river mouth, which induces a decrease of sediment fluxes and associated total organic carbon (OC) inputs. Conversely, the increase of OC contents and the concomitant decrease of organic matter lability seaward (**Table 3.1** ; Lamarque et al., 2022, 2021) suggest that the intensity of anoxic remineralization in the WGMP is rather controlled by the quality than the quantity of organic matter.

Owing to the high hydrodynamics of the Bay of Biscay continental shelf (Cirac et al., 2000; Jouanneau et al., 1989), it is particularly relevant to compare the biogeochemical functioning of the WGMP to that of other high-energy RiOMars. Based on its morphology, the moderate discharge of sediments from the Gironde and the hydrodynamics dominated by storms and waves, the continental shelf off the Gironde may be considered as a Marine Dispersal Dominated (MDD) system (Walsh and Nittrouer, 2009). These environments are characterized by moderate sediment discharges from rivers and a high hydrodynamics precluding sedimentation near the river mouth. In contrast, the high-energy RiOMars (i.e., RiOMars of type 1) included in the classification of Blair and Aller (2012) are deltaic systems. Among them, the most energetic environments are Subaqueous Delta Clinoform (SDC ; e.g., the Amazon delta, the gulf of Papua deltaic complex, Walsh and Nittrouer, 2009). However, hydrodynamics in SDC environments is dominated by tides rather than storms. In fact, a too high hydrodynamics (i.e., significant wave height > 2 m) precludes the formation of a SDC. The

second difference between SDC and MDD (i.e., the WGMP) systems is the sediment discharge (Walsh and Nittrouer, 2009). Indeed, only rivers or groups of rivers having a sediment discharge > 100 Mt y^{-1} appear able to produce a SDC. Therefore, given (1) the seasonal average of significant waves heights between 2 and 3.5 m in the Bay of Biscay (Charles et al., 2012) and (2) the relatively modest discharge of sediments of the Gironde estuary (~ 1.5 Mt y^{-1}, Jouanneau et al., 1999), the depositional environment of the WGMP fundamentally differs from that of RiOMars of type 1. As the WGMP is not a delta, it is not directly connected to its main sediment source with an upper limit of mud deposits ~ 30 m depth against less than 10 m for the RiOMars of type 1. In these systems organic matter is extensively remineralized in the shallowest area that acts as a suboxic organic matter incinerator due frequent resuspension of a mobile layer of ~ 10 - 200 cm thick depending on sites (Aller, 2004; Aller et al., 2008; Blair and Aller, 2012; Zhu et al., 2016). These sediments are eventually transferred to a deeper zone where they accumulate (Aller, 2004; Walsh et al., 2004). The deeper location of the WGMP results in the absence of mobile muds acting as an organic matter incinerator. Indeed, while in RiOMars of type 1 the transit of sediments through a shallow suboxic incinerator results in OC loads typically < 0.4 mgC m^{-2} (Aller et al., 2008; Blair and Aller, 2012), they range between 0.4 and 1.5 mgC m^{-2} in the first decimeters of the WGMP sediments (Dubosq et al., 2021). Hence, the biogeochemical functioning of the WGMP does not correspond to those of RiOMars of type 1 according to the classification of Blair and Aller (2012) in spite of the direct influence of the Gironde and the energetic character of the Bay of Biscay continental shelf. However, the WGMP obviously does not match with the two others types of RiOMars (i.e., small mountainous systems and low energetics environments, respectively) defined by Blair and Aller (2012). It seems therefore reasonable to consider the WGMP as a system representative of a fourth group of RiOMars, which the characteristics need to be defined.

Part B – Implications of the biogeochemical functioning of the WGMP on the ecosystem

3.4 Organic carbon remineralization rates by the different degradation pathways

3.4.1 Spatial structuration of organic carbon remineralization rates

In order to quantitatively estimate the relative importance of each pathway of organic carbon (OC) remineralization, OC remineralization rates were computed based on (1) stoichiometric ratios of remineralization processes from Froelich et al. (1979) and on (2) diffusive fluxes of dissolved compounds implies in these processes. Diffusive fluxes of nitrate, Mn_d, Fe_d and sulfate were computed using the Fick's First Law of Diffusion applied to the sediment (i.e., $J = -\Phi Ds\frac{dC}{dz}$, where J corresponds to the flux, Φ to the sediment porosity, Ds to the molecular

diffusion coefficient from Schulz and Zabel (2006) corrected for tortuosity according to Rasmussen and Jorgensen (1992) and $\frac{dC}{dz}$ to the gradients of concentrations). For aerobic respiration, we used diffusive oxygen uptakes (DOU) computed with the Berg model (Berg et al., 1998). Since DOU are related to consumption of dissolved oxygen by aerobic respiration and oxidation of reduced compounds (Canfield et al., 1993; Galloway, 2014; Glud, 2008), they were corrected for upward fluxes of ammonium, Mn_d and Fe_d using (1) these fluxes computed with the Fick's First Law of Diffusion applied to the sediment and (2) stoichiometric ratios of oxidation reactions (Hyacinthe et al., 2001; Wang and Van Cappellen, 1996).

Estimates of OC remineralization rates show that organic matter in the sediments of the WGMP is mainly remineralized by aerobic respiration and sulfate reduction. The sum of other pathways represents less than 10% of total remineralization (data not shown). Obviously, the importance of suboxic processes is possibly underestimate if an efficient coupling between oxidation of reduced compounds (i.e., ammonium, Mn_d, Fe_d) and reduction of newly produced oxidized forms occurs. This uncertainty is related to the fact that these calculations were performed considering a steady state. However, as the shape of dissolved compounds over the first decimeters of sediments did not present marked variations between cruises (**Figure 3.5**), this assumption seems reasonable. Only the surface layers of proximal stations may differ from the steady state due to their remobilization or inputs of sandy sediments during seasonal energetic events (Jouanneau et al., 1989; Lesueur et al., 2002). These layers may in a some extend act as an unsteady batch reactor (Aller, 2004). However, the rather similar intensity of aerobic respiration at the station 1 between seasons, except in April 2018 (**Figures 3.9** and **3.10**), suggests a quick equilibration of dissolved oxygen distributions in surface sediments and that a steady state may be assumed at least at the scale of the cruise. Such remobilizations of sediments are believe to promote suboxic remineralization processes. However, the low contents of Mn_{Asc} and Fe_{Asc} in these layers due to their relatively high grain-size in comparison to the rest of the WGMP likely precludes a significant suboxic remineralization. In fact, the relatively low importance of suboxic remineralization processes in comparison to other energetic RiOMars is consistent with the absence of mobile muds due to the depositional environment of the WGMP (*see section 3.3*).

OC remineralization rates by aerobic respiration ranged from 4.5 to 27.8 gC m^{-2} y^{-1} (**Figures 3.9** and **3.10**). Interestingly, they did not vary monotonously along the bathymetric transect (**Figure 3.9**). They were almost equivalent at the stations 1, 2, 3 and 8 but significantly higher at the stations 10 and 4. These latter stations can be considered as hot spots for aerobic respiration at the scale of the WGMP, namely areas with higher remineralization rates in comparison to other sites (Bianchi et al., 2018; McClain et al., 2003). The only exception to

this global pattern is the station 2 whose the intensity of aerobic respiration was significantly different from the station 10 but not from the station 4 (**Figure 3.9**). The high lability of organic matter in surface sediments of the station 10 (EHAA/THAA = 41 ± 13% in October 2021, **Table 3.1**), in comparison to the rest of the WGMP (EHAA/THAA from 20 ± 4% to 27 ± 4% in October 2021; **Table 3.1**), is likely the cause of the higher rates of aerobic respiration observed at this site. Rates of OC remineralization coupled to sulfate reduction were lower than those of aerobic respiration with values between 0.4 and 10.3 gC m^{-2} y^{-1} (**Figures 3.9** and **3.10**). Contrary to aerobic respiration rates, they markedly decreased seaward with significantly higher values at proximal stations (i.e. 1 and 10) consistently with sulfate profiles (**Figures 3.1** and **3.5**). These two sites can therefore be considered as hot spots for sulfate reduction at the scale of the WGMP.

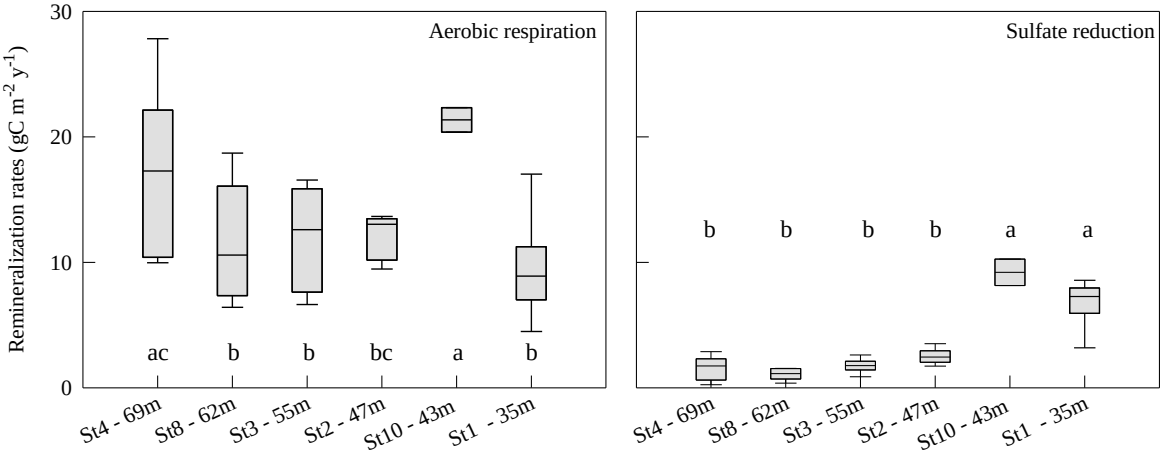

Figure 3.9: Organic carbon remineralization rates by aerobic respiration and sulfate reduction in sediments of the WGMP, estimated from measurements performed along a cross-shelf bathymetric transect during the six cruises led between 2016 and 2021. The significance of the differences between stations was assessed using an Analysis of Variance (ANOVA) coupled to a Tukey test. Stations labelled with the same letter are not significantly different.

These estimates of remineralization rates allow defining the spatial structuration of biogeochemical processes in the WGMP. Firstly, there is a clear distinction between the proximal area that is a hot spot for sulfate reduction and the distal part where this process is much less intense. The particular biogeochemical functioning of the proximal area, namely a diagenetic regime divided in two layers (*see section 3.1*), highly supports this distinction. Concerning the distal area, the significantly higher aerobic respiration rate at the station 4 suggests a subdivision of this area in two zones: (1) a central part (i.e., stations 2, 3 and 8) having moderate aerobic respiration rates and (2) an outer part represented by the station 4, which is a hot spot for organic matter remineralization by aerobic respiration (**Figure 3.10**).

3.4.2 Seasonal dynamic of organic carbon remineralization rates

Consistently with the constancy of profiles of dissolved compounds between cruises, rates of OC remineralization coupled to sulfate reduction did not much vary temporally (**Figure 3.10**). Conversely, the intensity of aerobic respiration was highly variable with globally higher rates in spring and lower ones in autumn (**Figure 3.10**). The amplitude of these seasonal variations was relatively low at the shallowest stations (e.g., stations 1 and 2; **Figures 3.9** and **3.10**) and increased seaward. The higher and lower rates of aerobic respiration were measured in April 2018 and October 2016, respectively. Interestingly, April 2018 corresponds to a cruise performed during the spring bloom and October 2016 to the one during which the longest stratification and the most pronounced deoxygenations were measured (Dubosq et al., 2022). This suggests that aerobic respiration rates in the WGMP are sensitive to seasonal events, and the occurrence of "hot" and "cold moments" for aerobic respiration rates, namely shorts periods with higher and lower reactions rates relative to longer periods (McClain et al., 2003).

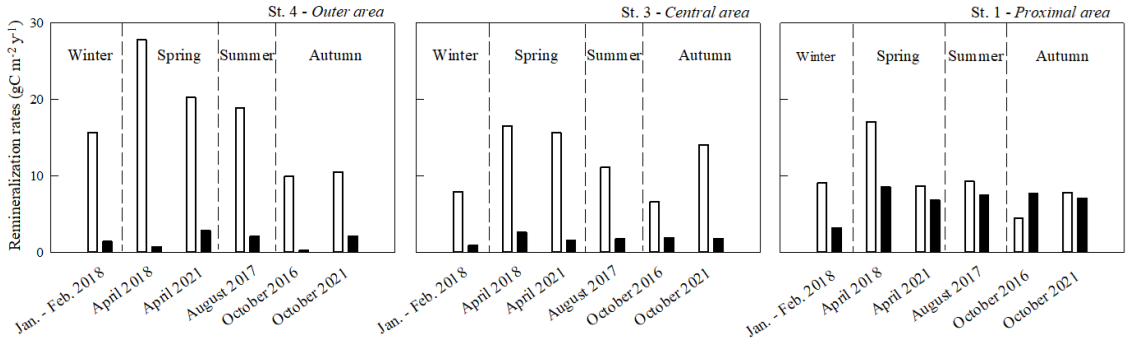

Figure 3.10: Seasonal variations of organic carbon remineralization rates by aerobic respiration (white) and sulfate reduction (black) at three sampled stations. Each station is representative of one of the three parts of the WGMP (*see section 3.4.1*).

3.4.3 Factors controlling the variability of organic carbon remineralization rates by aerobic respiration

Benthic oxygen consumption, and the associated rates of aerobic respiration, are influenced by numerous parameters as temperature (Braeckman et al., 2014; Jorgensen et al., 2022), availability of dissolved oxygen (Norkko et al., 2019; Rabouille et al., 2021), quantity and quality of organic matter inputs (Braeckman et al., 2014; Jorgensen et al., 2022; Pastor et al., 2011b), faunal abundances and its bioturbation activities (Arndt et al., 2013; Kristensen and Mikkelsen, 2003; Norkko et al., 2019), and sedimentary processes (Hulot et al., 2023).

A way to define the respective influence of these parameters on the variability of aerobic respiration rates is to build statistical models linking aerobic respiration rates with explanatory variables (e.g., Braeckman et al., 2014; Link et al., 2013). In this work, we built two models using a forward stepwise regression and a path-analysis. In the forward stepwise regression, the

explanatory variable that best and significantly improves the model is added at each step. The analysis ends when the addition of new variables no longer significantly improves the model. The path-analysis is a regression model that calculates path coefficients reflecting the relationships of the explanatory variables with aerobic respiration rates. Path coefficients do not correspond to simple correlations between aerobic respiration rates and the explanatory variables but also take into account the correlation of explanatory variables between them (Wright, 1934). Hence, compared to the forward stepwise regression, this analysis allows unravelling the influence of co-correlated explanatory variables. Indeed, if two of them are correlated, the model attributes a higher coefficient to the best correlated with aerobic respiration rates and a lower coefficient to the second one. Positive coefficients indicate that an increase of the value of the explanatory variable induces an increase of aerobic respiration rates and conversely (Tritah and Daoud, 2021; Valenzuela and Bachmann, 2017).

Prior to performed analyses, the explanatory variables to be included in the models have been selected. If several variables were available to describe a same parameter (e.g., OC and THAA contents as descriptors of the quantity of organic matter), the best correlated with aerobic respiration rates was selected. The variables retained to build the models were:

1) The saturation of dissolved oxygen in bottom water, describing the deoxygenation of bottom water
2) The content of Phaeo-*a* in surface sediments, describing both the availability of labile organic matter and the intensity of primary production
3) The salinity of surface water, describing the inputs from the Gironde
4) The abundance of macrofauna, describing the quantity of benthic macrofauna

The temperature of bottom water and the content of THAA in surface sediments, which describes the quantity of organic matter available, were initially included in the models. However, as they negatively contributed to the models while an increase of these parameters typically enhanced remineralization rates (Braeckman et al., 2014; Jorgensen et al., 2022; Pastor et al., 2011b; Song et al., 2016), they have been excluded.

The model built with the stepwise forward regression explained 65.2% of the variability of aerobic respiration rates. The first variable included in the regression was the content of Phaeo-*a* in surface sediments ($r^2_{aj.}$ = 0.538). The oxygen saturation of bottom water was the second variable selected and improves the explanation of the variability of aerobic respiration rates of ~ 7% (r^2_{aj} = 0.610). The last variable that significantly improves the model was the abundance

of benthic macrofauna. Its addition improves the description of ~ 4% ($r^2aj.$ = 0.652). The salinity of surface water was not included because it did not significantly improve the model.

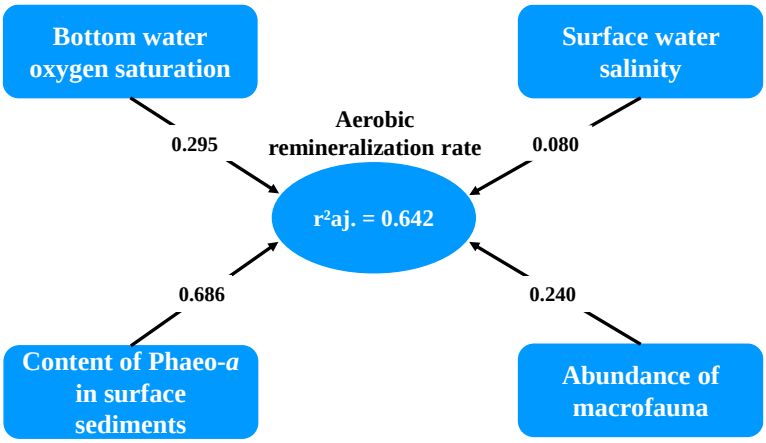

Figure 3.11: Path-analysis showing relationships of the variability of aerobic respiration rates at the SWI with several environmental parameters. The adjusted determination coefficient ($r^2aj.$) represents the part of the variance of aerobic respiration rates at the SWI explained by the combination of environmental parameters. Path coefficients are labeled on arrows linking explanatory variables to aerobic respiration rates. The analysis was performed using the software SmartPLS 4 (Ringle et al., 2022).

The model built using the path-analysis explained 64.2% of the variance of aerobic respiration rates at the SWI (**Figure 3.11**). It shows that the content of Phaeo-*a* in surface sediment explains the main part of the variance while bottom water oxygen saturation and abundances of macrofauna have almost equal contributions. At last, the low contribution of fluvial inputs described by surface salinity may be related to the fact that only one cruise was carried out during a flood (i.e., January – February 2018 ; Dubosq et al., 2022). The important contribution of the content of Phaeo-*a* in surface sediments, and so of primary production, is likely highly related to the cruise of April 2018 during which the highest Phaeo-*a* contents and aerobic respiration rates were concomitantly measured. Such an influence of organic matter inputs related to a bloom is classic for temperate coastal environments. However, it is usually restricted from days to weeks due to the high degradability of these labile compounds (Glud, 2008). In addition to this short-term effect, the influence of Phaeo-*a* contents on aerobic respiration rates is also likely due to the higher contents of pigments (i.e., Chl-*a* and Phaeo-*a*) usually measured at the station 4 (**Table 3.1**; Lamarque et al., 2022) that may partly explain the higher respiration rates measured at this station (**Figures 3.9** and **3.10**). The influence of macrofauna on aerobic respiration rates at the SWI may be related to an increase of the degradability of organic compounds through ingestion (Kristensen and Mikkelsen, 2003) and to a mixture of refractory with more labile compounds, which promotes co-oxidation processes usually referred to as "priming" (Aller and Cochran, 2019; Bianchi, 2012). These statistical models highlight the influence of seasonal events (i.e., spring bloom, deoxygenations) on the

variations of aerobic respiration rates at the SWI. This contrasts with anaerobic remineralization processes, which are more variable spatially than temporally (*see section 3.1*).

3.5 Total organic carbon remineralization rates and efficiencies in the WGMP

Estimates of OC remineralization rates based on diffusive fluxes have been useful to characterize the biogeochemical structuration and functioning of the WGMP. However, they do not take into account remineralization processes in relation to fauna activities. The sum of remineralization rates computed from diffusive fluxes therefore underestimates the total remineralization of OC in sediments. Indeed, it is not usually assessed from diffusive fluxes but rather goes through the estimate of Total Oxygen Uptakes (TOU) by sediments. TOU correspond to the quantity of oxygen consumed by heterotrophic metabolisms (fauna and microorganisms) and by the oxidation of reduced compounds produced during anaerobic remineralization of organic matter (Glud, 2008). As (1) the most of reduced compounds produced during organic matter remineralization are ultimately oxidized and (2) oxygen is the terminal electron acceptor, TOU are commonly used as a proxy of total benthic remineralization (Chen et al., 2022; Glud, 2008; Jorgensen et al., 2022).

In the WGMP, TOU ranged from 4.4 ± 1.2 to 12.1 ± 3.6 mmol m^{-2} d^{-1} (**Figure 3.12**). They were higher in the proximal area (i.e., stations 1 and 10) except in April 2021 when they were also high at the stations 2 and 3 with values of 11.4 ± 5.1 and 12.1 ± 3.6 mmol m^{-2} d^{-1}, respectively. Except these two high fluxes, TOU were rather similar from stations 2 to 4 with no marked seasonal differences (**Figure 3.12**). These results highlight a more intense organic matter remineralization at proximal stations. It is most likely due to higher abundance of benthic macrofauna (Lamarque et al., 2022). Indeed, oxygen consumption by fauna activities at these stations represents between 50 and 80% of the TOU (**Figure 3.12**). However, due to the transient nature of the surface layer, TOU most likely underestimate the total remineralization at proximal sites. Interestingly, although the station 4 is a hot spot for aerobic respiration at the SWI (*see section 3.4*), the similarity of TOU in the central and outer WGMP indicates that similar amounts of organic matter are remineralized from station 2 to station 4. The increase of the DOU/TOU ratio from ~ 0.5 at the station 2 to ~ 1 at the station 4 indicates that the influence of fauna activities on organic matter remineralization decreases with depth. It may influence remineralization (1) by direct remineralization or by enhancing the degradability of organic matter through ingestion and digestion (Glud, 2008; Jorgensen et al., 2022; Kristensen and Mikkelsen, 2003), (2) by enhancing organic matter degradation through injection of oxygen in anoxic sediments (Aller, 1994; Jorgensen et al., 2022; Kristensen, 2000; Kristensen and Mikkelsen, 2003) or (3) by priming (Aller, 1994; Aller and Cochran, 2019).

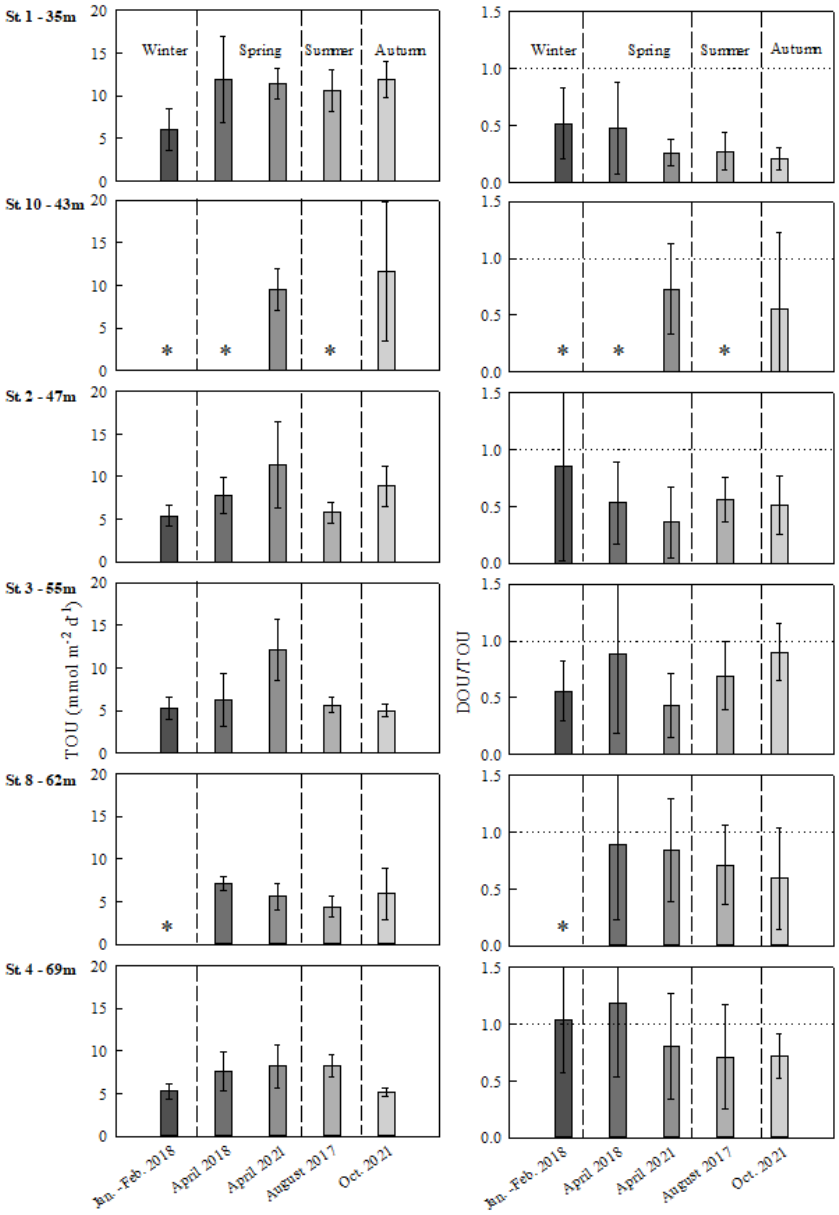

Figure 3.12: Total Oxygen Uptakes (TOU) and DOU/TOU ratios measured at the six stations of the WGMP investigated between 2017 and 2021. Asterisks (*) indicate that the station was not sampled during the cruise.

The wide use of TOU as a proxy of total remineralization allows comparing the intensity of remineralization in the WGMP with that of other systems. At global scale, mean TOU on inner and outer shelves are of 27 ± 16 and 14 ± 14 mmol m^{-2} d^{-1}, respectively (**Table 3.2** ; Jorgensen et al., 2022). In comparison, TOU and so the intensity of total remineralization in the WGMP are relatively low. More specifically, minimums TOU measured in the WGMP are consistent with those observed on other continental shelves while maximum values are in the lower range (**Table 3.2**). In fact, they are quite similar to values measured in sediments of the East China Sea shelf, which have relatively low organic carbon contents and are fueled with weakly labile organic matter (S.-H. Kim et al., 2020; Song et al., 2016). This similarity suggests that the low reactivity of the WGMP sediments could be related to the refractory character of organic matter

inputs from the Gironde (Etcheber et al., 2007; Savoye et al., 2012). Indeed prior to reach the continental shelf, it is extensively remineralized within the estuary turbid maximum, which acts as a fluidized bed reactor (Abril et al., 1999; Savoye et al., 2012). These observations therefore suggest an influence of Gironde inputs on the biogeochemical functioning of the WGMP.

Table 3.2: Total Oxygen Uptakes and organic carbon (OC) contents of sediments (when available) measured on several continental shelves and margins in various areas.

Location	System	Depth	OC	TOU	References
		m	%	mmol m^{-2} d^{-1}	
West European Shelf	West Gironde Mud Patch	30 - 70	0.26 - 1.52	4.4 - 12.1	*This study*
Global scale	Inner shelf	10 - 50		27 ± 16	Jørgensen et al., 2022
	Outer shelf	50 - 200		14 ± 14	
West European Shelf	Northwestern Adriatic coast	25 - 45		2.4 - 34.8	Tahey et al., 1996
	Gulf of Finland	36 - 75		6.3 - 17.7	Almroth et al., 2009
	Rhône prodelta	24 - 89	1.0 - 2.0	7.0 - 15.9	Pastor et al., 2011a, 2011b
		20 - 98	0.82 - 1.09	5.1 - 28.6	Lansard et al., 2008
		9 -192	0.82 - 2.38	3.7 - 23.8	Lansard et al., 2009
West Atlantic Shelf	Mid-Atlantic Bight	11 - 17	0.2 - 2.1	4.8 - 67	Laursen and Seitzinger, 2002
	Louisiana shelf	16 - 20		3.9 - 19.9	Murrell and Lehrter, 2011
	Gulf of Mexico	12 - 30		0.8 - 56.4	Rowe et al., 2002
	Eastern Canadian continental shelf	18 - 255		10.6 - 32.6	Grant et al., 1991
East Pacific Shelf	Washington shelf	42 - 161	0.6 - 1.8	5.3 - 18.3	Duineveld et al., 1997
Western Pacific Shelf	East China Sea shelf, Yellow Sea	17 - 81	0.21 - 1.20	1.7 - 17.6	Song et al., 2016
	East China Sea continental shelf	40 - 96	0.11 - 1.40	5.8 - 16.4	Kim et al., 2020
	New Zeland continental shelf	4.2 - 360	0.5 - 2.6	3.2 - 29.3	Giles et al., 2007
Arctic Shelf	Bering sea continental shelf	35 - 161		3.7 - 10.5	Rowe and Phoel, 1992
Indian Ocean Shelf	Kenyan shelf	50 - 200		9.8 - 36	Duineveld et al., 1997

As TOU represent the total remineralization, they can be converted in total OC remineralization rates using a respiratory quotient (RQ; i.e., OC/O_2 ratio ; Jørgensen et al., 2022; Kim et al., 2020). As RQ varies among environments depending on the nature of organic matter and was not yet estimated in the WGMP, we used a value of 0.85, which is representative of outer continental shelves (i.e., 50 - 200 m depth ; Jørgensen et al., 2022). Total OC remineralization rates were computed using mean values of the TOU measured from 2017 to 2021. As TOU are likely not a reliable proxy of total remineralization in the proximal area, calculations were restricted to the distal one.

Mean total benthic OC remineralization rates from station 2 to station 4 between 2017 and 2021 ranged from 21 ± 4 to 29 ± 9 gC m^{-2} y^{-1} (**Table 3.3**). Based on these values and on previously published OC carbon burial rates (Dubosq et al., 2021), it is possible to computed efficiencies of OC remineralization and burial (**Table 3.3** ; Kim et al., 2020; Middelburg, 2019).

Values of remineralization efficiencies (i.e., total OC remineralization rates/(total OC remineralization rates + OC burial rates)) indicate that less than half of the OC deposited in the WGMP is recycled on a multi-decennial scale. This results in high OC burial efficiencies, which are consistent with qualitative estimates based on OC/SA ratios (Dubosq et al., 2021). Given mass accumulations rates measured in the central and distal WGMP (Dubosq et al., 2021), burial efficiencies are consistent with that estimated in other marine environments at the global scale (Canfield, 1994; McKee et al., 2004). In comparison to RiOMars, OC burial efficiencies in the WGMP are close to that measured in RiOMars of type 3 (Blair and Aller, 2012). These environments correspond to systems of small mountainous river on active margins with moderate sediment accumulation rates but that receive highly refractory organic matter, which results in relatively high burial efficiencies (Blair and Aller, 2012). Concerning RiOMars located on passive margins, such high burial efficiencies (50 - 60%) at these sedimentation rates were measured on the Mackenzie shelf (Blair and Aller, 2012; Goñi et al., 2005). In this environment, high burial efficiencies are directly due to inputs of highly refractory organic matter (i.e., kerogen and pre-aged soil organic matter; Goñi et al., 2005). These comparisons reinforce the idea that inputs of poorly bioavailable organic matter from the Gironde (Etcheber et al., 2007; Savoye et al., 2012) are a major factor influencing biogeochemical processes and carbon cycle in the WGMP.

Table 3.3: Mean Total Oxygen Uptakes (TOU) computed from measurements performed at the stations 2, 3, 8 and 4 between 2017 and 2021. Total OC remineralization rates were calculated from mean TOU using a respiratory quotient of 0.85. Remineralization (and burial) efficiencies were computed as the ratios of total OC remineralization (or burial) rates to organic carbon inputs (i.e., sum of total OC remineralization and burial rates). *data from Dubosq et al. (2021)

	Mean TOU	Total OC benthic remineralization	OC burial rates*	Remineralization efficiency	Burial efficiency
	mmol m^{-2} d^{-1}	gC m^{-2} y^{-1}	gC m^{-2} y^{-1}	%	%
Station 2	7.9 ± 2.4	29 ± 9	32 ± 16	48 ± 39	52 ± 42
Station 3	6.8 ± 3.0	26 ± 11	36 ± 8	41 ± 27	59 ± 39
Station 8	5.8 ± 1.1	21 ± 4	45 ± 6	32 ± 11	68 ± 22
Station 4	6.9 ± 1.6	26 ± 6	44 ± 9	37 ± 16	63 ± 27

3.6 Consequences of the biogeochemical functioning of the WGMP

3.6.1 Sediment oxygen consumption: a key factor controlling the bottom water deoxygenation in the WGMP?

At global scale, RiOMars are among environments subjected to deoxygenations (Fennel and Testa, 2019; Wang et al., 2021). In these systems, sediment oxygen consumption may reach almost one third of the total consumption within the deoxygenated layer (Capet et al., 2013; Fennel and Testa, 2019; Yu et al., 2015). This value can even reach more than 50% in the few

meters above sediments as observed on the Louisiana shelf (Quiñones-Rivera et al., 2007; Yu et al., 2015). In these environments, deoxygenations are partly related to the stratification of the water column, isolating bottom water in which dissolved oxygen is progressively depleted (e.g., Cai et al., 2011; Feng et al., 2012; Wang et al., 2021). In the WGMP, the establishment of a thermal stratification induces a deoxygenation of bottom water whose the intensity increases with the duration of stratification (Dubosq et al., 2022). Moreover, a relation between dissolved oxygen concentrations and pH of bottom water showed that dissolved oxygen consumption was primarily related to respiration (Dubosq et al., 2022). Hence, to make a first assessment of the influence of the benthic compartment on deoxygenations, we estimated the role of sediment of oxygen consumption on the stock of dissolved oxygen in bottom water over the duration of the cruises of April 2018 and 2021, August 2017 and October 2021 (~ 14 days). The stock of dissolved oxygen was computed at each cruise based on (1) the volume of bottom water on a 1 m section from the proximal to the distal WGMP and (2) the average of dissolved oxygen concentrations measured in bottom water at studied stations. Results showed that at the scale of a cruise, the sediment may consume between 2.6 % (April 2018) and 3.6 % (October 2021) of the stock of dissolved oxygen in bottom water.

During the cruises of April and October 2021, the stations 1 and 10, located in the proximal area and spaced by ~ 6 km, were investigated 9 and 11 days apart, respectively. At the two periods, bottom oxygen concentrations were 3.2% (April 2021) and 3.7% (October 2021) lower at the station 10. Thus, considering the duration between the measurements at the two sites, we estimated that between 60 and 76% of the decrease of dissolved oxygen concentrations could be related to sediment consumption. These values are consistent with studies performed on other RiOMars (Quiñones-Rivera et al., 2007; Yu et al., 2015) and suggest an important role of the benthic compartment in the establishment of bottom water deoxygenations. However, it is important to note that these calculations were performed assuming a static water mass. Given the relatively weak residual currents on the Bay of Biscay continental shelf (i.e.; 3 cm s^{-1}; Le Boyer et al., 2013), this assumption seems reasonable for the duration considered in calculations. However, poleward current pulses of several days and mean velocities > 10 cm s^{-1} also occur on the continental shelf (Kersalé et al., 2016). Hence, an accurate estimate of the role of the benthic compartment on deoxygenations seems to require a better characterization of bottom water circulation and of the extension of deoxygenations as well as the quantification of benthic oxygen uptakes over a larger area of the continental shelf.

3.6.2 The WGMP sediment: a major source of nitrogenous nutrients for the continental shelf off the Gironde?

In the WGMP, the intensity of bottom water deoxygenation appears partly influenced by the intensity of primary production in the water column (Dubosq et al., 2022). As the intensity of primary production is closely related to the availability of nutrients, the relative contributions of the WGMP and of the Gironde estuary to nutrient inputs to the shelf have been estimated. Fluxes of nitrogenous nutrients (i.e., nitrate and ammonium) from the WGMP were computed by multiplying the average of nutrient fluxes measured from the stations 1 to 4 between August 2017 and October 2021 by the area of the WGMP (i.e., 420 km²). Nutrient supplies from the Gironde were computed based on (1) nitrate (34 – 154 µM) and ammonium (0.1 – 1.5 µM) concentrations measured at low tide, 1 m below the surface, near the mouth of the estuary (PK86 of the estuary ; Liénart et al., 2018) between August 2017 and October 2021 (one measure per month) and (2) the corresponding mean daily river discharge extracted from the data portal *hydro.eaufrance.fr*. Nitrate and ammonium concentrations in the Gironde were extracted from the SOMLIT database (*https://www.somlit.fr/gironde/*; Cocquempot et al., 2019). The flux of nitrogenous nutrients from the WGMP was of ~ 73 Mmol y^{-1} while that from the Gironde was of ~ 3.9 Gmol y^{-1}. The total input of nitrogenous nutrients from the WGMP to the water column represents less than 2% of that of the Gironde. The intensity of the primary production on the shelf off the Gironde appears therefore mainly supported by nutrient supplies from the Gironde. Accordingly, as the intensity of deoxygenations is likely influenced by that of primary production (Dubosq et al., 2022), nutrient supplies from the Gironde indirectly influence deoxygenations. Interestingly, this low contribution of the WGMP relative to that of the Gironde is of the same order of magnitude of that measured on the northern part of the East China Sea (S.-H. Kim et al., 2020). Indeed, in this area presenting TOU similar to that measured in the WGMP (**Table 3.2**), the benthic production of nitrogenous nutrients represents ~ 6% of the nitrogen requirements for primary production.

4. Conclusion

The processes of organic matter remineralization in sediments of the WGMP follow the classical diagenetic sequence. They are spatially structured with a clear distinction between the proximal and the distal area. In the proximal WGMP, the sedimentary context related to the high hydrodynamics results in a diagenetic regime divided into two layers with a high sulfate reduction within relic sediments. In fact, a comparative study of the iron and sulfur cycles highlights that the biogeochemical functioning of relic sediments is clearly different from the rest of the WGMP. In the distal area, sulfate reduction is lower and the diagenetic sequence gradually expands seaward likely due to a decrease in organic matter lability and/or an increase

in bioturbation. The distal area appears to be composed of two subareas, namely a central part with moderate aerobic respiration rates and an outer part, which is a hot spot for organic matter remineralization by aerobic respiration. The steady-state profiles of dissolved compounds between cruises suggest that biogeochemical processes do not vary much seasonally over the first decimeters of sediments. Only aerobic respiration rates presented marked temporal variations in response to seasonal events such as spring bloom and the deoxygenation of bottom water. The intensity of total organic carbon remineralization is low in comparison to other continental shelves, likely due to the relatively low and refractory organic matter inputs from the Gironde. Owing to the characteristics of the area (i.e., fluvial discharge, mean significant wave height, hydrodynamics dominated by storms and waves), the WGMP does not act as an organic matter incinerator like the high-energy RiOMars included in the classification of Blair and Aller (2012). Indeed, less than half of organic carbon inputs to the WGMP would be recycled. This suggests that it may belong to a fourth category of RiOMars that needs to be accurately characterized.

Points clés du Chapitre 3

- Dans les sédiments de la Vasière Ouest Gironde, la matière organique est reminéralisée selon la séquence diagénétique classique.
- La Vasière Ouest Gironde peut être divisée en :
    - Une zone proximale où l'important hydrodynamisme induit un régime diagénétique en deux couches, une moderne et une relique, avec notamment une importante réduction des sulfates dans les sédiments reliques.
    - Une zone distale caractérisée par une plus faible réduction des sulfates et par une dilation de la séquence diagénétique vers le large.
- La zone distale peut être subdivisée en une zone centrale où l'intensité de la respiration aérobie est modérée et une zone externe où elle est significativement plus importante.
- Les variations de l'intensité de la respiration aérobie semblent être principalement liées à des évènements saisonniers tels que l'efflorescence printanière ou les désoxygénations des eaux de fond.
- L'intensité des processus de reminéralisation anaérobies ne semble pas varier saisonnièrement.
- Comparativement à d'autres environnements de plateaux continentaux, l'intensité de la reminéralisation du carbone organique dans les sédiments de la Vasière Ouest Gironde est assez faible, probablement en raison des apports de matière organique peu bio-disponibles de la Gironde.
- A l'échelle pluridécennale, moins de la moitié du carbone organique déposé est reminéralisé.
- En raison des caractéristiques de son environnement de dépôt, le fonctionnement biogéochimique de la Vasière Ouest Gironde diffère de celui des RiOMars de haute énergie (type 1) inclus dans la classification de Blair and Aller (2012).
- La Vasière Ouest Gironde semble correspondre à un quatrième type de RiOMars.

Chapitre 4

Processus de diagenèse précoce à l'échelle pluriséculaire dans un système de marge continentale tempérée sous l'influence d'un grand fleuve (La Vasière Ouest Gironde, golfe de Gascogne)

Dubosq N.[1], Deflandre B.[1], Rigaud S.[2], Eynaud F.[1], Danilo M.[1], Cordier M-A.[3], Perello M-C.[1], Labourdette N.[3], Grémare A.[1], Schmidt S.[3]

[1] Univ. Bordeaux, CNRS, Bordeaux INP, EPOC, UMR 5805, F-33600 Pessac, France
[2] Université de Nîmes, EA 7352 CHROME, F-30021 Nîmes, France
[3] CNRS, Univ. Bordeaux, Bordeaux INP, EPOC, UMR 5805, F-33600 Pessac, France

Chapitre écrit sous la forme d'un article – *A soumettre*

Les chapitres précédents se sont attachés à caractériser la structuration et le fonctionnement biogéochimique de la Vasière Ouest Gironde de l'échelle saisonnière à pluridécennale. Afin de compléter ce travail, des carottes sédimentaires d'environ 3 m ont été prélevées et analysées. Cela a permis de caractériser le recyclage et le stockage du carbone organique ainsi que le devenir de différents éléments impliqués dans les processus de la diagenèse précoce (Mn, Fe, P, S, Ca, Si) à l'échelle pluriséculaire.

Résumé

Les marges continentales sous l'influence de grands fleuves sont des environnements majeurs pour le recyclage et le stockage du carbone organique et des éléments qui lui sont associés. Malgré cette importance, la caractérisation de leur fonctionnement biogéochimique à partir de carottes pluri-métriques a été principalement restreinte à de grands systèmes tropicaux et subtropicaux tels que le delta de l'Amazone ou encore la ceinture de vase de la mer de Chine orientale. Afin de compléter la caractérisation du fonctionnement biogéochimique des marges continentales sous l'influence de grands fleuves à l'échelle pluriséculaire, la Vasière Ouest Gironde (VOG) est prise comme modèle de système tempéré soumis à un fort hydrodynamisme. Des carottes d'interface et des carottes « Kullenberg » pluri-métriques ont été échantillonnées à deux stations, localisées dans la zone centrale et la zone distale de la VOG. Ces carottes ont été datées et leurs caractéristiques physiques et biogéochimiques ont été analysées. Dans ces dépôts sédimentaires couvrant les 400 dernières années, la matière organique est reminéralisée selon la séquence diagénétique classique. Aux deux stations étudiées, la réduction des sulfates est limitée en profondeur. Cela semble lié à la labilité et la biodisponibilité de la matière organique, en partie contrôlée par son adsorption sur les particules sédimentaires qui la protège de la dégradation. En profondeur des carottes, la constance de la charge en carbone organique des sédiments (i.e., 0.40 – 0.59 mgC m^{-2}) montre que la quantité de matière organique préservée à l'échelle pluriséculaire est en partie contrôlée par la taille des particules déposées. Ces valeurs indiquent également que la VOG n'agit pas comme un « incinérateur » pour la matière organique, contrairement aux marges continentales de haute énergie sous l'influence de grands fleuves déjà étudiées. Les mesures de phases particulaires et dissoutes ainsi que le calcul d'indices de saturation des eaux porales vis-à-vis de plusieurs phases minérales indiquent que la VOG est un puits pour plusieurs éléments via l'adsorption sur les particules sédimentaires (carbone organique, fer, manganèse) ou la précipitation de minéraux authigènes comme l'apatite (P), la pyrite (S) ou les argiles (Si). Une augmentation de la granulométrie des particules déposées, estimée au début du 20^{e} siècle, semble avoir diminué la capacité de la VOG à stocker le carbone organique, le soufre, le fer, le manganèse et le phosphore. Cette diminution, qui affecte probablement la séquestration de certains contaminants métalliques dont les oxyhydroxydes de manganèse et de fer sont des phases porteuses, pourrait s'accentuer en raison des changements globaux actuels.

Mots-clés : RiOMar, plateau continental, diagenèse précoce, carbone organique, biogéochimie

1. Introduction

Continental margins influenced by large rivers have primary production, sedimentation and organic carbon (OC) burial rates among the highest of oceanic environments (McKee et al., 2004). These systems are therefore of major importance for global biogeochemical cycles. Indeed, it is estimated that about 90% of oceanic OC burial occurs in these environments (Hedges and Keil, 1995; McKee et al., 2004). However, it is also evaluated that between 55 and 80% of riverine organic matter inputs are degraded within River-dominated Ocean Margins (RiOMars, Burdige, 2005; Blair and Aller, 2012). In sediments, this degradation follows a sequence of reactions, the order of which depends on their free energy yield (Froelich et al., 1979). The by-products of these reactions can react with other compounds to form authigenic phases such as carbonates (Middelburg et al., 1987; Mucci, 2004, 1988), pyrite (Jorgensen et al., 2019), apatite (Ruttenberg and Berner, 1993), vivianite (Egger et al., 2015; Rothe et al., 2016) or authigenic clays (Chong et al., 2018; Michalopoulos and Aller, 2004). The formation of these minerals and their compositions depend on many factors as their solubility (Middelburg et al., 1987), the kinetics of precipitation (Mucci, 1988), the concentrations of dissolved compounds that favor or inhibit precipitation (Michalopoulos and Aller, 2004; Mucci, 2004, 1986) or the interaction with other biogeochemical processes (Egger et al., 2015).

The study of multi-metric sediment cores allows the characterization of organic matter remineralization and burial of OC and other elements on a multi-century or even longer time scales (Charbonnier et al., 2019). With respect to RiOMars, studies of early diagenesis processes based on such long cores have been extensively conducted on the continental shelf influenced by the Amazon river (Aller et al., 1991, 1996, 1986; Aller and Blair, 2006, 1996; Michalopoulos and Aller, 2004). It is an energetic environment where the frequent resuspension of sediments and the large inputs of reactive iron result in the dominance of suboxic remineralization processes and an efficient remineralization of organic matter (Aller et al., 1996, 1986; Aller and Blair, 1996). In this system, only few sulfide minerals are formed and authigenic minerals are typical of low sulfate environments (e.g., siderite and vivianite ; Aller et al., 1986). In addition, large inputs of reactive iron favor the formation of authigenic clays from dissolved silica and cations such as iron, potassium or magnesium (Aller, 2014; Michalopoulos and Aller, 2004). A study conducted on the inner shelf of the East China Sea showed that subtropical mobile mud belts have the same main characteristics as tropical ones (Zhu et al., 2016). In deeper areas of these environments, which are less affected by hydrodynamics as well as in sediments underlying mobile muds, diagenesis is dominated by sulfidic conditions and more pyrite formation occurs (Aller et al., 2004; Lin et al., 2000). In low-energy RiOMars, iron and sulfur are typically buried in the form of iron sulfide minerals

(Aller et al., 2004; Pastor et al., 2011a; Sommerfield et al., 2001). Studies of long cores performed in RiOMars have focused on tropical and subtropical deltaic systems, such as the East China Sea mobile mud belt or the Amazon and Mississippi deltas. However, studies of diagenetic processes in high-energy RiOMars in temperate regions are still scarce, especially on relatively long time scales.

In this context, the West Gironde Mud Patch (WGMP) appears of particular interest because it is a temperate non-deltaic RiOMar located in a high-energy environment (i.e., the Bay of Biscay continental shelf, Northeast Atlantic). Long-term diagenetic transformations have recently been studied on the continental slope of the southern part of the Bay of Biscay, from 150 to 2000 m depth (Charbonnier et al., 2019). In these sediments, remineralization of organic matter mainly occurs through sulfate reduction and methane genesis. Futhermore, measurements of dissolved and particulate compounds indicate the precipitation of authigenic carbonates and phosphorus minerals. However, long-term diagenetic transformations on the continental shelf off the Gironde, one of the main rivers flowing into the Bay of Biscay, have yet to be characterized. In fact, until now, biogeochemical studies carried out on the WGMP were limited to interface cores (Massé et al., 2016; Relexans et al., 1992). Moreover, the study of element burial has been focused on the OC (Dubosq et al., 2021). This study therefore aims to characterize, on a multi-century scale, (1) the processes of organic matter remineralization and their controlling factors, (2) the efficiency of OC sequestration and (3) the fate of other elements involved in early diagenesis (i.e., Mn, Fe, P, S, Ca and Si) in the sediments of the WGMP. Through this work, this study aims to complete the characterization of the biogeochemical functioning of RiOMars on a multi-century scale by using the WGMP as a model of a temperate and energetic RiOMar.

2. Material and methods

2.1 Study site

The West Gironde Mud Patch is a well-defined temperate sedimentary patch located on the continental shelf of the Bay of Biscay, ~ 40 km off the Gironde (**Figure 4.1**). It is surrounded by sands and extends between 30 and 75 m depth with an area of ~ 420 km^2 (Massé et al., 2016). It is directly influenced by sediment inputs from the Gironde, which are higher during river floods (Constantin et al., 2018; Jouanneau et al., 1989; Lesueur et al., 2002; Weber et al., 1991). However, due to the relatively long residence time of particles in the estuary (12 - 24 months ; Saari et al., 2010), which acts as a fluidized bed reactor, organic matter inputs to the shelf are poorly bioavailable (Abril et al., 1999; Savoye et al., 2012). The WGMP is also subject to a high hydrodynamics associated with storms and swells whose the amplitude can reach 15 m

on a decennial scale and 25 m on a centennial scale (Cirac et al., 2000; Jouanneau et al., 1989). The high hydrodynamics of the area controls the amount and type of the sediments currently deposited in the WGMP (Dubosq et al., 2021). In its proximal shallow part, recent deposits are mainly composed of sands and overlay finer relic sediments. Conversely, in the central and distal areas, which are less subject to hydrodynamics, a more continuous silty clay sedimentation occurs (Dubosq et al., 2021).

2.2 Sampling

The JERICObent-7 cruise took place in July 2019 on the R/V "Côtes de la Manche" (Deflandre, 2019). Cores of ~ 3 m length were sampled in the central and distal parts of the WGMP using a Kullenberg corer (**Figure 4.1**). Due to the potential loss of the sediment core top during coring, undisturbed interface cores were sampled with an UWITEC® monocorer. Interface cores were sliced under a dinitrogen atmosphere every 0.5 cm over the first cm then every 1 cm until 4 cm and every 2 cm until the core bottom. Kullenberg cores were first cut into sections of 50 cm then sliced under a dinitrogen atmosphere. The two first and last cm of each section that had been exposed to the air were removed. For the first section, 3 cm of sediments were sampled every 5 cm to have a sufficient resolution to make a reliable connection with interface cores. For the following sections, this sampling was performed every 10 cm until reaching the bottom of the section or underlying sands and gravels. Each slice was first subsampled for methane and particulate sulfides measurements using truncated syringes. Samples for methane analyses were sealed in pre-weighted glass vials with 1 mL of 1 M NaOH. Syringes for particulate sulfide measurements were put in anaerobic hermetic sealed jars and stored in the freezer. Sediments were then subsampled and frozen for porosity and solid phase analyses. The remaining sediment was centrifuged under a dinitrogen atmosphere to recover sediment pore waters that were filtered (0.2 µm), treated and stored according to the subsequent analyses to be performed. An interface core was sampled and maintained in *in situ* conditions for the determination of the oxygen (O_2) penetration depth. Profiles of O_2 were performed within 3 hours after sampling using Clark-type microelectrodes (Revsbech, 1989) with a tip diameter of 100 µm and a response time < 5 seconds (OX-100 *Unisense S/A*) and a Field Microprofiling System coupled to a motorized micromanipulator controlled by a computer (*Unisense S/A*). An interface core was carefully extruded for radionuclides analyses, every 0.5 cm until 4 cm depth then every 1 cm until the core bottom.

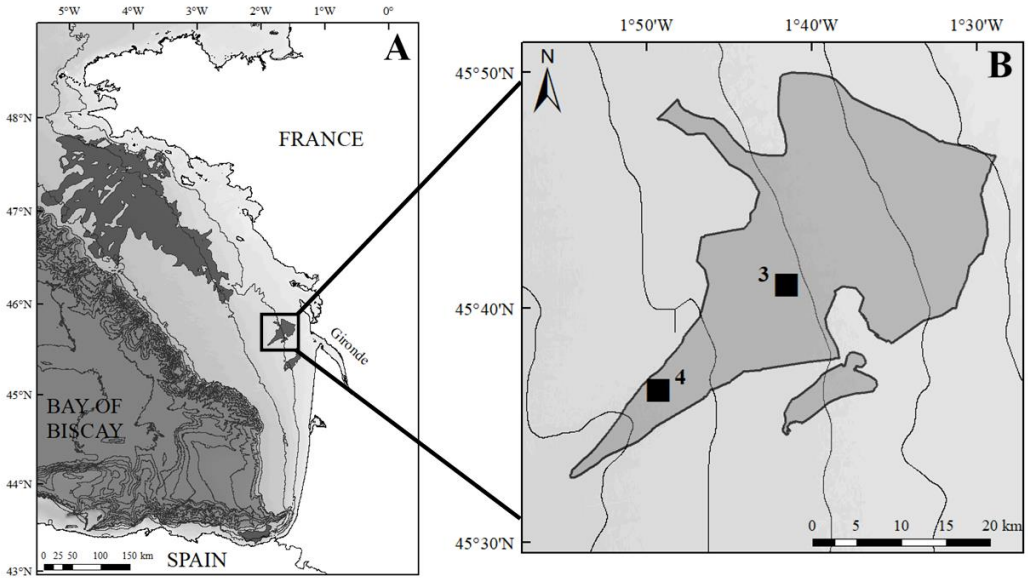

Figure 4.1: Maps of the Bay of Biscay with the locations of mud patches (gray areas, **A**) and of the WGMP with the locations of sampling stations (**B**).

2.3 Physical characteristics of sediments

Sediment porosity was assessed by comparing sediment weight before and after freeze-drying by assuming a particle density of 2.65 g cm^{-3}. Porosity was corrected for salt content (Burdige, 2006). Sediment grain-size was measured on freeze-dried sediments using a Malvern Mastersizer 2000 laser particle size analyzer. Surface area (SA) of sediments was measured on a subsample of freeze-dried sediment using a Gemini® VII Surface Area Analyzer (2390a model; Micromeritics®) by a multi-point BET method (Aller and Blair, 2006; Mayer, 1994a). Sediment was homogenized and degassed overnight at 150°C prior to the analysis.

2.4 Radiocarbon ages and ^{210}Pb

Profiles of ^{210}Pb in excess ($^{210}Pb_{xs}$, $T_{1/2}$ = 22.3 years) were established based on ^{210}Pb and ^{226}Ra measurements performed on interface and Kullenberg cores using a high efficiency, broad energy gamma detector equipped with a Cryo-Cycle II (Mirion) (Dubosq et al., 2021). These profiles were used to reconcile interface and Kullenberg cores and to estimate current sedimentation rates.

Radiocarbon ($T_{1/2}$ = 5730 years) dating were performed on carbonated shells sampled in sediments. The measurements were carried out by the "Laboratoire de Mesure du Carbone 14" (LMC14, Saclay, France) using an Accelerator Mass Spectrometer. However, due to the scarcity of shells, only a few layers have been dated. Radiocarbon ages were corrected for the local reservoir age, which corresponds to an offset between atmospheric and marine dating due to the lower ^{14}C activity in the ocean compared to the atmosphere (Alves et al., 2018). This difference is related to the lower content and longer residence time of ^{14}C in the ocean. For this study, the local reservoir age (i.e., 495 ± 17 years) was estimated from the difference between

radiocarbon ages and those estimated from the ^{210}Pb-based chronology at the same depth (Treinen-Crespo et al., 2021). The local reservoir age estimated from our data is consistent with that previously used in the Bay of Biscay (i.e., 405 years ; Mary et al., 2017).The oldest age measured in our cores (464 ± 47 years) was determined at the station 3, on shells sampled within a muddy layer mixed with the sandy substratum (**Figure 4.2**). The age of the lower limit of the homogeneous mud deposits is estimated to be 344 ± 47 and 399 ± 47 years at the stations 3 and 4, respectively (**Figure 4.2**). Thus, the two cores cover almost the same period, namely the last 400 years. However, the lower thickness of mud deposits at the distal site (i.e., station 4) suggests a lower overall sedimentation rate compared to the central site (i.e, station 3). These results are consistent with previous dating performed at the base of mud deposits, which estimated that most of the WGMP sediments were deposited in the last five to six centuries (Lesueur et al., 2002, 1996). Interestingly, the agreement between ^{14}C and ^{210}Pb-dating (**Figure 4.2**) suggests a fairly constant mean sedimentation rate throughout the evolution of the WGMP.

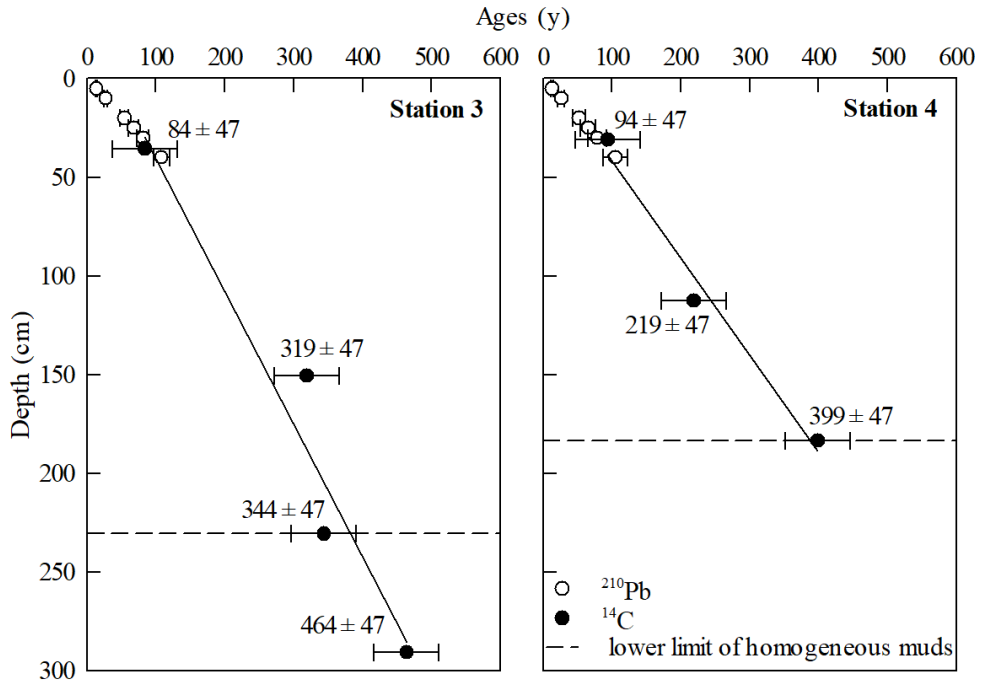

Figure 4.2: Ages of deposits in the central and distal areas of the WGMP assessed from ^{14}C and $^{210}Pb_{xs}$ measurements. Labels correspond to radiocarbon ages.

2.5 Pore waters analyses

Pore waters were analyzed for nutrients using a QuAAtro (nitrate, nitrite and ammonium) and an AA3 (dissolved silicate) continuous segmented flow analyzers (*Seal Analytical*, Aminot and Kérouel, 2007). The measurement of certified standards showed (*MOOS, NRCC*) a reproducibility better than 2%. Dissolved iron (Stookey, 1970), manganese (Charbonnier and Anschutz, 2019; Madison et al., 2011), inorganic phosphorus (Murphy and Riley, 1962) and sulfides (Fonselius et al., 1999) were measured by spectrophotometry. Major dissolved

compounds (i.e., Cl^-, SO_4^{2-}, Ca^{2+}, K^+, Na^+, Mg^{2+}) were measured by ionic chromatography (Dionex Corporation, 1986). Concentrations of dissolved inorganic carbon (DIC) were assessed by flow injection analysis according to Hall and Aller (1992). The reproducibility of these analyses was better than 5%. pH was measured using a micro-probe just after recovering pore waters by centrifugation. Methane concentrations were measured using an HP 5890A gas chromatograph with a reproducibility better than 5%.

Profiles of dissolved oxygen (10 and 15 profiles for stations 3 and 4, respectively) were processed using the software ProbeFlux, an improved version of PrO_2Flux (Deflandre and Duchêne, 2010). It allows defining the sediment-water interface and the oxygen penetration depth. For each profile, microelectrodes were recalibrated from the O_2 concentration measured a few cm above the sediment-water interface with a SDOT 300 equipped with an Aanderaa 3835 ADDI optode (*NKE Instrumentation)* and the zero-oxygen concentration in the anoxic sediment.

2.6 Solid phase analyses

Particulate organic carbon (OC), total carbon and nitrogen contents were measured on a subsample of crushed homogenized freeze-dried sediments using a CHN analyzer. For OC measurements, sediments were first acidified with HCl 10% to remove carbonates. Contents of inorganic carbon were assessed by the difference of total and OC contents then converted in carbonate contents considering that most inorganic carbon corresponds to calcium carbonates. Stable carbon isotopic ratio ($\delta^{13}C$) of OC was measured on decarbonated (0.5 M H_2SO_4) crushed freeze-dried sediments using a Sercon® IRMS. Chlorophyll–*a* (Chl-*a*) and Phaeophytin-*a* (Phaeo-*a*) contents were measured on thawed frozen sediments using a Perkin Elmer® LS-55 spectrofluorometer after an overnight extraction with 90% acetone (Neveux and Lantoine, 1993). The Chl-*a*/(Chl-*a* + Phaeo-*a*) ratio was used as a descriptor of the lability of vegetal biomass. Contents of Total and Enzymatically Hydrolysable Amino Acids (THAA and EHAA, respectively) were measured on triplicates on freeze-dried sediments. THAA were extracted by an acid hydrolysis (6 M HCl) during 24h at 110°C. EHAA were extracted according to the biometric method approach (Mayer et al., 1995). THAA and EHAA were analyzed by derivation to form fluorescent amino compounds that were separated by reverse-phase High-Performance Liquid Chromatography (1260 Infinity model, *Agilent*) on a Phenomenex® Kinetex 5 µm EVO C18 column and detected by fluorescence from 340 to 450 nm using an excitation wavelength of 338 nm. The EHAA/THAA ratio was used as a descriptor of bulk organic matter lability (Grémare et al., 2005). Due to the time required to perform extractions and to the availability of the equipment, amino acids were only measured on

selected layers of the cores sampled at the station 3. These layers were selected based on OC and pigments data.

Selective extractions were performed on 100 mg of a subsample of crushed homogenized freeze-dried sediments to assess particulate contents of manganese, iron and phosphorus (Anschutz and Deborde, 2016). The most reactive fraction (Mn_{Asc}, $Fe_{Asc,}$ P_{Asc}) was extracted with an ascorbate solution under shaking for 24h (Anschutz et al., 2005; Kostka and Luther, 1994). This fraction includes amorphous manganese and iron oxyhydroxydes (easily reducible) and the associated phosphorus (Anschutz et al., 2005; Anschutz and Deborde, 2016). The acid-soluble fraction (Mn_{HCl}, $Fe_{HCl,}$ P_{HCl}) was extracted using a solution of 1 M HCl under shaking for 24h. This fraction includes that extracted with the ascorbate leaching but also more crystallized iron and manganese oxyhydroxydes, iron monosulfides, carbonates and hydrous-aluminosilicates, authigenic, biogenic and detrital apatite (Kostka and Luther, 1994; Raiswell et al., 1994; Ruttenberg, 1992). Extracted iron, manganese and phosphorus were then measured in the centrifuged and diluted (1:10) extraction solution by spectrophotometry according to Stookey (1970) for iron, Anschutz and Deborde (2016) for phosphorus and Charbonnier and Anschutz (2019) for manganese. The analysis of a standard (MESS-2, *NRCC*) showed a reproducibility of these measurements better than 7%.

Acid Volatile Sulfides (AVS) and Chromium Reducible Sulfides (CRS) were sequentially extracted on 2 - 5 g of thawed frozen sediments in close jars under a dinitrogen atmosphere (Gagnon et al., 1995; Hsieh and Yang, 1989). AVS include mackinawite and poorly crystalized greigite while CRS correspond to sulfur associated with pyrite (Gagnon et al., 1995; Hsieh and Yang, 1989; Rickard and Morse, 2005). AVS were extracted at room temperature during 18h using a 20% $SnCl_2$ solution in 9 M HCl. H_2S produced were trapped in a 20% ZnAc solution in 2 M NaOH (Gagnon et al., 1995; Hsieh and Yang, 1989). After the replacement of the trap under a dinitrogen atmosphere, CRS were extracted during 48h at room temperature using a 1 M $CrCl_2$ solution in 0.5 M HCl (Gagnon et al., 1995). All solutions were degassed with dinitrogen prior to extractions. Trapped sulfides were then measured by spectrophotometry according to the method of Fonselius et al., (1999) modified to measure high sulfide concentrations. On interface cores, CRS measurements were restricted to the distal site.

2.7 Data treatments

Saturation indexes of pore waters with respect to calcite, hydroxyapatite, rhodochrosite and manganese sulfide were computed based on pH and the concentrations of dissolved compounds using the software PHREEQC (Parkhurst and Appelo, 1999). The significance of the correlations between surface area of sediments and particulate manganese and iron and between

particulate iron and phosphorus contents were assessed using Spearman's rank correlation coefficients (software SigmaPlot 14).

3. Results

3.1 Physical characteristics of sediments and organic compounds

At the two sites, vertical distributions of median grain-size (D50) varied similarly and allowed dividing the cores in three distinct sections. The first top three decimeters of sediments presented a median grain-size around 20 µm (**Figure 4.3**). Then, it decreased to ~ 10 µm and remained almost constant until the base of muddy sediments that overlaid a coarser sandy substratum (**Figure 4.3**). The transition from the substratum to homogeneous muds was progressive at the central site but sharp at the distal one. Consistently with dating, both stations presented almost the same sedimentary sequence but on a lower thickness in the distal area. A noticeable difference between the two sites was a layer of coarser sediments (D50 ~ 21 µm) at 60.5 cm depth at the central site (**Figure 4.3**).

At the station 3, OC contents presented a classical decrease with depth over the first 20 cm from ~ 1.1 to 0.6 – 0.7 %. Then, they unusually increased from 35 - 40 cm depth to values between 0.8 and 1.1% (**Figure 4.3**). As this variation was concomitant with a shift of D50, OC contents were normalized to particle surface area (SA) to minimize variations strictly related to grain - size changes (Aller and Blair, 2006; Mayer, 1994a, 1994b). OC loads (i.e., OC/SA ratios) were of 1.52 mgC m^{-2} at the sediment-water interface (SWI) and decreased with depth to values of 0.40 - 0.56 mgC m^{-2} at ~ 40 - 50 cm depth. Then, they were relatively constant until the base of muddy sediments and increased in the bottom sandy layers (**Figure 4.3**). At the distal site, the profile of OC loads was similar in muddy sediments. However, except for the deeper layer, sandy deposits of the substratum did not have higher OC loads than the rest of the core. The lability of bulk organic matter, assessed with the EHAA/THAA ratio, was the highest at the SWI (31 ± 2 %) and decreased with depth to values ranging from 13% to 18% (**Figure 4.3**). Interestingly, the coarser layer observed at 60.5 cm depth at the central station was characterized by a lower lability of organic matter with an EHAA/THAA ratio of 10%.

Depth profiles of Chl-*a* and Phaeo-*a* contents had a shape close to those of OC contents with a maximum at the SWI followed by a gradual decrease with depth until reaching quite constant values (**Figure 4.3**). Interestingly, these values were close to zero for Chl-*a* (< 0.2 µg g^{-1}) but between 2 and 3 µg g^{-1} for Phaeo-*a*. The lability of vegetal biomass, assessed with the Chl-*a*/(Chl-*a*+Phaeo-*a*) ratio, decreased with depth from ~ 12% at the core top to values ~ 5% between 10 and 20 cm.

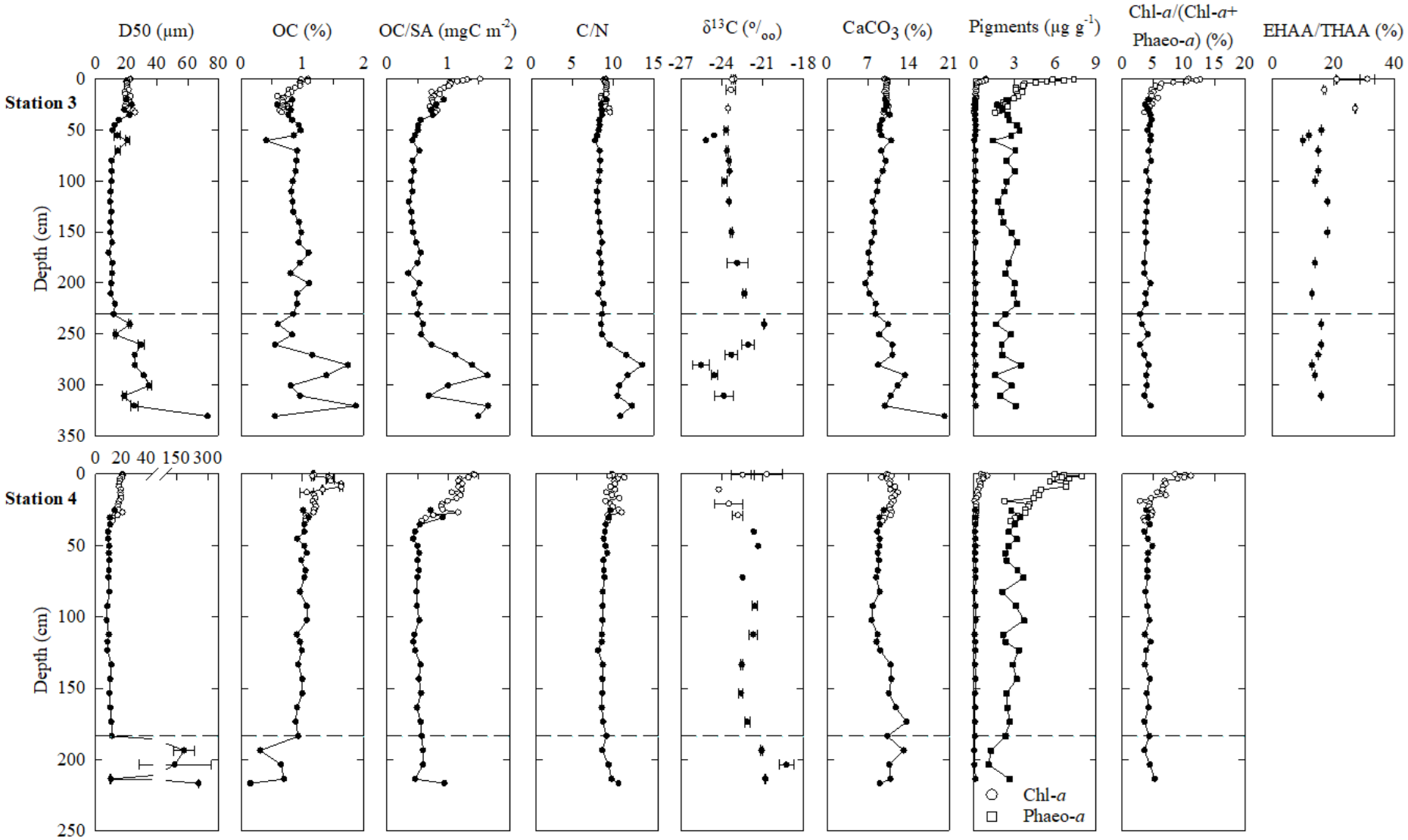

Figure 4.3: Depth profiles of median grain size (D50), OC content, OC load (OC/SA), C/N, $\delta^{13}C$, carbonate and pigment contents, Chl-*a*/(Chl-*a*+Phaeo-*a*) and EHAA/THAA ratios in interface (white) and Kullenberg (black) cores collected in the central and distal WGMP. The dash line represents the lower limit of homogeneous muddy sediments.

Depth profiles of the C/N ratio were similar at both sites with slightly higher values in the top 30 cm (i.e, from 8.5 to 10.5) than in the finer sediments below 40 cm depth (~ 8.0 - 8.5). Conversely, vertical distributions of $\delta^{13}C$ differed between the two stations. At the central site, it was rather constant over the first 200 cm of sediments with values between -23.1 and -23.8 ‰ and increased at -20.9 ‰ at the base of muddy sediments (**Figure 4.3**). At the distal site, $\delta^{13}C$ was highly variable in the first 30 cm of sediments (i.e., from -20.7 to -24.2 ‰). In the finer sediments below, it less varied and was higher (i.e., from -21.3 to -22.6 ‰) than at the central site. At last, sandy deposits at the core bottom of the central station were characterized by lower values of $\delta^{13}C$, which is consistent with the higher C/N ratios. On the contrary, the bottom layers of the distal station had a higher $\delta^{13}C$ than the rest of the core with values up to -19.3 ‰ (**Figure 4.3**).

3.2 Pore waters composition

At both stations, the vertical distribution of dissolved redox compounds showed a classic diagenetic sequence. Dissolved oxygen concentrations presented a sharp gradient at the SWI with penetration depths of 0.39 ± 0.10 and 0.49 ± 0.05 cm at the central and distal stations, respectively (**Figure 4.4**). Nitrate concentrations decreased from the SWI until to disappear between 2 and 10 cm depth. Depth profiles of dissolved iron and manganese had the same shapes with a maximum a few centimeters below the SWI followed by a progressive decrease with depth until reaching low and constant values (**Figure 4.4**). Interestingly, background concentrations of dissolved iron were close to zero in depth (< 5 µM) while that of dissolved manganese ranged from 4 to 17 µM. Below the maximum of dissolved iron, sulfate concentrations progressively decreased at both stations (**Figure 4.4**). At the central site, this decrease was more sharply in the first 70.5 cm. Then, sulfate concentrations decreased almost linearly until reaching constant values (~ 7 mM) around 230 cm. This stabilisation of sulfate concentrations was also observed at the distal site but less deeply (i.e., 153 cm). At this station, a gradient of sulfate concentrations in the first decimeters was not clearly observed, although lower concentrations were measured in the Kullenberg core. As sulfate was not totally consummed, methane concentrations were not surprisingly low (< 4 µM; data not shown). Surprisingly, sulfide concentrations remained always below 3 µM (data not shown).

Concentrations of the by-products of organic matter remineralization (i.e., ammonium, DIC, DIP) increased with depth. The increases of DIC and ammonium reflected almost exactly the depletion of sulfate. Indeed, at the central site their concentration gradients were higher in the first 70 cm. Then, their concentrations increased almost linearly with depth until constant values (**Figure 4.4**). Although DIP also accumulated with depth, its concentrations were rather

constant between 60 and 140 cm, contrary to ammonium and DIC. Depth profiles of these compounds showed almost the same variations at the distal site.

Concentrations of some other dissolved compounds that are not involved in organic matter remineralization also varied with depth. Vertical distributions of calcium were similar at both sites with constant concentrations (~ 10.3 mM) in the top 30 cm followed by a decrease with depth until ~ 5 mM at the base of muddy sediments (**Figure 4.4**). Magnesium concentrations also decreased with depth at both sites from ~ 54 mM at the SWI to ~ 50 – 51 mM at the bottom of the cores. Profiles of dissolved silica showed classic shapes (Chong et al., 2018; Dixit et al., 2001). Indeed, concentrations were low in bottom water (< 5 µM), markly higher in the first centimeter of sediment (~ 130 – 170 µM) and progressively increased with depth until reaching a maximum between 5 and 20 cm. Below this maximum, concentrations decreased then remained relatively constant ~ 270 – 280 µM (**Figure 4.4**).

3.3 Inorganic particulate compounds

Contents of particulate manganese, iron and phosphorus showed similar variations with depth at both sites. Over the first centimeters, they decreased until almost constant values (**Figure 4.4**). This was more marked for manganese due to an important accumulation of reactive oxyhydroxydes at the SWI. These decreases were concomitant with an increase of the concentrations of their respective dissolved forms (**Figure 4.4**). However, because DIP is a by-product of organic matter remineralization, its concentrations continued to increase after the stabilization of particulate phosphorus contents in contrast to dissolved iron and manganese. In the finer silty clay sediments of the middle section of the cores, particulate manganese, iron and phosphorus contents were higher than in the overlying slightly coarser deposits (**Figure 4.4**). At the distal site they presented a maximum between 92 and 122 cm depth, associated with a layer of finer sediments (D50 ~ 9 µm). In the coarser layers at the bottom of the cores, the two sites presented contrasted variations of manganese, iron and phosphorus contents. At the central site, they were lower than in the middle of the core while at the distal site, the variations depended on the considered element (**Figure 4.4**).

Contents of AVS were lower than 12 µmol g^{-1} at both stations (**Figure 4.4**). At the central one, they tended to increase with depth from 0.3 µmol g^{-1} at a few cm depth to ~ 8.5 µmol g^{-1} at the lower limit of homogeneous muds. At the distal station, they did not linearly increase with depth but presented a maximum ~ 100 cm depth. CRS contents were clearly higher than AVS ones with values comprised between 13 and 87 µmol g^{-1} in the Kullenberg cores (**Figure 4.4**). At the distal station, CRS contents were higher in the finer sediments of the middle section of the core than in the first decimeters. This difference is well-marked by a sharp increase of CRS contents between the two sections (**Figure 4.4**).

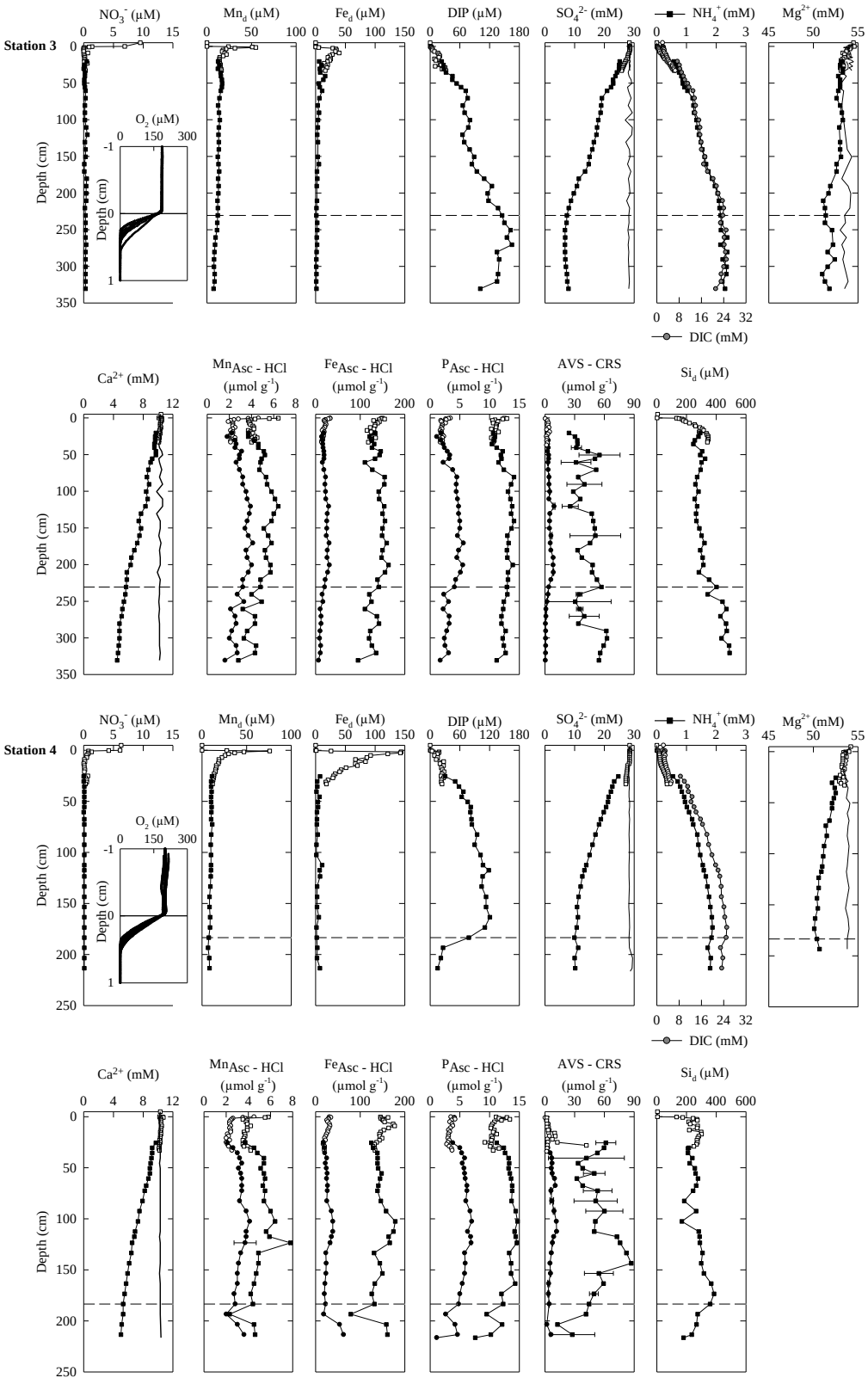

Figure 4.4 : Depth profiles of oxygen (O_2), nitrate (NO_3^-), dissolved manganese (Mn_d), iron (Fe_d) and inorganic phosphorus (DIP), sulfate (SO_4^{2-}), ammonium (NH_4^+), dissolved inorganic carbon (DIC), calcium (Ca^{2+}), dissolved silica (Si_d) and magnesium (Mg^{2+}), AVS (circles) and CRS (squares), particulate manganese (Mn_{Asc}, Mn_{HCl}), iron (Fe_{Asc}, Fe_{HCl}) and phosphorus (P_{Asc}, P_{HCl}). White and black symbols correspond to the interface and Kullenberg cores, respectively. The dash line represents the lower limit of homogeneous muddy sediments. The solid line corresponds to theorical concentrations of calcium, sulfate and magnesium calculated from chloride concentrations using the DITTMAR ratios.

Variations of carbonate contents with depth were closely related to grain-size changes. At the central station, they were higher (~10.2%) in the top coarser silts (D50 ~ 19 – 26 µm) than in the underlying finer sediments (D50 ~ 8 – 14 µm) for which values ranged from 6.6 to 9.6%, excepted in the coarser layer at 60.5 cm depth (**Figure 4.3**). Sandy layers at the core bottom were characterized by variable but relatively high carbonate contents in comparison to overlying sediments. The distal site presented similar vertical changes but with slightly higher values in the first decimeters (~11%) and a noticeable increase at the base of muddy sediments (**Figure 4.3**).

4. Discussion

To complete the characterization of the biogeochemical functioning of RiOMars, the WGMP is used as a model of a high-energy temperate RiOMar. The structuration of the sedimentary record and the origin of organic matter are first characterized prior to discuss the capability of the WGMP to recycle and bury organic matter on a multi-century scale. Then, as early diagenesis processes influence the biogeochemical cycles of other compounds, their fate is characterized on this time scale.

4.1 Structuration of the sedimentary record and origin of organic matter

The division of the sedimentary record in three sections based on grain-size highlights distinct periods in the development of the WGMP (Lesueur et al., 2002). At both stations, muddy sediments covered coarser layers. However, despite this apparent similarity, these bottom sandy layers presented marked differences. At the distal station, they correspond to the sandy substratum whose the marine origin is confirmed by values of $\delta^{13}C$ comprised between - 21.1 and - 19.3‰, which are typical of marine plankton (Fontugne and Jouanneau, 1987). In contrast, the bottom layers of the core sampled at the central station correspond to a mix of silty clay sediments with the sandy substratum. The lower $\delta^{13}C$ and higher C/N ratio mark the more terrigenous origin of these sediments in comparison to the bottom layer of the distal station.

The constant values of $\delta^{13}C$ and C/N in the homogeneous muddy sediments in the central section of the cores indicate that the sources of organic matter, and so of associated sediments, were constants throughout these deposits. More precisely, organic matter is a mix of terrestrial and marine organic matters, characterized by values of $\delta^{13}C$ of -25.9‰ and -20.5‰ (Fontugne and Jouanneau, 1987), respectively. However, values of $\delta^{13}C$ highlight a higher influence of terrestrial inputs at the central ($\delta^{13}C$ ~ -23‰) than at the distal site (~ -22‰). At the central station, the layer of coarser (D50 ~ 21 µm) and more terrigenous ($\delta^{13}C$ ~ -25.2‰) deposits observed at 60.5 cm depth likely reflects an event of high hydrodynamics such as those reported by previous sedimentological studies (Lesueur et al., 1991, 1996, 2002). The fact that only one

such event was observed in our cores is likely due to the sampling resolution or to a homogenization of thin coarser layers with finer deposits by bioturbation.

The more superficial sedimentary section characterized by a higher D50 had already been observed on cores sampled during the 1990's (Lesueur et al., 2002). Two hypotheses had been proposed to explain this shift of grain-size. The first proposed explanation was based on sediment reworking by trawling, which has been simulated as resulting in a loss of the finest fraction of sediments (Mengual et al., 2019). This has already been observed in intensively trawled areas of the Northwest Iberian shelf (Oberle et al., 2016). A higher bottom trawling effort in the WGMP compared to adjacent areas (Lamarque et al., 2021) and the presence of trawling tracks, observed in 2018 with a multibeam echosounder and a side scan sonar (*H. Gillet, personal communica*tion), seem to reinforce this hypothesis. In contrast, it must be note that no typical anomalies related to bottom trawling were observed on profiles of dissolved compounds. However, as they reach a new steady state a few months after such a disturbance (van de Velde et al., 2018), it does not mean that bottom trawling has no lasting effect on sediments. The second hypothesis proposed to explain the presence of top coarser sediments was the occurrence of particular hydrological conditions from 1987 to 1991 (Lesueur et al., 2002). During these years, low river discharges associated to particular tidal conditions related to lunar cycles would have lowered Gironde inputs to the shelf due to the retention of the estuary turbid maximum in the upper estuary and thus favored the dominance of the sedimentation of silts and fine sands from the continental shelf. In fact, during the last decades the estuary turbid maximum migrated upstream due to geomorphological changes of the estuary and the decrease of river discharges (Jalón-Rojas et al., 2021). Accordingly, as the expulsion of sediments from the estuary is favored when the estuary turbid maximum is located in the lower estuary (Lesueur et al., 1996), its migration landward has likely reduced sediments inputs to the continental shelf. However, as in the central area $\delta^{13}C$ did not indicate any changes in sediment origin between the middle and top sections of the deposits (**Figure 4.3**), it is unlikely that the reduction of particles inputs favored the dominance of sediments from the shelf as suggested by Lesueur et al. (2002). Another possible explanation of the gran-size shift is a modification of the grain-size of the sediments supplied to the shelf. The shift is observed between the horizons 34 - 37 cm and 39 - 42 cm at the central station and a bit shallower at the distal one (i.e., between the horizons 28 - 30 cm and 30 - 32 cm). By taking a depth of grain-size change of 38 and 30 cm at the central and distal sites respectively, and by using the corresponding sediment accumulation rates (i.e., 0.37 ± 0.04 and 0.38 ± 0.06 cm y^{-1}, respectively), we estimate that the shift of grain-size would have occurred between 1904 and 1926 at the central site, and between 1925 and 1951 at the distal one. This period is characterized by an extensive anthropic management within the estuary and in the watershed of the Gironde (Lesueur et al., 1996). On

the one hand, many hydroelectric dams have been built in the first half of the 20th century on the Dordogne and Garonne Rivers, the two main tributaries of the Gironde estuary (e.g., dams of Marège, Pinet, Thuriès and of the Jourdanie). It is likely that they have reduced the supply of fine sediments to the continental shelf, as previously observed in other environments (Sun et al., 2020). On the other hand, the management of the estuary have favored the export of sediments to the continental shelf (Allen et al., 1979; Lesueur et al., 2001, 1996) but also the trapping of finest particles within the estuary, thus limiting the export of the finest fraction of sediments to ocean (Lesueur et al., 1996). This may explain the shift of gran-size observed in the WGMP and is consistent with the fact that the $\delta^{13}C$ of organic matter did not change. An increase of hydrodynamics would also have explained the increase of grain-size. However, as wave heights in the Bay of Biscay have decreased between 1980 and 2000 (Dupuis et al., 2006) and are expected to decrease further in the next decades (Charles et al., 2012), this hypothesis can be ruled out. To summary, the variation of gran-size observed ~ 30 - 38 cm depth may be related to several forcing such as bottom trawling, management within the estuary and in the watershed of the Gironde, geomorphological changes of the estuary and a decrease of river discharges. However, unravelling these influences on the grain-size of particles deposited in the WGMP is tricky due to their concomitant effect. At the central site, as $\delta^{13}C$ did not vary between the middle and the upper sections of the core, the higher C/N ratio measured in the first decimeters of sediments suggests an input of more degraded organic matter since the shift of grain-size.

4.2 Organic matter recycling and burial: influence of organic matter reactivity and bioavailability

At both sites, organic matter is remineralized according to the classic diagenetic sequence described by Froelich et al., (1979). It is remineralized by aerobic respiration in the first millimeters of sediments then by denitrification until the disappearance of nitrate in the following centimeters (**Figure 4.4**). Subsequently, remineralization goes through the reduction of manganese then iron oxyhydroxydes. These reactions produce dissolved manganese and iron that diffuse to the SWI where they may be oxidized by oxygen, nitrate or manganese oxyhydroxydes for dissolved iron (Canfield et al., 1993; Hyacinthe et al., 2001). This leads to enrichments of reactive manganese and iron oxyhydroxydes (i.e., Mn_{Asc} and Fe_{Asc}) in the top centimeters of sediments (**Figure 4.4**). Then, sulfate reduction occurs from between 9 and 15 cm depth until the bottom of the cores. As sulfate is still measured in depth (> 6.5 mM between 240 and 300 cm at the central site and > 9.9 mM between 153 and 203 cm at the distal one), it is consistent that no methane production occurs because it is an energetically less favorable degradation pathway (Alperin et al., 1994; Burdige, 2006; Hoehler et al., 1994). The variation

of the intensity of OC remineralization by sulfate reduction with depth was assessed from OC remineralization rates. They were estimated from stoichiometric ratios of sulfate reduction (Froelich et al., 1979) and diffusive fluxes of sulfate calculated using the Fick's first law of diffusion applied to the sediment. At the central site, OC remineralization rates by sulfate reduction were higher between 17 and 70.5 cm depth (7.5 mgC m^{-2} d^{-1}) than between 70.5 and 220 depth (4.3 mgC m^{-2} d^{-1}). At the distal site, the mismatch between the interface and Kullenberg cores prevents the observation of an attenuation of sulfate consumption in the first decimeters. However, OC remineralization rates by sulfate reduction were of 6.9 mg m^{-2} d^{-1} between 30.5 and 123.5 cm, which is close to that estimated at the central site. At both stations, the stabilization of sulfate, ammonium and DIC concentrations in depth (**Figure 4.4**) highlights a limitation of organic matter remineralization by the availability of degradable organic matter (Aller, 2014). The decrease of the lability of organic matter in the first decimeters of sediments, highlighted by the Chl-*a*/(Chl-*a* + Phaeo-*a*) and EHAA/THAA ratios (**Figure 4.3**), may partly explain this limitation and the variation of OC remineralization rates with depth. The limitation of remineralization by organic matter lability is likely related to the refractory nature of sediment inputs from the Gironde (Abril et al., 1999; Etcheber et al., 2007; Savoye et al., 2012). However, the lability ratios become constant several decimeters above the variation of the sulfate gradient observed at 70.5 cm at the central site. The constant values of OC loads (0.40 - 0.59 mgC m^{-2}) since ~ 40 - 50 cm (**Figure 4.3**) may also explain the limitation of remineralization. Indeed, they correspond to a threshold from which organic matter is less reactive and available for degradation owing to a physical protection related to its sorption on particles (Blair and Aller, 2012; Hedges and Keil, 1995; Mayer, 1994a). However, like for descriptors of organic matter lability, constant values of OC loads are observed shallower than the variation of the sulfate gradient. This suggests that both the bioavailability and lability of organic matter control the intensity of its degradation on a multi-century scale. The limitation of organic matter remineralization is observed at the boundary between the homogeneous muds and the sandy substratum at the central site (~ 230.5 cm, **Figure 4.4**) and some decimeters above this boundary at the distal one (153.5 cm; **Figure 4.4**). Considering that muddy sediments accumulate since ~ 400 years (**Figure 4.2**) and assuming a mean continuous sedimentation, this suggests that sulfate reduction ended after less than 400 years at the distal site. Such a limitation was also observed on long muddy sediment cores (1 to 3.5 m length) sampled between 550 and 2000 m depth on the continental slope of the Landes shelf located in the southern part of the Bay of Biscay (Charbonnier et al., 2019). At these stations that are partly influenced by the Gironde and the Loire, sulfate is not entirely consumed and its concentrations also tend to be constant in depth (Charbonnier et al., 2019). This suggests that a major part of the Bay of Biscay

could be a carbon-limited system, partly due to the refractory nature of continental organic matter inputs.

The scarcity of shells required for dating rules out the possibility to estimate OC burial rates at different periods throughout the history of the WGMP. However, a qualitative assessment of OC burial efficiencies can be performed using OC loads (Blair and Aller, 2012; Dubosq et al., 2021). Briefly, values < 0.4 mgC m^{-2} are typical of environments with an enhanced organic matter remineralization while those > 1.0 mgC m^{-2} indicate an efficient preservation possibly related to high organic matter inputs (e.g., upwelling areas) or an inefficient degradation (e.g., low oxygen areas ; Blair and Aller, 2012; Mayer, 1994a). The constant and relatively low values of OC loads (i.e., 0.40 – 0.59 mgC m^{-2}) observed in the middle section of the cores at both sites are typical of non-deltaic shelves and indicate that organic matter is relatively efficiently remineralized on a multi-century scale. However, the WGMP does not act as an organic matter "incinerator" like previously studied high-energy RiOMars (e.g., the Amazon mobile mud belt, the gulf of Papua deltaic complex) in which OC loads are typically < 0.4 mgC m^{-2} (Aller et al., 2008; Aller and Blair, 2006). Although the central and distal parts of the WGMP are relatively efficient to store OC on a multi-decennial scale (Dubosq et al., 2021), it is not the case on longer times scales. This lower efficiency of OC preservation is likely related to a longer period of remineralization. However, the efficiency of OC preservation may also have been influenced by the change of sedimentation in the first half of the 20^{th} century (*see section 4.1*). The stabilization of OC loads to values of 0.40 - 0.59 mgC m^{-2} suggests that the preservation of organic matter in these sediments could be related to a physical protection due to its sorption on particles (Mayer, 1994a). Accordingly, the quantity of organic matter ultimately buried appears directly controlled by the size of deposited particles.

4.3 Burial of elements on a multi-century scale

4.3.1 Formation of authigenic minerals

By-products of organic matter remineralization produced during early diagenesis may react to form authigenic carbonate, phosphorus or sulfide minerals (Jorgensen et al., 2019; Mucci, 2004; Rothe et al., 2016; Ruttenberg and Berner, 1993). As the precipitation of authigenic minerals induces an equilibrium between the particulate and dissolved phases, the depth profiles of dissolved compounds may highlight the occurrence of such reactions. It is the case for dissolved manganese whose the decrease of concentrations in depth highlights a consumption. This could be due to the precipitation of pure or mixed manganese carbonates (Middelburg et al., 1987; Mucci, 2004). However, to be validated, this hypothesis has to be supported by an uptake of DIC. This can be inferred by using ammonium as a conservative tracer of organic matter remineralization (Ruttenberg and Berner, 1993). Indeed, as DIC and ammonium are both

by-products of organic matter remineralization, a precipitation of carbonates would result in a decoupling of their profiles. However the constancy of the DIC/NH_4^+ ratio with depth indicates that no or negligible carbonate precipitation occurs in these sediments (**Figure 4.5**). This absence of carbonate precipitation in spite of the oversaturation of pore waters with respect to calcite (**Figure 4.6**) may be due to the adsorption of phosphates on calcite surfaces inhibiting precipitation (Lin and Singer, 2006; Mucci, 1986). As no carbonate precipitation occurs, the equilibrium of dissolved manganese with the particulate phase is most likely due to the adsorption of manganese on calcite. Indeed, this process results in a decrease of dissolved manganese concentrations below the threshold of saturation with respect to rhodochrosite (i.e., $MnCO_3$; Middelburg et al., 1987; Mucci, 2004), as observed at both sites (**Figure 4.6**). Other possible processes for removing dissolved manganese from pore waters include its adsorption on or co-precipitation with iron sulfides, or precipitation of manganese sulfides (Arakaki and Morse, 1993; Stockdale et al., 2010). The large undersaturation of pore waters with respect to manganese sulfides (saturation index < - 5; **Figure 4.6**) shows that if sulfides manganese are formed in these sediments, it is likely through a co-precipitation with iron sulfides.

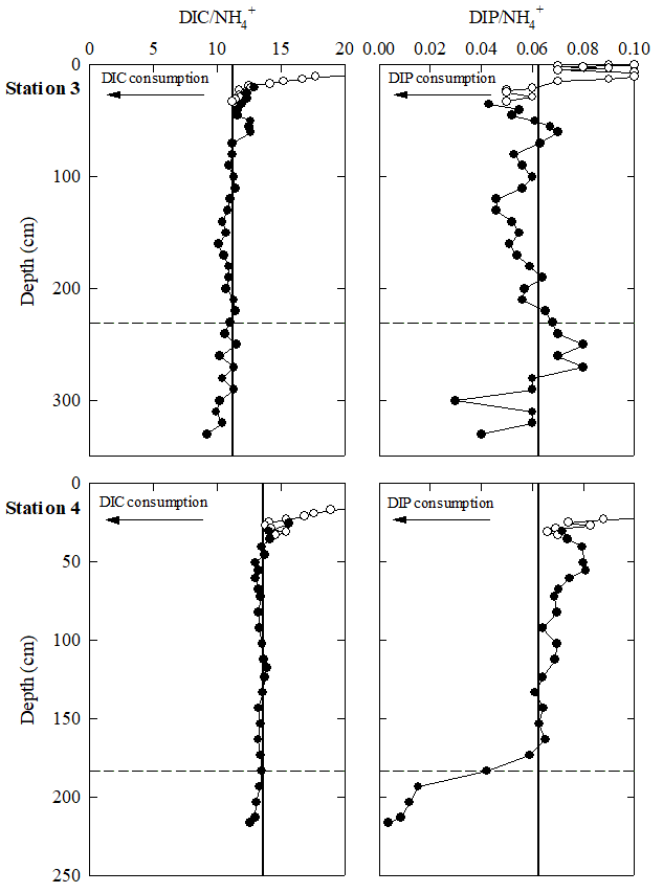

Figure 4.5: Depth profiles of DIC/NH_4^+ and DIP/NH_4^+ ratios at the central and distal stations in interface (white) and Kullenberg (black) cores. The dash line represents the lower limit of homogeneous muddy sediments. Solid lines correspond to the mean DIC/NH_4^+ ratio in muddy sediments of the Kullenberg core and of the theoretical DIP/NH_4^+ ratio resulting of sulfate reduction (Froelich et al., 1979), respectively.

The calcium uptake being not related to carbonate precipitation, it is most likely due to the formation of authigenic Ca-P phases as hydroxyapatite whose saturation index is > 0 (**Figure 4.6**). The depth profile of the DIP/NH_4^+ ratio highlights an uptake of DIP and confirms the precipitation of phosphorus minerals (**Figure 4.5** ; Ruttenberg, 2014; Ruttenberg and Berner, 1993). This consumption is well marked between 80 and 180 cm depth at the central station and appears restricted at the core bottom at the distal one (**Figure 4.5**). However, the consumption of DIP at the central site seems not to be sufficient to completely explain the calcium uptake. On the depth range 70.5 - 170.5 cm, on which sulfate and calcium concentrations decreased linearly, the fluxes of calcium and sulfate calculated using the Fick's first law of diffusion applied to the sediment are of ~ 31 µmol m^{-2} d^{-1} and ~ 155 µmol m^{-2} d^{-1}, respectively. Considering that during sulfate reduction 1 µmol of DIP is produced for an uptake of 53 µmol of sulfate (Froelich et al., 1979), ~ 3 µmol m^{-2} d^{-1} of DIP is estimated to be produced on this depth range. Thus, by taking a Ca:P stoichiometric ratio of 10:6 for apatite minerals (Slomp, 2011), we can estimate that if all the produced DIP was consumed for apatite precipitation, it would support only ~ 16% of the calcium uptake. As DIP is therefore obviously not the main source of phosphorus for the precipitation of Ca-P minerals, their formation is most likely supported by particulate organic phosphorus produced by fermentation during the first stages of organic matter degradation (Ruttenberg and Berner, 1993). Further studies on phosphorus speciation in these sediments could solve this issue by carrying out sequential extractions according to the SEDEX method (Ruttenberg, 1992; Ruttenberg and Berner, 1993). Indeed if organic phosphorus actually supports the precipitation of authigenic minerals, a decrease of particulate organic phosphorus should be observed in parallel to an increase of contents of authigenic phosphorus (Ruttenberg and Berner, 1993).

Particulate sulfide (AVS and CRS) contents and the decrease of dissolved iron concentrations with depth until a background < 5 µM indicate the formation of iron sulfide minerals (e.g. Burdige, 2006; Deflandre et al., 2002; Jorgensen et al., 2019). The high contents of CRS relative to AVS show that dissolved sulfides produced during sulfate reduction are ultimately buried under the form of pyrite. This is consistent with the very low concentrations of dissolved sulfides (i.e., < 3 µM). The formation of pyrite in the central and distal areas of the WGMP that are less subjected to hydrodynamics and have higher sedimentation rates is consistent with observations performed in other energetic RiOMars like the Gulf of Papua deltaic complex, the East China sea continental shelf and the Mississippi delta where a higher pyrite formation occurs in areas with higher sedimentation rates (Aller et al., 2004; Lin et al., 2000; Lin and Morse, 1991). Interestingly, contents of particulate sulfides may be used to assess the rate of OC remineralization: higher contents indicate higher rates of sulfate reduction and so of organic matter remineralization (Sundby et al., 2004). Hence, the higher CRS contents in

the middle section of the distal core compared to the first 30 cm suggest that sulfate reduction rates were higher before the shift of grain-size. This shift has likely influenced the quantity of OC inputs to the WGMP and so the intensity of sulfate reduction. Indeed at equivalent sedimentation rate, as larger-size particles have typically lower OC contents than finer ones (Mayer, 1994a), the OC input is lower. At a constant OC content, a decrease of sedimentation rates could have the same effect. However, the chronology based on radiocarbon dating and $^{210}Pb_{xs}$ does not clearly highlight a variation of sedimentation rates at the distal site (**Figure 4.2**).

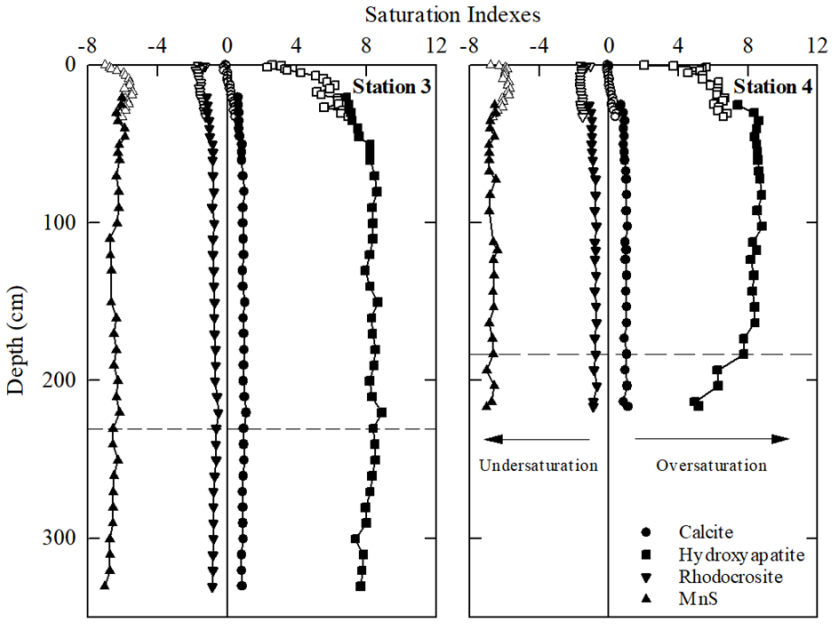

Figure 4.6: Pore waters saturation indexes for calcite, hydroxyapatite, rhodochrosite and manganese sulfide (MnS) at the central and distal stations computed for interface (white) and Kullenberg (black) cores using the software PHREEQC (Parkhurst and Appelo, 1999). The dash line represents the lower limit of homogeneous muds.

Another interesting point concerns dissolved silica. The quick increase of concentrations in the first decimeters of sediments (**Figure 4.4**) is due to a dissolution of particulate biogenic silica (Chong et al., 2018; Michalopoulos and Aller, 2004). The subsequent decrease of concentrations highlights the formation of authigenic clays through a « reverse weathering » process (Chong et al., 2018; Dixit et al., 2001; Michalopoulos and Aller, 2004). Briefly, it corresponds to a formation of aluminosilicates from reactive silica and dissolved cations (Aller, 2014). Hence, the uptake of dissolved magnesium observed at both sites seems to confirm its occurrence (**Figure 4.4**). In depth, the stabilization of dissolved silica concentrations indicates an equilibrium between the dissolution of biogenic silica and the precipitation of clays (Chong et al., 2018). The formation of authigenic clays in the WGMP is consistent with observations made in other RiOMars like the Mississippi and the Amazon deltas where it is estimated that ~ 40% and ~ 90% of the biogenic silica buried is converted to authigenic clays, respectively (Michalopoulos and Aller, 2004; Presti and Michalopoulos, 2008).

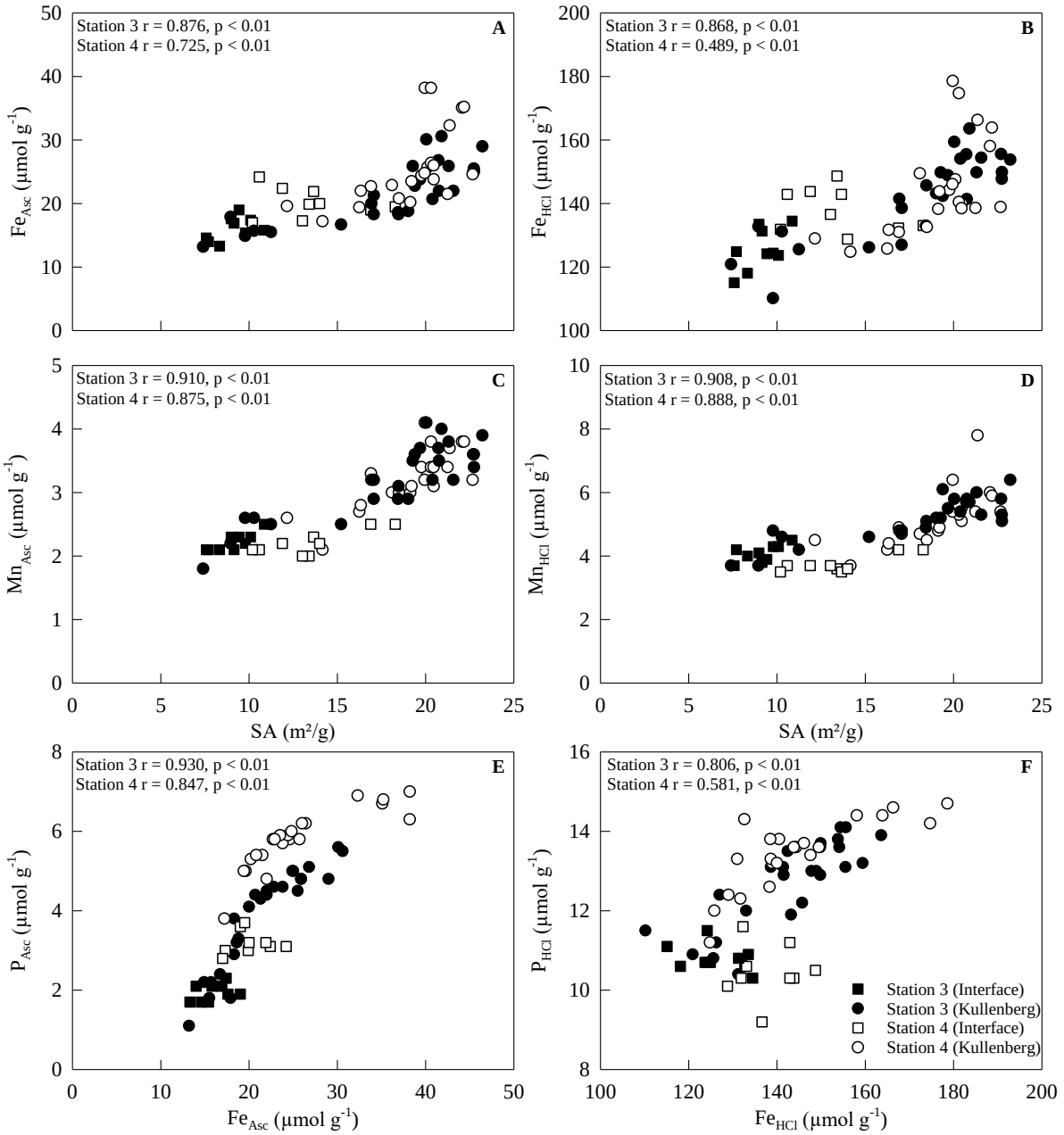

Figure 4.7: Particulate iron and manganese extracted using an ascorbate (Fe_{Asc} (**A**), Mn_{Asc} (**C**)) and a 1 M HCL solutions (Fe_{HCl} (**B**), Mn_{HCl} (**D**)) against surface area of sediments (SA) and particulate phosphorus (P_{Asc} (**E**), P_{HCl} (**F**)) against particulate iron. Only the data measured in silty clay sediments below the horizon of the reduction of iron oxyhydroxydes are included.

4.3.2 Burial of particulate iron and manganese oxyhydroxydes : implications for the sequestration of phosphorus and metallic contaminants

Contents of particulate manganese, iron and phosphorus seem to vary according to grain-size changes. This relationship is confirmed by significant correlations between surface area of sediments and particulate iron and manganese below the horizon of particulate iron reduction (**Figure 4.7**). Manganese and iron oxyhydroxydes are indeed coated on the surface of particles (Poulton and Raiswell, 2005). This implies that their burial on a multi-century scale depends on grain-size and so of the type of sedimentation. Thus, the variation of grain-size of particles

deposited in the WGMP in the first half of the 20th century (*see section 4.1*) indirectly lowered the capability of the WGMP to store iron and manganese oxyhydroxydes.

In marine sediments, the biogeochemical cycle of phosphorus is closely related to that of iron due to the adsorption of phosphates on iron oxyhydroxydes (Anschutz et al., 1998; Sundby, 2006; Sundby et al., 1992). This results in correlations of particulate iron and phosphorus extracted with ascorbate and 1 M HCl solutions (**Figure 4.7**). The better correlation obtained for the ascorbate extraction is due to the fact that only the phosphorus associated with iron is extracted with that method while the 1 M HCl solution also extracts authigenic and detrital phosphorus phases such as apatite (Ruttenberg, 1992; Slomp, 2011). However, the relative high correlations between Fe_{HCl} and P_{HCl} (0.806 and 0.581 at the central and distal sites, respectively) suggest that iron oxyhydroxydes are a relatively large sink for phosphorus compared to apatite.

Some metallic contaminants have a strong affinity with iron and manganese oxyhydroxydes (e.g., arsenic, cobalt, mercury, nickel, lead, cadmium ; Chaillou et al., 2008; Mucci et al., 2003; Rigaud et al., 2013; Shi et al., 2021). Hence, the shift of the grain - size of deposited particles may have indirectly lower the capability of the WGMP to store these contaminants on multi-decennial and multi-century scales. In the current context of global changes, the fluvial discharge of the Gironde tends to decrease (ongoing and projected ; Schmidt et al., 2017), thus lowering the exports of sediments to the continental shelf. This could result in a decrease of sedimentation rates and reinforce the diminishing capability of the WGMP to store iron and manganese oxyhydroxydes and associated metallic contaminants. Since the quantity of OC buried in the WGMP is closely related to mass accumulation rates (Dubosq et al., 2021), this could also reduce the capability of the WGMP to store OC. Such a decrease of OC preservation during the last decades has been observed on the East China Sea shelf, influenced by the Yangtze river (Sun et al., 2020). In this system, the building of the Three Gorges Dam in 2003 appears to have reduced sedimentation rates, increased the sand content in sediments of the subaqueous delta and triggered the erosion of its shallower part (Yang et al., 2011), thus altering OC sequestration (Sun et al., 2020).

5. Conclusion

The sampling of sediment cores of ~ 3 m length in the central and distal WGMP showed that deposits may be divided into three sections. The lower layers corresponded to the sandy substratum, which is mixed with silty sediments in the central area. Above the substratum, muddy sediments were rather homogeneous until a slight shift to coarser sediments ~ 30 - 38 cm depth depending on the site. In sediments, organic matter is remineralized according to the classical diagenetic sequence. However, due to relatively high sulfate concentrations in depth,

no methane genesis occurs. Compared to tropical and subtropical high-energy RiOMars, the occurrence of sulfate reduction and pyrite formation over most of the sedimentary column is consistent with the lower hydrodynamics and higher sedimentation rates of the central and distal areas of the WGMP. In depth, organic matter remineralization is limited by organic matter lability and bioavailability. This limitation seems to be induced by the refractory nature of organic matter inputs from the Gironde and the sorption of organic matter on particles, which physically prevents its degradation. The constancy of OC loads in depth indicates that the amount of OC ultimately buried is controlled by the size of particles. The relatively high values of OC sediment loads (i.e., 0.40 - 0.59 mgC m^{-2}) compared to other high-energy RiOMars (i.e., typically < 0.40 mgC m^{-2}) indicates that the WGMP does not act as an "incinerator" of organic matter in contrast to the Amazon delta or the mobile mud belt of the East China Sea (Blair and Aller, 2012).

By-products of organic matter remineralization and other dissolved compounds react to form authigenic minerals. The formation of authigenic clays, highlighted by dissolved silica and magnesium uptakes, is consistent with previous observations in other RiOMars. Surprisingly, no or negligible carbonate precipitation occurs. The calcium consumption seems therefore related to apatite precipitation, which is likely mainly sustained by particulate organic phosphorus. However, much of the buried phosphorus appears to be associated with iron oxyhydroxydes. The increase of grain-size observed ~ 30 - 38 cm depth and estimated at the first half of the 20^{th} century, appears to have decreased the capability of the WGMP to store OC, particulate sulfides and manganese and iron oxyhydroxydes. This directly impacted the sequestration of phosphorus and likely of some metallic contaminants having a strong affinity for these oxyhydroxydes. This decreasing trend is expected to increase in the next decades due to the decrease of Gironde discharges related to climate change. Through the characterization of the WGMP on a multi-century scale, this study provides an example of the long-term biogeochemical functioning of a high-energy temperate RiOMar.

Points clés du Chapitre 4

- Dans les sédiments, la matière organique est reminéralisée selon la séquence diagénétique classique. Cependant, il n'y a pas de méthanogenèse en raison des concentrations en sulfates relativement élevées à la base des sédiments vaseux.
- En profondeur, la reminéralisation de la matière organique est limitée par la disponibilité de matière organique dégradable. Cette limitation est liée à une diminution de la labilité de la matière organique avec la profondeur ainsi qu'à son adsorption sur les particules sédimentaires qui la protège de la dégradation.
- Dans la Vasière Ouest Gironde, la reminéralisation de la matière organique est plus efficace à l'échelle pluriséculaire qu'à l'échelle pluridécennale. Cependant, elle n'agit pas comme un « incinérateur » pour la matière organique, contrairement aux RiOMars de haute énergie déjà étudiés.
- A l'échelle pluriséculaire, la quantité de carbone organique séquestrée dans la Vasière Ouest Gironde semble contrôlée par la taille des particules déposées.
- La Vasière Ouest Gironde est un puits pour plusieurs éléments via :
    - La précipitation de minéraux authigènes (pyrite, apatite, argiles).
    - L'adsorption de composés sur les particules sédimentaires (carbone organique, oxyhydrohydes de fer et de manganèse).
- Malgré la précipitation d'apatite, la majeure partie du phosphore enfoui semble être adsorbée sur les oxyhydroxydes de fer.
- Une augmentation de la taille des particules déposées, estimée au début du 20^{e} siècle, semble avoir diminuer la capacité de la Vasière Ouest Gironde à stocker le carbone organique, le soufre, le fer, le manganèse et le phosphore.

Synthèse et perspectives

Les marges continentales sous l'influence de grands fleuves (RiOMars pour *River-dominated Ocean Margins*) jouent un rôle majeur dans les cycles biogéochimiques globaux. La classification de ces systèmes en trois catégories par Blair and Aller (2012) a permis une compréhension globale de leur fonctionnement biogéochimique. Cependant, cette classification était avant tout basée sur des systèmes tropicaux et subtropicaux. De plus, les RiOMars de haute énergie (type 1) avaient uniquement été caractérisés à partir de l'étude de grands systèmes deltaïques. L'étude de la Vasière Ouest Gironde (VOG) paraissait donc particulièrement intéressante pour compléter la caractérisation du fonctionnement biogéochimique des RiOMars. En effet, c'est un système sédimentaire tempéré non-deltaïque, localisé dans un environnement de fort hydrodynamisme et sous l'influence d'un fleuve avec un flux de sédiments modéré. Ainsi, ce travail de thèse a notamment permis de mettre en évidence l'originalité de son fonctionnement biogéochimique, de l'échelle saisonnière à pluriséculaire, par rapport aux RiOMars précédemment étudiés.

1. Structuration et fonctionnement biogéochimique de la Vasière Ouest Gironde de l'échelle saisonnière à pluridécennale

Dans la VOG, la structuration spatiale des processus sédimentaires influence fortement celle des processus biogéochimiques. Elle permet notamment de diviser la VOG en une zone proximale et une zone distale (**Figure 5.1**). La limite entre ces deux zones a été déterminée à partir des caractéristiques des sédiments de surface et est estimée aux alentours de 42.5 m de profondeur (Lamarque et al., 2021). Dans la zone distale, où la sédimentation silto-argileuse est plutôt continue, la séquence diagénénétique se dilate progressivement vers le large (**Figure 5.1**). Cette dilatation est probablement liée à une diminution de la labilité de la matière organique et à une augmentation de la bioturbation avec la profondeur. La variation de l'intensité de la respiration aérobie à l'interface eau-sédiment au sein de la zone distale a permis de la subdiviser en une zone centrale où l'intensité de la respiration aérobie est modérée et une zone externe où elle est significativement plus élevée (**Figure 5.1**). Contrairement à la sédimentation plutôt continue observée dans la zone distale, le fort hydrodynamisme de la zone proximale induit une structuration verticale de la colonne sédimentaire en deux parties distinctes, à savoir une couche superficielle sablo-vaseuse transitoire inférieure à 10 cm d'épaisseur recouvrant des sédiments reliques plus fins. Cette structuration induit un régime diagénétique en deux couches présentant des fonctionnements biogéochimiques différents. Dans la couche superficielle transitoire, la matière organique est reminéralisée par respiration aérobie et par des processus de reminéralisation suboxiques. Au contraire, la réduction des sulfates est le processus de reminéralisation dominant dans les vases reliques. Au-delà des processus de recyclage de la matière organique, les mesures de différentes phases dissoutes et particulaires ont mis en

évidence un fonctionnement différent des cycles biogéochimiques du fer et du soufre entre les vases reliques et les sédiments du reste de la VOG. En effet, les sulfures particulaires produits dans les sédiments sont principalement sous forme d'Acid Volatile Sulfides (AVS) et probablement de soufre élémentaire dans les vases reliques alors qu'ils sont convertis en pyrite dans les sédiments du reste de la VOG (**Figure 5.1**). Cette différence semble liée à une charge en oxyhydroxydes de fer réactifs plus importante dans les vases reliques qui favorise l'oxydation des sulfures dissous et limite la conversion des AVS en pyrite.

La réalisation de missions d'échantillonnage saisonnières a montré que l'intensité des processus de reminéralisation anaérobies de la matière organique ne variait pas entre les saisons. Au contraire, l'intensité de la respiration aérobie présentait une dynamique temporelle bien marquée liée à des évènements saisonniers tels que l'efflorescence printanière ou la désoxygénation des eaux de fond.

Les flux d'oxygène benthiques totaux ont été utilisés comme descripteur de l'intensité de la reminéralisation totale du carbone organique. Cela a mis en évidence que l'intensité du recyclage du carbone organique dans la VOG était faible en comparaison d'autres environnements de plateaux continentaux. Cette intensité de reminéralisation relativement faible est probablement liée au fait que la matière organique apportée à la VOG depuis l'estuaire de la Gironde a déjà été intensément reminéralisée et est par conséquent plutôt réfractaire et peu biodisponible (Abril et al., 1999; Etcheber et al., 2007; Savoye et al., 2012). Cela induit une faible efficacité du recyclage du carbone organique, estimée entre 32 ± 11 et 48 ± 39% dans la zone distale, et un stockage du carbone organique plutôt efficace à l'échelle pluridécennale. A l'échelle de la VOG, les taux de séquestration du carbone organique à cette échelle de temps varient entre 7 ± 9 et 45 ± 6 gC m^{-2} an^{-1} (**Figure 5.1** ; Dubosq et al., 2021). Ils sont contrôlés à la fois par les quantités d'apports sédimentaires et l'intensité de l'hydrodynamisme qui influencent la quantité et la nature de sédiments déposés aux différents sites. Ces taux de séquestration du carbone organique sont parmi les plus élevés de ceux mesurés dans l'Atlantique nord est. Ainsi, bien que la VOG ne soit pas un puits majeur pour le carbone organique en raison de sa superficie relativement faible, le stockage du carbone organique dans l'ensemble des vasières du plateau continental du golfe de Gascogne est potentiellement important à l'échelle globale.

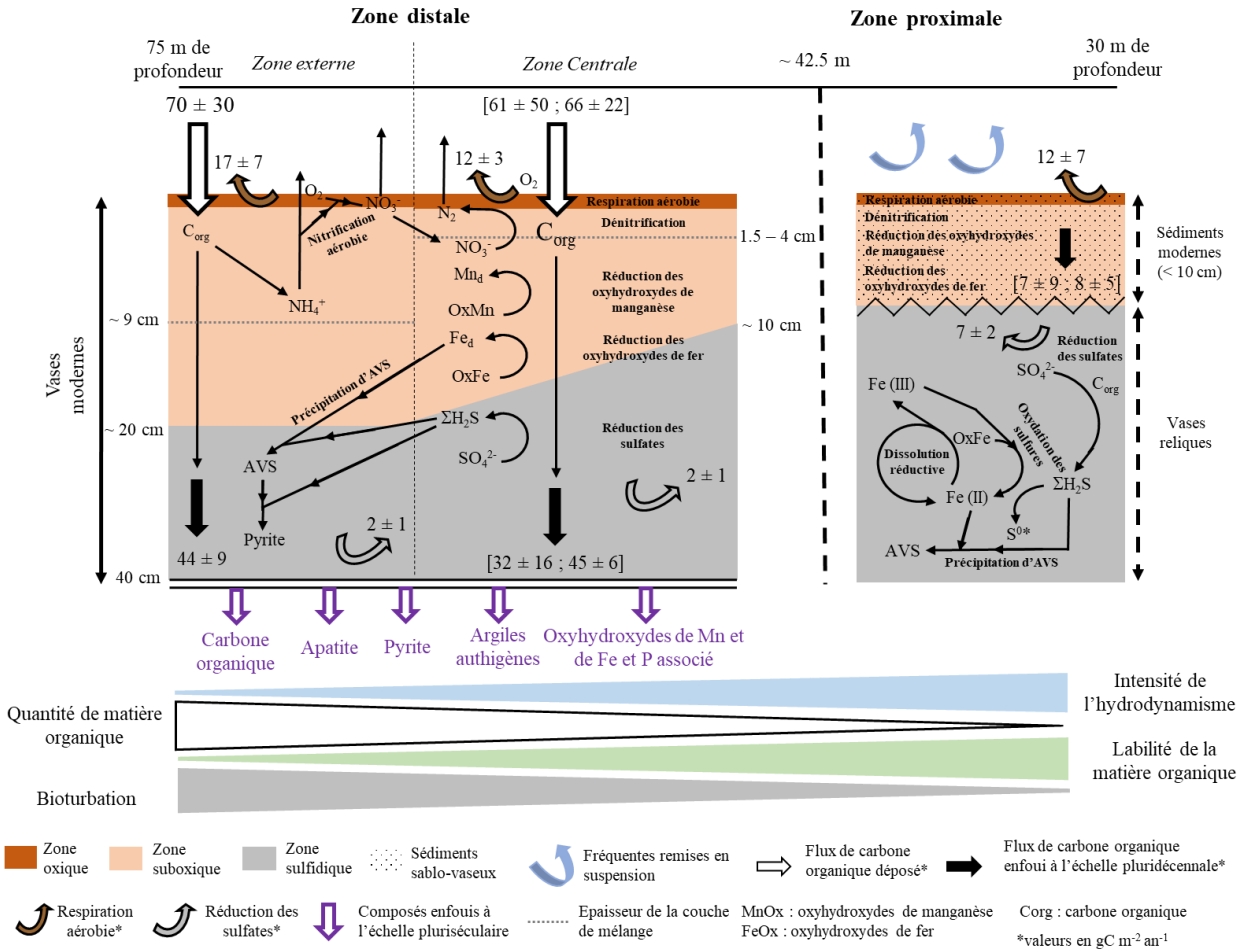

Figure 5.1 : Schéma conceptuel du fonctionnement biogéochimique du compartiment benthique de la Vasière Ouest Gironde établi à partir des mesures réalisées entre octobre 2016 et 2021. Il est important de noter des fonctionnements sédimentaires et biogéochimiques différents entre les zones proximales et distales. Les zones externes et centrales sont des subdivisions de la zone distale. Elles se différencient par l'intensité de la respiration aérobie à l'interface eau-sédiment et par l'épaisseur de la couche de mélange. *Bien que le soufre élémentaire n'ait pas été mesuré dans le cadre de cette étude, il est probable qu'il se forme lors de l'oxydation des sulfures par les oxyhydroxydes de fer.

2. Fonctionnement biogéochimique de la Vasière Ouest Gironde de l'échelle pluridécennale à pluriséculaire

Le prélèvement de carottes longues dont l'enregistrement sédimentaire couvrait les derniers 400 ans a permis de caractériser le fonctionnement biogéochimique de la VOG sur de plus longues échelles de temps. Les résultats montrent qu'au-delà de 15 cm de profondeur, la matière organique est reminéralisée par réduction des sulfates. En profondeur des carottes, la constance des concentrations de sulfates témoigne d'une limitation de la reminéralisation de la matière organique. Cela est probablement lié à la diminution de sa labilité ainsi qu'à une protection physique de la matière organique contre la dégradation via son adsorption sur les particules sédimentaires. Ainsi, la quantité de matière organique préservée dans les sédiments à l'échelle pluriséculaire semble directement contrôlée par la taille des particules déposées. Les charges en carbone organique des sédiments (i.e., ratio OC/SA) indiquent que la matière organique est plus efficacement reminéralisée à l'échelle pluriséculaire qu'à l'échelle pluridécennale. Cela peut être lié à une plus longue durée de dégradation mais également à un changement des apports sédimentaires vers le début du 20^{e} siècle.

Ce travail a montré que dans les sédiments de la VOG, les produits de la reminéralisation de la matière organique (e.g., sulfures, fer dissous, phosphates) ainsi que d'autres éléments (e.g., silicium, magnésium) sont stockés sous forme de minéraux authigènes (**Figure 5.1)** tels que l'apatite, la pyrite ou encore les argiles authigènes formées à partir de silice dissoute via un processus de « reverse weathering ». Les résultats indiquent également une absence de précipitation de carbonates authigènes. A l'image du carbone organique, la séquestration de certains éléments tels que le fer et le manganèse semble être fortement influencée par la taille des particules déposées en raison de l'adsorption de leurs oxyhydroxydes sur celles-ci. Cela impacte directement la séquestration du phosphore qui a une forte affinité avec les oxyhydroxydes de fer. Par conséquent, une augmentation de la taille des particules déposées à partir de la première moitié du 20^{e} siècle semble avoir diminué la capacité de la VOG à stocker ces éléments ainsi que le carbone organique. De plus, il est probable que ce changement ait également diminué la capacité de la VOG à stocker des contaminant métalliques ayant une forte affinité avec les oxyhydroxydes de manganèse et de fer.

3. La Vasière Ouest Gironde : un nouveau modèle de RiOMar?

Le fait que la VOG ne soit pas un delta se traduit notamment par une limite supérieure des dépôts vaseux plus profonde (~ 30 m) que dans les RiOMars énergétiques déjà étudiés où les sédiments vaseux commencent à se déposer au maximum vers 10 m de profondeur. Cette

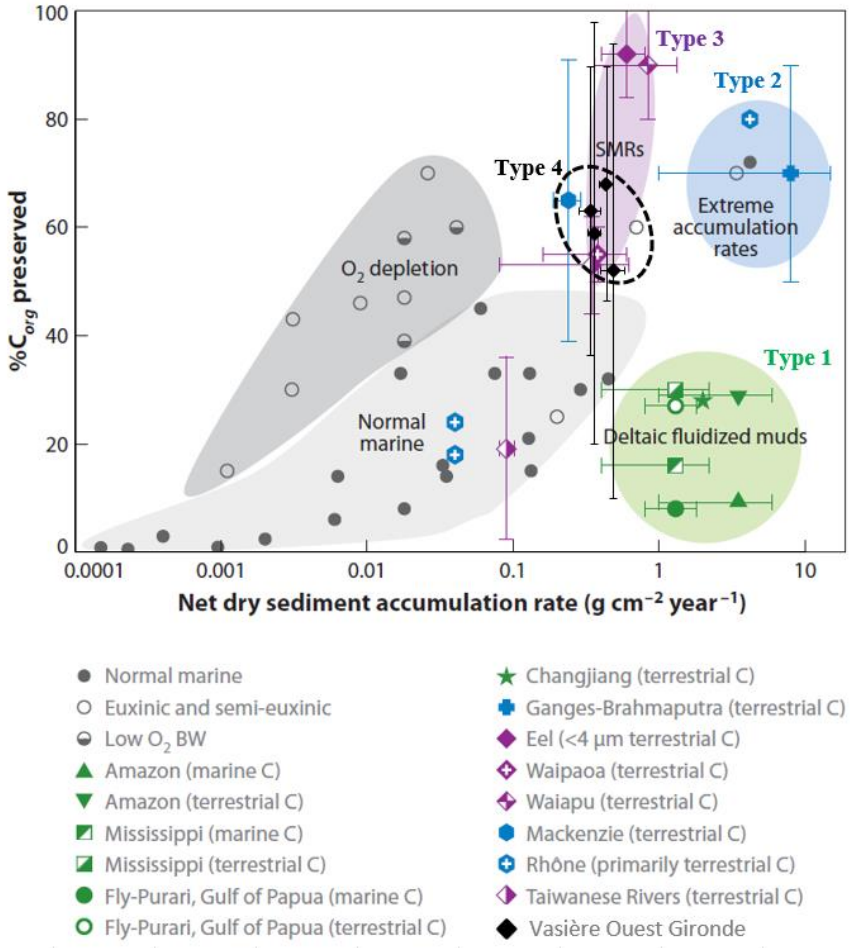

Figure 5.2 : Efficacité d'enfouissement du carbone organique en fonction des taux d'accumulation de sédiments pour plusieurs systèmes de marges continentales sous l'influence de fleuves. Cette figure permet de distinguer les trois types de RiOMars définis par Blair and Aller (2012) ainsi que le type 4 proposé sur la base de l'étude du fonctionnement biogéochimique de la Vasière Ouest Gironde. Pour la Vasière Ouest Gironde, seules les stations du transect nord où la sédimentation est continue (i.e., 2,3,8 et 4) sont représentées. Modifié d'après Blair and Aller (2012).

différence morphologique de la VOG induit l'absence d'une large étendue de vases mobiles fréquemment remises en suspension où la matière organique est efficacement reminéralisée. Par conséquent et contrairement aux RiOMars de type 1 de la classification de Blair and Aller (2012), la VOG ne fonctionne pas comme « un incinérateur » mais séquestre efficacement la matière organique. En effet, plus la moitié du carbone organique déposé dans la VOG est séquestré à l'échelle pluridécennale (**Figure 5.1** et **5.2**). Bien que ce stockage soit moins efficace à l'échelle pluriséculaire, les charges en carbone organique mesurées en profondeur restent typiques de plateau continentaux non-deltaïques (i.e., 0.4 – 1 mgC m^{-2}) et sont supérieures à celles mesurées dans les RiOMars énergétiques qualifiés « d'incinérateurs » (i.e., > 0.4 mgC m^{-2} ; Blair and Aller, 2012). Ainsi, malgré l'important hydrodynamisme du golfe de Gascogne, le fonctionnement biogéochimique de la VOG diffère fortement de celui des RiOMars de type 1. De plus, ses caractéristiques ne correspondent pas non plus aux deux autres

types de RiOMars, à savoir des systèmes de faible énergie avec d'importants taux d'accumulation de sédiments (type 2) ou influencés par des rivières de montagne et caractérisés par des apports sédimentaires épisodiques liés aux tempêtes (type 3). Cela nous amène à proposer un quatrième type de RiOMars dont la VOG pourrait être un site modèle. Ces RiOMars de type 4 pourraient inclure des systèmes sédimentaires de marge passive présentant une préservation du carbone organique efficace malgré des taux de sédimentation modérés en raison d'apports de matière organique plutôt réfractaires. Bien qu'initialement regroupé avec les RiOMars de type 1 (**Figure 5.2**), le plateau continental influencé par le fleuve Mackenzie au nord du Canada semble davantage correspondre à cette quatrième catégorie étant donné ses taux d'accumulation de sédiment, de séquestration du carbone organique et le caractère réfractaire de la matière organique apportée par le fleuve (**Figure 5.2** ; Blair and Aller, 2012; Goñi et al., 2005; Kim et al., 2022).

4. Perspectives

Ce travail a permis de caractériser pour la première fois le fonctionnement biogéochimique de la VOG et de le comparer à celui d'autres RiOMars. Cependant, la structuration spatiale des processus biogéochimiques et l'intensité de la reminéralisation de la matière organique n'ont été caractérisées qu'à partir de mesures effectuées sur six stations. Afin de pallier cette limite, une cartographie de la consommation benthique d'oxygène a été réalisée en juin 2022 (mission JERICObent-8 ; Deflandre, 2022). Les données de cette campagne ont été traitées dans le cadre du stage de master 2 de Margot Porcher (Porcher, 2023).

Mon travail de thèse a notamment permis de quantifier la capacité de la VOG à stocker et recycler le carbone organique. Cependant, de nombreux facteurs pouvant influencer ces processus tels que la température (Marchand et al., 2020), la disponibilité en oxygène dissous (Wakelin et al., 2020), les débits de la Gironde (Schmidt et al., 2017) et donc les apports sédimentaires, l'hydrodynamisme (Charles et al., 2012) et les communautés benthiques (Marchand et al., 2020) sont susceptibles de varier dans les prochaines décennies en réponse aux changements globaux. Dans ce contexte, la prévision de l'évolution du fonctionnement biogéochimique de la VOG par modélisation est prévue dans la cadre du projet RiOMar (Programme Prioritaire de Recherche Océan et Climat).

Dans la cadre de ce travail, les taux de reminéralisation du carbone organique par les différents processus de reminéralisation ont été estimés à partir des flux diffusifs de composés dissous. Par conséquent, ces calculs ne prennent pas en compte les processus transitoires tels que la bioirrigation ou la remise en suspension de sédiments pouvant induire des couplages entre l'oxydation de composés réduits et la réduction subséquente des composés oxydés

nouvellement formés. Ainsi, il est probable que l'importance des processus de reminéralisation suboxiques aient été sous-estimée. De plus, les mesures de phases particulaires et dissoutes ont permis de mettre en évidence la formation de plusieurs phases authigènes sur l'ensemble de la colonne sédimentaire. Cependant, les taux de stockage des éléments inclus dans ces minéraux authigènes (e.g., Si, S, P) n'ont pas été quantifiés. La quantification de ces processus pourrait être réalisée par modélisation (Katsev et al., 2007; Munhoven, 2021; Paraska et al., 2014; Yakushev et al., 2017) et permettrait d'affiner la compréhension du fonctionnement biogéochimique de la VOG de l'échelle saisonnière à pluriséculaire.

Références

Abril, G., Etcheber, H., Le Hir, P., Bassoullet, P., Boutier, B., Frankignoulle, M., 1999. Oxic/anoxic oscillations and organic carbon mineralization in an estuarine maximum turbidity zone (The Gironde, France). Limnology and Oceanography 44, 1304–1315. https://doi.org/10.4319/lo.1999.44.5.1304

Accornero, A., Picon, P., Bovée, F. de, Charrière, B., Buscail, R., 2003. Organic carbon budget at the sediment–water interface on the Gulf of Lions continental margin. Continental Shelf Research 23, 79–92. https://doi.org/10.1016/S0278-4343(02)00168-1

Allen, G.P., Castaing, P., 1977. Carte de répartition des sédiments superficiels sur le plateau continental du Golfe de Gascogne. Bulletin Institut de Géologie du Bassin d'Aquitaine (Bordeaux) 255–261.

Allen, G.P., Castaing, P., Froidefond, J.M., Migniot, C., 1979. Quelques effets à long terme des aménagements sur la sédimentation dans l'estuaire de la gironde. Publications du CNEXO : Actes de Colloques 115–138.

Aller, R., Aller, J., Blair, N., Mackin, J., Rude, P., Stupakoff, I., Patchineelam, S., Boehme, S., Knoppers, B., 1991. Biogeochemical Processes in Amazon Shelf Sediments. Oceanography 4, 27–32. https://doi.org/10.5670/oceanog.1991.18

Aller, R., Aller, J., Kemp, P., 2001. "Effects of particle and solute transport on rates and extent of remineralization in bioturbated sediments," in: Organism-Sediment Interactions. University of South Carolina Press, USA, pp. 315–333.

Aller, R.C., 2014. Sedimentary Diagenesis, Depositional Environments, and Benthic Fluxes, in: Treatise on Geochemistry. Elsevier, pp. 293–334. https://doi.org/10.1016/B978-0-08-095975-7.00611-2

Aller, R.C., 2004. Conceptual models of early diagenetic processes: The muddy seafloor as an unsteady, batch reactor. Journal of Marine Research 62, 815–835. https://doi.org/10.1357/0022240042880837

Aller, R.C., 1998. Mobile deltaic and continental shelf muds as suboxic, fluidized bed reactors. Marine Chemistry 61, 143–155. https://doi.org/10.1016/S0304-4203(98)00024-3

Aller, R.C., 1994. Bioturbation and remineralization of sedimentary organic matter: effects of redox oscillation. Chemical Geology 114, 331–345. https://doi.org/10.1016/0009-2541(94)90062-0

Aller, R.C., Aller, J.Y., 1998. The effect of biogenic irrigation intensity and solute exchange on diagenetic reaction rates in marine sediments. Journal of Marine Research 56, 905–936. https://doi.org/10.1357/002224098321667413

Aller, R.C., Blair, N.E., 2006. Carbon remineralization in the Amazon–Guianas tropical mobile mudbelt: A sedimentary incinerator. Continental Shelf Research, Special Issue in Honor of Richard W. Sternberg's Contributions to Marine Sedimentology 26, 2241–2259. https://doi.org/10.1016/j.csr.2006.07.016

Aller, R.C., Blair, N.E., 1996. Sulfur diagenesis and burial on the Amazon shelf: Major control by physical sedimentation processes. Geo-Marine Letters 16, 3–10. https://doi.org/10.1007/BF01218830

Aller, R.C., Blair, N.E., Brunskill, G.J., 2008. Early diagenetic cycling, incineration, and burial of sedimentary organic carbon in the central Gulf of Papua (Papua New Guinea). Journal of Geophysical Research 113, F01S09. https://doi.org/10.1029/2006JF000689

Aller, R.C., Blair, N.E., Xia, Q., Rude, P.D., 1996. Remineralization rates, recycling, and storage of carbon in Amazon shelf sediments. Continental Shelf Research 16, 753–786. https://doi.org/10.1016/0278-4343(95)00046-1

Aller, R.C., Cochran, J.K., 2019. The Critical Role of Bioturbation for Particle Dynamics, Priming Potential, and Organic C Remineralization in Marine Sediments: Local and Basin Scales. Frontiers in Earth Science 7. https://doi.org/10.3389/feart.2019.00157

Aller, R.C., Mackin, J.E., Cox, R.T., 1986. Diagenesis of Fe and S in Amazon inner shelf muds: apparent dominance of Fe reduction and implications for the genesis of ironstones. Continental Shelf Research 6, 263–289. https://doi.org/10.1016/0278-4343(86)90064-6

Aller, Robert.C., Hannides, A., Heilbrun, C., Panzeca., C., 2004. Coupling of early diagenetic processes and sedimentary dynamics in tropical shelf environments: the Gulf of Papua deltaic complex. Continental Shelf Research 24, 2455–2486. https://doi.org/10.1016/j.csr.2004.07.018

Almroth, E., Tengberg, A., Andersson, J.H., Pakhomova, S., Hall, P.O.J., 2009. Effects of resuspension on benthic fluxes of oxygen, nutrients, dissolved inorganic carbon, iron and manganese in the Gulf of Finland, Baltic Sea. Continental Shelf Research 29, 807–818. https://doi.org/10.1016/j.csr.2008.12.011

Alperin, M.J., Albert, D.B., Martens, C.S., 1994. Seasonal variations in production and consumption rates of dissolved organic carbon in an organic-rich coastal sediment. Geochimica et Cosmochimica Acta 58, 4909–4930. https://doi.org/10.1016/0016-7037(94)90221-6

Alves, E.Q., Macario, K., Ascough, P., Bronk Ramsey, C., 2018. The Worldwide Marine Radiocarbon Reservoir Effect: Definitions, Mechanisms, and Prospects. Reviews of Geophysics 56, 278–305. https://doi.org/10.1002/2017RG000588

Aminot, A., Kérouel, R., 2007. Dosage automatique des nutriments dans les eaux marines: méthodes en flux continu. Ifremer, France.

Andrews, D., Bennett, A., 1981. Measurements of diffusivity near the sediment-water interface with a fine-scale resistivity probe. Geochimica et Cosmochimica Acta 45, 2169–2175. https://doi.org/10.1016/0016-7037(81)90069-7

Anschutz, P., Chaillou, G., 2009. Deposition and fate of reactive Fe, Mn, P, and C in suspended particulate matter in the Bay of Biscay. Continental Shelf Research 29, 1038–1043. https://doi.org/10.1016/j.csr.2008.12.022

Anschutz, P., Deborde, J., 2016. Spectrophotometric determination of phosphate in matrices from sequential leaching of sediments: Phosphate Analysis in Leaching Matrices. Limnology and Oceanography: Methods 14, 245–256. https://doi.org/10.1002/lom3.10085

Anschutz, P., Dedieu, K., Desmazes, F., Chaillou, G., 2005. Speciation, oxidation state, and reactivity of particulate manganese in marine sediments. Chemical Geology 218, 265–279. https://doi.org/10.1016/j.chemgeo.2005.01.008

Anschutz, P., Zhong, S., Sundby, B., Mucci, A., Gobeil, C., 1998. Burial efficiency of phosphorus and the geochemistry of iron in continental margin sediments. Limnology and Oceanography 43, 53–64. https://doi.org/10.4319/lo.1998.43.1.0053

Arakaki, T., Morse, J.W., 1993. Coprecipitation and adsorption of Mn(II) with mackinawite (FeS) under conditions similar to those found in anoxic sediments. Geochimica et Cosmochimica Acta 57, 9–14. https://doi.org/10.1016/0016-7037(93)90463-7

Arndt, S., Jørgensen, B.B., LaRowe, D.E., Middelburg, J.J., Pancost, R.D., Regnier, P., 2013. Quantifying the degradation of organic matter in marine sediments: A review and synthesis. Earth-Science Reviews 123, 53–86. https://doi.org/10.1016/j.earscirev.2013.02.008

Berg, P., Risgaard-Petersen, N., Rysgaard, S., 1998. Interpretation of measured concentration profiles in sediment pore water. Limnology and Oceanography 43, 1500–1510. https://doi.org/10.4319/lo.1998.43.7.1500

Berner, R.A., 1990. Atmospheric Carbon Dioxide Levels Over Phanerozoic Time. Science 249, 1382–1386. https://doi.org/10.1126/science.249.4975.1382

Berner, R.A., 1982. Burial of organic carbon and pyrite sulfur in the modern ocean; its geochemical and environmental significance. American Journal of Science 282, 451–473. https://doi.org/10.2475/ajs.282.4.451

Berthois, L., Le Calvez, Y., 1959. Deuxième contribution à l'étude de la sédimentation dans le golfe de Gascogne. Revue des travaux de l'institut des pêches maritimes 23, 323–377.

Bianchi, T.S., 2012. The role of terrestrially derived organic carbon in the coastal ocean: A changing paradigm and the priming effect. Proceedings of the National Academy of Sciences 109, 5134–5134. https://doi.org/10.1073/pnas.1202757109

Bianchi, T.S., 2011. The role of terrestrially derived organic carbon in the coastal ocean: A changing paradigm and the priming effect. Proceedings of the National Academy of Sciences 108, 19473–19481. https://doi.org/10.1073/pnas.1017982108

Bianchi, T.S., Cui, X., Blair, N.E., Burdige, D.J., Eglinton, T.I., Galy, V., 2018. Centers of organic carbon burial and oxidation at the land-ocean interface. Organic Geochemistry 115, 138–155. https://doi.org/10.1016/j.orggeochem.2017.09.008

Blair, N.E., Aller, R.C., 2012. The Fate of Terrestrial Organic Carbon in the Marine Environment. Annual Review of Marine Science 4, 401–423. https://doi.org/10.1146/annurev-marine-120709-142717

Blair, N.E., Leithold, E.L., Aller, R.C., 2004. From bedrock to burial: the evolution of particulate organic carbon across coupled watershed-continental margin systems. Marine Chemistry, New Approaches in Marine Organic Biogeochemistry: A Tribute to the Life and Science of John I. Hedges 92, 141–156. https://doi.org/10.1016/j.marchem.2004.06.023

Borja, A., Amouroux, D., Anschutz, P., Gómez-Gesteira, M., Uyarra, M.C., Valdés, L., 2019. The Bay of Biscay, in: World Seas: An Environmental Evaluation. Elsevier, pp. 113–152. https://doi.org/10.1016/B978-0-12-805068-2.00006-1

Bourillet, J.-F., Zaragosi, S., Mulder, T., 2006. The French Atlantic margin and deep-sea submarine systems. Geo-Marine Letters 26, 311–315. https://doi.org/10.1007/s00367-006-0042-2

Braeckman, U., Foshtomi, M.Y., Van Gansbeke, D., Meysman, F., Soetaert, K., Vincx, M., Vanaverbeke, J., 2014. Variable Importance of Macrofaunal Functional Biodiversity for Biogeochemical Cycling in Temperate Coastal Sediments. Ecosystems. https://doi.org/10.1007/s10021-014-9755-7

Breitburg, D., Levin, L.A., Oschlies, A., Grégoire, M., Chavez, F.P., Conley, D.J., Garçon, V., Gilbert, D., Gutiérrez, D., Isensee, K., Jacinto, G.S., Limburg, K.E., Montes, I., Naqvi, S.W.A., Pitcher, G.C., Rabalais, N.N., Roman, M.R., Rose, K.A., Seibel, B.A., Telszewski, M., Yasuhara, M., Zhang, J., 2018. Declining oxygen in the global ocean and coastal waters. Science. https://doi.org/10.1126/science.aam7240

Burdige, D.J., 2011. Estuarine and Coastal Sediments – Coupled Biogeochemical Cycling, in: Treatise on Estuarine and Coastal Science. Elsevier, pp. 279–316. https://doi.org/10.1016/B978-0-12-374711-2.00511-8

Burdige, D.J., 2007. Preservation of Organic Matter in Marine Sediments: Controls, Mechanisms, and an Imbalance in Sediment Organic Carbon Budgets? Chemical Reviews 107, 467–485. https://doi.org/10.1021/cr050347q

Burdige, D.J., 2006. Geochemistry of marine sediments. Princeton University Press, Princeton, NJ.

Burdige, D.J., 2005. Burial of terrestrial organic matter in marine sediments: A re-assessment: Terrestrial organic matter in marine sediments. Global Biogeochemical Cycles 19. https://doi.org/10.1029/2004GB002368

Burdige, D.J., 1993. The biogeochemistry of manganese and iron reduction in marine sediments. Earth-Science Reviews 35, 249–284. https://doi.org/10.1016/0012-8252(93)90040-E

Cai, W.-J., 2011. Estuarine and Coastal Ocean Carbon Paradox: CO_2 Sinks or Sites of Terrestrial Carbon Incineration? Annual Review of Marine Science 3, 123–145. https://doi.org/10.1146/annurev-marine-120709-142723

Cai, W.-J., Hu, X., Huang, W.-J., Murrell, M.C., Lehrter, J.C., Lohrenz, S.E., Chou, W.-C., Zhai, W., Hollibaugh, J.T., Wang, Y., Zhao, P., Guo, X., Gundersen, K., Dai, M., Gong, G.-C., 2011. Acidification of subsurface coastal waters enhanced by eutrophication. Nature Geoscience 4, 766–770. https://doi.org/10.1038/ngeo1297

Canfield, D.E., 1994. Factors influencing organic carbon preservation in marine sediments. Chemical Geology 114, 315–329. https://doi.org/10.1016/0009-2541(94)90061-2

Canfield, D.E., Jørgensen, B.B., Fossing, H., Glud, R., Gundersen, J., Ramsing, N.B., Thamdrup, B., Hansen, J.W., Nielsen, L.P., Hall, P.O.J., 1993. Pathways of organic carbon oxidation in three continental margin sediments. Marine Geology 113, 27–40. https://doi.org/10.1016/0025-3227(93)90147-N

Capet, A., Beckers, J.-M., Grégoire, M., 2013. Drivers, mechanisms and long-term variability of seasonal hypoxia on the Black Sea northwestern shelf – is there any recovery after eutrophication? Biogeosciences 10, 3943–3962. https://doi.org/10.5194/bg-10-3943-2013

Carbonel, P., Moyes, J., Peypouquet, J.P., 1975. Utilisation des ostracodes pour la mise en évidence et l'évolution d'une lagune Holocène à l'ouest de la Gironde, Golfe de Biscaye. Bulletin of American paleontology, Biology and Paleobiology of Ostracoda 65, 445–462.

Castaing, P., 1981. Le transfert à l'océan des suspensions estuariennes : cas de la Gironde (Thèse de doctorat). Université de Bordeaux I, Bordeaux.

Castaing, P., Froidefond, J.M., Lazure, P., Weber, O., Prud'homme, R., Jouanneau, J.M., 1999. Relationship between hydrology and seasonal distribution of suspended sediments on

the continental shelf of the Bay of Biscay. Deep Sea Research Part II: Topical Studies in Oceanography 46, 1979–2001. https://doi.org/10.1016/S0967-0645(99)00052-1

Cauwet, G., Gadel, F., de Souza Sierra, M.M., Donard, O., Ewald, M., 1990. Contribution of the Rhône River to organic carbon inputs to the northwestern Mediterranean Sea. Continental Shelf Research 10, 1025–1037. https://doi.org/10.1016/0278-4343(90)90073-U

Chaillou, G., Schäfer, J., Blanc, G., Anschutz, P., 2008. Mobility of Mo, U, As, and Sb within modern turbidites. Marine Geology 254, 171–179. https://doi.org/10.1016/j.margeo.2008.06.002

Charbonnier, C., Anschutz, P., 2019. Spectrophotometric determination of manganese in acidified matrices from (pore)waters and from sequential leaching of sediments. Talanta 195, 778–784. https://doi.org/10.1016/j.talanta.2018.12.012

Charbonnier, C., Mouret, A., Howa, H., Schmidt, S., Gillet, H., Anschutz, P., 2019. Quantification of diagenetic transformation of continental margin sediments at the Holocene time scale. Continental Shelf Research 180, 63–74. https://doi.org/10.1016/j.csr.2019.04.015

Charles, E., Idier, D., Delecluse, P., Déqué, M., Le Cozannet, G., 2012. Climate change impact on waves in the Bay of Biscay, France. Ocean Dynamics 62, 831–848. https://doi.org/10.1007/s10236-012-0534-8

Chen, Z., Nie, T., Zhao, X., Li, J., Yang, B., Cui, D., Li, X., 2022. Organic carbon remineralization rate in global marine sediments: A review. Regional Studies in Marine Science 49, 102112. https://doi.org/10.1016/j.rsma.2021.102112

Chong, L.S., Berelson, W.M., McManus, J., Rollins, N.E., 2018. Meter-Scale Early Diagenesis of Organic Matter Buried Within Deep-Sea Sediments Beneath the Amazon River Plume. Frontiers in Marine Science 5, 250. https://doi.org/10.3389/fmars.2018.00250

Ciavatta, S., Kay, S., Saux-Picart, S., Butenschön, M., Allen, J.I., 2016. Decadal reanalysis of biogeochemical indicators and fluxes in the North West European shelf-sea ecosystem. Journal of Geophysical Research: Oceans 121, 1824–1845. https://doi.org/10.1002/2015JC011496

Cirac, P., Berne, S., Castaing, P., Weber, O., 2000. Processus de mise en place et d'évolution de la couverture sédimentaire superficielle de la plate-forme nord-aquitaine. Oceanologica Acta 23, 663–686. https://doi.org/10.1016/S0399-1784(00)00110-9

Cocquempot, L., Delacourt, C., Paillet, J., Riou, P., Aucan, J., Castelle, B., Charria, G., Claudet, J., Conan, P., Coppola, L., Hocdé, R., Planes, S., Raimbault, P., Savoye, N., Testut, L., Vuillemin, R., 2019. Coastal Ocean and Nearshore Observation: A French Case Study. Frontiers in Marine Science 6.

Constantin, S., Doxaran, D., Derkacheva, A., Novoa, S., Lavigne, H., 2018. Multi-temporal dynamics of suspended particulate matter in a macro-tidal river Plume (the Gironde) as observed by satellite data. Estuarine, Coastal and Shelf Science 202, 172–184. https://doi.org/10.1016/j.ecss.2018.01.004

Corbett, D.R., McKee, B., Duncan, D., 2004. An evaluation of mobile mud dynamics in the Mississippi River deltaic region. Marine Geology 209, 91–112. https://doi.org/10.1016/j.margeo.2004.05.028

Cornwell, J.C., Morse, J.W., 1987. The characterization of iron sulfide minerals in anoxic marine sediments. Marine Chemistry, IX International Symposium on the Chemistry of the Mediterranean 22, 193–206. https://doi.org/10.1016/0304-4203(87)90008-9

Dalsgaard, T., Nielsen, L.P., Brotas, V., Viaroli, P., Underwood, G., Nedwell, D., Sundbäck, K., Rysgaard, S., Miles, A., Bartoli, M., Dong, L., Thornton, D., Ottosen, L., Castaldelli, G., Risgaard-Petersen, N., 2000. Protocol handbook for NICE-Nitrogen cycling in estuaries: A project under the EU research programme.

Deflandre, B., 2022. JERICOBENT-8 (THE REBIRTH) cruise, Côtes De La Manche R/V. https://doi.org/10.17600/18001913

Deflandre, B., 2019. JERICOBENT-7 cruise, Côtes De La Manche R/V. https://doi.org/10.17600/18001022

Deflandre, B., 2016. JERICOBENT. https://doi.org/10.18142/284

Deflandre B., 2016. JERICOBENT-1 cruise, Côtes De La Manche R/V. https://doi.org/10.17600/16010400

Deflandre, B., Duchêne, J.-C., 2010. PRO2FLUX – A software program for profile quantification and diffusive O2 flux calculations. Environmental Modelling & Software 25, 1059–1061. https://doi.org/10.1016/j.envsoft.2009.10.015

Deflandre, B., Gagné, J.-P., Sundby, B., Mucci, A., Guignard, C., Anschutz, P., 2000. The 1996 flood event : disruption of the ongoing diagenesis of saguenay fjord sediments. The Canadian Geotechnical Society 117–122.

Deflandre, B., Mucci, A., Gagné, J.-P., Guignard, C., Sundby, Bjørn, S., 2002. Early diagenetic processes in coastal marine sediments disturbed by a catastrophic sedimentation event. Geochimica et Cosmochimica Acta 66, 2547–2558. https://doi.org/10.1016/S0016-7037(02)00861-X

Deflandre, B., Schafer, J., Coynel, A., Mauffret, A., Burgeot, T., 2021. MAGMA cruise, Côtes De La Manche R/V. https://doi.org/10.17600/18000861

Deng, B., Zhang, J., Wu, Y., 2006. Recent sediment accumulation and carbon burial in the East China Sea. Global Biogeochemical Cycles 20. https://doi.org/10.1029/2005GB002559

Dias, J.M.A., Jouanneau, J.M., Gonzalez, R., Araújo, M.F., Drago, T., Garcia, C., Oliveira, A., Rodrigues, A., Vitorino, J., Weber, O., 2002. Present day sedimentary processes on the northern Iberian shelf. Progress in Oceanography, Benthic processes and dynamics at the NW Iberian Margin: results of the OMEX II Program 52, 249–259. https://doi.org/10.1016/S0079-6611(02)00009-5

Diaz, R.J., Rosenberg, R., 2008. Spreading Dead Zones and Consequences for Marine Ecosystems. Science. https://doi.org/10.1126/science.1156401

Dionex Corporation, 1986. Method for the determination of trace sulfate in brine. Sunnyvale, CA.

Dixit, S., Van Cappellen, P., van Bennekom, A.J., 2001. Processes controlling solubility of biogenic silica and pore water build-up of silicic acid in marine sediments. Marine Chemistry 73, 333–352. https://doi.org/10.1016/S0304-4203(00)00118-3

Dubosq, N., Schmidt, S., Sudre, J., Rigaud, S., Lamarque, B., Danilo, M., Grémare, A., Deflandre, B., 2022. First observations of seasonal bottom water deoxygenation off the Gironde estuary (Bay of Biscay, North East Atlantic). Frontiers in Marine Science 9, 1006453. https://doi.org/10.3389/fmars.2022.1006453

Dubosq, N., Schmidt, S., Walsh, J.P., Grémare, A., Gillet, H., Lebleu, P., Poirier, D., Perello, M.-C., Lamarque, B., Deflandre, B., 2021. A first assessment of organic carbon burial in the West Gironde Mud Patch (Bay of Biscay). Continental Shelf Research 221, 104419. https://doi.org/10.1016/j.csr.2021.104419

Duineveld, G.C.A., De Wilde, P.A.W.J., Berghuis, E.M., Kok, A., Tahey, T., Kromkamp, J., 1997. Benthic respiration and standing stock on two contrasting continental margins in the western Indian Ocean: the Yemen-Somali upwelling region and the margin off Kenya. Deep Sea Research Part II: Topical Studies in Oceanography 44, 1293–1317. https://doi.org/10.1016/S0967-0645(97)00006-4

Dupuis, H., Michel, D., Sottolichio, A., 2006. Wave climate evolution in the Bay of Biscay over two decades. Journal of Marine Systems 63, 105–114. https://doi.org/10.1016/j.jmarsys.2006.05.009

Edenborn, H.M., Belzile, N., Mucci, A., Lebel, J., Silverberg, N., 1986. Observations on the diagenetic behavior of arsenic in a deep coastal sediment. Biogeochemistry 2, 359–376. https://doi.org/10.1007/BF02180326

Egger, M., Jilbert, T., Behrends, T., Rivard, C., Slomp, C.P., 2015. Vivianite is a major sink for phosphorus in methanogenic coastal surface sediments. Geochimica et Cosmochimica Acta 169, 217–235. https://doi.org/10.1016/j.gca.2015.09.012

Epping, E., van der Zee, C., Soetaert, K., Helder, W., 2002. On the oxidation and burial of organic carbon in sediments of the Iberian margin and Nazaré Canyon (NE Atlantic).

Progress in Oceanography 52, 399–431. https://doi.org/10.1016/S0079-6611(02)00017-4

Etcheber, H., Relexans, J.-C., Beliard, M., Weber, O., Buscail, R., Heussner, S., 1999. Distribution and quality of sedimentary organic matter on the Aquitanian margin (Bay of Biscay). Deep Sea Research Part II: Topical Studies in Oceanography 46, 2249–2288. https://doi.org/10.1016/S0967-0645(99)00062-4

Etcheber, H., Taillez, A., Abril, G., Garnier, J., Servais, P., Moatar, F., Commarieu, M.-V., 2007. Particulate organic carbon in the estuarine turbidity maxima of the Gironde, Loire and Seine estuaries: origin and lability. Hydrobiologia 588, 245–259. https://doi.org/10.1007/s10750-007-0667-9

Feng, Y., DiMarco, S.F., Jackson, G.A., 2012. Relative role of wind forcing and riverine nutrient input on the extent of hypoxia in the northern Gulf of Mexico. Geophysical Research Letters 39. https://doi.org/10.1029/2012GL051192

Fennel, K., Testa, J.M., 2019. Biogeochemical Controls on Coastal Hypoxia. Annual Review of Marine Science 11, 105–130. https://doi.org/10.1146/annurev-marine-010318-095138

Feral, A., 1970. Interprétation sédimentologique et paléogéographique des formations alluviales frandriennes de l'estuaire de la Gironde et de ses dépendances marines (Thèse de doctorat). Université de Bordeaux I, Bordeaux.

Findlay, A.J., 2016. Microbial impact on polysulfide dynamics in the environment. FEMS Microbiology Letters 363, fnw103. https://doi.org/10.1093/femsle/fnw103

Fonselius, S., Dyrssen, D., Yhlen, B., 1999. Determination of hydrogen sulphide, in: Grasshoff, K., Kremling, K., Ehrhardt, M. (Eds.), Methods of Seawater Analysis. Wiley-VCH Verlag GmbH, Weinheim, Germany, pp. 91–100. https://doi.org/10.1002/9783527613984.ch5

Fontanier, C., Deflandre, B., Rigaud, S., Mamo, B., Dubosq, N., Lamarque, B., Langlet, D., Schmidt, S., Lebleu, P., Poirier, D., Cordier, M.A., Grémare, A., 2022. Live (stained) benthic foraminifera from the West-Gironde Mud Patch (Bay of Biscay, NE Atlantic): Assessing the reliability of bio-indicators in a complex shelf sedimentary unit. Continental Shelf Research 232, 104616. https://doi.org/10.1016/j.csr.2021.104616

Fontugne, M.R., Jouanneau, J.-M., 1987. Modulation of the particulate organic carbon flux to the ocean by a macrotidal estuary: Evidence from measurements of carbon isotopes in organic matter from the Gironde system. Estuarine, Coastal and Shelf Science 24, 377–387. https://doi.org/10.1016/0272-7714(87)90057-6

Foucault, A., Raoult, J.-F., Cecca, F., Platevoet, B., 2014. Dictionnaire de Géologie, 8e édition. ed. Dunod.

Froelich, P.N., Klinkhammer, G.P., Bender, M.L., Luedtke, N.A., Heath, G.R., Cullen, D., Dauphin, P., Hammond, D., Hartman, B., Maynard, V., 1979. Early oxidation of organic matter in pelagic sediments of the eastern equatorial Atlantic: suboxic diagenesis. Geochimica et Cosmochimica Acta 43, 1075–1090. https://doi.org/10.1016/0016-7037(79)90095-4

Gagnon, C., Mucci, A., Pelletier, É., 1996. Vertical distribution of dissolved sulphur species in coastal marine sediments. Marine Chemistry 52, 195–209. https://doi.org/10.1016/0304-4203(95)00099-2

Gagnon, C., Mucci, A., Pelletier, É., 1995. Anomalous accumulation of acid-volatile sulphides (AVS) in a coastal marine sediment, Saguenay Fjord, Canada. Geochimica et Cosmochimica Acta 59, 2663–2675. https://doi.org/10.1016/0016-7037(95)00163-T

Galloway, J.N., 2014. The Global Nitrogen Cycle, in: Treatise on Geochemistry. Elsevier, pp. 475–498. https://doi.org/10.1016/B978-0-08-095975-7.00812-3

Galy, V., France-Lanord, C., Beyssac, O., Faure, P., Kudrass, H., Palhol, F., 2007. Efficient organic carbon burial in the Bengal fan sustained by the Himalayan erosional system. Nature 450, 407–410. https://doi.org/10.1038/nature06273

Gan, S., Schmidt, F., Heuer, V.B., Goldhammer, T., Witt, M., Hinrichs, K.-U., 2020. Impacts of redox conditions on dissolved organic matter (DOM) quality in marine sediments off the River Rhône, Western Mediterranean Sea. Geochimica et Cosmochimica Acta 276, 151–169. https://doi.org/10.1016/j.gca.2020.02.001

Gilbert, D., Rabalais, N.N., Díaz, R.J., Zhang, J., 2010. Evidence for greater oxygen decline rates in the coastal ocean than in the open ocean. Biogeosciences 7, 2283–2296. https://doi.org/10.5194/bg-7-2283-2010

Giles, H., Pilditch, C.A., Nodder, S.D., Zeldis, J.R., Currie, K., 2007. Benthic oxygen fluxes and sediment properties on the northeastern New Zealand continental shelf. Continental Shelf Research 27, 2373–2388. https://doi.org/10.1016/j.csr.2007.06.007

Gillet, H., Deflandre, B., 2018. JERICOBENT-5-TH cruise, Thalia R/V. https://doi.org/10.17600/18000425

Glud, R.N., 2008. Oxygen dynamics of marine sediments. Marine Biology Research 4, 243–289. https://doi.org/10.1080/17451000801888726

Goñi, M.A., Yunker, M.B., Macdonald, R.W., Eglinton, T.I., 2005. The supply and preservation of ancient and modern components of organic carbon in the Canadian Beaufort Shelf of the Arctic Ocean. Marine Chemistry 93, 53–73. https://doi.org/10.1016/j.marchem.2004.08.001

Gordon, E.S., Goñi, M.A., Roberts, Q.N., Kineke, G.C., Allison, M.A., 2001. Organic matter distribution and accumulation on the inner Louisiana shelf west of the Atchafalaya

River. Continental Shelf Research 21, 1691–1721. https://doi.org/10.1016/S0278-4343(01)00021-8

Grant, J., Emerson, C.W., Hargrave, B.T., Shortle, J.L., 1991. Benthic oxygen consumption on continental shelves off eastern Canada. Continental Shelf Research, Proceedings of the Canadian Continental Shelf Seabed Symposium (CS) 11, 1083–1097. https://doi.org/10.1016/0278-4343(91)90092-K

Grasshoff, K., Ehrhardt, M., Kremling, K., Almgren, T. (Eds.), 1983. Methods of seawater analysis, 2nd rev. and extended ed. ed. Verlag Chemie, Weinheim.

Grémare, A., Gutiérrez, D., Anschutz, P., Amouroux, J.M., Deflandre, B., Vétion, G., 2005. Spatio-temporal changes in totally and enzymatically hydrolyzable amino acids of superficial sediments from three contrasted areas. Progress in Oceanography 65, 89–111. https://doi.org/10.1016/j.pocean.2005.02.016

Gröger, M., Maier-Reimer, E., Mikolajewicz, U., Moll, A., Sein, D., 2013. NW European shelf under climate warming: implications for open ocean – shelf exchange, primary production, and carbon absorption. Biogeosciences 10, 3767–3792. https://doi.org/10.5194/bg-10-3767-2013

Halewood, E., Opalk, K., Custals, L., Carey, M., Hansell, D.A., Carlson, C.A., 2022. Determination of dissolved organic carbon and total dissolved nitrogen in seawater using High Temperature Combustion Analysis. Frontiers in Marine Science 9.

Hall, P. 0. J., Aller, R.C., 1992. Rapid, small-volume, flow injection analysis for SCO_2, and NH_4^+ in marine and freshwaters. Limnology and Oceanography 37, 1113–1119. https://doi.org/10.4319/lo.1992.37.5.1113

Hedges, J.I., Keil, R.G., 1995. Sedimentary organic matter preservation: an assessment and speculative synthesis. Marine Chemistry 49, 81–115. https://doi.org/10.1016/0304-4203(95)00008-F

Herman, P.M.J., Soetaert, K., Middelburg, J.J., Heip, C., Lohse, L., Epping, E., Helder, W., Antia, A.N., Peinert, R., 2001. The seafloor as the ultimate sediment trap—using sediment properties to constrain benthic–pelagic exchange processes at the Goban Spur. Deep Sea Research Part II: Topical Studies in Oceanography 48, 3245–3264. https://doi.org/10.1016/S0967-0645(01)00039-X

Hoehler, T.M., Alperin, M.J., Albert, D.B., Martens, C.S., 1994. Field and laboratory studies of methane oxidation in an anoxic marine sediment: Evidence for a methanogen-sulfate reducer consortium. Global Biogeochemical Cycles 8, 451–463. https://doi.org/10.1029/94GB01800

Hsieh, Y.P., Yang, C.H., 1989. Diffusion methods for the determination ofreduced inorganic sulfur species in sediments. Limnology and Oceanography 34, 1126–1130. https://doi.org/10.4319/lo.1989.34.6.1126

Hu, L., Shi, X., Bai, Y., Qiao, S., Li, L., Yu, Y., Yang, G., Ma, D., Guo, Z., 2016. Recent organic carbon sequestration in the shelf sediments of the Bohai Sea and Yellow Sea, China. Journal of Marine Systems 155, 50–58. https://doi.org/10.1016/j.jmarsys.2015.10.018

Hulot, V., Metzger, E., Thibault de Chanvalon, A., Mouret, A., Schmidt, S., Deflandre, B., Rigaud, S., Beneteau, E., Savoye, N., Souchu, P., Le Merrer, Y., Maillet, G.M., 2023. Impact of an exceptional winter flood on benthic oxygen and nutrient fluxes in a temperate macrotidal estuary: Potential consequences on summer deoxygenation. Frontiers in Marine Science 10.

Hulth, S., Blackburn, T.H., Hall, P.O.J., 1994. Arctic sediments (Svalbard): consumption and microdistribution of oxygen. Marine Chemistry 46, 293–316. https://doi.org/10.1016/0304-4203(94)90084-1

Hulth, S., Tengberg, A., Landén, A., Hall, P.O.J., 1997. Mineralization and burial of organic carbon in sediments of the southern Weddell Sea (Antarctica). Deep Sea Research Part I: Oceanographic Research Papers 44, 955–981. https://doi.org/10.1016/S0967-0637(96)00114-8

Hyacinthe, C., Anschutz, P., Carbonel, P., Jouanneau, J.-M., Jorissen, F.J., 2001. Early diagenetic processes in the muddy sediments of the Bay of Biscay. Marine Geology 177, 111–128. https://doi.org/10.1016/S0025-3227(01)00127-X

Jalón-Rojas, I., Dijkstra, Y.M., Schuttelaars, H.M., Brouwer, R.L., Schmidt, S., Sottolichio, A., 2021. Multidecadal Evolution of the Turbidity Maximum Zone in a Macrotidal River Under Climate and Anthropogenic Pressures. Journal of Geophysical Research: Oceans 126. https://doi.org/10.1029/2020JC016273

Jorgensen, B.B., 2021. Sulfur Biogeochemical Cycle of Marine Sediments. Geochemical Perspectives 145–307. https://doi.org/10.7185/geochempersp.10.2

Jorgensen, B.B., Findlay, A.J., Pellerin, A., 2019. The Biogeochemical Sulfur Cycle of Marine Sediments. Frontiers in Microbiology 10. https://doi.org/10.3389/fmicb.2019.00849

Jorgensen, B.B., Wenzhöfer, F., Egger, M., Glud, R.N., 2022. Sediment oxygen consumption: Role in the global marine carbon cycle. Earth-Science Reviews 228, 103987. https://doi.org/10.1016/j.earscirev.2022.103987

Jouanneau, J.-M., Weber, O., Champilou, N., Cirac, P., Muxika, I., Borja, A., Pascual, A., Rodríguez-Lázaro, J., Donard, O., 2008. Recent sedimentary study of the shelf of the

Basque country. Journal of Marine Systems, Oceanography of the Bay of Biscay 72, 397–406. https://doi.org/10.1016/j.jmarsys.2007.03.013

Jouanneau, J.M., Weber, O., Cremer, M., Castaing, P., 1999. Fine-grained sediment budget on the continental margin of the Bay of Biscay. Deep Sea Research Part II: Topical Studies in Oceanography 46, 2205–2220. https://doi.org/10.1016/S0967-0645(99)00060-0

Jouanneau, J.M., Weber, O., Drago, T., Rodrigues, A., Oliveira, A., Dias, J.M.A., Garcia, C., Schmidt, S., Reyss, J.L., 2002. Recent sedimentation and sedimentary budgets on the western Iberian shelf. Progress in Oceanography, Benthic processes and dynamics at the NW Iberian Margin: results of the OMEX II Program 52, 261–275. https://doi.org/10.1016/S0079-6611(02)00010-1

Jouanneau, J.M., Weber, O., Latouche, C., Vernet, J.P., Dominik, J., 1989. Erosion, non-deposition and sedimentary processes through a sedimentological and radioisotopic study of surficial deposits from the "Ouest-Gironde vasière" (Bay of Biscay). Continental Shelf Research 9, 325–342. https://doi.org/10.1016/0278-4343(89)90037-X

Katsev, S., Chaillou, G., Sundby, B., Mucci, A., 2007. Effects of progressive oxygen depletion on sediment diagenesis and fluxes: A model for the lower St. Lawrence River Estuary. Limnology and Oceanography 52, 2555–2568. https://doi.org/10.4319/lo.2007.52.6.2555

Keil, R., 2017. Anthropogenic Forcing of Carbonate and Organic Carbon Preservation in Marine Sediments. Annual Review of Marine Science 9, 151–172. https://doi.org/10.1146/annurev-marine-010816-060724

Kersalé, M., Marié, L., Le Cann, B., Serpette, A., Lathuilière, C., Le Boyer, A., Rubio, A., Lazure, P., 2016. Poleward along-shore current pulses on the inner shelf of the Bay of Biscay. Estuarine, Coastal and Shelf Science 179, 155–171. https://doi.org/10.1016/j.ecss.2015.11.018

Kim, D., Kim, J.-H., Tesi, T., Kang, S., Nogarotto, A., Park, K., Lee, D.-H., Jin, Y.K., Shin, K.-H., Nam, S.-I., 2022. Changes in the burial efficiency and composition of terrestrial organic carbon along the Mackenzie Trough in the Beaufort Sea. Estuarine, Coastal and Shelf Science 275, 107997. https://doi.org/10.1016/j.ecss.2022.107997

Kim, H.-C., Son, S., Kim, Y.H., Khim, J.S., Nam, J., Chang, W.K., Lee, J.-H., Lee, C.-H., Ryu, J., 2017. Remote sensing and water quality indicators in the Korean West coast: Spatio-temporal structures of MODIS-derived chlorophyll-*a* and total suspended solids. Marine Pollution Bulletin 121, 425–434. https://doi.org/10.1016/j.marpolbul.2017.05.026

Kim, S.-H., Lee, J.S., Kim, K.-T., Kim, S.-L., Yu, O.H., Lim, D., Kim, S.H., 2020. Low benthic mineralization and nutrient fluxes in the continental shelf sediment of the northern East China Sea. Journal of Sea Research 164, 101934. https://doi.org/10.1016/j.seares.2020.101934

Kim, Y.H., Son, S., Kim, H.-C., Kim, B., Park, Y.-G., Nam, J., Ryu, J., 2020. Application of satellite remote sensing in monitoring dissolved oxygen variabilities: A case study for coastal waters in Korea. Environment International 134, 105301. https://doi.org/10.1016/j.envint.2019.105301

Kostka, J.E., Luther, G.W., 1994. Partitioning and speciation of solid phase iron in saltmarsh sediments. Geochimica et Cosmochimica Acta 58, 1701–1710. https://doi.org/10.1016/0016-7037(94)90531-2

Koutsikopoulos, C., Le Cann, B., 1996. Physical processes and hydrological structures retated to the Bay of Biscay anchovy. Scientia Marina 9–19.

Kristensen, E., 2000. Organic matter diagenesis at the oxic/anoxic interface in coastal marine sediments, with emphasis on the role of burrowing animals. Hydrobiologia 426, 1–24. https://doi.org/10.1023/A:1003980226194

Kristensen, E., Kostka, J. E., 2005. Macrofaunal burrows and irrigation in marine sediment: Microbiological and biogeochemical interactions, in: Kristensen, Erik, Haese, R.R., Kostka, Joel E. (Eds.), Coastal and Estuarine Studies. American Geophysical Union, Washington, D. C., pp. 125–157. https://doi.org/10.1029/CE060p0125

Kristensen, E., Mikkelsen, O.L., 2003. Impact of the burrow-dwelling polychaete Nereis diversicolor on the degradation of fresh and aged macroalgal detritus in a coastal marine sediment. Marine Ecology Progress Series 265, 141–153.

Kuehl, S.A., DeMaster, D.J., Nittrouer, C.A., 1986. Nature of sediment accumulation on the Amazon continental shelf. Continental Shelf Research 6, 209–225. https://doi.org/10.1016/0278-4343(86)90061-0

Kuzyk, Z.Z.A., Gobeil, C., Goñi, M.A., Macdonald, R.W., 2017. Early diagenesis and trace element accumulation in North American Arctic margin sediments. Geochimica et Cosmochimica Acta 203, 175–200. https://doi.org/10.1016/j.gca.2016.12.015

Labry, C., Herbland, A., Delmas, D., Laborde, P., Lazure, P., Froidefond, J., Jegou, A.-M., Sautour, B., 2001. Initiation of winter phytoplankton blooms within the Gironde plume waters in the Bay of Biscay. Marine Ecology Progress Series 212, 117–130.

Lamarque, B., 2022. Biodiversité et fonctionnement de l'écosystème benthique dans la Vasière Ouest Gironde (These de doctorat). Bordeaux, Université de Bordeaux.

Lamarque, B., Deflandre, B., Galindo Dalto, A., Schmidt, S., Romero-Ramirez, A., Garabetian, F., Dubosq, N., Diaz, M., Grasso, F., Sottolichio, A., Bernard, G., Gillet, H., Cordier,

M.-A., Poirier, D., Lebleu, P., Derriennic, H., Danilo, M., Murilo Barboza Tenório, M., Grémare, A., 2021. Spatial Distributions of Surface Sedimentary Organics and Sediment Profile Image Characteristics in a High-Energy Temperate Marine RiOMar: The West Gironde Mud Patch. Journal of Marine Science and Engineering 242. https://doi.org/10.3390/jmse9030242

Lamarque, B., Deflandre, B., Schmidt, S., Bernard, G., Dubosq, N., Diaz, M., Lavesque, N., Garabetian, F., Grasso, F., Sottolichio, A., Rigaud, S., Romero-Ramirez, A., Cordier, M.-A., Poirier, D., Danilo, M., Grémare, A., 2022. Spatiotemporal dynamics of surface sediment characteristics and benthic macrofauna compositions in a temperate high-energy River-dominated Ocean Margin. Continental Shelf Research 247, 104833. https://doi.org/10.1016/j.csr.2022.104833

Lanoux, A., Etcheber, H., Schmidt, S., Sottolichio, A., Chabaud, G., Richard, M., Abril, G., 2013. Factors contributing to hypoxia in a highly turbid, macrotidal estuary (the Gironde, France). Environmental Science Processes and Impacts 15, 585–595. https://doi.org/10.1039/c2em30874f

Lansard, B., Rabouille, C., Denis, L., Grenz, C., 2009. Benthic remineralization at the land–ocean interface: A case study of the Rhône River (NW Mediterranean Sea). Estuarine, Coastal and Shelf Science 81, 544–554. https://doi.org/10.1016/j.ecss.2008.11.025

Lansard, B., Rabouille, C., Denis, L., Grenz, C., 2008. In situ oxygen uptake rates by coastal sediments under the influence of the Rhône River (NW Mediterranean Sea). Continental Shelf Research 28, 1501–1510. https://doi.org/10.1016/j.csr.2007.10.010

Laursen, A.E., Seitzinger, S.P., 2002. The role of denitrification in nitrogen removal and carbon mineralization in Mid-Atlantic Bight sediments. Continental Shelf Research 22, 1397–1416. https://doi.org/10.1016/S0278-4343(02)00008-0

Le Boyer, A., Charria, G., Le Cann, B., Lazure, P., Marié, L., 2013. Circulation on the shelf and the upper slope of the Bay of Biscay. Continental Shelf Research 55, 97–107. https://doi.org/10.1016/j.csr.2013.01.006

Legeleux, F., Reyss, J., Bonte, P., Organo, C., 1994. Concomitant enrichments of uranium, molybdenum and arsenic in suboxic continental-margin sediments. Oceanologica Acta 17, 417–429.

Leithold, E.L., Perkey, D.W., Blair, N.E., Creamer, T.N., 2005. Sedimentation and carbon burial on the northern California continental shelf: the signatures of land-use change. Continental Shelf Research 25, 349–371. https://doi.org/10.1016/j.csr.2004.09.015

Lesueur, P., 1992. Les vasières de la plate-forme Ouest-Gironde (France) : modèle faciologique et archive sédimentaire des flux côtiers (These de doctorat). Université de Bordeaux 1, Bordeaux.

Lesueur, P., Jouanneau, J.-M., Boust, D., Tastet, J.-P., Weber, O., 2001. Sedimentation rates and fluxes in the continental shelf mud fields in the Bay of Biscay (France). Continental Shelf Research 21, 1383–1401. https://doi.org/10.1016/S0278-4343(01)00004-8

Lesueur, P., Tastet, J.P., 1994. Facies, internal structures and sequences of modern Gironde-derived muds on the Aquitaine inner shelf, France. Marine Geology 120, 267–290. https://doi.org/10.1016/0025-3227(94)90062-0

Lesueur, P., Tastet, J.P., Marambat, L., 1996. Shelf mud fields formation within historical times: examples from offshore the Gironde estuary, France. Continental Shelf Research 16, 1849–1870. https://doi.org/10.1016/0278-4343(96)00013-1

Lesueur, P., Tastet, J.P., Weber, O., 2002. Origin and morphosedimentary evolution of fine-grained modern continental shelf deposits: the Gironde mud fields (Bay of Biscay, France). Sedimentology 49, 1299–1320. https://doi.org/10.1046/j.1365-3091.2002.00498.x

Lesueur, P., Tastet, J.-P., Weber, O., Sinko, J.-A., 1991. Modèle faciologique d'un corps sédimentaire pélitique de plate-forme : la vasière Ouest-Gironde (France). Oceanologica Acta sp., 143–153.

Levin, L.A., 2018. Manifestation, Drivers, and Emergence of Open Ocean Deoxygenation. Annual Review of Marine Science 10, 229–260. https://doi.org/10.1146/annurev-marine-121916-063359

Li, M., Lee, Y.J., Testa, J.M., Li, Y., Ni, W., Kemp, W.M., Di Toro, D.M., 2016. What drives interannual variability of hypoxia in Chesapeake Bay: Climate forcing versus nutrient loading? Geophysical Research Letters 43, 2127–2134. https://doi.org/10.1002/2015GL067334

Li, M., Peng, C., Wang, M., Xue, W., Zhang, K., Wang, K., Shi, G., Zhu, Q., 2017. The carbon flux of global rivers: A re-evaluation of amount and spatial patterns. Ecological Indicators 80, 40–51. https://doi.org/10.1016/j.ecolind.2017.04.049

Liénart, C., Savoye, N., David, V., Ramond, P., Rodriguez Tress, P., Hanquiez, V., Marieu, V., Aubert, F., Aubin, S., Bichon, S., Boinet, C., Bourasseau, L., Bozec, Y., Bréret, M., Breton, E., Caparros, J., Cariou, T., Claquin, P., Conan, P., Corre, A.-M., Costes, L., Crouvoisier, M., Del Amo, Y., Derriennic, H., Dindinaud, F., Duran, R., Durozier, M., Devesa, J., Ferreira, S., Feunteun, E., Garcia, N., Geslin, S., Grossteffan, E., Gueux, A., Guillaudeau, J., Guillou, G., Jolly, O., Lachaussée, N., Lafont, M., Lagadec, V., Lamoureux, J., Lauga, B., Lebreton, B., Lecuyer, E., Lehodey, J.-P., Leroux, C., L'Helguen, S., Macé, E., Maria, E., Mousseau, L., Nowaczyk, A., Pineau, P., Petit, F., Pujo-Pay, M., Raimbault, P., Rimmelin-Maury, P., Rouaud, V., Sauriau, P.-G., Sultan, E., Susperregui, N., 2018. Dynamics of particulate organic matter composition in

coastal systems: Forcing of spatio-temporal variability at multi-systems scale. Progress in Oceanography 162, 271–289. https://doi.org/10.1016/j.pocean.2018.02.026

Lin, S., Huang, K.-M., Chen, S.-K., 2000. Organic carbon deposition and its control on iron sulfide formation of the southern East China Sea continental shelf sediments. Continental Shelf Research 20, 619–635. https://doi.org/10.1016/S0278-4343(99)00088-6

Lin, S., Morse, J.W., 1991. Sulfate reduction and iron sulfide mineral formation in Gulf of Mexico anoxic sediments. American Journal of Science 291, 55–89. https://doi.org/10.2475/ajs.291.1.55

Lin, Y.-P., Singer, P.C., 2006. Inhibition of calcite precipitation by orthophosphate: Speciation and thermodynamic considerations. Geochimica et Cosmochimica Acta 70, 2530–2539. https://doi.org/10.1016/j.gca.2006.03.002

Link, H., Chaillou, G., Forest, A., Piepenburg, D., Archambault, P., 2013. Multivariate benthic ecosystem functioning in the Arctic – benthic fluxes explained by environmental parameters in the southeastern Beaufort Sea. Biogeosciences 10, 5911–5929. https://doi.org/10.5194/bg-10-5911-2013

Lofi, J., Werber, O., 2001. SCOPIX - digital processing of X-ray images for the enhancement of sedimentary structures in undisturbed core slabs. Geo-Marine Letters 20, 182–186. https://doi.org/10.1007/s003670000051

Ludwig, W., Probst, J.-L., Kempe, S., 1996. Predicting the oceanic input of organic carbon by continental erosion. Global Biogeochemical Cycles 10, 23–41. https://doi.org/10.1029/95GB02925

Luo, X., Bai, X., Tan, Q., Ran, C., Chen, H., Xi, H., Chen, F., Wu, L., Li, C., Zhang, S., Zhong, X., Tian, S., 2022. Particulate organic carbon exports from the terrestrial biosphere controlled by erosion. CATENA 209, 105815. https://doi.org/10.1016/j.catena.2021.105815

Luther, G.W., Kostka, J.E., Church, T.M., Sulzberger, B., Stumm, W., 1992. Seasonal iron cycling in the salt-marsh sedimentary environment: the importance of ligand complexes with Fe(II) and Fe(III) in the dissolution of Fe(III) minerals and pyrite, respectively. Marine Chemistry, Progress in Marine Chemistry 40, 81–103. https://doi.org/10.1016/0304-4203(92)90049-G

Madison, A.S., Tebo, B.M., Luther, G.W., 2011. Simultaneous determination of soluble manganese(III), manganese(II) and total manganese in natural (pore)waters. Talanta 84, 374–381. https://doi.org/10.1016/j.talanta.2011.01.025

Marchand, M.L., Hattab, T., Niquil, N., Albouy, C., Loc'h, F.L., Lasram, F.B.R., 2020. Climate change in the Bay of Biscay: Changes in spatial biodiversity patterns could be driven

by the arrivals of southern species. Marine Ecology Progress Series 647, 17. https://doi.org/10.3354/meps13401

Mary, Y., Eynaud, F., Colin, C., Rossignol, L., Brocheray, S., Mojtahid, M., Garcia, J., Peral, M., Howa, H., Zaragosi, S., Cremer, M., 2017. Changes in Holocene meridional circulation and poleward Atlantic flow: the Bay of Biscay as a nodal point. Climate of the Past 13, 201–216. https://doi.org/10.5194/cp-13-201-2017

Masqué, P., Isla, E., Sanchez-Cabeza, J.A., Palanques, A., Bruach, J.M., Puig, P., Guillén, J., 2002. Sediment accumulation rates and carbon fluxes to bottom sediments at the Western Bransfield Strait (Antarctica). Deep Sea Research Part II: Topical Studies in Oceanography, FRUELA - A Carbon Flux Study in the Antarctic Peninsula Area 49, 921–933. https://doi.org/10.1016/S0967-0645(01)00131-X

Massé, C., Meisterhans, G., Deflandre, B., Bachelet, G., Bourasseau, L., Bichon, S., Ciutat, A., Jude-Lemeilleur, F., Lavesque, N., Raymond, N., Grémare, A., Garabetian, F., 2016. Bacterial and macrofaunal communities in the sediments of the West Gironde Mud Patch, Bay of Biscay (France). Estuarine, Coastal and Shelf Science, Special Issue: Functioning and dysfunctioning of Marine and Brackish Ecosystems 179, 189–200. https://doi.org/10.1016/j.ecss.2016.01.011

Mayer, L.M., 1994a. Surface area control of organic carbon accumulation in continental shelf sediments. Geochimica et Cosmochimica Acta 58, 1271–1284. https://doi.org/10.1016/0016-7037(94)90381-6

Mayer, L.M., 1994b. Relationships between mineral surfaces and organic carbon concentrations in soils and sediments. Chemical Geology 114, 347–363. https://doi.org/10.1016/0009-2541(94)90063-9

Mayer, L.M., Linda L., S., Sawyer, T., Plante, C.J., Jumars, P.A., Sel, R.L., 1995. Bioavailable amino acids in sediments: A biomimetic, kinetics based approach. Limnology and Oceanography 40, 511–520. https://doi.org/10.4319/lo.1995.40.3.0511

McCave, I.N., 1972. Shelf Sediment Transport, Process and Pattern, in: Swift, D.J.P., Duane, D.B., Pilkey, O.H. (Eds.), Transport and Escape of Fine-Grained Sediment from Shelf Areas. Dowden, Hutchinson & Ross, Stroudsburg, Pa., pp. 225–248.

McClain, M.E., Boyer, E.W., Dent, C.L., Gergel, S.E., Grimm, N.B., Groffman, P.M., Hart, S.C., Harvey, J.W., Johnston, C.A., Mayorga, E., McDowell, W.H., Pinay, G., 2003. Biogeochemical Hot Spots and Hot Moments at the Interface of Terrestrial and Aquatic Ecosystems. Ecosystems 6, 301–312. https://doi.org/10.1007/s10021-003-0161-9

McKee, B.A., Aller, R.C., Allison, M.A., Bianchi, T.S., Kineke, G.C., 2004. Transport and transformation of dissolved and particulate materials on continental margins influenced

by major rivers: benthic boundary layer and seabed processes. Continental Shelf Research 24, 899–926. https://doi.org/10.1016/j.csr.2004.02.009

Ménesguen, A., Dussauze, M., Dumas, F., Thouvenin, B., Garnier, V., Lecornu, F., Répécaud, M., 2019. Ecological model of the Bay of Biscay and English Channel shelf for environmental status assessment part 1: Nutrients, phytoplankton and oxygen. Ocean Modelling 133, 56–78. https://doi.org/10.1016/j.ocemod.2018.11.002

Mengual, B., Le Hir, P., Cayocca, F., Garlan, T., 2019. Bottom trawling contribution to the spatio-temporal variability of sediment fluxes on the continental shelf of the Bay of Biscay (France). Marine Geology 414, 77–91. https://doi.org/10.1016/j.margeo.2019.05.009

Michalopoulos, P., Aller, R.C., 2004. Early diagenesis of biogenic silica in the Amazon delta: alteration, authigenic clay formation, and storage. Geochimica et Cosmochimica Acta 68, 1061–1085. https://doi.org/10.1016/j.gca.2003.07.018

Middelburg, J.J., 2019. Carbon Processing at the Seafloor, in: China's Provincial Economic Competitiveness and Policy Outlook for the 13th Five-Year Plan Period (2016-2020). Springer Singapore, Singapore, pp. 57–75. https://doi.org/10.1007/978-3-030-10822-9_4

Middelburg, J.J., De Lange, G.J., van Der Weijden, C.H., 1987. Manganese solubility control in marine pore waters. Geochimica et Cosmochimica Acta 51, 759–763. https://doi.org/10.1016/0016-7037(87)90086-X

Mouret, A., Anschutz, P., Deflandre, B., Chaillou, G., Hyacinthe, C., Deborde, J., Etcheber, H., Jouanneau, J.-M., Grémare, A., Lecroart, P., 2010. Oxygen and organic carbon fluxes in sediments of the Bay of Biscay. Deep Sea Research Part I: Oceanographic Research Papers 57, 528–540. https://doi.org/10.1016/j.dsr.2009.12.009

Moyes, J., 1974. Un exemple d'étude paléoécologique et paléogéographique : la vasière Ouest-Gironde et son évolution durant l'Holocène. Bulletin Institut de Géologie du Bassin d'Aquitaine 3–20.

Mucci, A., 2004. The Behavior of Mixed Ca–Mn Carbonates in Water and Seawater: Controls of Manganese Concentrations in Marine Porewaters. Aquatic Geochemistry 10, 139–169. https://doi.org/10.1023/B:AQUA.0000038958.56221.b4

Mucci, A., 1988. Manganese uptake during calcite precipitation from seawater: Conditions leading to the formation of a pseudokutnahorite. Geochimica et Cosmochimica Acta 52, 1859–1868. https://doi.org/10.1016/0016-7037(88)90009-9

Mucci, A., 1986. Growth kinetics and composition of magnesian calcite overgrowths precipitated from seawater: Quantitative influence of orthophosphate ions. Geochimica et Cosmochimica Acta 50, 2255–2265. https://doi.org/10.1016/0016-7037(86)90080-3

Mucci, A., Boudreau, B., Guignard, C., 2003. Diagenetic mobility of trace elements in sediments covered by a flash flood deposit: Mn, Fe and As. Applied Geochemistry 18, 1011–1026. https://doi.org/10.1016/S0883-2927(02)00207-X

Mucci, A., Richard, L.-F., Lucotte, M., Guignard, C., 2000. The Differential Geochemical Behavior of Arsenic and Phosphorus in the Water Column and Sediments of the Saguenay Fjord Estuary, Canada. Aquatic Geochemistry 6, 293–324. https://doi.org/10.1023/A:1009632127607

Mucci, A., Starr, M., Gilbert, D., Sundby, B., 2011. Acidification of Lower St. Lawrence Estuary Bottom Waters. Atmosphere - Ocean 49, 206–218. https://doi.org/10.1080/07055900.2011.599265

Muller-Karger, F.E., 2005. The importance of continental margins in the global carbon cycle. Geophysical Research Letters 32, L01602. https://doi.org/10.1029/2004GL021346

Munhoven, G., 2021. Model of Early Diagenesis in the Upper Sediment with Adaptable complexity – MEDUSA (v. 2): a time-dependent biogeochemical sediment module for Earth system models, process analysis and teaching. Geoscientific Model Development 14, 3603–3631. https://doi.org/10.5194/gmd-14-3603-2021

Murphy, J., Riley, J.P., 1962. A modified single solution method for the determination of phosphate in natural waters. Analytica Chimica Acta 27, 31–36. https://doi.org/10.1016/S0003-2670(00)88444-5

Murrell, M.C., Lehrter, J.C., 2011. Sediment and Lower Water Column Oxygen Consumption in the Seasonally Hypoxic Region of the Louisiana Continental Shelf. Estuaries and Coasts 34, 912–924. https://doi.org/10.1007/s12237-010-9351-9

NASA Ocean Color. (USA, NASA) Availabile at: https://oceancolor.gsfc.nasa.gov/

Neveux, J., Lantoine, F., 1993. Spectrofluorometric assay of chlorophylls and phaeopigments using the least squares approximation technique. Deep Sea Research Part I: Oceanographic Research Papers 40, 1747–1765. https://doi.org/10.1016/0967-0637(93)90030-7

Nittrouer, C.A., Sharara, M.T., DeMaster, D.J., 1983. Variations of sediment texture on the Amazon continental shelf. Journal of Sedimentary Research 53, 179–191. https://doi.org/10.1306/212F8184-2B24-11D7-8648000102C1865D

Norkko, J., Pilditch, C.A., Gammal, J., Rosenberg, R., Enemar, A., Magnusson, M., Granberg, M.E., Lindgren, J.F., Agrenius, S., Norkko, A., 2019. Ecosystem functioning along gradients of increasing hypoxia and changing soft-sediment community types. Journal of Sea Research 153, 101781. https://doi.org/10.1016/j.seares.2019.101781

Oberle, F.K.J., Swarzenski, P.W., Reddy, C.M., Nelson, R.K., Baasch, B., Hanebuth, T.J.J., 2016. Deciphering the lithological consequences of bottom trawling to sedimentary

habitats on the shelf. Journal of Marine Systems 159, 120–131. https://doi.org/10.1016/j.jmarsys.2015.12.008

Oms, P.-E., 2019. Transferts multi-échelles des apports continentaux dans le golfe de Gascogne (Thèse de doctorat). Université de Bretagne occidentale - Brest.

Oschlies, A., Brandt, P., Stramma, L., Schmidtko, S., 2018. Drivers and mechanisms of ocean deoxygenation. Nature Geoscience 11, 467–473. https://doi.org/10.1038/s41561-018-0152-2

Paraska, D.W., Hipsey, M.R., Salmon, S.U., 2014. Sediment diagenesis models: Review of approaches, challenges and opportunities. Environmental Modelling & Software 61, 297–325. https://doi.org/10.1016/j.envsoft.2014.05.011

Parkhurst, D.L., Appelo, C. a. J., 1999. User's guide to PHREEQC (Version 2)-a computer program for speciation, batch-reaction, one-dimensional transport, and inverse geochemical calculations. Water-Resources Investigations Report 312. https://doi.org/10.3133/WRI994259

Parra, M., Castaing, P., Jouanneau, J.-M., Grousset, F., Latouche, C., 1999. Nd–Sr Isotopic composition of present-day sediments from the Gironde Estuary, its draining basins and the WestGironde mud patch (SW France). Continental Shelf Research 19, 135–150. https://doi.org/10.1016/S0278-4343(98)00083-1

Pastor, L., Cathalot, C., Deflandre, B., Viollier, E., Soetaert, K., Meysman, F.J.R., Ulses, C., Metzger, E., Rabouille, C., 2011a. Modeling biogeochemical processes in sediments from the Rhône River prodelta area (NW Mediterranean Sea). Biogeosciences 8, 1351–1366. https://doi.org/10.5194/bg-8-1351-2011

Pastor, L., Deflandre, B., Viollier, E., Cathalot, C., Metzger, E., Rabouille, C., Escoubeyrou, K., Lloret, E., Pruski, A.M., Vétion, G., Desmalades, M., Buscail, R., Grémare, A., 2011b. Influence of the organic matter composition on benthic oxygen demand in the Rhône River prodelta (NW Mediterranean Sea). Continental Shelf Research 31, 1008–1019. https://doi.org/10.1016/j.csr.2011.03.007

Pastor, L., Rabouille, C., Metzger, E., Thibault de Chanvalon, A., Viollier, E., Deflandre, B., 2018. Transient early diagenetic processes in Rhône prodelta sediments revealed in contrasting flood events. Continental Shelf Research 166, 65–76. https://doi.org/10.1016/j.csr.2018.07.005

Pond, S., Pickard, G.L., 2007. Introductory dynamical oceanography, 3. ed., reprinted. ed. Butterworth-Heinemann, Oxford.

Porcher, M., 2023. Etude des facteurs influençant la reminéralisation du carbone organique dans les sédiments de la Vasière Ouest Gironde (golfe de Gascogne). Université de Bordeaux.

Poulton, S.W., Raiswell, R., 2005. Chemical and physical characteristics of iron oxides in riverine and glacial meltwater sediments. Chemical Geology 218, 203–221. https://doi.org/10.1016/j.chemgeo.2005.01.007

Presti, M., Michalopoulos, P., 2008. Estimating the contribution of the authigenic mineral component to the long-term reactive silica accumulation on the western shelf of the Mississippi River Delta. Continental Shelf Research 28, 823–838. https://doi.org/10.1016/j.csr.2007.12.015

Puillat, I., Lazure, P., Jégou, A.M., Lampert, L., Miller, P.I., 2004. Hydrographical variability on the French continental shelf in the Bay of Biscay, during the 1990s. Continental Shelf Research 24, 1143–1163. https://doi.org/10.1016/j.csr.2004.02.008

Pujos, M., 1976. Ecologie des foraminifères benthiques et des thécamoebiens de la Gironde et du plateau continental Sud-Gascogne. Application à la connaissance du Quaternaire terminal de la région Ouest-Gironde (Thèse de doctorat). Université de Bordeaux I, Bordeaux.

Qiao, S., Shi, X., Wang, G., Zhou, L., Hu, B., Hu, L., Yang, G., Liu, Y., Yao, Z., Liu, S., 2017. Sediment accumulation and budget in the Bohai Sea, Yellow Sea and East China Sea. Marine Geology 390, 270–281. https://doi.org/10.1016/j.margeo.2017.06.004

Quiñones-Rivera, Z., Wissel, B., Justić, D., Fry, B., 2007. Partitioning oxygen sources and sinks in a stratified, eutrophic coastal ecosystem using stable oxygen isotopes. Marine Ecology Progress Series 342, 69–83. https://doi.org/10.3354/meps342069

Rabouille, C., Conley, D.J., Dai, M.H., Cai, W.-J., Chen, C.T.A., Lansard, B., Green, R., Yin, K., Harrison, P.J., Dagg, M., McKee, B., 2008. Comparison of hypoxia among four river-dominated ocean margins: The Changjiang (Yangtze), Mississippi, Pearl, and Rhône rivers. Continental Shelf Research 28, 1527–1537. https://doi.org/10.1016/j.csr.2008.01.020

Rabouille, C., Denis, L., Dedieu, K., Stora, G., Lansard, B., Grenz, C., 2003. Oxygen demand in coastal marine sediments: comparing in situ microelectrodes and laboratory core incubations. Journal of Experimental Marine Biology and Ecology 285–286, 49–69. https://doi.org/10.1016/S0022-0981(02)00519-1

Rabouille, C., Lansard, B., Owings, S.M., Rabalais, N.N., Bombled, B., Metzger, E., Richirt, J., Eitel, E.M., Boever, A.D., Beckler, J.S., Taillefert, M., 2021. Early Diagenesis in the Hypoxic and Acidified Zone of the Northern Gulf of Mexico: Is Organic Matter Recycling in Sediments Disconnected From the Water Column? Frontiers in Marine Science 8, 604330. https://doi.org/10.3389/fmars.2021.604330

Raiswell, R., Canfield, D.E., 2012. The Iron Biogeochemical Cycle Past and Present. Geochemical Perspectives 1, 1–220. https://doi.org/10.7185/geochempersp.1.1

Raiswell, R., Canfield, D.E., Berner, R.A., 1994. A comparison of iron extraction methods for the determination of degree of pyritisation and the recognition of iron-limited pyrite formation. Chemical Geology 111, 101–110. https://doi.org/10.1016/0009-2541(94)90084-1

Rasmussen, H., Jorgensen, B., 1992. Microelectrode studies of seasonal oxygen uptake in a coastal sediment: role of molecular diffusion. Marine Ecology Progress Series 81, 289–303. https://doi.org/10.3354/meps081289

Ratmaya, W., Laverman, A.M., Rabouille, C., Akbarzadeh, Z., Andrieux-Loyer, F., Barillé, L., Barillé, A.-L., Le Merrer, Y., Souchu, P., 2022. Temporal and spatial variations in benthic nitrogen cycling in a temperate macro-tidal coastal ecosystem: Observation and modeling. Continental Shelf Research 235, 104649. https://doi.org/10.1016/j.csr.2022.104649

Relexans, J.-C., Lin, R.G., Castel, J., Etcheber, H., Laborde, P., 1992. Response of biota to sedimentary organic matter quality of the West Gironde mud patch, Bay of Biscay (France). Oceanologica Acta 15, 639–649.

Retho, M., Quemener, L., Le Gall, C., Repecaud, M., Souchu, P., Gabellec, R., Manach, S., 2020. MOLIT Vilaine data and metadata from Coriolis Data Centre. https://doi.org/10.17882/46529

Revsbech, N.P., 1989. An oxygen microsensor with a guard cathode. Limnology and Oceanography 34, 474–478. https://doi.org/10.4319/lo.1989.34.2.0474

Rickard, D., Luther, G.W., 2007. Chemistry of Iron Sulfides. Chemical Reviews 107, 514–562. https://doi.org/10.1021/cr0503658

Rickard, D., Morse, J.W., 2005. Acid volatile sulfide (AVS). Marine Chemistry 97, 141–197. https://doi.org/10.1016/j.marchem.2005.08.004

Rigaud, S., Radakovitch, O., Couture, R.-M., Deflandre, B., Cossa, D., Garnier, C., Garnier, J.-M., 2013. Mobility and fluxes of trace elements and nutrients at the sediment–water interface of a lagoon under contrasting water column oxygenation conditions. Applied Geochemistry 31, 35–51. https://doi.org/10.1016/j.apgeochem.2012.12.003

Ringle, C.M., Wende, S., Becker, J.-M., 2022. SmartPLS4.

Roman, M.R., Brandt, S.B., Houde, E.D., Pierson, J.J., 2019. Interactive Effects of Hypoxia and Temperature on Coastal Pelagic Zooplankton and Fish. Frontiers in Marine Science 6.

Rossignol-Strick, M., 1985. A Marine Anoxic Event on the Brittany Coast, July 1982. Journal of Coastal Research 1, 11–20.

Rothe, M., Kleeberg, A., Hupfer, M., 2016. The occurrence, identification and environmental relevance of vivianite in waterlogged soils and aquatic sediments. Earth-Science Reviews 158, 51–64. https://doi.org/10.1016/j.earscirev.2016.04.008

Rowe, G.T., Kaegi, M.E.C., Morse, J.W., Boland, G.S., Briones, E.G.E., 2002. Sediment Community Metabolism Associated with Continental Shelf Hypoxia, Northern Gulf of Mexico. Estuaries 25, 1097–1106.

Rowe, G.T., Phoel, W.C., 1992. Nutrient regeneration and oxygen demand in Bering Sea continental shelf sediments. Continental Shelf Research 12, 439–449. https://doi.org/10.1016/0278-4343(92)90085-X

Ruttenberg, K.C., 2014. The Global Phosphorus Cycle, in: Treatise on Geochemistry. Elsevier, pp. 499–558. https://doi.org/10.1016/B978-0-08-095975-7.00813-5

Ruttenberg, K.C., 1992. Development of a sequential extraction method for different forms of phosphorus in marine sediments. Limnology and Oceanography 37, 1460–1482. https://doi.org/10.4319/lo.1992.37.7.1460

Ruttenberg, K.C., Berner, R.A., 1993. Authigenic apatite formation and burial in sediments from non-upwelling, continental margin environments. Geochimica et Cosmochimica Acta 57, 991–1007. https://doi.org/10.1016/0016-7037(93)90035-U

Saari, H.-K., Schmidt, S., Castaing, P., Blanc, G., Sautour, B., Masson, O., Cochran, J.K., 2010. The particulate 7Be/210Pbxs and 234Th/210Pbxs activity ratios as tracers for tidal-to-seasonal particle dynamics in the Gironde estuary (France): Implications for the budget of particle-associated contaminants. Science of The Total Environment 408, 4784–4794. https://doi.org/10.1016/j.scitotenv.2010.07.017

Savoye, N., David, V., Morisseau, F., Etcheber, H., Abril, G., Billy, I., Charlier, K., Oggian, G., Derriennic, H., Sautour, B., 2012. Origin and composition of particulate organic matter in a macrotidal turbid estuary: The Gironde Estuary, France. Estuarine, Coastal and Shelf Science, ECSA 46 Conference Proceedings 108, 16–28. https://doi.org/10.1016/j.ecss.2011.12.005

Schmidt, S., 2020. Depth profiles of selected radionuclides and grain size in marine sediments of the West Gironde Mud Patch (Bay of Biscay). https://doi.org/10.17882/77523

Schmidt, S., Bernard, C., Escalier, J.-M., Etcheber, H., Lamouroux, M., 2017. Assessing and managing the risks of hypoxia in transitional waters: a case study in the tidal Garonne River (South-West France). Environmental Science and Pollution Research 24, 3251–3259. https://doi.org/10.1007/s11356-016-7654-5

Schmidt, S., Deflandre, B., 2018. JERICOBENT-5 cruise, Côtes De La Manche R/V. https://doi.org/10.17600/18000471

Schmidt, S., Diallo, I.I., Derriennic, H., Fallou, H., Lepage, M., 2019. Exploring the Susceptibility of Turbid Estuaries to Hypoxia as a Prerequisite to Designing a Pertinent Monitoring Strategy of Dissolved Oxygen. Frontiers in Marine Science 6, 352. https://doi.org/10.3389/fmars.2019.00352

Schmidt, S., Howa, H., Diallo, A., Martín, J., Cremer, M., Duros, P., Fontanier, C., Deflandre, B., Metzger, E., Mulder, T., 2014. Recent sediment transport and deposition in the Cap-Ferret Canyon, South-East margin of Bay of Biscay. Deep Sea Research Part II: Topical Studies in Oceanography 104, 134–144. https://doi.org/10.1016/j.dsr2.2013.06.004

Schmidt, S., Howa, H., Mouret, A., Lombard, F., Anschutz, P., Labeyrie, L., 2009. Particle fluxes and recent sediment accumulation on the Aquitanian margin of Bay of Biscay. Continental Shelf Research, 100 Years of Research within the Bay of Biscay 29, 1044–1052. https://doi.org/10.1016/j.csr.2008.11.018

Schulz, H.D., Zabel, M., 2006. Marine Geochemistry. Springer Berlin, Heidelberg, Berlin, Heidelberg.

Shi, M., Min, X., Ke, Y., Lin, Z., Yang, Z., Wang, S., Peng, N., Yan, X., Luo, S., Wu, J., Wei, Y., 2021. Recent progress in understanding the mechanism of heavy metals retention by iron (oxyhydr)oxides. Science of The Total Environment 752, 141930. https://doi.org/10.1016/j.scitotenv.2020.141930

Slomp, C.P., 2011. Phosphorus Cycling in the Estuarine and Coastal Zones, in: Treatise on Estuarine and Coastal Science. Elsevier, pp. 201–229. https://doi.org/10.1016/B978-0-12-374711-2.00506-4

Sommerfield, C.K., Aller, R.C., Nittrouer, C.A., 2001. Sedimentary Carbon, Sulfur, and Iron Relationships in Modern and Ancient Diagenetic Environments of the Eel River Basin (U.S.A.). Journal of Sedimentary Research 71, 335–345. https://doi.org/10.1306/2DC40947-0E47-11D7-8643000102C1865D

Song, G., Liu, S., Zhu, Z., Zhai, W., Zhu, C., Zhang, J., 2016. Sediment oxygen consumption and benthic organic carbon mineralization on the continental shelves of the East China Sea and the Yellow Sea. Deep Sea Research Part II: Topical Studies in Oceanography 124, 53–63. https://doi.org/10.1016/j.dsr2.2015.04.012

Steckbauer, A., Klein, S.G., Duarte, C.M., 2020. Additive impacts of deoxygenation and acidification threaten marine biota. Global Change Biology 26, 5602–5612. https://doi.org/10.1111/gcb.15252

Stockdale, A., Davison, W., Zhang, H., Hamilton-Taylor, J., 2010. The Association of Cobalt with Iron and Manganese (Oxyhydr)oxides in Marine Sediment. Aquatic Geochemistry 16, 575–585. https://doi.org/10.1007/s10498-010-9092-1

Stookey, L.L., 1970. Ferrozine---a new spectrophotometric reagent for iron. Analytical Chemistry 42, 779–781. https://doi.org/10.1021/ac60289a016

Sun, X., Fan, D., Liu, M., Liao, H., Tian, Y., 2020. The fate of organic carbon burial in the river-dominated East China Sea: Evidence from sediment geochemical records of the last 70 years. Organic Geochemistry 143, 103999. https://doi.org/10.1016/j.orggeochem.2020.103999

Sundby, B., 2006. Transient state diagenesis in continental margin muds. Marine Chemistry 102, 2–12. https://doi.org/10.1016/j.marchem.2005.09.016

Sundby, B., Gobeil, C., Silverberg, N., Alfonso, M., 1992. The phosphorus cycle in coastal marine sediments. Limnology and Oceanography 37, 1129–1145. https://doi.org/10.4319/lo.1992.37.6.1129

Sundby, B., Martinez, P., Gobeil, C., 2004. Comparative geochemistry of cadmium, rhenium, uranium, and molybdenum in continental margin sediments. Geochimica et Cosmochimica Acta 68, 2485–2493. https://doi.org/10.1016/j.gca.2003.08.011

Tahey, T., Duineveld, G., Dewilde, P., Berghuis, E., Kok, A., 1996. Sediment O-2 demand, density and biomass of the benthos and phytopigments along the northwestern Adriatic coast: The extent of Po enrichment. Oceanologica Acta 19, 117–130.

Taillefert, M., Hover, V.C., Rozan, T.F., Theberge, S.M., Luther, G.W., 2002. The influence of sulfides on soluble organic-Fe(III) in anoxic sediment porewaters. Estuaries 25, 1088–1096. https://doi.org/10.1007/BF02692206

Testa, J.M., Kemp, W.M., 2011. Oxygen – Dynamics and Biogeochemical Consequences, in: Treatise on Estuarine and Coastal Science. Elsevier, pp. 163–199. https://doi.org/10.1016/B978-0-12-374711-2.00505-2

Treinen-Crespo, C., Barbara, L., Villaescusa, J.A., Schmidt, S., Pearson, A., Carriquiry, J.D., 2021. Revisiting the marine reservoir age in Baja California continental margin sediments using ^{14}C and ^{210}Pb dating. Quaternary Geochronology 66, 101178. https://doi.org/10.1016/j.quageo.2021.101178

Triana, K., Wahyudi, A.J., 2021. Dissolved oxygen variability of Indonesian seas over decades as detected by satellite remote sensing. IOP Conference Series: Earth Environmental. Science 925, 012003. https://doi.org/10.1088/1755-1315/925/1/012003

Tritah, S., Daoud, M., 2021. Les fondements conceptuels et théoriques de la méthode des équations structurelles PLS. https://doi.org/10.5281/ZENODO.4474527

Valenzuela, S., Bachmann, I., 2017. Path Analysis, in: Matthes, J., Davis, C.S., Potter, R.F. (Eds.), The International Encyclopedia of Communication Research Methods. Wiley, pp. 1–9. https://doi.org/10.1002/9781118901731.iecrm0181

van de Velde, S., Van Lancker, V., Hidalgo-Martinez, S., Berelson, W.M., Meysman, F.J.R., 2018. Anthropogenic disturbance keeps the coastal seafloor biogeochemistry in a transient state. Scientific Reports 8, 5582. https://doi.org/10.1038/s41598-018-23925-y

Van den Thillart, G., Dalla Via, J., Vitali, G., Cortesi, P., 1994. Influence of long-term hypoxia exposure on the energy metabolism of Solea solea. I. Critical O_2 levels for aerobic and anaerobic metabolism. Marine Ecology Progress Series 104, 109–117. https://doi.org/10.3354/meps104109

van Weering, T.C.E., de Stigter, H.C., Boer, W., de Haas, H., 2002. Recent sediment transport and accumulation on the NW Iberian margin. Progress in Oceanography, Benthic processes and dynamics at the NW Iberian Margin: results of the OMEX II Program 52, 349–371. https://doi.org/10.1016/S0079-6611(02)00015-0

van Weering, Tj.C.E., Hall, I.R., de Stigter, H.C., McCave, I.N., Thomsen, L., 1998. Recent sediments, sediment accumulation and carbon burial at Goban Spur, N.W. European Continental Margin (47–50°N). Progress in Oceanography 42, 5–35. https://doi.org/10.1016/S0079-6611(98)00026-3

Vigneaux, M., Allen, G.P., Caralp, M., Carbonel, P., Castaing, P., Cirac, P., Dumon, J.C., Gonthier, E., Klingebiel, A., Latouche, C., Moyes, J., Naudin, J.J., Parra, M., Peypouquet, J.P., Prud'homme, R., Pujos-Lamy, A., Pujos, M., 1971. Bilan d'étude d'environnement marin et applications dans le Golfe de Gascogne. Presented at the Colloque International sur l'exploitation des océans, Bordeaux, p. 66.

Vincent, A., Kurc, G., 1969. Hydrologie, variations saisonnières de la situation thermique dans le Golfe de Gascogne en 1967. Revue des Travaux de l'Institut des Pêches Maritimes 79–96.

Wakelin, S.L., Artioli, Y., Holt, J.T., Butenschön, M., Blackford, J., 2020. Controls on near-bed oxygen concentration on the Northwest European Continental Shelf under a potential future climate scenario. Progress in Oceanography 187, 102400. https://doi.org/10.1016/j.pocean.2020.102400

Walsh, J.P., Nittrouer, C.A., 2009. Understanding fine-grained river-sediment dispersal on continental margins. Marine Geology 263, 34–45. https://doi.org/10.1016/j.margeo.2009.03.016

Walsh, J.P., Nittrouer, C.A., Palinkas, C.M., Ogston, A.S., Sternberg, R.W., Brunskill, G.J., 2004. Clinoform mechanics in the Gulf of Papua, New Guinea. Continental Shelf Research 24, 2487–2510. https://doi.org/10.1016/j.csr.2004.07.019

Wang, K., Cai, W.-J., Chen, J., Kirchman, D., Wang, B., Fan, W., Huang, D., 2021. Climate and Human-Driven Variability of Summer Hypoxia on a Large River-Dominated Shelf

as Revealed by a Hypoxia Index. Frontiers in Marine Science 8, 634184. https://doi.org/10.3389/fmars.2021.634184

Wang, Y., Van Cappellen, P., 1996. A multicomponent reactive transport model of early diagenesis: Application to redox cycling in coastal marine sediments. Geochimica et Cosmochimica Acta 60, 2993–3014. https://doi.org/10.1016/0016-7037(96)00140-8

Weber, O., Jouanneau, J.M., Ruch, P., Mirmand, M., 1991. Grain-size relationship between suspended matter originating in the Gironde estuary and shelf mud-patch deposits. Marine Geology 96, 159–165. https://doi.org/10.1016/0025-3227(91)90213-N

Włodarska-Kowalczuk, M., Mazurkiewicz, M., Górska, B., Michel, L.N., Jankowska, E., Zaborska, A., 2019. Organic Carbon Origin, Benthic Faunal Consumption, and Burial in Sediments of Northern Atlantic and Arctic Fjords (60–81°N). Journal of Geophysical Research: Biogeosciences 124, 3737–3751. https://doi.org/10.1029/2019JG005140

Wright, S., 1934. The Method of Path Coefficients. Annals of Mathematical Statistics 5, 161–215. https://doi.org/10.1214/aoms/1177732676

Yakushev, E.V., Protsenko, E.A., Bruggeman, J., Wallhead, P., Pakhomova, S.V., Yakubov, S.Kh., Bellerby, R.G.J., Couture, R.-M., 2017. Bottom RedOx Model (BROM v.1.1): a coupled benthic–pelagic model for simulation of water and sediment biogeochemistry. Geoscientific Model Development 10, 453–482. https://doi.org/10.5194/gmd-10-453-2017

Yang, B., Gao, X., Zhao, J., Liu, Y., Xie, L., Lv, X., Xing, Q., 2021. Summer deoxygenation in a bay scallop (Argopecten irradians) farming area: The decisive role of water temperature, stratification and beyond. Marine Pollution Bulletin 173, 113092. https://doi.org/10.1016/j.marpolbul.2021.113092

Yang, S.L., Milliman, J.D., Li, P., Xu, K., 2011. 50,000 dams later: Erosion of the Yangtze River and its delta. Global and Planetary Change 75, 14–20. https://doi.org/10.1016/j.gloplacha.2010.09.006

Yao, P., Zhao, B., Bianchi, T.S., Guo, Z., Zhao, M., Li, D., Pan, H., Wang, J., Zhang, T., Yu, Z., 2014. Remineralization of sedimentary organic carbon in mud deposits of the Changjiang Estuary and adjacent shelf: Implications for carbon preservation and authigenic mineral formation. Continental Shelf Research 91, 1–11. https://doi.org/10.1016/j.csr.2014.08.010

Yu, L., Fennel, K., Laurent, A., Murrell, M.C., Lehrter, J.C., 2015. Numerical analysis of the primary processes controlling oxygen dynamics on the Louisiana shelf. Biogeosciences 12, 2063–2076. https://doi.org/10.5194/bg-12-2063-2015

Zhai, W., Zhao, H., Su, J., Liu, P., Li, Y., Zheng, N., 2019. Emergence of Summertime Hypoxia and Concurrent Carbonate Mineral Suppression in the Central Bohai Sea, China. Journal

of Geophysical Research: Biogeosciences 124, 2768–2785. https://doi.org/10.1029/2019JG005120

Zhang, H., Davison, W., Mortimer, R.J.G., Krom, M.D., Hayes, P.J., Davies, I.M., 2002. Localised remobilization of metals in a marine sediment. Science of The Total Environment 296, 175–187. https://doi.org/10.1016/S0048-9697(02)00078-5

Zhu, C., Wagner, T., Talbot, H.M., Weijers, J.W.H., Pan, J.-M., Pancost, R.D., 2013. Mechanistic controls on diverse fates of terrestrial organic components in the East China Sea. Geochimica et Cosmochimica Acta 117, 129–143. https://doi.org/10.1016/j.gca.2013.04.015

Zhu, M.-X., Chen, K.-K., Yang, G.-P., Fan, D.-J., Li, T., 2016. Sulfur and iron diagenesis in temperate unsteady sediments of the East China Sea inner shelf and a comparison with tropical mobile mud belts (MMBs): S and Fe Diagenesis in Sediments. Journal of Geophysical Research: Biogeosciences 121, 2811–2828. https://doi.org/10.1002/2016JG003391

Annexe 1

Spatial Distributions of Surface Sedimentary Organics and Sediment Profile Image Characteristics in a High-Energy Temperate Marine RiOMar: The West Gironde Mud Patch

Bastien Lamarque[1], Bruno Deflandre[2], Adriana Galindo Dalto[3], Sabine Schmidt[2], Alicia Romero-Ramirez[1], Frédéric Garabetian[1], Nicolas Dubosq[2], Mélanie Diaz[2], Florent Grasso[4], Aldo Sottolichio[2], Guillaume Bernard[1], Hervé Gillet[2], Marie-Ange Cordier[2], Dominique Poirier[2], Pascal Lebleu[2], Hervé Derriennic[2], Martin Danilo[2], Márcio Murilo Barboza Tenório[3] and Antoine Grémare[1]

[1]UMR EPOC, Université de Bordeaux, CNRS, UMR 5805, Station Marine d'Arcachon, 2 rue du Professeur Jolyet, F33120 Arcachon, France
[2]UMR EPOC, Université de Bordeaux, CNRS, UMR 5805, Bâtiments B18/B18N, Allée Geoffroy Saint-Hilaire, F33615 Pessac CEDEX, France
[3]Departamento de Biologia Marinha, Instituto de Biologia, Universidade Federal do Rio de Janeiro, CEP 21941-902 Rio de Janeiro, Brazil
[4]IFREMER Brest—DYNECO/DHYSED, Centre de Bretagne, CS 10070, 29280 Plouzané, France

Article publié en 2021 dans la revue *Journal of Marine Science and Engineering*

Abstract

The spatial distributions of (1) surface sediment characteristics ($D_{0.5}$, Sediment Surface Area (SSA), Particulate Organic Carbon (POC), Chlorophyll-*a* (Chl-*a*), Phaeophytin-*a* (Phaeo-*a*), Total and Enzymatically Hydrolyzable Amino Acids (THAA, EHAA), $\delta^{13}C$) and (2) sediment profile image (apparent Redox Potential Discontinuity (aRPD), numbers and depths of biological traces) characteristics were quantified based on the sampling of 32 stations located within the West Gironde Mud Patch (Bay of Biscay, NE Atlantic) in view of (1) assessing the spatial structuration of a temperate river-dominated ocean margin located in a high-energy area, (2) disentangling the impacts of hydrodynamics and bottom trawling on this structuration, and (3) comparing the West Gironde Mud Patch with the Rhône River Prodelta (located in a low-energy area). Results support the subdivision of the West Gironde Mud Patch in a proximal and a distal part and show (1) the existence of depth gradients in surface sedimentary organics characteristics and bioturbation within the distal part; (2) no evidence for a significant effect of bottom trawling, as opposed to Bottom Shear Stress, on the West Gironde Mud Patch spatial structuration; and (3) major discrepancies between spatial structuration in the West Gironde Mud Patch and the Rhône River Prodelta, which were attributed to differences in tidal regimes, sedimentation processes, and local hydrodynamics, which is in agreement with current river-dominated ocean margin typologies.

Keywords: RiOMar, surface sediment, spatial distribution, sedimentary organics, bioturbation

1. Introduction

Continental margins are the interface between land and the open ocean, where 50 to 80% of continental Particulate Organic Carbon (POC) inputs are mineralized [1–3]. Less than 5% of these inputs are transferred to the deep ocean [4], the remaining part being buried in continental margin sediments. River-dominated ocean margins (RiOMars), defined as margins impacted by major rivers freshwater and/or sediment discharges (e.g., plumes of Amazon, Yangtze or Mississippi Rivers), are the main marine primary depositional areas of riverine particulate continental inputs [2, 5]. They account for 40 to 50% of continental POC burial occurring in continental margins [2, 3, 6]. Burial is tightly cued by biogeochemical processes taking place at the water–sediment interface [3, 5, 7]. Therefore, assessments of the structuration and functioning of the benthic components of marine RiOMars are key issues to reach a comprehensive understanding of the marine contribution to global biogeochemical cycles [1, 3].

Benthic macrofauna plays a major role in the biogeochemistry of the top centimeters of the sediment column through bioturbation (i.e., sediment mixing and bioirrigation [8]). This includes both changes in the spatial distribution and the temporal dynamics of electron acceptors, which influence mineralization fluxes [9–11]. Mostly based on the analysis of macrofauna vertical distribution within the sediment column and X-rays radiographies, Rhoads et al. [12] first proposed a conceptual model describing the response of macrofauna and surface sediments to the inputs of major rivers. According to this model, macrofauna spatial distribution is mainly determined by (1) physical disturbance induced by intense continental inputs, and (2) reduction in Particulate Organic Matter (POM) availability due to the limitation of primary production in turbid river plumes. In proximal (i.e., the closest to the river mouth) parts of RiOMars, high and irregular sedimentation rates induce sedimentary instability, precluding the establishment of mature macrobenthic communities. Moreover, high turbidity limits primary production and results in mainly low (and refractory) POM concentrations in surface sediments. Accordingly, RiOMar proximal areas are characterized by low bioturbation intensities and low mineralization fluxes. Conversely, in distal (i.e., deeper) parts, sedimentation is lower and primary production is higher, allowing for the establishment of mature macrobenthic communities, high bioturbation intensities, and mineralization fluxes.

Several studies have compared RiOMars based on either the characterization/quantification of geomorphological [5] or biogeochemical [3] processes. Their results highlighted the major effect of energetic regimes on RiOMar morphologies [5] and POC mineralization/burial intensities [3]. This later study drew a clear distinction between (1) low-energy systems, with both significant sedimentation rates and carbon preservation (later referred as type 1), and (2)

high-energy tidal and/or wave systems with both high sediment oxygenation and low carbon preservation rates (later referred as type 2). It evidenced that the spatial distributions of the benthic components of RiOMars are cued by both riverine inputs and marine hydrodynamics. This categorization was mostly based on tropical/subtropical systems, the Rhône River being the only major (type 1) considered temperate RiOMar. Moreover, both studies considered RiOMars and their continuity with fluvial systems in their entirety, even though McKee et al. [5] underlined the interest of differencing RiOMar sub-environments and comparing RiOMar types. Thus, there is still a clear need to document the spatial structuration of a potential temperate type 2 RiOMar and to compare it with a temperate type 1 one.

Together with the bottom shear stress induced by both waves and bottom currents, bottom trawling is contributing to control sediment resuspension in coastal areas [13–20]. As such, it can deeply affect surface sediments, benthic macrofauna and bioturbation [13, 21– 24]. RiOMar mud fields are organically enriched as compared to surrounding sediments and often constitute preferential fishing areas [19, 20]. Therefore, it is also important to unravel the role of both hydrodynamics and bottom trawling in controlling the structuration of benthic ecosystems in RiOMars.

The present study is aiming at (1) improving current knowledge regarding the spatial structuration of a potential temperate type 2 RiOMar, (2) disentangling the potential effects of hydrodynamics and bottom trawling in controlling this structuration, and (3) comparing this spatial structuration with the one of a type 1 temperate RiOMar (i.e., the Rhône River Prodelta [3]). It is based on the synoptic sampling of a large number of stations and the quantitative analysis of (1) surface sediment characteristics and (2) Sediment Profile Images (SPI).

2. Materials and Methods

2.1 The West Gironde Mud Patch

The West Gironde Mud Patch (WGMP) is a 420 km^2 sedimentary body located in the Bay of Biscay 40 km off the Mouth of the Gironde Estuary (**Figure 6.1**). This relict paleovalley/depression constitutes the primary depocenter (sedimentation rates between less than 1 and 5 $mm \cdot y^{-1}$ [25, 26]) of fine particles originating from the Gironde Estuary, which presents an annual mean water discharge of 944 $m^3 \cdot s^{-1}$ [27] and daily discharge up to 7500 $m^3.s^{-1}$ during wintertime [28]. The WGMP is located in a macro-tidal environment with a tidal range from 1.5 to 5 m [26, 29]. The continental shelf around the Mouth of the Gironde Estuary is dominated by strong swells/waves, which can reach maximal amplitudes of 15 m and time periods of 15 s during winter storms [30]. These hydrological conditions prevent the

sedimentation of fine particles in the immediate vicinity of the Mouth of the Estuary. Therefore, the WGMP can a priori be considered as a potential temperate type 2 RiOMar [5].

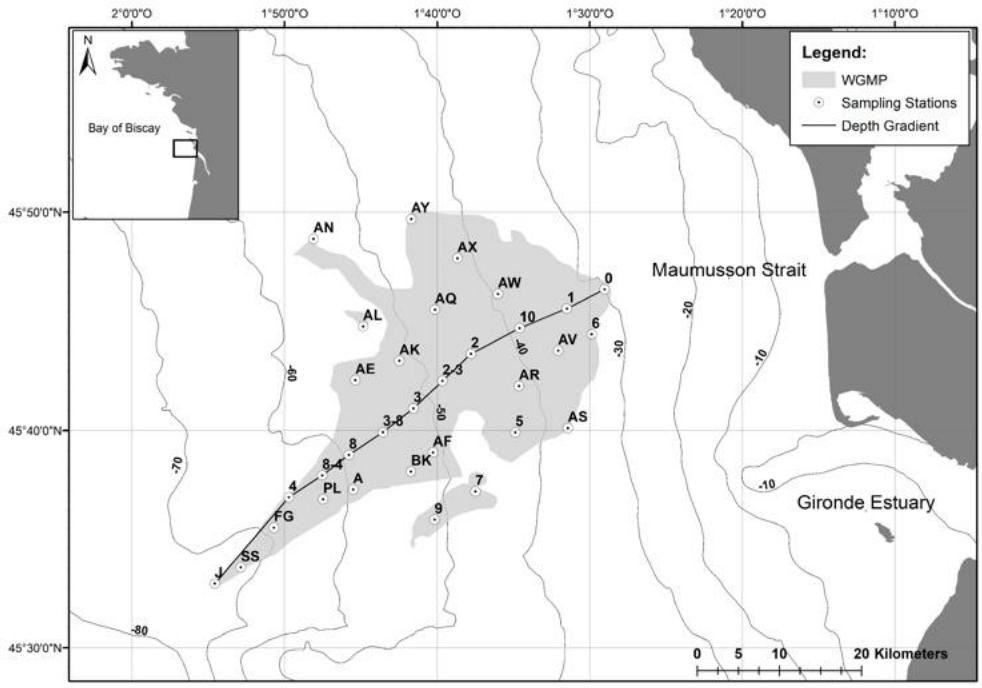

Figure 6.1. Map showing the location of the West Gironde Mud Patch along the French Atlantic coast, the locations of the 32 sampled stations, and the depth gradient sampled for X-ray radiographies and amino acids. The delimitation of the West Gironde Mud Patch (WGMP) is based on the acoustic measurements achieved during the JERICOBENT-5-TH cruise [48] and the surface sediment granulometry assessed during the present study [49].

The sedimentology of the WGMP has been extensively studied based on stratigraphic sequences, palynological data, X-rays radiographies, and radiochronographies [25, 26, 31– 38, 39–43]. Sedimentological surveys have attributed a major role to hydrodynamics in controlling the spatial structuration of the WGMP [25, 26, 35, 38, 42]. This paradigm was based on both (1) the segmentation between a proximal and a distal part with no modern persistent sedimentation in the former due to strong hydrodynamics, and (2) the decreasing frequency of occurrence of vertical erosional sequences within the sediment column with station depth. The occurrence of spatial zonation in the distal part has also been addressed [25, 26, 35, 38, 42] but without reaching a clear conclusion due to a limited number of sampled stations and to the lack of a fine quantitative assessment of bioturbation. Benthic macrofauna composition and associated biogeochemical processes have been largely neglected as well, with only two studies based on the sampling of a limited number of stations [44, 45]. The WGMP is a preferential fishing area [46] where several benthic species are commercially exploited, including the Norway lobster (*Nephrops norvegicus*) and the common sole (*Solea solea*). Bottom trawls are commonly deployed in the area [46], and it has been suggested that their use may constitute a significant source of disturbance for benthic habitats [26, 38, 47]. Based on Vessel Monitoring

System data, Mengual et al. [19, 20] showed that the Benthic Trawling Effort (BTE) in the WGMP can be locally intense (up to 10 times trawled·y^{-1}) and seems to increase with depth.

2.2 Sampling of Surface Sediment and Sediment Profile Images

This study is based on samples collected during the JERICOBENT-5 cruise [49], which took place in June 2018 on board of the R/V Côtes de la Manche. Thirty-two stations located between 32.5 and 78 m depth, and allowing for a full coverage of the WGMP were sampled for both surface sediment characteristics and Sediment Profile Images (SPIs; **Figure 6.1, Table A6.1**). At each station, a sediment core (10 cm internal diameter) was collected using an Uwitec® (Mondsee, Austria) monotube-corer. The upper top centimeter (i.e., 0–1 cm depth layer) was carefully extruded and split in two subsamples immediately frozen (−20 °C) for further analyses of (1) grain size, Sediment Surface Area (SSA; [50]), Particulate Organic Carbon (POC), and OC isotopic ratio; and (2) chloropigments. Total and Enzymatically Hydrolyzable Amino Acids (THAA and EHAA) were assayed at 11 stations distributed along a depth gradient (see **Figure 6.1**). At these stations, a second core was collected for X-rays radiographies (SCOPIX system; [51]). EHAA were not assayed at station J due to a technical problem. At all stations, between 4 and 8 SPIs were taken (at stations PL and J, respectively) using a sediment profile imager (Ocean Imaging Systems®, Pocasset, USA) [52] fitted with a D7100 camera (Nikon®, Tokyo, Japan).

2.3 Analysis of Surface Sediment Characteristics

Grain size was measured on duplicated aliquots of each sediment sample using a Master Sizer laser microgranulometer (Malvern Panalytical®, Malvern, UK), which allowed for the computation of median diameter ($D_{0.5}$). SSAs were measured on freeze-dried sediments, previously degassed overnight at 150 °C, using a Gemini VII 2390 Series Surface Area Analyzer (Micromeritics®, Norcross, USA) with the multi-point Brunauer–Emmett–Teller method [50]. POC was assayed using a LECO® (St. Joseph, USA) CS 200 analyzer, after 2M HCl overnight decarbonatation of previously freeze-dried sediments [53].

THAA and EHAA were analyzed on duplicates. THAA were extracted by acid hydrolysis. EHAA were extracted following the biomimetic approach proposed by Mayer et al. [54]. THAA and EHAA were analyzed by derivation to form fluorescent amino compounds with the presence of the thiol 3-mercaptopropionic acid (MPA). Fluorescent derivatives were separated by reverse-phase High-Performance Liquid Chromatography (Agilent®, Santa Clara, USA; 1260 INFINITY model) on a Phenomenex® (Torrance, USA) Kinetex 5 µm EVO C18 column using non-linear gradient of methanol–acetate buffer (pH = 7, 40 mM), and detected by

fluorescence from 340 to 450 nm using an excitation wavelength of 338 nm. The EHAA/THAA ratio was used as a lability index of bulk sedimentary organics [55–57].

Chlorophyll-*a* (Chl-*a*) and Phaeophytin-*a* (Phaeo-*a*) were assayed on thawed frozen (−20 °C) sediment after overnight acetone extraction (90% final concentration) using a Perkin Elmer® LS-55 spectrofluorometer following Neveux and Lantoine [58]. Pigment data are lacking for station BK due to sample loss. All organic concentrations were normalized for SSA (i.e., expressed in terms of mass per SSA). The Chl-*a*/(Chl-*a* + Phaeo-*a*) ratio was used as a lability index of vegetal biomass [55, 56].

For the analysis of OC isotopic ratio, replicated freeze-dried sediment samples were decarbonated (1M HCl) and later analyzed using a Thermo Scientific® Delta V plus IRMS coupled with a Thermo Scientific® (Waltham, USA) Flash 2000 EA. Raw measurements were converted in usual $\delta^{13}C$ units [59].

2.4 Analysis of Sediment Profile Images

Individual SPI were analyzed for (1) apparent Redox Potential Discontinuity (aRPD) thickness, (2) numbers of biogenic structures (tubes, burrows, oxic voids, feeding pits), (3) numbers of epi- and infauna, and (4) maximal depths of oxic voids within the sediment column. For the stations presenting a surface sandy layer, the upper limit for the computation of aRPD thickness was set below the transient top coarser sediment layer. Image analyses were achieved using the SpiArcBase software [60] and mean values and standard deviations were computed for each station. In addition, all SPIs were visually inspected for the presence of potential traces of bottom trawling. This included the presence of clasts and furrows [61, 62], and of a surface puzzle fabric [63].

2.5 Spatial Distribution of Bottom Shear Stress and Trawling Effort

The spatial distribution of Bottom Shear Stress (BSS) was computed from a tridimensional numerical model deployed and validated over the study area [64]. This model, stretching from the Gironde Estuary to the continental shelf, is based on the MARS3D hydrodynamic model [65] and the WAVE WATCH III® wave model [66]. Its curvilinear mesh resolution is approximately 0.5 × 0.5 km^2 over the WGMP. The model integrates realistic hydro-meteorological forcing (i.e., wind, tide, surge, and river flow). BSS was computed as the combination of current-induced and wave-induced components following Soulsby's formulation [67]. A more detailed description of the model can be found in Grasso et al. [68]. Simulations achieved during the present study provided hourly outputs over the whole year

preceding the JERICOBENT-5 cruise. In order to account for intense hydrodynamic events, 95th percentiles were used to characterize BSS intensities.

The spatial distribution of Bottom Trawling Effort (BTE), within and around the WGMP, was assessed based on vessel Automatic Identification System (AIS) data collected by Global Fishing Watch [69, 70]. Raw (daily) BTE were available with a 1/100 degree (corresponding to 1.77 km^2 cells) spatial resolution. For each cell, daily BTE were summed over the whole year preceding the JERICOBENT-5 cruise. Summed BTE were expressed both in terms of h.km^{-2}.y^{-1} and number of times trawled.y^{-1}. The conversion between these two units was achieved following Mengual et al. [19, 20].

2.6 Analysis of WGMP Data

2.6.1 Sediment Characteristics and Sediment Profile Images

For both sediment (i.e., SSA, POC, Chl-*a*, Phaeo-*a*, Chl-*a*/(Chl-*a* + Phaeo-*a*) ratio and $\delta^{13}C$) and SPI (i.e., aRPD thickness; maximal oxic void depth; mean numbers of tubes, burrows, oxic voids, feeding structures, epifauna and infauna) characteristics, hierarchical clustering (Euclidean distance and average group linking) and Principal Components Analyses (PCAs) were used to define groups of stations and to assess relationships between variables. THAA, EHAA, and EHAA/THAA ratios were not included, since data were missing at some stations. Station depth, BSS, and BTE were introduced as supplementary variables in both PCAs. SIMilarity PROFile procedures (SIMPROF; [71]) were used to test for the statistical significance of differences between station groups resulting from hierarchical clustering. SIMilarity PERcentage analysis (SIMPER; [72]) was used to identify the SPI characteristics contributing the most to between-group differences. All analyses were run on normalized data using the PRIMER® 6 software package [73].

Multivariate analyses supported the distinction between a proximal and a distal part in the WGMP (see Section 4.1). Simple linear regression models were used to assess the significance of the relationships between station depth and both surface sediment and SPI characteristics in the whole WGMP and in the sole distal part to avoid confounding effects resulting from (1) the high between-station variability in the proximal part and (2) major differences in sediment and SPI characteristics between parts. The same approach was used to assess the significance of the relationships between station depths and their coordinates on the first component of both PCAs.

2.6.2 Bottom Shear Stress and Trawling Effort

BSS 95th percentiles and summed BTE were mapped using the ArcGIS Desktop® 10.6 software. The relationships between BSS 95th percentiles, summed BTE within cells containing sampled stations, and (1) station depth, (2) surface sediment characteristics, and (3) SPI characteristics were assessed using simple linear regression models at the scale of the whole WGMP and/or its sole distal part. Multiple linear regression models were used to test for additive effects of BSS and BTE.

2.7 Comparisons with the Rhône River Prodelta

The Rhône River Prodelta (RRP) is a ca 265 km^2 [74] depositional system, located in the Gulf of Lions (North Mediterranean Sea). It is supplied with particles from the Rhône River, which presents a mean annual water discharge of 1700 m·s^{-1} and massive flood events (i.e., up to 11,000 m^3·s^{-1}; [75]). The RRP is located in an environment with micro-tidal conditions (i.e., maximal tidal range of 0.4–0.5 m) and wave mean heights of 1–1.5 m [76]. During winter storms, wave heights can exceptionally reach 3–4 m, with periods of about 6–7 s [77, 78]. These conditions allow for the sedimentation of fine particles at the immediate vicinity of the river mouth. Sedimentation rates are about 40 cm·y^{-1} in the proximal part (i.e., 5–30 m depth) of the RRP and between 1 and 10 cm·y^{-1} in its distal part (30–100 m depth; [74, 79, 80]). According to the classifications established by McKee et al. [5] and Blair and Aller [3], the RRP therefore constitutes a low-energy (type 1) temperate RiOMar in direct continuity with the Rhône River.

WGMP results collected during the present study were compared with those originating from the Chaccra cruise (April 2007), which took place in a comparable situation in terms of river flows [56] and during which the same parameters (i.e., $D_{0.5}$, POC, chloropigments, THAA, EHAA, $\delta^{13}C$, and SPI characteristics) were measured at 7–10 stations located in the RRP [56 ,81 , 82]. Since modern sedimentation was shown to be restricted to the distal part of the WGMP (see above), the comparison was achieved between the sole WGMP distal part and the whole RRP. All organic concentrations were expressed in terms of sediment DW (eventually standardized for $D_{0.5}$), since no SSA data were available for the RRP. For the same reason, we used mean instead of maximal oxic void depth. Mean values of WGMP and RRP characteristics were compared using one-way ANOVAs.

3. Results

3.1 Surface Sediment Characteristics

Except for two stations (i.e., stations 0 and 10), all particle size distributions were unimodal. There were marked differences in surface median sediment grain size ($D_{0.5}$) among shallow stations (**Figure 6.2A**). $D_{0.5}$ was minimal at station AV (13.5 µm) and maximal at station 0 (64.6 µm). Conversely, deep stations featured a narrower range (i.e., between 14.9 and 24.8 µm at stations 7 and 2, respectively) of $D_{0.5}$. Sediment Surface Area (SSA) was also more dispersed at shallow stations (i.e., between 3.4 and 14.2 $m^2 \cdot gDW^{-1}$ at stations AW and AV, respectively) (**Figure 6.2B**) than at deep stations (i.e., between 6.1 and 9.8 $m^2 \cdot gDW^{-1}$ at stations 2 and 4, respectively).

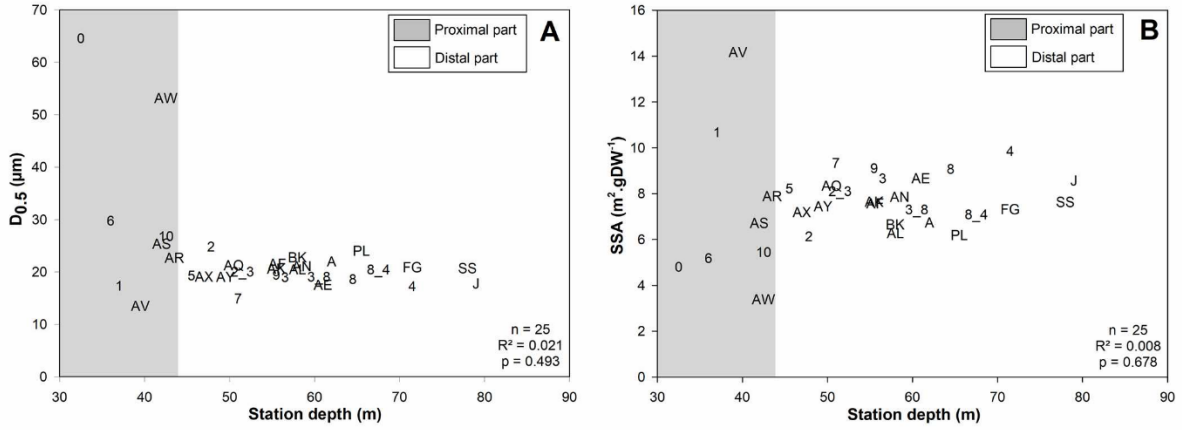

Figure 6.2. Relationships between station depth and: $D_{0.5}$ (**A**); Sediment Surface Area (SSA; (**B**)). Gray areas represent the proximal part (z < 42.5 m) of the WGMP. Station codes are the same as in Figure 6.1 and Table A6.1. Statistical results refer to the sole WGMP distal part.

At the scale of the whole WGMP, SSA significantly decreased with increasing $D_{0.5}$ following an exponential model ($y = 4.268 + 51.982 \times e^{-0.134x}$; $n = 32$, $R^2 = 0.830$, $p < 0.001$). $D_{0.5}$, all surface sediment organic concentrations and Chl-*a*/(Chl-*a* + Phaeo-*a*) ratio (**Table A6.1**) correlated significantly with station depth, which was not the case for SSA and $\delta^{13}C$ (**Table A6.2**). When considering only the distal part (see Section 4.1 for the delimitation between the proximal and distal parts), the correlations between station depth, $D_{0.5}$, Chl-*a*, and Chl-*a*/(Chl-*a* + Phaeo-*a*) were not significant (**Table A6.2**).

Particulate Organic Carbon (POC) concentrations were between 0.50 and 2.06 $mg.m^{-2}$ at stations AV and J, respectively. POC correlated positively with depth in the distal part of the West Gironde Mud Patch (WGMP; **Figure 6.3A**, **Table A6.2**). Total Hydrolyzable Amino Acid (THAA) concentrations were between 0.18 and 0.69 $mg \cdot m^{-2}$ at stations 10 and J respectively (**Table A6.1**). THAA correlated positively with station depth in both the whole WGMP and the

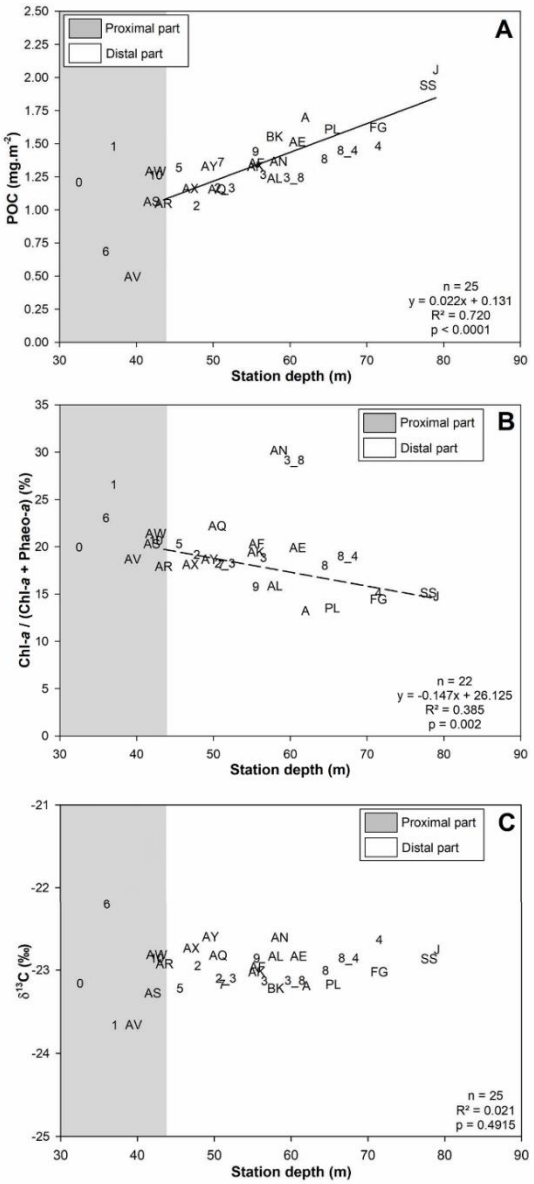

Figure 6.3. Relationships between station depth and main surface sediment characteristics: Particulate Organic Carbon concentration (POC; (**A**)); Chl-*a*/(Chl-*a*+Phaeo-*a*) ratio (**B**) and $\delta^{13}C$ (**C**). Gray areas represent the proximal part (z < 42.5 m) of the WGMP. Station codes are the same as in Figure 6.1 and Table A6.1. The continuous line represents the linear regression linking station depth and POC concentration within the distal part of the WGMP, and the dotted line represents the linear regression linking station depth and Chl-*a*/(Chl-*a*+Phaeo-*a*) ratio within the distal part of the WGMP (excluding stations AN and 3_8).

distal part of the WGMP (**Table A6.2**). Enzymatically Hydrolyzable Amino Acids (EHAA) concentrations also correlated significantly with station depth at the scale of the whole WGMP, with values ranging from 0.047 mg·m^{-2} (station 10) to 0.109 mg.m^{-2} (stations 8–4). However, this correlation was not significant in the sole distal part. EHAA/THAA ratios ranged from 15.5 (station 8) to 26.6% (station 10) (**Table A6.1**). They did not significantly correlate with station depth when considering either the whole WGMP or its sole distal part (**Table A6.2**). Stations AN and 3_8 constituted clear outliers (i.e., featuring high ratios as regard to their depth) in the

relationship linking station depth and Chl-*a*/(Chl-*a* + Phaeo-*a*) ratio (**Figure 6.3B**). When excluding these two stations, this relationship was significantly negative in the distal part of the WGMP (**Table A6.2**). $\delta^{13}C$ values presented a narrow variation range with values from −23.66‰ to −22.20‰ at stations 1 and 6, respectively. Variability relative to station depth was more marked in the proximal than in the distal part of the WGMP, where all $\delta^{13}C$ values were around −23‰ (**Figure 6.3C**).

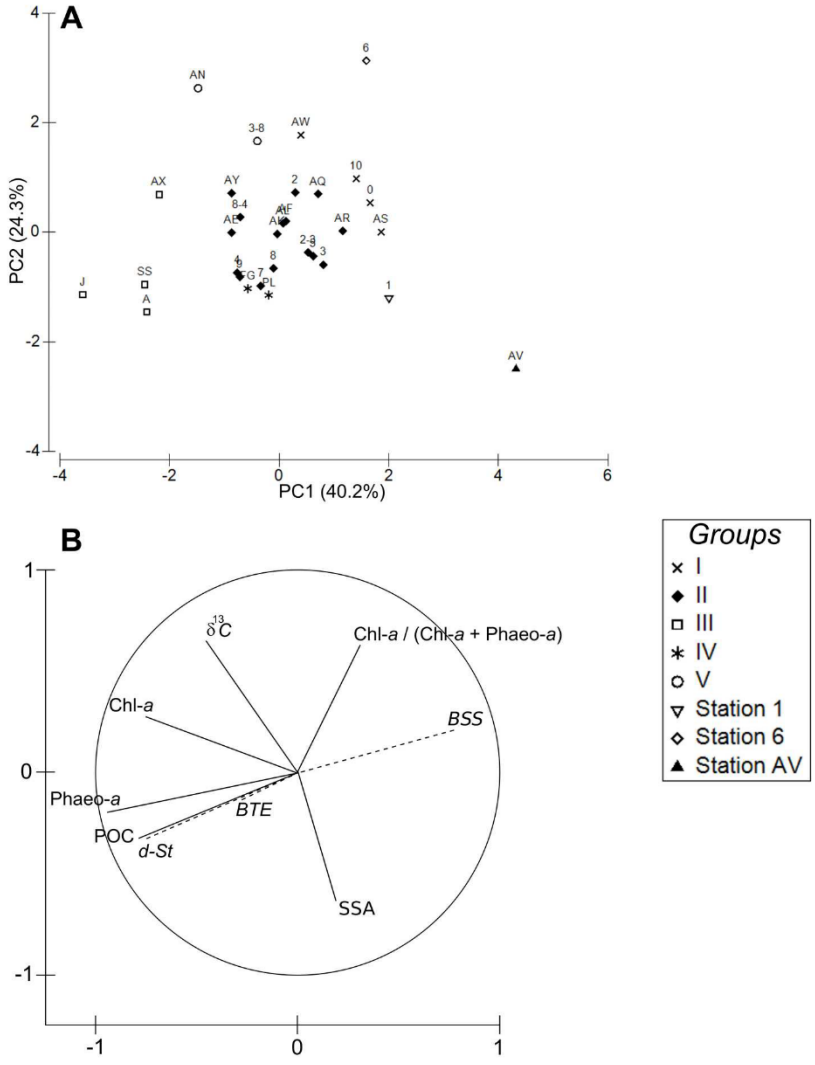

Figure 6.4. Principal component analysis based on normalized surface sediment characteristics (Sediment Surface Area (SSA), POC, Chl-*a*, Phaeo-*a*, Chl-*a*/(Chl-*a*+Phaeo-*a*) ratio and $\delta^{13}C$). Projection of stations on the first plane of the Principal Components Analysis (PCA) (**A**) and correlations of the variables with the first two components (**B**). Station depth (*d-St*), Bottom Shear Stress (*BSS*) and Bottom Trawling Effort (*BTE*) were used as supplementary variables. Group identification was achieved through the coupling of hierarchical clustering with a SIMilarity PROFile (SIMPROF) procedure. Station codes are the same as in Figure 6.1 and Table A6.1.

The first two components of the Principal Component Analysis (PCA) based on surface sediment characteristics accounted for 64.5% (i.e., 40.2% and 24.3% for the first and the second principal component, respectively) of the total variance (**Figure 6.4A**). The first component was defined by organic concentrations. The second component was mostly driven by the

opposition between Chl-*a*/(Chl-*a* + Phaeo-*a*) ratio and $\delta^{13}C$ on one side, and SSA on the other side (**Figure 6.4B**). Hierarchical clustering and the associated SIMPROF procedure resulted in the identification of 5 groups and 3 "isolated" stations (**Figure 6.4A**). Stations of group I, together with stations 1, 6, and AV, were all shallow (i.e., from 32.5 to 42.5 m depth). Group II was mostly composed of stations from the median part of the WGMP (i.e., from 43.5 to 60.5 m depth) except for stations AE, 8, 8-4, and 4, which were deeper (i.e., 31, 64.5, 67.5, and 71.5 m, respectively). Group III was composed of deep stations (i.e., from 62 to 79 m depth) except for station AX (z = 47.0 m). Stations of group IV (i.e., FG and PL) constituted apparent outliers to this overall pattern mostly due to their low Chl-*a*/(Chl-*a* + Phaeo-*a*) ratios and $\delta^{13}C$ values compared to other deep stations. Likewise, stations of group V (i.e., AN and 3-8) differed in Chl-*a* concentrations and Chl-*a*/(Chl-*a* + Phaeo-*a*) ratios. Overall, the coordinates of stations on the first axis of the PCA correlated significantly with station depth at the scale of both the whole WGMP and its sole distal part ($n = 31$, $R^2 = 0.561$, $p < 0.001$; $n = 24$, $R^2 = 0.366$, $p = 0.002$).

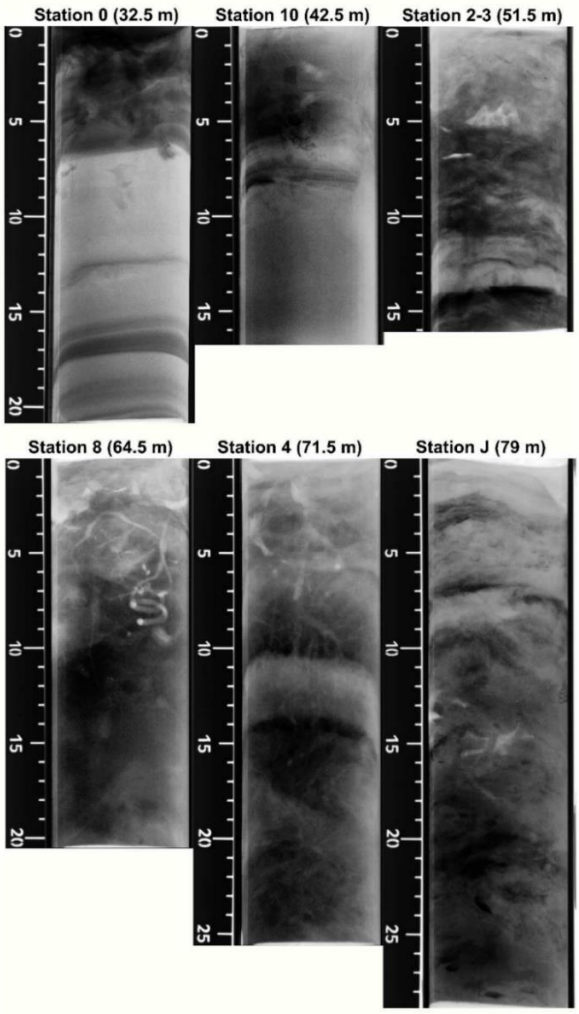

Figure 6.5. Examples of X-rays radiographies (positives; scale in cm) collected at six stations located along the sampled depth gradient (*see Figure 6.1*). Station codes are the same as in Figure 6.1 and Table A6.1.

3.2 X-Rays Radiographies

Examples of X-rays radiographies are shown in **Figure 6.5**. Stations 0 and 10 showed the presence of a ca. 6–7 cm thick surface sandy layer. Station 10 also presented traces of biological mixing within this layer. Both stations showed laminae corresponding to the denser particles deposits in the sediment column (z ≈13; 16; 17; 19 cm at station 0 and z ≈8 cm at station 10). These structures were less numerous at deeper stations. Nevertheless, some larger structures were observable: (1) at station 2–3 where a coarse layer (z≈14/15 cm) was overlaid by a finer one (11 < z < 14 cm), and (2) at station 4 where two denser (centimeter scaled) layers surrounded a finer one (10 < z < 14.5 cm). Overall, X-rays radiographies clearly showed an increase in the thickness of the bioturbated layer between stations 10 and J, whereas station 0 presented only superficial biological reworking within the surface sandy layer.

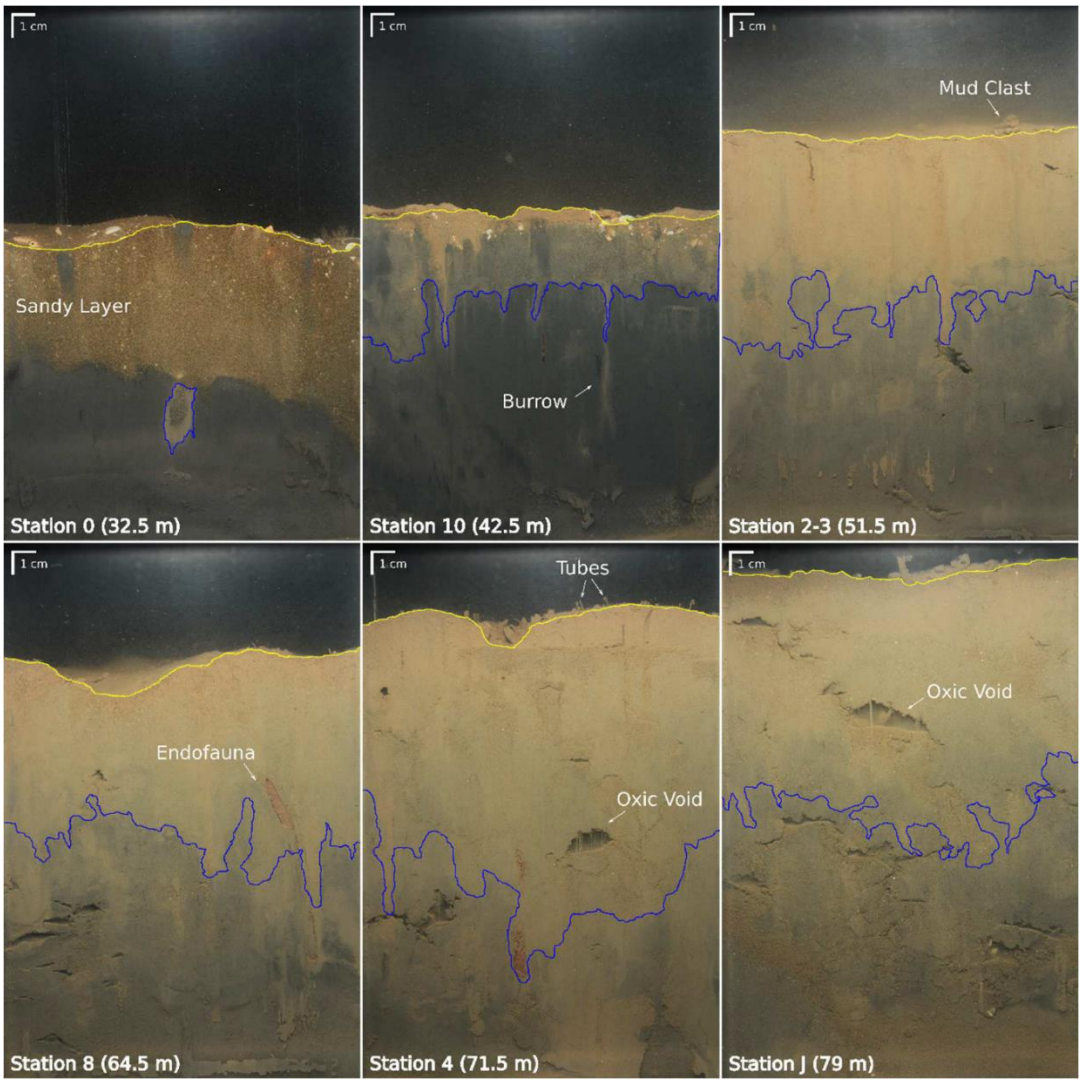

Figure 6.6. Examples of Sediment Profile Images (SPI) collected at six stations located along the depth gradient sampled for X-rays radiographies (see Figure 6.1). Yellow lines represent sediment–water interfaces and blue lines represent apparent Redox Potential Discontinuity (aRPD) thicknesses. Stations are the same as in Figure 6.5, and codes are the same as in Figure 6.1 and Table A6.1.

3.3 Sediment Profile Images

Overall, 186 Sediment Profiles Images (SPI) were captured. Representative examples (**Figure 6.6**) show the increases in the mean values of: (1) aRPD thickness, (2) total number of biological traces (i.e., biogenic structures + epi + infauna), and (3) the thickness of the sediment layer containing biogenic structures with station depth. They also clearly show the presence of a top coarser sediment layer covering dark mud at station 0.

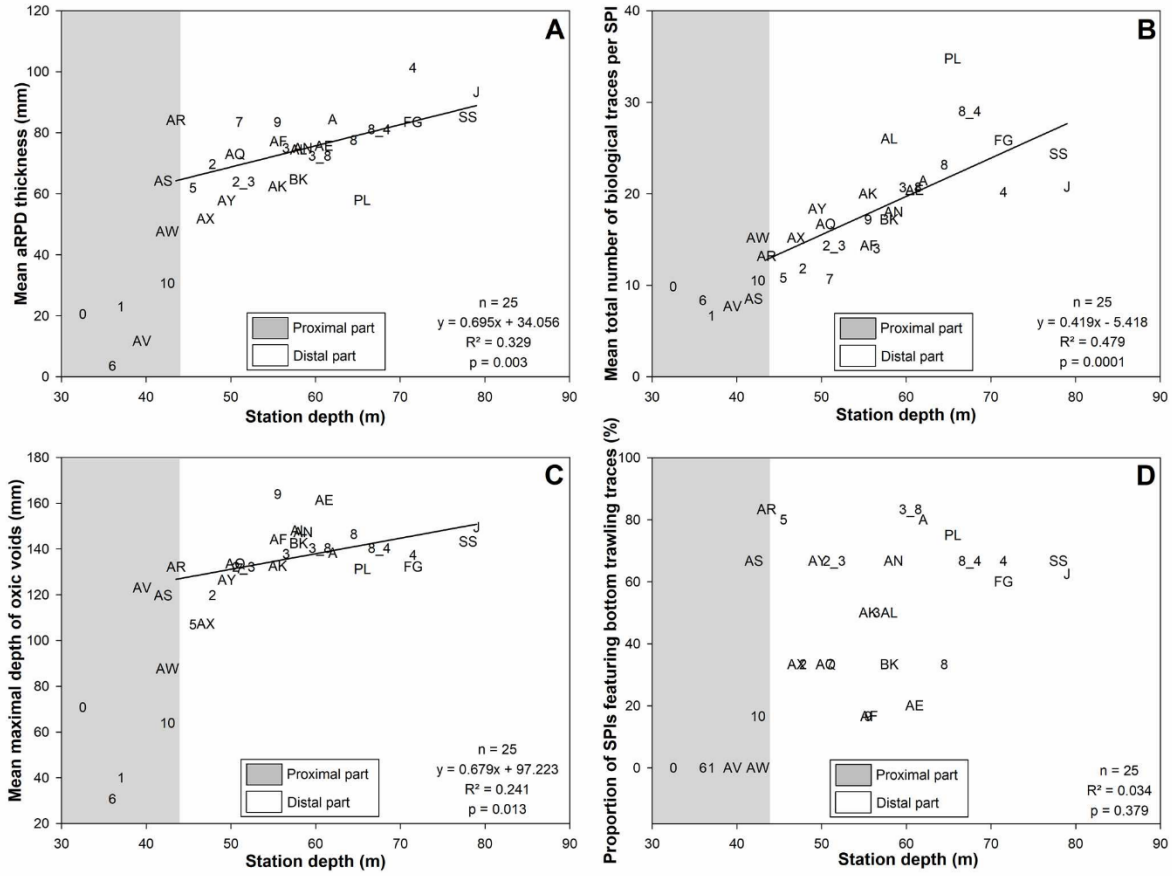

Figure 6.7. Relationships between station depth and mean main SPI characteristics: aRPD thickness (**A**), total number of biological traces per SPI (**B**), maximal depth of oxic voids (**C**), and proportion of SPIs featuring bottom trawling traces (**D**). Gray areas represent the proximal part (z < 42.5 m) of the WGMP. Station codes are the same as in Figure 6.1 and Table A6.1. Continuous lines represent the linear regressions linking station depth and mean SPI characteristics within the distal part of the WGMP.

At the scale of the whole WGMP, all SPI characteristics correlated significantly with station depth except for the number of infauna (**Table A6.2**). All significant correlations were positive except for number of epifauna. Examples of such relationships are given in **Figure 6.7** for mean (1) aRPD thickness, (2) total number of biological traces (i.e., biogenic structures + epi- and infauna), and (3) maximal depth of oxic voids. These three parameters presented low values and, for some of them (i.e., aRPD thickness and maximum depth of oxic void), there was a high between-station variability in the proximal part. Within the distal part, they correlated

significantly with station depth (**Table A6.2**), which was also the case of most other SPI characteristics (i.e., except for burrow and infauna numbers). All significant correlations were positive except for the number of epifauna. For both the whole WGMP and its sole distal part, the proportions of explained variance remained low (**Table A6.2**). They were higher for aRPD thickness, oxic void number and maximal depth, and tube number. This proportion was higher for the total number of biological traces than for any individual SPI characteristic.

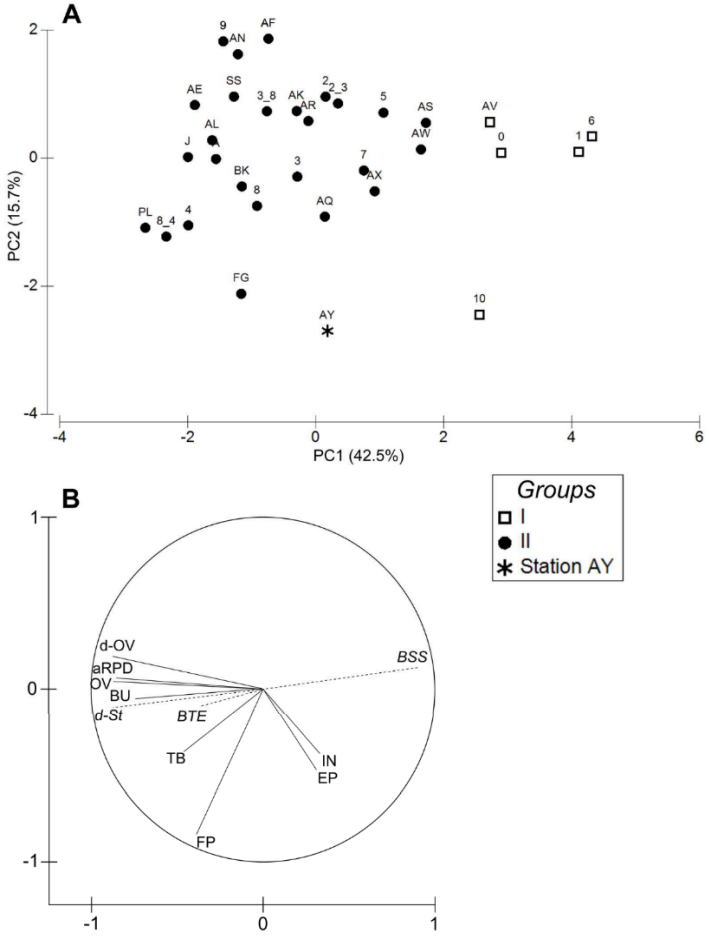

Figure 6.8. Principal component analysis based on normalized mean SPI characteristics (aRPD: aRPD thickness; BU: number of burrows; OV and d-OV: number and maximal depth of oxic voids; FP: number of feeding pits; TB: tubes; EP: epifauna and IN: infauna). Projection of stations on the first plane of the PCA (**A**), and correlations of the variables with its first two components (**B**). Station depth (*d-St*), Bottom Shear Stress (*BSS*), and Bottom Trawling Effort (*BTE*) were used as supplementary variables. Group identification was achieved through the coupling of hierarchical clustering with a SIMPROF procedure. Station codes are the same as in Figure 6.1 and Table A6.1.

The first two components of the PCA based on SPI characteristics explained 58.2% (i.e., 42.5% and 15.7% for the first and the second principal component, respectively) of the total variance (**Figure 6.8A**). The first component was mainly characterized by a set of co-correlated subsurface features (i.e., number and maximal depth of oxic voids, number of burrows and aRPD thickness). The second component was mostly driven by the number of feeding pits

(**Figure 6.8B**). Hierarchical clustering and the associated SIMPROF procedure resulted in the identification of three groups of stations (**Figure 6.8A**), one of them including only a single station. Group I was composed of five of the seven shallowest stations (i.e., stations 0, 1, 6, 10, and AV), and group II was composed of all other stations except station AY due to a high number of epifauna. The SPI characteristics accounting most for differences between groups I and II were (1) aRPD thickness (22.3%), (2) oxic void maximal depth (22.0%), (3) burrow number (14.4%), and (4) oxic void number (13.5%). The coordinates of stations on the first axis of the PCA correlated significantly with station depth at the scale of both the whole WGMP and its sole distal part ($n = 32$, $R^2 = 0.757$, $p < 0.001$; $n = 25$, $R^2 = 0.601$, $p < 0.001$; respectively).

Mud clasts were observed in 80 out of 186 SPIs, whereas furrows were recorded on only two images and surface puzzle fabrics were never observed. SPIs from five of the shallowest stations did not show any of these traces at all (**Figure 6.7D**). There was otherwise high among-station variability in the proportion of SPI containing such features. The proportion of SPI featuring traces indicative of bottom trawling correlated significantly with station depth at the scale of the whole WGMP, but this correlation was not significant within the sole distal part (**Table A6.2**).

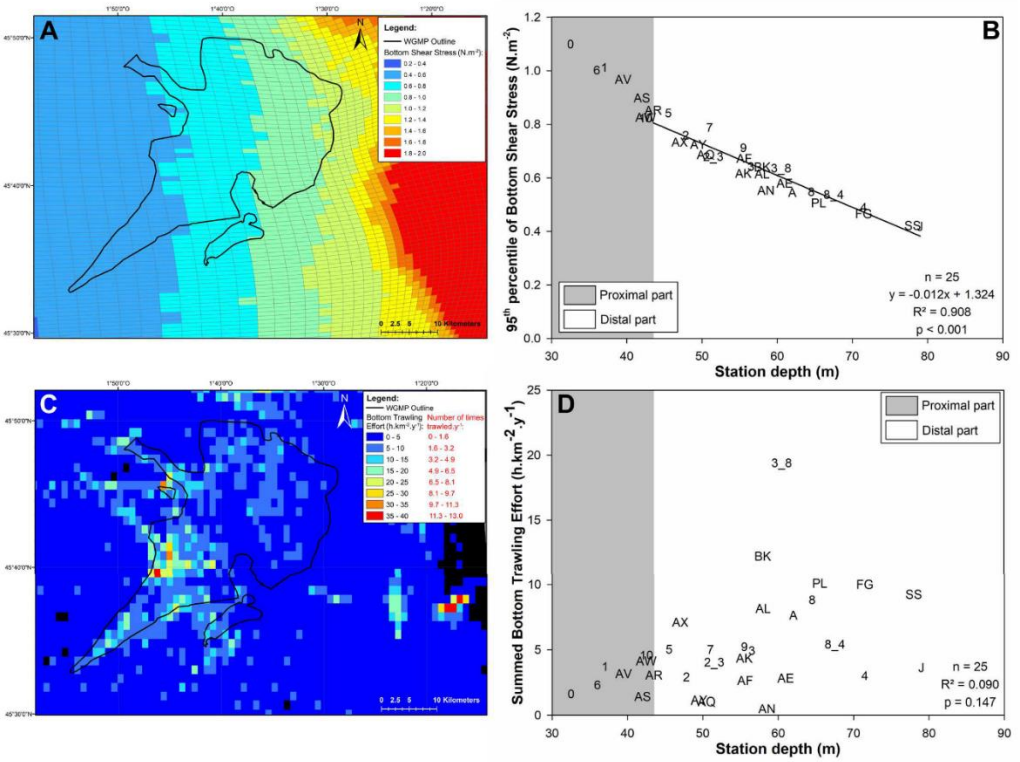

Figure 6.9. Spatial mapping of 95th percentile of Bottom Shear Stress during the year preceding the JERICOBENT-5 cruise (**A**), relationship with station depth within cells including sampled stations (**B**), summed Bottom Trawling Effort during the year preceding the JERICOBENT-5 cruise (**C**), and relationship with station depth within cells including sampled stations (**D**). Gray areas represent the proximal part (z < 42.5 m) of the WGMP. Station codes are the same as in Figure 6.1 and Table A6.1.

3.4 Bottom Shear Stress and Bottom Trawling Effort

BSS 95th percentiles significantly decreased with station depth at the scale of the whole WGMP and of its sole distal part (**Figure 6.9A,B** and **Table A6.2**). Their values within cells containing sampled stations were between 0.42 at station J and 1.10 N·m^{-2} at station 0 (**Figure 6.9B** and **Table A6.1**). In the distal part, POC, Phaeo-*a*, and THAA correlated negatively with BSS 95th percentiles. This was also the case for six (i.e., aRPD thickness; numbers of oxic voids, feeding pits, tubes; maximal depth of oxic voids; and total number of biological traces; **Table A6.3**) of the 10 SPI characteristics assessed during the present study. Moreover, at the scale of the sole WGMP distal part, the coordinates of stations on the first axis of the PCAs based on both surface sediment and SPI characteristics correlated significantly with BSS (n = 24, R^2 = 0.348, p = 0.002; and n = 25, R^2 = 0.547, p < 0.001; respectively).

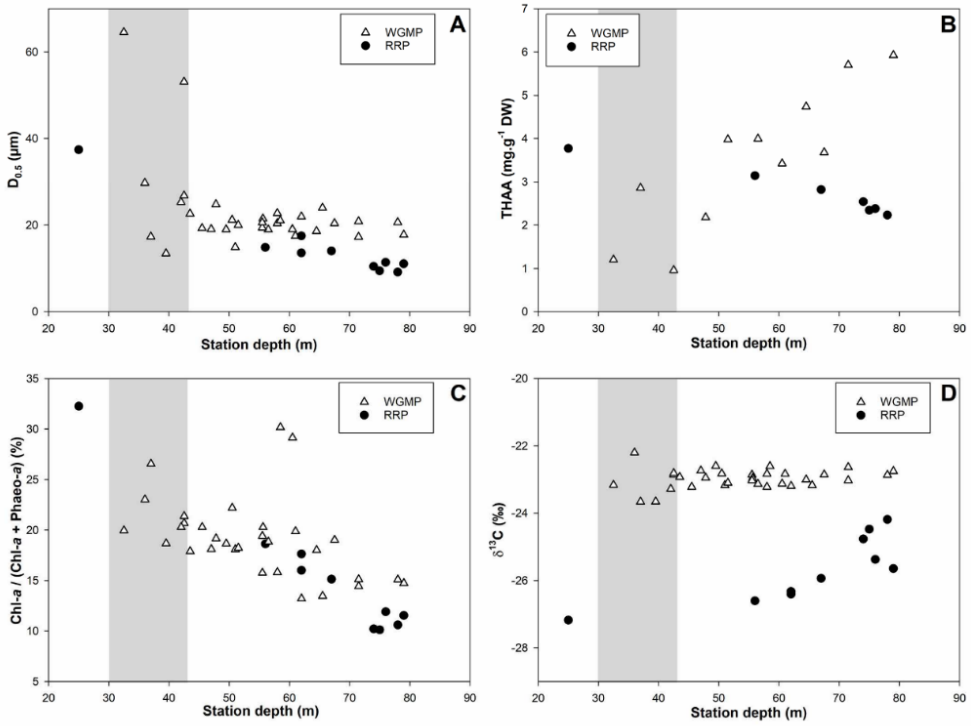

Figure 6.10. Relationships between station depth and main surface sediment characteristics in the WGMP and the Rhône River Prodelta (RRP): $D_{0.5}$ (**A**), Total Hydrolyzable Amino Acids (THAA (**B**)), Chl-*a*/(Chl-*a*+Phaeo-*a*) ratio (**C**), and $\delta^{13}C$ (**D**). Gray areas represent the proximal part of the WGMP (z < 42.5 m).

Bottom Trawling Effort (BTE) tended to be higher in the WGMP than in adjacent areas (**Figure 6.9C**). It was low in the shallowest part (i.e., 35 < z < 50 m) of the WGMP. Deeper, BTE was highly heterogeneous with some cells being heavily trawled between 55 and 60 m depth (i.e., up to 39.6 h·km^{-2}·y^{-1} and 12.9 times trawled·y^{-1}; **Figures 6.9C**), while some others were only lightly affected. BTE within cells containing sampled stations was between 0.48 and 19.4 h·km^{-2}·y^{-1} (0.2 and 6.3 times trawled.y^{-1} for stations AN and 3-8, respectively; **Figure 6.9D** and **Table A6.1**). Four sampled stations (3-8, BK, PL, and FG) were located in cells

featuring a BTE higher than 10 $h \cdot km^{-2} \cdot y^{-1}$ (**Figure 6.9D** and **Table A6.1**). BTE within cells containing sampled stations correlated positively with station depth at the scale of the whole WGMP, but this correlation was not significant in the sole distal part (**Table A6.2**). In the distal part, there was no significant correlation between BTE and any surface sediment or SPI individual characteristic (including the proportion of SPI featuring traces indicative of bottom trawling), except for (1) $\delta^{13}C$, (2) Chl-*a*/(Chl-*a* + Phaeo-*a*), and (3) numbers of tube and total biological traces (which was largely affected by tube number; **Table A6.3**). Moreover, at the scale of the sole WGMP distal part, the coordinates of stations on the first axis of the PCAs based on both surface sediment and SPI characteristics did not correlate significantly with BTE (n = 24, R^2 = 0.003, p = 0.813; and n = 25, R^2 = 0.038, p = 0.347; respectively).

3.5 Comparison with the Rhône River Prodelta

The relationships between station depth and $D_{0.5}$, THAA, Chl-*a*/(Chl-*a* + Phaeo-*a*), and $\delta^{13}C$ in both the distal part of the WGMP and the Rhône River Prodelta (RRP) show clear differences between the two systems (**Figure 6.10**). With the exception of the RRP shallowest station, surface sediments were significantly ($p < 0.001$) coarser in the distal part of the WGMP (mean $D_{0.5}$ of 20.2 µm) than in the RRP (i.e., mean $D_{0.5}$ of 12.0 µm; **Figure 6.10A**). Mean THAA concentrations were significantly higher in the distal part of the WGMP than in the RRP (mean values and standard deviations of 4.20 ± 1.23 $mg \cdot gDW^{-1}$ and 2.75 ± 0.55 $mg \cdot gDW^{-1}$, respectively; p = 0.013). Moreover, changes in THAA concentrations relative to station depth showed opposite patterns in the two systems with increasing values with increasing depth in the distal part of the WGMP and decreasing values with increasing depth in the RRP (**Figure 6.10B**). The same result was found after standardization for $D_{0.5}$. Similar discrepancies between systems were found for POC and EHAA concentrations even though mean POC concentrations were significantly lower in the distal part of the WGMP (1.09 ± 0.24 vs. 1.39 ± 0.29%DW in the RRP; p = 0.021), and mean EHAA concentrations did not significantly differ between systems (0.76 ± 0.13 vs. 0.77 ± 0.19 $mg \cdot gDW^{-1}$, in the distal part of the WGMP and the RRP, respectively; p = 0.846). Chl-*a*/(Chl-*a* + Phaeo-*a*) ratio significantly decreased with increasing station depth in both systems (**Figure 6.10C**) with no significant difference in their mean values (p = 0.105). EHAA/THAA ratios did not correlate significantly with station depth in either system (p = 0.202 and p = 0.950 in the distal part of the WGMP and the RRP, respectively). Their mean value was significantly lower in the distal part of the WGMP than in the RRP (19.8 ± 3.4% and 27.7 ± 1.5%, respectively; p <0.001). The pattern of changes in $\delta^{13}C$ relative to station depth clearly differed between systems with significantly increasing values with increasing station depth in the RRP (p = 0.005) and no significant change in the distal part of the

WGMP. Their mean value was significantly ($p < 0.001$) less negative in the WGMP (−22.9‰) than in the RRP (−25.7‰).

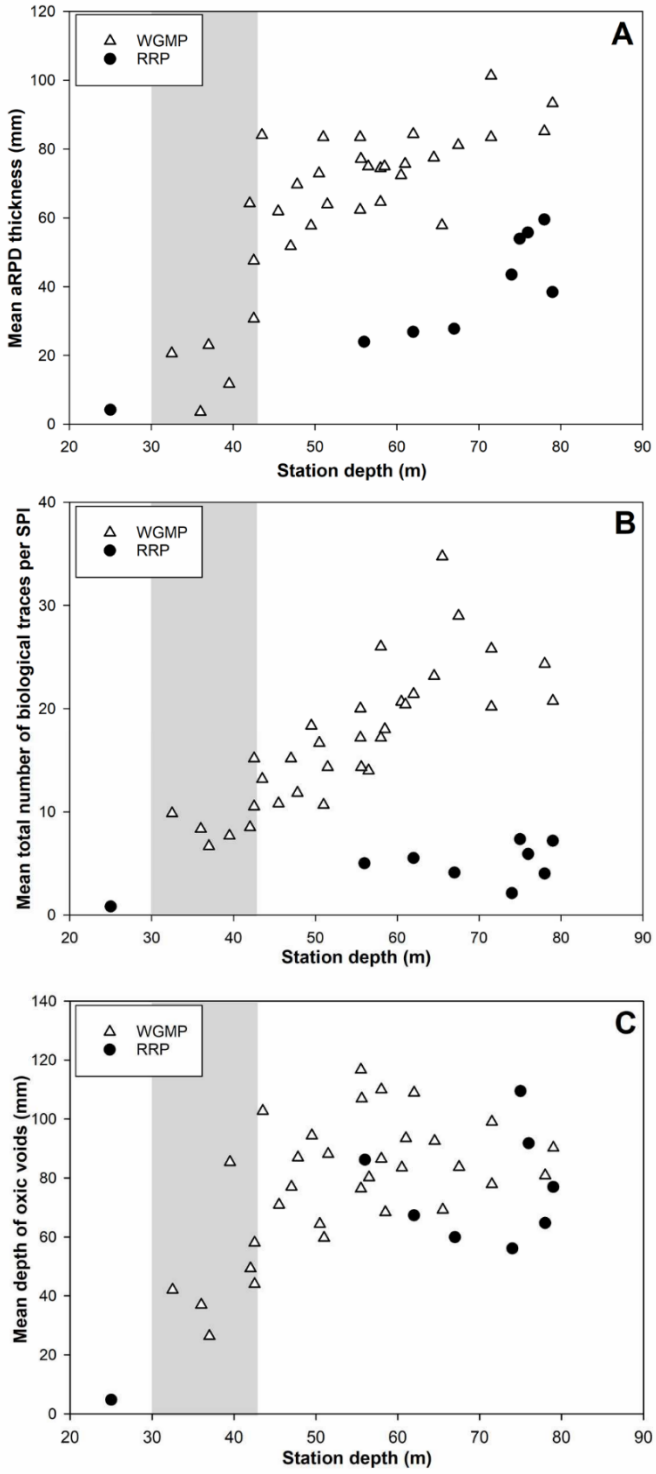

Figure 6.11. Relationships between station depth and mean main SPI characteristics in the WGMP and the RRP: aRPD thickness (**A**), total number of biological traces per SPI (**B**), and depth of oxic voids (**C**). Grey areas represent the proximal part of the WGMP (z < 42.5 m).

The relationships between station depth and (1) aRPD thickness, (2) total number of biological traces per SPI, and (3) depth of oxic voids in both the distal part of the WGMP and the RRP are shown in **Figure 6.11**. The two systems presented strong differences. aRPD thickness increased with station depth in both the distal part of the WGMP and in the RRP ($p = 0.003$ and $p = 0.002$, respectively; **Figure 6.11A**), but its mean was significantly higher in the distal part of the WGMP (74.8 ± 11.7 vs. 37.0 ± 18.1 mm in the RRP; $p < 0.001$). The mean total number of biological traces was also significantly higher in the distal part of the WGMP (**Figure 6.11B**; 19.1 ± 5.9 vs. 4.7 ± 2.2 per SPI in the RRP; $p < 0.001$). There were similar differences for the mean numbers of burrows, oxic voids, and tubes ($p < 0.001$ in all cases). Mean oxic void depth significantly increased with station depth in the RRP ($p = 0.022$) but not in the distal part of the WGMP ($p = 0.745$). Its mean value was also significantly higher, although to a lower extent, in the distal part of the WGMP (**Figure 6.11C**; 86.7 ± 15.0 vs. 68.5 ± 29.4 mm, in the RRP; $p = 0.023$).

4. Discussion

4.1 Spatial Structuration

4.1.1 Subdivision between Proximal and Distal Parts

Up to now, only two studies have considered the spatial distribution of surface sediment grain size and organic contents in the West Gironde Mud Patch (WGMP; [44, 45]). Both studies relied on the sampling of only three stations, and their results supported the original [26, 34, 40] distinction between a proximal and a distal part. Our sampling plan was based on 32 stations, which allowed showing a significant correlation between surface sediment characteristics (as summarized by the first component of the corresponding PCA) and station depth. Data analysis resulted in the identification of three main groups of stations presenting different surface sediment characteristics. Stations of groups I (together with stations 1, 6, and AV) were all shallow ($z < 42.5$ m) and tended to present coarse surface sediments and low concentrations in Particular Organic Carbon (POC) and chloropigments. A high between-station variability in $D_{0.5}$ and Sediment Surface Area (SSA) was nevertheless recorded in this group, most likely reflecting spatial differences in the transient deposition of coarse sediments [25, 26, 40] as observed during the present study on the Sediment Profile Images (SPIs) collected at station 0. Therefore, our results clearly support that the stations of group I, and associated isolated stations are constitutive of the proximal part of the WGMP as stated by Jouanneau et al. [35] and Lesueur et al. [26, 34].

The spatial zonation of the WGMP has also been studied based on X-rays radiographies of long sediment cores [26, 34, 35, 40, 43]. Lesueur and Tastet [43] computed a crude index of bioturbation (i.e., the proportion of reworked sediment volume) based on these radiographies. They proposed to subdivide the WGMP in three parts based on the values of this index, which increased with station depth. The shallowest part could be considered as mostly representative of the proximal and the two others of the distal part (Lesueur and Tastet [43]). However, this conclusion clearly suffered from (1) the inability of X-rays radiographies to precisely assess bioturbation and (2) the use of long sediment cores, which did not allow for the preservation of the sediment–water interface. The X-rays radiographies collected during the present study were achieved on cores collected using a lightweight interface corer, which allowed for a better preservation of this interface. Results confirmed previous observations in showing (1) the occurrence of sandy layers in the top sediment column of the three stations sampled within the proximal part (see above); (2) the presence, especially at shallow stations, of laminae attributed by Lesueur and Tastet [43] to the deposition of dense and coarse particles following high energy events; and (3) a limitation of bioturbation to the top of the sediment column at shallow stations, whereas the thickness of the mixed sediment layer was clearly higher at deep stations. During the present study, we also used Sediment Profile Imagery, which allowed for (1) an in situ 2D visualization of the sedimentary column without disturbing the sediment–water interface and (2) a multiparametric assessment of modern bioturbation through the analysis of biological traces [63]. This resulted in the identification of two main groups of stations delimited by a ca. 42.5 m depth threshold, which further supports the distinction between a proximal part where bioturbation is limited and a distal part where it is much higher (**Figure 6.7A–C**).

4.1.2 Spatial Structuration of the Distal Part

Previous sedimentological surveys have shown the occurrence of two major depth gradients in the distal part [26, 34, 35, 40, 43]. The first related to the frequency of occurrence of erosional surfaces and subsequent vertical decreasing granulometric sequences (see above), and the second related to bioturbation. However, these surveys did not account for modern biogeochemical processes taking place in the top of the sediment column. This issue was tackled by Relexans et al. [44] and later by Massé et al. [45] based on the analyses of surface sedimentary organics and benthic fauna composition. However, results remained largely inconclusive regarding the possible existence of spatial gradients due to limited sampling efforts.

During the present study, we sampled 25 stations within the distal part. Based on the multivariate analysis of their surface sediment characteristics, these stations were mostly distributed among two main groups, which were clearly related to station depth as confirmed by

the significance of the correlations linking station depth with (1) POC, THAA, and Phaeo-*a* concentrations and (2) the coordinates of stations on the first component of the PCA based on surface sediment characteristics within the distal part of the WGMP. A significant correlation was also found for the Chl-*a*/(Chl-*a* + Phaeo-*a*) ratio when excluding two outliers. Thus, our results clearly support the occurrence of a depth gradient in surface sediment characteristics within the distal part of the WGMP. This gradient was linked to changes in sedimentary organic characteristics and independent of changes in sediment granulometry, since all organic concentrations were normalized to SSA.

The two statistical approaches used to assess the existence of a potential depth gradient based on SPI characteristics led to apparently different conclusions. On the one hand, regression analyses showed significant correlations between most individual characteristics and station depth, and there was a significant correlation between station depth and station coordinates on the first component of the PCA based on SPI characteristics. On the other hand, the hierarchical clustering based on the whole set of SPI characteristics together with the associated SIMPROF procedure failed to identify significantly differing station subgroups. Most of the assessed individual SPI characteristics correlated significantly with station depth, and for five of them, this was indicative of an increase in bioturbation with station depth. This trend was particularly marked for (1) sediment oxidation (aRPD), (2) burrowing (oxic void number), and (3) thickness of the mixed sediment layer (oxic void maximal depth). Conversely, neither infauna nor burrow numbers did significantly correlate with station depth. For infauna, this may result from undersampling. For burrow number, this probably results from (1) large spatial extensions at highly bioturbated deep stations, which complicates the distinction between burrows and may induce an underestimation of their number; and (2) stronger difficulties in identifying burrows (i.e., oxidized structures) within sediment columns featuring thicker aRPDs at deep stations. Interestingly, the positive correlation with station depth was more pronounced for the total number of biological traces (although this last parameter included the epifauna number, which correlated negatively with station depth) than for any SPI individual characteristic. This can be interpreted as a reduction (by summation) of the lack of fit of the regression models linking station depth and individual SPI characteristics, which further supports the existence of a gradient of increasing bioturbation along the depth gradient within the distal part of the WGMP. The fact that hierarchical clustering based on SPI characteristics did not allow differentiating station subgroups is likely caused by (1) the use of normalized data, which resulted in the attribution of the same weight to all considered parameters, including those that did not correlate significantly with station depth (i.e., burrow and infauna numbers); and (2) the noise generated by the lack of fit of the regression models linking station depth and individual SPI characteristics, which differed between characteristics for a given station (as exemplified above

for the total number of biological traces). Therefore, our interpretation of SPI data is that they also support the existence of a depth gradient of increasing bioturbation within the distal part.

4.1.3 Overall Conclusion

Based on a wide range of surface sediment characteristics and the use of an image analysis technique specifically designed for the top of the sediment column, our results clearly confirm the subdivision of the WGMP in a proximal and a distal part put forward by previous sedimentological surveys and support the proposed 40–45 m depth limit between these two parts [26, 43]. They also show the existence of a depth gradient resulting from modern sedimentation and bioturbation processes taking place in the distal part of the WGMP.

4.2 Disentangling the Potential Effects of Hydrodynamics and Bottom Trawling

The potential impacts of hydrodynamics and bottom trawling on the spatial distributions of surface sediment and SPI characteristics were tested by the simultaneous assessments of the spatial distributions of (1) Bottom Shear Stress (BSS), (2) Bottom Trawling Effort (BTE), (3) surface sediment characteristics, and (4) SPI features. When considering the whole WGMP, the correlations between both BSS and BTE with station depth impaired the unraveling of the role of these two factors in controlling the spatial distribution of surface sediment and SPI characteristics. More generally, the correlation between environmental characteristics and fishing effort clearly constitutes a major issue when assessing the impact of benthic trawling on benthic systems [23,83,84]. During the present study, this difficulty was overcome by considering spatial changes recorded in the sole distal part where (1) BTE did not correlate significantly with station depth, (2) the ranges of $D_{0.5}$ and SSA were narrower, and one of these two parameters correlated significantly with both BSS and BTE (see Queirós et al. [24] for a similar approach).

The 95th BSS percentiles recorded during the present studies were between 0.4 and 1.1 N.m^{-2}. These values can be compared with those computed in the Gulf of Lions using a similar model (i.e., a 90th percentile around 0.05 N·m^{-2} at a 30 m depth; [85]). Moreover, based on simultaneous assessments of BSS and Suspended Particulate Matter concentration, Dufois et al. [78] concluded that resuspension was induced over a critical BSS threshold of 0.35 N·m^{-2} at a 20 m deep station within the Rhône River Prodelta. Although caution should clearly be taken since sediment roughness and rheological properties were not assessed during the present study, this supports the hypothesis according to which sediment resuspension may take place over the whole WGMP [47]. Moreover, the 95th percentile value of BSS correlated negatively with station depth, which largely corresponded to the dominance of its wave-induced component relative to its current-induced component and is also coherent with the dominant role attributed

to waves in controlling the spatial structuration of the WGMP [26]. Although collected over different periods (June 2017–June 2018 vs. 2005–2013) and using different positioning systems (i.e., Automatic Identification System vs. Vessel Monitoring System), the absolute values and the spatial distribution of BTE observed during the present study were fully consistent with the one reported by Mengual et al. [19, 20]. BTE was clearly higher within the distal part with a maximal average number of times trawled.y^{-1} of 12.9.

Several lines of evidence suggest that the effect of bottom trawling on the spatial distributions of both surface sediment and SPI characteristics was limited as compared to the influence of hydrodynamics. First, there were significant correlations between three (four when excluding the two above-mentioned outliers for Chl-*a*/(Chl-*a* + Phaeo-*a*)) of surface sediment characteristics and BSS, whereas only $\delta^{13}C$ (although featuring a very restricted range of variation) and Chl-*a*/(Chl-*a* + Phaeo-*a*) (when excluding the two above-mentioned outliers) correlated significantly with BTE. Second, most of the SPI individual characteristics correlated negatively with BSS, whereas the number of tubes was the only individual SPI characteristic significantly correlating with BTE. Furthermore, this last result is not supporting a strong effect of bottom trawling, since BTE is generally assumed to negatively impact benthic bioturbation [24, 83, 84, 86–89]. Along the same line, the correlation between tube number and BTE was positive, which here again is not supporting a strong influence of bottom trawling, since according to the literature, tube-building species tend to be rare or even absent in trawled areas [61,62,90]. Third, stations coordinates of the PCAs based on both surface sediment and SPI characteristics correlated significantly with BSS, but not BTE. Fourth, the incorporation of BTE with BSS in multiple regression models did not improve the description of either the surface sediment or the SPI characteristics assessed during the present study. None of the correlations that were not significant using BSS alone as the independent variable became significant when incorporating BTE as a second independent variable. Moreover, for most characteristics correlating significantly with BSS alone (i.e., all except tube number and total number of biological traces), the incorporation of BTE resulted in poorer descriptions. Therefore, BTE did not account as well for changes in surface sediment and SPI characteristics assessed not described by changes in BSS.

Overall, the only rationale for a significant impact of bottom trawling was the sometimes high (i.e., up to ca 80%) proportion of SPI featuring trawling traces. However, these proportions were highly variable between stations and did not correlate significantly with BTE. Moreover, the trawling traces recorded during the present study almost exclusively consisted in mud clasts with almost no furrows and no puzzle fabrics at all. This is an important point, since the direct causality linking bottom trawling and the presence of mud clasts appears still questionable [91,

92]. For example, similar proportions of SPI featuring trawling traces (including mud clasts) have been reported in several areas of the Gulf of Lions experimenting different BTE [61,62,93], which further highlights the difficulty in unambiguously associating the presence of mud clasts with bottom trawling.

Based on these rationales, our overall conclusion is that the assessment of the spatial distributions of both SPI characteristics and BTE recorded during the present study does not support the hypothesis according to which bottom trawling is a key factor in controlling the spatial structuration of the WGMP. However, it should be pointed out that this conclusion may partly result from differences in spatial scales associated with the assessments of BTE (i.e., a few km^2) and SPI characteristics (i.e., typically a few m^2). BTE is known to induce spatially heterogeneous effects on benthic habitats even within experimentally heavily trawled areas [94], which led Smith et al. [95] to recommend collecting a high number of SPIs (i.e., ca. 30, which is much more than achieved during the present study) at each station to infer the impact of bottom trawling (see also [86, 96], for the interest of complementary approaches). BTE was not spatially homogeneous over each of the 1.77 km^2 cells considered during the present study, which may have hampered the detection of significant correlations between BTE and both surface sediment and SPI characteristics measured over much smaller spatial scales. Differences in temporal scales associated with the assessment of BTE (i.e., one year during the present study) and the kinetics of recovery of benthic habitats may have had the same effect as well.

4.3 Comparison with the Rhône River Prodelta

4.3.1 Surface Sediment Characteristics

$\delta^{13}C$ values differed between the distal part of the WGMP and the Rhône River Prodelta (RRP) regarding both their absolute values and their changes relative to station depth. In the RRP, $\delta^{13}C$ ranged from −24.2‰ to −27.2‰ and significantly increased with station depth, whereas in the distal part of the WGMP, they were close to −23‰ and did not change significantly with station depth. In the RRP, these results have been interpreted as reflecting the dominance of a continental source of organic matter and its gradual mixing with marine sources through a series of resuspension/sedimentation events occurring within the prodelta itself [74, 81, 97–99]. In the WGMP, $\delta^{13}C$ values around −23‰ have been reported in suspended particulate material both at the Mouth of the Gironde Estuary and in the inner part of the Bay of Biscay Continental Shelf [100]. These values were interpreted as resulting from an early mixing between (1) a continental/terrestrial source (with a mean $\delta^{13}C$ of −25.9‰), (2) estuarine sources generated by autochthonous processes due to long estuarine residence times

[101, 102], and (3), a marine planktonic source (with a mean $\delta^{13}C$ of −20.5‰). Such an early mixing within the Gironde Estuary is largely resulting from its macro-tidal regime [100,103]. Our own results support this interpretation and suggest the lack of subsequent significant mixing with marine sources in the WGMP itself. Overall, the discrepancies in the $\delta^{13}C$ between the two systems are indicative of major differences in the timing and the nature of the processes involved in the mixing of continental and marine sources of sedimented Particulate Organic Matter (POM).

Our results show a lack of correlation between station depth and $D_{0.5}$ and the presence of coarser sediment in the distal part of the WGMP, despite a lower water discharge and a long (i.e., 1–2 years in the Estuarine Turbidity Maximum) particle residence time in the Gironde Estuary [104, 105]. There were also marked differences between systems in both sedimentary organics concentrations and their changes relative to station depth. THAA concentrations were higher in the WGMP, where they increased with station depth conversely to what was observed in the RRP. Such opposite patterns were also observed for POC and, to lesser extent, EHAA. In the RRP, spatial changes in $D_{0.5}$ and surface sediment concentrations were interpreted as resulting from (1) a particle sorting relative to size induced by the succession of sedimentation/resuspension events [106] and (2) the progressive dilution of a highly dominant continental POM source originating from the Rhône River [55, 56, 74, 81, 97– 99]. The Gironde River is also the dominant source of particles fueling the WGMP [31, 32, 41], and successive sedimentation/resuspension events are largely responsible for the transfer of particles at depth in this system as well [26]. Therefore, the same two key driving factors are inducing major differences in the spatial structuration of the two systems. The lack of depth gradient in particle size in the distal part of the WGMP suggests that particle sorting is not predominantly controlled by particle size in the WGMP. Density may constitute an alternative sorting cue as suggested by the preferential sedimentation of denser particles following major resuspension events [43]. In coastal sediments, low-density particles are organically enriched and behave similar to smaller ones with regard to particle sorting [107]. Therefore, a density-driven particle sorting could account for the depth gradients observed in the distal part of the WGMP; low-density (and organically enriched) particles being preferentially settled and trapped in deeper areas irrespective of their size, which would account for increasing bulk organic concentrations with station depth. At this stage, this only constitutes a working hypothesis, and it will certainly prove interesting to assess spatial changes in the proportion of low-density particles during future studies taking place in the WGMP.

EHAA/THAA ratios were lower in the distal part of the WGMP than in the RRP. This is

indicative of a lower lability of sedimented POM, which may be linked to the long residence time of particles in the Gironde Estuary [104, 105] and the predominance of degradation processes in its Estuarine Turbidity Maximum [101, 108–110]. Conversely Chl-*a*/(Chl-*a* + Phaeo-*a*) ratios did not significantly differ between areas. These two indices showed the same pattern of change relative to station depth in both systems with (1) a significant decrease in Chl-*a*/(Chl-*a* + Phaeo-*a*) ratios and (2) no significant change in EHAA/THAA ratios. In the RRP, the discrepancy between the two indices has been attributed to the fact that the Chl-*a*/(Chl- *a* + Phaeo-*a*) ratio is representing a highly labile vegetal fraction of the sediment POM, whereas the EHAA/THAA ratio is representative of the lability of the bulk nitrogenous fraction of sedimentary organics [56, 57]. This suggests that both in the WGMP and the RRP, degradation processes occurring during the transfer of deposited particles at depth are mostly affecting a highly labile fraction of POM. Since this component is contributing only to a small fraction of bulk sedimentary organics, this is also in agreement with the lack of significant changes in $\delta^{13}C$ with station depth.

Overall, the WGMP and RRP present strong similarities. Both are alimented by particles originating from major rivers. Moreover, the transfer of particles along their depth gradient is cued by sorting processes associated with the succession of sedimentation and resuspension sequences. Major differences between the two systems first refer to the tidal regime and marine hydrodynamics, which result in a much earlier mixing between continental and marine POM in the Gironde estuarine system. More specifically, this mixing is largely taking place in the RRP itself and conversely upstream the WGMP, namely in the Gironde Estuary and near its mouth. Other major differences between the two systems are linked to sedimentary organic concentrations and their patterns of change relative to station depth. We hypothesized that this may result from different particle sorting processes (i.e., mostly cued by particle size and particle density in the RRP and the WGMP, respectively) associated with successive sedimentation/resuspension events. These differences support the distinction between type 1 and type 2 prodeltas [3, 5] for temperate areas.

4.3.2. Bioturbation

In both systems, the aRPD thickness, the total number of biological traces, and the thickness of the bioturbated layer increased with station depth in accordance with the negative impact of disturbance on bioturbation described by the Pearson and Rosenberg [111] and Rhoads et al. [12] models. However, the nature of the dominant disturbance itself differs between systems. In the RRP, the shallowest stations are mostly submitted to high sedimentation rates [74, 79, 80, 112] and associated organic matter inputs caused by river floods [56]. This results in sediment instability and organic enrichment, which largely affect benthic macrofauna

composition and limit bioturbation [56]. In the distal part of the RRP, continental inputs are diluted and sediment stability is higher, which results in increasing bioturbation. In the proximal part of the WGMP, strong Bottom Shear Stress (BSS) precludes modern sedimentation [25, 26]. It also largely controls the composition of resident fauna, which is largely dominated by suspension feeders (mostly the small-sized bivalve *Kurtiella bidentata* and the ophiuroid *Amphiura filiformis*; [45]) that are not efficient bioturbators under such environmental conditions.

There were also important differences in bioturbation between the distal parts of the WGMP and the RRP. These differences refer both to overall intensity and change relative to station depth. In the distal part of the WGMP, bioturbation intensity tended to increase with station depth together with decreasing BSS, which is coherent with the Rhoads et al. [12] model. Conversely, in the distal part of the RRP, there was no clear correlation between station depth and bioturbation intensity. Salen-Picard et al. [113] reported the existence of a positive impact of Rhone River floods on the abundance of subsurface feeders (i.e., potentially strong bioturbators) at a 70 m deep station with a time lag of ca. 33 months. Therefore, the lack of significant correlation between bioturbation intensity with station depth in the distal part of the RRP may result from opposite gradients in three potentially controlling factors, namely: (1) organic matter availability, which decreases with station depth; (2) the positive impact of floods on the abundance of strong bioturbators, which also decreases with station depth; and (3) sediment stability, which conversely increases with station depth. According to this hypothesis, the lack of gradient in bioturbation intensity in relation with station depth would result from an equilibrium between organic matter availability and sediment stability and therefore conforms to the Rhoads et al. [12] model.

Differences between overall bioturbation intensities between systems are not easy to account for. According to the Rhoads et al. [12] model, bioturbation intensity results from the interaction between organic matter availability (eventually through its effect on benthic macrofauna) and physical disturbances [12]. POC sediment concentrations were quite similar in both areas, which was also true for amino acid concentrations when accounting for their bioavailability (i.e., EHAA). The comparison of benthic macrofauna abundance, biomass, and feeding types between systems is clearly complicated by the fact that they were not sampled using the same gear (i.e., an Hamon grab for Massé et al. [45] vs. a Van Veen grab for Bonifácio et al. [56]). Nevertheless, it showed no obvious difference in the nature and abundance of major potential bioturbators. During the present study, we considered the effect of hydrodynamics, sedimentation, and bottom trawling as potential sources of physical disturbances within the WGMP. Therefore, these three sources of physical disturbances could also account for

differences between systems. As exemplified by differences in (1) WGMP and RRP morphologies [5], and (2) the upper depth limit allowing for modern sedimentation [25, 26, 114], hydrodynamics is stronger in the WGMP and therefore cannot directly account for higher bioturbation intensity in this area. Conversely, sedimentation rates are higher in the RRP; however, they decrease with depth to reach ca. 0.63 $cm.y^{-1}$ at 73 m [114, 115], which is close to the sedimentation rates (i.e., between 0.15 and 0.50 $cm.y^{-1}$) recorded in the WGMP between 45 and 71 m [25, 26]. Therefore, it is unlikely as well that differences in sedimentation can account for differences in bioturbation intensity between systems. Automatic Identification System (AIS) data collected by Global Fishing Watch [69, 70] are available only since 2012. Therefore, we computed the spatial distribution of BTE in the Rhône River for the June 2017–June 2018. Results (available on request to B.L.) showed an overall higher (i.e., by a factor of 2.3) BTE in the RRP than in the WGMP. However, the spatial distribution of BTE clearly differed between systems. BTE was maximal in the shallowest part of the RRP and then decreased with depth so that it was not higher in the distal part of the RRP than in the WGMP. Assuming stability in BTE in the RRP between 2007 and 2017, therefore, our conclusion is that differences in the intensity of the physical disturbance caused by bottom trawling are probably not responsible for differences in bioturbation intensity between systems as well.

Overall, the identification of the cause of difference in bioturbation intensities between the WGMP and RRP distal parts will clearly require additional studies. There are several ways forward: (1) the comparative assessment of sediment mechanical properties (Dorgan et al. [116]) in both systems, (2) the refinement of the comparison of benthic macrofauna composition through the use of the same sampling gear (see above), and (3) considering the temporal dynamics of bioturbation in both systems. Within the WGMP, Jouanneau et al. [35] indeed described the alternation of calm periods during which bioturbation is high and periods following strong storms during which bioturbation traces are destroyed. Along the same line, Bonifácio et al. [56] showed that river floods induce a quick (i.e., within 1–2 months) change in bioturbation within the RRP. Considering possible impacts of temporal dynamics may be important as well for all parameters/processes considered during the present study. This could be tackled by seasonally sampling along a depth gradient as already achieved for the RRP by Bonifácio et al. [56].

5. Conclusions

Our results first support the spatial subdivision of the West Gironde Mud Patch (WGMP) in a proximal and a distal part. They also show the existence of depth gradients in surface sedimentary organics characteristics and bioturbation within the distal part and suggest that

these gradients are more related to hydrodynamics than bottom trawling. The comparison with the Rhône River Prodelta finally highlights major discrepancies. These discrepancies refer to (1) the mixing of continental and marine sources of particulate organic matter that is taking place in the Gironde Estuary versus the Rhône River Prodelta itself, and (2) opposite patterns of changes in sedimentary organic concentrations relative to depth, which may result from particle sorting processes during sedimentation/resuspension cycles mainly cued by particle size in the Rhône River Prodelta and density in the WGMP. Overall, our results support the distinction between type 1 and type 2 river-dominated ocean margins [3,5] in temperate areas.

Author Contributions

Conceptualization, B.L., B.D. and A.G.; Data curation, B.L.; Formal analysis, B.L. and A.G.; Funding acquisition, B.D. and A.G.; Investigation, B.L., B.D., S.S., N.D., G.B. and A.G.; Methodology, B.L., B.D., S.S., M.D., F.G. (Florent Grasso), A.S., H.G. and A.G.; Project administration, A.G.; Resources, B.L., B.D., A.G.D., S.S., A.R.-R., F.G. (Frédéric Garabetian), N.D., M.D., F.G. (Florent Grasso), A.S., G.B., H.G., M.-A.C., D.P., P.L., H.D., M.D. and M.M.B.T.; Software, B.L., A.G.D., A.R.-R., M.D., F.G. (Florent Grasso) and H.G.; Validation, B.L., B.D. and A.G.; Visualization, B.L. and A.G.; Writing—original draft, B.L. and A.G.; Writing— review and editing, B.L., B.D., S.S., A.R.-R., F.G. (Frédéric Garabetian), F.G. (Florent Grasso), A.S., G.B. and A.G. All authors have read and agreed to the published version of the manuscript.

Funding

This work is part of the PhD thesis of Bastien Lamarque (Bordeaux University). Bastien Lamarque was partly supported by a doctoral grant from the French “Ministère de l’Enseignement Supérieur, de la Recherche et de l’Innovation”. This work was supported by: (1) the JERICO-NEXT project (European Union’s Horizon 2020 Research and Innovation program under grant agreement no. 654410), (2) the VOG project (LEFE-CYBER and EC2CO-PNEC), and (3) the MAGMA project (COTE cluster of Excellence ANR-10-LABX-45). It also benefited from additional fundings allocated by the Conseil Régional Nouvelle Aquitaine and the Agence Française de la Biodiversité. Operations at sea were funded by the French Oceanographic Fleet.

Data Availability Statement

The data presented in this study are available in SEANOE at https://doi.org/10.17882/78991, [117].

Acknowledgments

The authors wish to thank the crew of the R/V Côtes de la Manche for their help during field sampling, Céline Labrune for sharing Rhône River Prodelta SPI data, and Marie Claire Perello and Pierre Touzerie for their help in the analysis of some samples and results.

Conflicts of Interest

The authors declare no conflict of interest. The funders had no role in the design of the study; in the collection, analyses, or interpretation of data; in the writing of the manuscript, or in the decision to publish the results.

Appendix A

Table A6.1. Location (WGS84, degrees, and decimal minutes) and depth of the 32 sampled stations, with associated mean values (± standard deviation) of surface sediment and SPI characteristics, and Bottom Trawling Effort within cells containing stations. Station positionings are shown in Figure 6.1. $D_{0.5}$: median grain size, SSA: Sediment Surface Area, POC: Particulate Organic Carbon, Chl-*a*: Chlorophyll-a, Phaeo-*a*: Phaeophytin-a, THAA: Total Hydrolyzable Amino Acids, EHAA: Enzymatically Hydrolyzable Amino Acids, aRPD: apparent Redox Potential Discontinuity thickness, Burrows: number of burrows, OV: number of oxic voids, OV depth: maximal depth of oxic voids, Tubes: number of tubes, Feeding pits: number of feeding pits, Epifauna: number of epifauna, Infauna: number of infauna, Clasts: number of clasts, Furrows: number of furrows, BSS: 95th percentile of Bottom Shear Stress, BTE: Summed Bottom Trawling Effort.

Station	Latitude N	Longitude W	Depth (m)	$D_{0.5}$ (µm)	SSA ($m^2.gDW^{-1}$)	POC ($mg.m^{-2}$)	Chl-*a* ($µg.m^{-2}$)	Phaeo-*a* ($µg.m^{-2}$)	Chl-*a*/(Chl-*a*+Phaeo-*a*) (%)	THAA ($mg.m^{-2}$)	EHAA ($mg.m^{-2}$)	EHAA/THAA (%)	$\delta^{13}C$ (‰)	Number of SPI	aRPD (mm)	Burrows ($nb.SPI^{-1}$)	OV ($nb.SPI^{-1}$)	OV depth (mm)	Tubes ($nb.SPI^{-1}$)	Feeding pits ($nb.SPI^{-1}$)	Epifauna ($nb.SPI^{-1}$)	Infauna ($nb.SPI^{-1}$)	Clasts ($nb.SPI^{-1}$)	Furrows ($nb.SPI^{-1}$)	BSS ($N.m^{-2}$)	BTE ($h.km^{-2}.y^{-1}$)
0	45°46.465'	1°29.016'	32.5	64.6 ± 28.5	4.8 ± 0.3	1.2 ± 0.1	0.15	0.62	19.9	0.25 ± 0.01	0.05 ± 0.00	21.7 ± 1.3	-23.2 ± 0.1	6	20.6 ± 12.7	2.5 ± 1.2	2.2 ± 1.8	70.8 ± 44.7	3.5 ± 3.0	0.0 ± 0.0	0.5 ± 0.5	1.2 ± 1.2	0.0 ± 0.0	0.0 ± 0.0	1.1	1.6
1	45°45.580'	1°31.489'	37	17.3 ± 1.1	10.7 ± 0.7	1.5 ± 0.0	0.26	0.71	26.6	0.27 ± 0.04	0.05 ± 0.01	19.0 ± 0.7	-23.7	6	23.0 ± 15.0	1.2 ± 0.8	0.7 ± 0.5	39.9 ± 46.2	3.3 ± 1.9	0.0 ± 0.0	0.5 ± 0.8	1.0 ± 1.3	0.0 ± 0.0	0.0 ± 0.0	1	3.7
2	45°43.511'	1°37.773'	47.8	24.8 ± 1.4	6.1 ± 0.2	1.0 ± 0.1	0.36	1.54	19.2	0.36 ± 0.04	0.09 ± 0.00	24.5 ± 1.7	-22.9 ± 0.0	6	69.7 ± 2.2	3.8 ± 0.8	3.8 ± 2.5	119.8 ± 20.5	3.2 ± 1.6	0.0 ± 0.0	0.2 ± 0.4	0.8 ± 0.8	0.2 ± 0.4	0.0 ± 0.0	0.8	2.9
3	45°41.007'	1°41.545'	56.5	19.0 ± 0.1	8.7 ± 0.2	1.3 ± 0.0	0.28	1.2	18.8	0.46 ± 0.03	0.08 ± 0.00	17.0 ± 0.5	-23.1 ± 0.3	6	74.9 ± 9.6	3.2 ± 1.5	5.2 ± 4.9	137.8 ± 28.4	4.0 ± 2.5	0.3 ± 0.5	0.3 ± 0.5	1.0 ± 0.9	1.3 ± 2.3	0.0 ± 0.0	0.6	4.9
4	45°36.924'	1°49.712'	71.5	17.3 ± 0.6	9.8 ± 0.5	1.5 ± 0.1	0.31	1.76	15.1	0.58 ± 0.00	0.10 ± 0.01	17.0 ± 2.4	-22.6 ± 0.4	6	101.3 ± 8.8	3.0 ± 1.1	6.8 ± 2.4	137.3 ± 15.0	9.5 ± 6.1	0.7 ± 0.5	0.0 ± 0.0	0.2 ± 0.4	2.3 ± 2.3	0.0 ± 0.0	0.5	3
5	45°39.911'	1°34.866'	45.5	19.3 ± 1.9	8.2 ± 0.1	1.3 ± 0.2	0.33	1.29	20.3	n/a	n/a	n/a	-23.2 ± 0.0	5	61.9 ± 5.7	3.2 ± 0.4	3.4 ± 1.8	106.9 ± 56.4	2.6 ± 2.2	0.0 ± 0.0	0.0 ± 0.0	1.6 ± 1.3	3.2 ± 3.4	0.0 ± 0.0	0.8	5
6	45°44.412'	1°29.868'	36	29.8 ± 0.8	5.2 ± 0.3	0.7 ± 0.2	0.19	0.65	23	n/a	n/a	n/a	-22.2	6	3.5 ± 3.0	0.8 ± 1.3	0.5 ± 0.8	30.6 ± 24.0	6.3 ± 4.8	0.0 ± 0.0	0.2 ± 0.4	0.5 ± 0.5	0.0 ± 0.0	0.0 ± 0.0	1	2.3
7	45°37.189'	1°37.486'	51	14.9 ± 0.5	9.3 ± 0.3	1.4 ± 0.2	0.41	1.88	18.1	n/a	n/a	n/a	-23.2 ± 0.4	6	83.4 ± 8.4	2.3 ± 0.8	3.0 ± 2.4	131.5 ± 12.4	3.2 ± 5.0	0.2 ± 0.4	0.7 ± 0.8	1.3 ± 1.0	0.2 ± 0.4	0.0 ± 0.0	0.8	5
8	45°38.873'	1°45.777'	64.5	18.6 ± 0.2	9.1 ± 0.1	1.4 ± 0.1	0.35	1.59	18	0.52 ± 0.01	0.08 ± 0.00	15.5 ± 0.8	-23.0 ± 0.1	6	77.5 ± 11.0	2.5 ± 0.5	8.8 ± 5.9	146.4 ± 10.2	9.8 ± 5.4	0.3 ± 0.5	0.0 ± 0.0	1.7 ± 1.0	1.8 ± 3.3	0.2 ± 0.4	0.5	8.8
9	45°35.890'	1°40.157'	55.5	19.4 ± 1.4	9.1 ± 0.3	1.4 ± 0.1	0.35	1.88	15.8	n/a	n/a	n/a	-22.9 ± 0.5	6	83.4 ± 12.3	3.2 ± 1.2	11.7 ± 2.4	163.9 ± 9.7	2.0 ± 1.3	0.0 ± 0.0	0.2 ± 0.4	0.2 ± 0.4	0.3 ± 0.8	0.0 ± 0.0	0.7	5.2
10	45°44.694'	1°34.587'	42.5	26.8 ± 1.0	5.4 ± 0.8	1.3 ± 0.4	0.15	0.57	20.7	0.18 ± 0.02	0.05 ± 0.00	26.6 ± 2.0	-22.9 ± 0.5	6	30.7 ± 6.2	2.5 ± 1.0	2.7 ± 2.3	63.9 ± 38.6	1.8 ± 1.2	0.7 ± 0.8	0.2 ± 0.4	2.7 ± 2.1	0.2 ± 0.4	0.0 ± 0.0	0.8	4.6
2_3	45°42.267'	1°39.646'	51.5	20.0 ± 0.4	8.1 ± 0.1	1.2 ± 0.1	0.32	1.44	18.2	0.49 ± 0.03	0.10 ± 0.00	20.7 ± 1.2	-23.1 ± 0.0	6	63.9 ± 10.9	3.0 ± 1.4	7.0 ± 3.0	132.0 ± 20.3	2.7 ± 2.3	0.0 ± 0.0	0.0 ± 0.0	1.7 ± 1.5	0.8 ± 0.8	0.0 ± 0.0	0.7	4
3_8	45°39.919'	1°43.552'	60.5	19.1 ± 0.5	7.3 ± 0.3	1.2 ± 0.1	0.68	1.65	29.1	0.47 ± 0.03	0.11 ± 0.00	22.6 ± 1.2	-23.1 ± 0.5	6	72.4 ± 8.5	3.2 ± 1.7	8.0 ± 3.3	140.3 ± 23.3	8.5 ± 4.3	0.0 ± 0.0	0.0 ± 0.0	1.0 ± 1.1	2.3 ± 2.3	0.0 ± 0.0	0.6	19.4
8_4	45°37.929'	1°47.529'	67.5	20.4 ± 2.4	7.1 ± 1.2	1.4 ± 0.2	0.4	1.71	19	0.52 ± 0.04	0.11 ± 0.01	21.2 ± 0.3	-22.9 ± 0.0	6	81.1 ± 11.0	3.8 ± 1.0	13.0 ± 5.2	140.4 ± 12.7	10.3 ± 7.2	0.5 ± 0.5	0.0 ± 0.0	1.3 ± 1.4	2.5 ± 2.3	0.0 ± 0.0	0.5	5.4
A	45°37.284'	1°45.508'	62	22.0 ± 0.4	6.7 ± 0.2	1.7 ± 0.1	0.46	2.99	13.2	n/a	n/a	n/a	-23.2 ± 0.1	5	84.3 ± 5.3	4.4 ± 1.5	9.6 ± 3.4	138.2 ± 19.9	5.6 ± 3.3	0.2 ± 0.4	0.0 ± 0.0	1.6 ± 1.3	2.2 ± 2.3	0.2 ± 0.4	0.5	7.6
AE	45°42.305'	1°45.361'	61	17.5 ± 1.3	8.7 ± 1.3	1.5 ± 0.1	0.44	1.77	19.9	n/a	n/a	n/a	-22.8 ± 0.4	5	75.6 ± 14.6	3.8 ± 1.1	10.8 ± 3.9	161.3 ± 8.8	5.2 ± 3.7	0.2 ± 0.4	0.0 ± 0.0	0.4 ± 0.9	0.2 ± 0.4	0.0 ± 0.0	0.6	2.8
AF	45°38.984'	1°40.254'	55.6	21.5 ± 0.1	7.6 ± 0.1	1.4 ± 0.1	0.35	1.37	20.3	n/a	n/a	n/a	-23.0 ± 0.2	6	77.1 ± 9.6	3.0 ± 0.6	10.0 ± 7.1	144.1 ± 37.9	1.2 ± 0.4	0.0 ± 0.0	0.2 ± 0.4	0.0 ± 0.0	0.3 ± 0.8	0.0 ± 0.0	0.7	2.6
AK	45°43.191'	1°42.472'	55.5	20.6 ± 0.0	7.6 ± 0.6	1.3 ± 0.0	0.37	1.54	19.4	n/a	n/a	n/a	-23.0 ± 0.3	4	62.3 ± 26.2	3.3 ± 1.0	11.3 ± 5.7	132.5 ± 23.4	3.8 ± 1.9	0.0 ± 0.0	0.0 ± 0.0	1.8 ± 1.0	1.3 ± 1.9	0.0 ± 0.0	0.6	4.3
AL	45°44.774'	1°44.853'	58	20.4 ± 1.7	6.3 ± 0.5	1.2 ± 0.2	0.27	1.44	15.8	n/a	n/a	n/a	-22.8 ± 0.5	6	74.4 ± 12.1	2.7 ± 1.0	9.8 ± 4.3	148.0 ± 12.6	13.2 ± 11.9	0.2 ± 0.4	0.0 ± 0.0	0.2 ± 0.4	0.7 ± 0.8	0.0 ± 0.0	0.6	8.1
AN	45°48.792'	1°48.100'	58.5	21.0 ± 1.8	7.8 ± 0.3	1.4 ± 0.0	0.78	1.8	30.2	n/a	n/a	n/a	-22.6 ± 0.1	6	74.9 ± 14.5	3.5 ± 2.4	10.7 ± 2.1	147.2 ± 24.8	3.5 ± 2.2	0.0 ± 0.0	0.0 ± 0.0	0.3 ± 0.5	2.8 ± 2.9	0.0 ± 0.0	0.6	0.5
AQ	45°45.532'	1°40.140'	50.5	21.2 ± 0.3	8.3 ± 0.1	1.2 ± 0.1	0.33	1.15	22.2	n/a	n/a	n/a	-22.8 ± 0.4	6	72.9 ± 14	2.5 ± 0.8	8.7 ± 3.1	133.4 ± 34.7	3.0 ± 4.0	0.3 ± 0.8	1.0 ± 0.6	1.2 ± 0.8	0.7 ± 1.2	0.0 ± 0.0	0.7	1
AR	45°42.034'	1°34.628'	43.5	22.6 ± 1.4	7.9 ± 0.3	1.0 ± 0.1	0.23	1.05	17.9	n/a	n/a	n/a	-22.9 ± 0.1	6	84.1 ± 9.2	2.5 ± 1.4	6.0 ± 2.9	132.1 ± 47.1	3.7 ± 2.7	0.2 ± 0.4	0.3 ± 0.5	0.5 ± 0.5	2.8 ± 2.6	0.0 ± 0.0	0.9	3
AS	45°40.103'	1°31.427'	42	25.3 ± 8.0	6.7 ± 0.4	1.1 ± 0.0	0.2	0.79	20.3	n/a	n/a	n/a	-23.3 ± 0.1	6	64.1 ± 9.5	2.0 ± 0.6	2.7 ± 3.2	119.6 ± 25.8	1.8 ± 1.3	0.0 ± 0.0	0.3 ± 0.5	1.7 ± 1.2	1.3 ± 1.5	0.0 ± 0.0	0.9	1.4
AV	45°43.660'	1°32.057'	39.5	13.4 ± 1.7	14.2 ± 1.2	0.5 ± 0.0	0.08	0.36	18.7	n/a	n/a	n/a	-23.7 ± 0.0	6	11.7 ± 14.5	1.8 ± 1.9	0.3 ± 0.8	123.0 ± 0.0	4.0 ± 2.8	0.0 ± 0.0	0.2 ± 0.4	1.3 ± 2.1	0.0 ± 0.0	0.0 ± 0.0	1	3.1
AW	45°46.252'	1°36.005'	42.5	53.1 ± 11.8	3.4 ± 0.6	1.3 ± 0.7	0.28	1.03	21.4	n/a	n/a	n/a	-22.8 ± 0.4	6	47.6 ± 9.3	2.0 ± 1.3	4.0 ± 3.7	87.6 ± 40.8	8.2 ± 4.0	0.0 ± 0.0	0.7 ± 0.5	0.3 ± 0.5	0.0 ± 0.0	0.0 ± 0.0	0.8	4.1
AX	45°47.892'	1°38.657'	47	19.1 ± 0.7	7.2 ± 0.6	1.2 ± 0.1	0.64	2.89	18.1	n/a	n/a	n/a	-22.7 ± 0.1	6	51.8 ± 3.9	3.0 ± 1.8	5.0 ± 3.0	107.2 ± 30.3	5.3 ± 5.0	0.2 ± 0.4	0.8 ± 1.2	0.8 ± 0.8	0.5 ± 0.8	0.0 ± 0.0	0.7	7.1
AY	45°49.688'	1°41.691'	49.5	19.0 ± 0.5	7.4 ± 0.1	1.3 ± 0.0	0.41	1.79	18.6	n/a	n/a	n/a	-22.6 ± 0.2	6	57.7 ± 11.9	3.8 ± 1.8	5.8 ± 3.3	126.4 ± 26.0	5.3 ± 4.0	0.5 ± 0.5	2.0 ± 1.4	0.8 ± 1.3	0.8 ± 1.0	0.0 ± 0.0	0.7	1.1
BK	45°38.109'	1°41.705'	58	22.7 ± 0.2	6.6 ± 0.0	1.6 ± 0.1	n/a	n/a	n/a	n/a	n/a	n/a	-23.2 ± 0.1	6	64.6 ± 8.4	3.7 ± 1.6	7.3 ± 2.9	142.3 ± 26.7	5.2 ± 4.1	0.5 ± 0.5	0.2 ± 0.4	0.3 ± 0.5	0.3 ± 0.5	0.0 ± 0.0	0.6	12.2
FG	45°35.524'	1°50.689'	71.5	20.9 ± 0.0	7.3 ± 0.1	1.6 ± 0.1	0.28	1.64	14.4	n/a	n/a	n/a	-23.0 ± 0.1	5	83.4 ± 15.1	2.4 ± 0.9	8.4 ± 3.3	132.2 ± 6.9	12.8 ± 7.2	0.6 ± 0.5	0.4 ± 0.9	1.2 ± 0.8	1.4 ± 1.7	0.0 ± 0.0	0.5	10
J	45°32.950'	1°54.563'	79	17.8 ± 0.5	8.6 ± 0.3	2.1 ± 0.3	0.53	3.08	14.7	n/a	n/a	n/a	-22.8 ± 0.1	8	93.3 ± 17.6	3.5 ± 0.8	10.1 ± 3.9	149.5 ± 25.4	6.1 ± 5.1	0.4 ± 0.7	0.0 ± 0.0	0.6 ± 0.7	1.4 ± 2.0	0.0 ± 0.0	0.4	3.6
PL	45°36.826'	1°47.471'	65.5	24.0 ± 0.2	6.2 ± 0.2	1.6 ± 0.1	0.22	1.44	13.5	n/a	n/a	n/a	-23.2 ± 0.0	4	57.8 ± 13.2	4.0 ± 1.8	18.0 ± 2.2	131.1 ± 19.3	11.5 ± 3.9	0.5 ± 1.0	0.0 ± 0.0	0.8 ± 1.5	6.8 ± 6.4	0.0 ± 0.0	0.5	10.1
SS	45°33.696'	1°52.863'	78	20.7 ± 0.1	7.6 ± 0.4	1.9 ± 0.2	0.44	2.46	15.1	0.69 ± 0.05	n/a	n/a	-22.9 ± 0.3	6	85.2 ± 14.4	2.3 ± 1.6	11.2 ± 5.8	143.1 ± 18.9	10.3 ± 7.3	0.0 ± 0.0	0.0 ± 0.0	0.5 ± 0.8	4.8 ± 5.0	0.0 ± 0.0	0.4	9.2

Table A6.2. Determination coefficients (R^2), associated probability levels (p), slopes and intercepts of the simple linear regression models linking station depth and assessed parameters within: (1) the whole WGMP and (2) its sole distal part. Bold types are indicative

		Whole WGMP					Distal area				
		n	R^2	p	Slope	Intercept	n	R^2	p	Slope	Intercept
Surface sediment characteristics	D_{50}	**32**	**0.182**	**0.015**	**-0.358**	**42.362**	25	0.021	0.493		
	SSA	32	0.013	0.533			25	0.008	0.678		
	POC	**32**	**0.578**	**<0.001**	**0.019**	**0.290**	**25**	**0.720**	**<0.001**	**0.022**	**0.131**
	Chl-*a*	**31**	**0.207**	**0.010**	**0.006**	**0.040**	24 22	0.008 0.011	0.682 0.638		
	Phaeo-*a*	**31**	**0.485**	**<0.001**	**0.039**	**-0.580**	**24** **22**	**0.185** **0.187**	**0.036** **0.044**	**0.024** **0.024**	**0.350** **0.347**
	Chl-*a* / (Chl-*a* + Phaeo-*a*)	**31**	**0.190**	**0.014**	**-0.144**	**26.990**	24 **22**	0.107 **0.385**	0.118 **0.002**	**-0.147**	**26.125**
	THAA	**11**	**0.873**	**<0.001**	**0.010**	**-0.113**	8	**0.850**	**0.001**	**0.009**	**-0.028**
	EHAA	**10**	**0.638**	**0.006**	**0.001**	**0.006**	7	0.089	0.515		
	EHAA / THAA	10	0.218	0.174			7	0.301	0.202		
	$\delta^{13}C$	32	0.041	0.267			25	0.021	0.492		
SPI characteristics	aRPD thickness	**32**	**0.598**	**<0.001**	**1.531**	**-18.413**	**25**	**0.329**	**0.003**	**0.695**	
	Number of burrows	**32**	**0.255**	**0.003**	**0.034**	**1.034**	25	<0.001	0.903		
	Number of oxic voids	**32**	**0.578**	**<0.001**	**0.262**	**-7.139**	**25**	**0.303**	**0.004**	**0.193**	**-2.743**
	Maximal depth of oxic voids	**32**	**0.498**	**<0.001**	**1.892**	**21.080**	**25**	**0.241**	**0.013**	**0.679**	**97.223**
	Number of feeding pits	**32**	**0.194**	**0.012**	**0.009**	**-0.260**	**25**	**0.168**	**0.042**	**0.009**	**-0.319**
	Number of tubes	**32**	**0.351**	**<0.001**	**0.169**	**-3.512**	**25**	**0.433**	**<0.001**	**0.244**	**-8.228**
	Number of epifauna	**32**	**0.133**	**0.040**	**-0.013**	**0.961**	**25**	**0.174**	**0.038**	**-0.020**	**-0.020**
	Number of infauna	32	0.053	0.204			25	0.022	0.475		
	Total number of biological traces	**32**	**0.654**	**<0.001**	**0.449**	**-7.325**	**25**	**0.479**	**<0.001**	**0.419**	**-5.418**
BSS	BSS 95th percentile	**32**	**0.926**	**<0.001**	**-0.014**	**1.469**	**25**	**0.908**	**<0.001**	**-0.012**	**1.324**
Trawling	Summed Bottom Trawling Effort	**32**	**0.180**	**0.016**	**0.138**	**-2.267**	25	0.090	0.147		
	Proportion of SPI featuring bottom trawling traces	**32**	**0.295**	**0.001**	**1.261**	**-24.374**	25	0.034	0.379		

Table A6.3. Determination coefficients (R^2), associated probability levels (p), slopes, and intercepts of the simple linear regression models linking 95th percentile of Bottom Shear Stress (BSS) and one-year summed Bottom Trawling Effort (BTE) within cells containing sampled stations, and assessed parameters within the distal part of the WGMP. Adjusted determination coefficients (R^2) and associated probability levels (p) of the multiple linear regression models linking the combination of BSS and BSS with assessed parameters within the distal part of the WGMP. Bold types are indicative of significant ($p < 0.05$) correlations and underlined types correspond to simple linear regression models without the outliers constituted by stations AN and 3_8.

		BSS					BTE					BSS + BTE	
		n	R^2	p	Slope	Intercept	n	R^2	p	Slope	Intercept	Adjusted R^2	p
Surface sediment characteristics	D_{50}	25	<0.001	0.890			25	0.007	0.686			<0.001	0.897
	SSA	25	<0.001	0.902			25	0.119	0.091			0.040	0.238
	POC	**25**	**0.603**	**<0.001**	**-1.591**	**2.399**	25	0.039	0.343			**0.567**	**0.001**
	Chl-*a*	24 22	0.020 0.012	0.514 0.634			24 22	0.019 0.005	0.518 0.765			<0.001	0.720
	Phaeo-*a*	**24** 22	**0.175** 0.177	**0.042** 0.052	**-1.878**	**2.939**	24 22	0.016 0.061	0.557 0.266			0.100	0.132
	Chl-*a* / (Chl-*a* + Phaeo-*a*)	24 **22**	0.070 **0.357**	0.210 **0.003**	**11.392**	**10.376**	24 **22**	<0.001 **0.420**	0.971 **0.001**	**-0.006**	**0.205**	<0.001	0.433
	THAA	8	**0.899**	**<0.001**	**-0.838**	**1.004**	8	0.025	0.708			**0.862**	**0.003**
	EHAA	7	0.052	0.624			7	0.076	0.547			<0.001	0.765
	EHAA / THAA	7	0.443	0.103			7	0.028	0.719			0.215	0.274
	$\delta^{13}C$	25	0.039	0.344			**25**	**0.272**	**0.008**	**-0.024**	**-22.806**	**0.325**	**0.005**
SPI characteristics	aRPD thickness	**25**	**0.181**	**0.034**	**-41.196**	**100.531**	25	0.010	0.635			0.153	0.062
	Number of burrows	25	0.014	0.571			25	0.003	0.793			<0.001	0.785
	Number of oxic voids	**25**	**0.402**	**<0.001**	**-17.711**	**19.618**	25	0.024	0.456			**0.347**	**0.003**
	Maximal depth of oxic voids	**25**	**0.219**	**0.018**	**-51.777**	**169.396**	25	0.001	0.858			0.154	0.061
	Number of feeding pits	**25**	**0.166**	**0.043**	**-0.741**	**0.692**	25	0.002	0.824			0.009	0.132
	Number of tubes	**25**	**0.428**	**<0.001**	**-19.387**	**18.187**	**25**	**0.283**	**0.006**	**0.456**	**3.378**	**0.539**	**<0.001**
	Number of epifauna	25	0.148	0.057			25	0.088	0.149			<0.001	0.708
	Number of infauna	25	0.012	0.602			25	0.012	0.610			0.120	0.094
	Total number of biological traces	**25**	**0.567**	**<0.001**	**-36.452**	**41.931**	**24**	**0.159**	**0.048**	**0.558**	**15.841**	**0.583**	**<0.001**
Trawling	Proportion of SPI featuring bottom trawling traces	25	0.030	0.407			25	0.052	0.273			<0.001	0.466

References

1. Aller, R.C. Mobile deltaic and continental shelf muds as suboxic, fluidized bed reactors. *Mar. Chem.* 1998, *61*, 143–155.
2. Burdige, D.J. Burial of terrestrial organic matter in marine sediments: A re-assessment. *Glob. Biogeochem. Cycles* 2005, *19*, 1–7.
3. Blair, N.E.; Aller, R.C. The fate of terrestrial organic carbon in the marine environment. *Ann. Rev. Mar. Sci.* 2012, *4*, 401–423.
4. Meade, R.H. River-sediment inputs to major deltas. In *Sea Level-Rise and Coastal Subsidence. Coastal Systems and Continental Margins*; Miliman, J.D., Haq, B.U., Eds.; Springer: Dordrecht, The Netherlands, 1996; Volume 2, pp. 63–85.
5. McKee, B.A.; Aller, R.C.; Allison, M.A.; Bianchi, T.S.; Kineke, G.C. Transport and transformation of dissolved and particulate materials on continental margins influenced by major rivers: Benthic boundary layer and seabed processes. *Cont. Shelf Res.* 2004, *24*, 899–926.
6. Hedges, J.I.; Keil, R.G. Sedimentary organic matter preservation: An assessment and speculative synthesis. *Mar. Chem.* 1995, *49*, 81–115.
7. Burdige, D.J. Estuarine and coastal sediments—Coupled biogeochemical cycling. In *Treatise on Estuarine and Coastal Science*; Wolanski, E., McLusky, D., Eds.; Academic Press: Cambridge, MA, USA, 2012; Volume 5, pp. 279–316.
8. Kristensen, E.; Penha-Lopes, G.; Delefosse, M.; Valdemarsen, T.; Quintana, C.O.; Banta, G.T. What is bioturbation? The need for a precise definition for fauna in aquatic sciences. *Mar. Ecol. Prog. Ser.* 2012, *446*, 285–302.
9. Aller, R.C. The effects of macrobenthos on chemical properties of marine sediment and overlying water. In *Animal-Sediment Relations*; McCall, P.L., Tevesz, M.J.S., Eds.; Springer: Boston, MA, USA, 1982; Volume 100, pp. 53–102.
10. Kristensen, E. Organic matter diagenesis at the oxic/anoxic interface in coastal marine sediments, with emphasis on the role of burrowing animals. *Hydrobiologia* 2000, *426*, 1–24.
11. Kristensen, E.; Kostka, J.E. Macrofaunal burrows and irrigation in marine sediment: Microbiological and biogeochemical interactions. In *Interactions Between Macro- and Microorganisms in Marine Sediments*; Kristensen, E., Haese, R.R., Kostka, J.E., Eds.; American Geophysical Union: Washington, DC, USA, 2013; pp. 125–157.
12. Rhoads, D.C.; Boesch, D.F.; Zhican, T.; Fengshan, X.; Liqiang, H.; Nilsen, K.J. Macrobenthos and sedimentary facies on the Changjiang delta platform and adjacent continental shelf, East China Sea. *Cont. Shelf Res.* 1985, *4*, 189–213.
13. Watling, L.; Norse, E.A. Disturbance of the seabed by mobile fishing gear: A comparison to

forest clearcutting. *Conserv. Biol.* 1998, *12*, 1180–1197.

14. Durrieu De Madron, X.; Ferré, B.; Le Corre, G.; Grenz, C.; Conan, P.; Pujo-Pay, M.; Buscail, R.; Bodiot, O. Trawling-induced resuspension and dispersal of muddy sediments and dissolved elements in the Gulf of Lion (NW Mediterranean). *Cont. Shelf Res.* 2005, *25*, 2387–2409.
15. Ferré, B.; Durrieu de Madron, X.; Estournel, C.; Ulses, C.; Le Corre, G. Impact of natural (waves and currents) and anthropogenic (trawl) resuspension on the export of particulate matter to the open ocean. Application to the Gulf of Lion (NW Mediterranean). *Cont. Shelf Res.* 2008, *28*, 2071–2091.
16. Palanques, A.; Guillén, J.; Puig, P. Impact of bottom trawling on water turbidity and muddy sediment of an unfished continental shelf. *Limnol. Oceanogr.* 2001, *46*, 1100–1110.
17. Palanques, A.; Puig, P.; Guillén, J.; Demestre, M.; Martín, J. Effects of bottom trawling on the Ebro continental shelf sedimentary system (NW Mediterranean). *Cont. Shelf Res.* 2014, *72*, 83–98.
18. Oberle, F.K.J.; Storlazzi, C.D.; Hanebuth, T.J.J. What a drag: Quantifying the global impact of chronic bottom trawling on continental shelf sediment. *J. Mar. Syst.* 2016, *159*, 109–119.
19. Mengual, B.; Cayocca, F.; Le Hir, P.; Draye, R.; Laffargue, P.; Vincent, B.; Garlan, T. Influence of bottom trawling on sediment resuspension in the 'Grande-Vasière' area (Bay of Biscay, France). *Ocean Dyn.* 2016, *66*, 1181–1207.
20. Mengual, B.; Le Hir, P.; Cayocca, F.; Garlan, T. Bottom trawling contribution to the spatio-temporal variability of sediment fluxes on the continental shelf of the Bay of Biscay (France). *Mar. Geol.* 2019, *414*, 77–91.
21. Thrush, S.F.; Dayton, P.K. Disturbance to marine benthic habitats by trawling and dredging: Implications for marine biodiversity. *Annu. Rev. Ecol. Syst.* 2002, *33*, 449–473.
22. Thrush, S.F.; Gray, J.S.; Hewitt, J.E.; Ugland, K.I. Predicting the effects of habitat homogenization on marine biodiversity. *Ecol. Appl.* 2006, *16*, 1636–1642.
23. Kaiser, M.J.; Collie, J.S.; Hall, S.J.; Jennings, S.; Poiner, I.R. Modification of marine habitats by trawling activities: Prognosis and solutions. *Fish Fish.* 2002, *3*, 114–136.
24. Queirós, A.M.; Hiddink, J.G.; Kaiser, M.J.; Hinz, H. Effects of chronic bottom trawling disturbance on benthic biomass, production and size spectra in different habitats. *J. Exp. Mar. Biol. Ecol.* 2006, *335*, 91–103.
25. Lesueur, P.; Jouanneau, J.M.; Boust, D.; Tastet, J.P.; Weber, O. Sedimentation rates and fluxes in the continental shelf mud fields in the Bay of Biscay (France). *Cont. Shelf Res.* 2001, *21*, 1383–1401.
26. Lesueur, P.; Tastet, J.P.; Weber, O. Origin and morphosedimentary evolution of fine-grained

modern continental shelf deposits: The Gironde mud fields (Bay of Biscay, France). *Sedimentology* 2002, *49*, 1299–1320

27. Doxaran, D.; Froidefond, J.M.; Castaing, P.; Babin, M. Dynamics of the turbidity maximum zone in a macrotidal estuary (the Gironde, France): Observations from field and MODIS satellite data. *Estuar. Coast. Shelf Sci.* 2009, *81*, 321–332.
28. Constantin, S.; Doxaran, D.; Derkacheva, A.; Novoa, S.; Lavigne, H. Multi-temporal dynamics of suspended particulate matter in a macro-tidal river Plume (the Gironde) as observed by satellite data. *Estuar. Coast. Shelf Sci.* 2018, *202*, 172–184.
29. Etcheber, H.; Schmidt, S.; Sottolichio, A.; Maneux, E.; Chabaux, G.; Escalier, J.M.; Wennekes, H.; Derriennic, H.; Schmeltz, M.; Quéméner, L.; et al. Monitoring water quality in estuarine environments: Lessons from the MAGEST monitoring program in the Gironde fluvial-estuarine system. *Hydrol. Earth Syst. Sci.* 2011, *15*, 831–840.
30. Cirac, P.; Berne, S.; Castaing, P.; Weber, O. Processus de mise en place et d'évolution de la couverture sédimentaire superficielle de la plate-forme nord-aquitaine. *Oceanol. Acta* 2000, *23*, 663–686.
31. Castaing, P.; Allen, G.P. Mechanisms controlling seaward escape of suspended sediment from the Gironde: A macrotidal estuary in France. *Mar. Geol.* 1981, *40*, 101–118.
32. Castaing, P.; Allen, G.; Houdart, M.; Moign, Y. Étude par télédétection de la dispersion en mer des eaux estuariennes issues de la Gironde et du Pertuis de Maumusson. *Oceanol. Acta* 1979, *2*, 459–469.
33. Castaing, P.; Philipps, I.; Weber, O. Répartition et dispersion des suspensions dans les eaux du plateau continental aquitain. *Oceanol. Acta* 1982, *5*, 85–96.
34. Longère, P.; Dorel, D. Etude des sédiments meubles de la vasière de la Gironde et des régions avoisinantes. *Rev. des Trav. l'Institut des Pêches Marit.* 1970, *34*, 233–256.
35. Jouanneau, J.M.; Weber, O.; Latouche, C.; Vernet, J.P.; Dominik, J. Erosion, non-deposition and sedimentary processes through a sedimentological and radioisotopic study of surficial deposits from the "Ouest-Gironde vasière" (Bay of Biscay). *Cont. Shelf Res.* 1989, *9*, 325–342.
36. Weber, O.; Jouanneau, J.M.; Ruch, P.; Mirmand, M. Grain-size relationship between suspended matter originating in the Gironde estuary and shelf mud-patch deposits. *Mar. Geol.* 1991, *96*, 159–165.
37. Lesueur, P.; Tastet, J.P. Les Vasières de plate-forme du Golfe de Gascogne (France). *Actes du III^e Colloque International « Océanographie du Golfe de Gascogne »* 1993, 181–184.
38. Lesueur, P.; Tastet, J.P. Facies, internal structures and sequences of modern Gironde-derived muds on the Aquitaine inner shelf, France. *Mar. Geol.* 1994, *120*, 267–290.
39. Gadel, F.; Jouanneau, J.M.; Weber, O.; Serve, L.; Comellas, L. Traceurs organiques dans

les dépôts de la vasière Ouest-Gironde (Golfe de Gascogne). *Oceanol. Acta* 1997, *20*, 687–695.

40. Parra, M.; Castaing, P.; Jouanneau, J.M.; Grousset, F.; Latouche, C. Nd-Sr isotopic composition of present-day sediments from the Gironde Estuary, its draining basins and the West Gironde mud patch (SW France). *Cont. Shelf Res.* 1998, *19*, 135–150.
41. Lesueur, P.; Weber, O.; Marambat, L.; Tastet, J.P.; Jouanneau, J.M.; Turon, J.L. Datation d'une vasière de plateforme atlantique au débouché d'un estuaire: La vasière à l'ouest de la Gironde (France) est d'âge historique (VIème siècle à nos jours). *Comptes rendus l'Académie des Sci. Série 2* 1989, *308*, 935–940.
42. Lesueur, P.; Tastet, J.P.; Weber, O.; Sinko, J.A. Modèle faciologique d'un corps sédimentaire pélitique de plate-forme la vasière Ouest-Gironde (France). *Oceanol. Acta* 1991, *11*, 143–153.
43. Lesueur, P.; Tastet, J.P.; Marambat, L. Shelf mud fields formation within historical times: Examples from offshore the Gironde estuary, France. *Cont. Shelf Res.* 1996, *16*, 1849–1870.
44. Relexans, J.C.; Lin, R.G.; Castel, J.; Etcheber, H.; Laborde, P. Response of biota to sedimentary organic matter quality of the west Gironde mud patch, Bay of Biscay (France). *Oceanol. Acta* 1992, *15*, 639–649.
45. Massé, C.; Meisterhans, G.; Deflandre, B.; Bachelet, G.; Bourasseau, L.; Bichon, S.; Ciutat, A.; Jude-Lemeilleur, F.; Lavesque, N.; Raymond, N.; et al. Bacterial and macrofaunal communities in the sediments of the West Gironde Mud Patch, Bay of Biscay (France). *Estuar. Coast. Shelf Sci.* 2016, *179*, 189–200.
46. Système d'Informations Halieutiques Ifremer. In *Activité des navires de pêche région Nouvelle-Aquitaine*; Ifremer: Paris, France, 2017.
47. Lesueur, P. Les Vasières de la Plate-Forme Ouest Gironde (France): Modèle Faciologique Et Archive Sédimentaire Des Flux Côtiers. Ph.D. Thesis, Université Bordeaux 1, Talence, France, 19 October 1992.
48. Gillet, H.; Deflandre, B. *JERICOBENT-5-TH cruise, RV Thalia*; Université de Bordeaux: Bordeaux, France, 2018.
49. Schmidt, S.; Deflandre, B. *JERICOBENT-5 cruise, RV Côtes De La Manche*; Université de Bordeaux: Bordeaux, France, 2018.
50. Mayer, L.M. Surface area control of organic carbon accumulation in continental shelf sediments. *Geochim. Cosmochim. Acta* 1994, *58*, 1271–1284.
51. Migeon, S.; Weber, O.; Faugeres, J.C.; Saint-Paul, J. SCOPIX: A new X-ray imaging system for core analysis. *Geo-Mar. Lett.* 1999, *18*, 251–255.
52. Rhoads, D.C.; Germano, J.D. Characterization of organism-sediment relations using

sediment profile imaging: An efficient method of remote ecological monitoring of the seafloor (Remots System). *Mar. Ecol. Prog. Ser.* 1982, *8*, 115–128.

53. Etcheber, H.; Relexans, J.C.; Beliard, M.; Weber, O.; Buscail, R.; Heussner, S. Distribution and quality of sedimentary organic matter on the Aquitanian margin (Bay of Biscay). *Deep. Res. Part II* 1999, *46*, 2249–2288.
54. Mayer, L.M.; Schick, L.L.; Sawyer, T.; Plante, C.J.; Jumars, P.A.; Self, R.L. Bioavailable amino acids in sediments: A biomimetic, kinetics based approach. *Limnol. Oceanogr.* 1995, *40*, 511–520.
55. Pastor, L.; Deflandre, B.; Viollier, E.; Cathalot, C.; Metzger, E.; Rabouille, C.; Escoubeyrou, K.; Lloret, E.; Pruski, A.M.; Vétion, G.; et al. Influence of the organic matter composition on benthic oxygen demand in the Rhône River prodelta (NW Mediterranean Sea). *Cont. Shelf Res.* 2011, *31*, 1008–1019.
56. Bonifácio, P.; Bourgeois, S.; Labrune, C.; Amouroux, J.M.; Escoubeyrou, K.; Buscail, R.; Romero-Ramirez, A.; Lantoine, F.; Vétion, G.; Bichon, S.; et al. Spatiotemporal changes in surface sediment characteristics and benthic macrofauna composition off the Rhône River in relation to its hydrological regime. *Estuar. Coast. Shelf Sci.* 2014, *151*, 196–209.
57. Wakeham, S.G.; Lee, C.; Hedges, J.I.; Hernes, P.J.; Peterson, M.L. Molecular indicators of diagenetic status in marine organic matter. *Geochim. Cosmochim. Acta* 1997, *61*, 5363–5369.
58. Neveux, J.; Lantoine, F. Spectrofluorometric assay of chlorophylls and phaeopigments using the least squares approximation technique. *Deep. Res. Part I* 1993, *40*, 1747–1765.
59. Coplen, T.B. Guidelines and recommended terms for expression of stable- isotope-ratio and gas-ratio measurement results. *Rapid Commun. Mass Spectrom* 2011, *25*, 2538–2560.
60. Romero-Ramirez, A.; Grémare, A.; Desmalades, M.; Duchêne, J.C. Semi-automatic analysis and interpretation of sediment profile images. *Environ. Model. Softw.* 2013, *47*, 42–54.
61. Rosenberg, R.; Grémare, A.; Amouroux, J.M.; Nilsson, H.C. Benthic habitats in the northwest Mediterranean characterised by sedimentary organics, benthic macrofauna and sediment profile images. *Estuar. Coast. Shelf Sci.* 2003, *57*, 297–311.
62. Rosenberg, R.; Nilsson, H.C.; Grémare, A.; Amouroux, J.M. Effects of demersal trawling on marine sedimentary habitats analysed by sediment profile imagery. *J. Exp. Mar. Biol. Ecol.* 2003, *285–286*, 465–477.
63. Germano, J.D.; Rhoads, D.C.; Valente, R.M.; Carey, D.A.; Solan, M. The use of sediment profile imaging (SPI) for environmental impact assessments and monitoring studies: Lessons learned from the past four decades. *Oceanogr. Mar. Biol. Annu. Rev.* 2011, *49*, 235–298.
64. Diaz, M.; Grasso, F.; Le Hir, P.; Sottolichio, A.; Caillaud, M.; Thouvenin, B. Modeling mud

and sand transfers between a macrotidal estuary and the continental shelf: Influence of the sediment transport parameterization. *J. Geophys. Res. Oceans* 2020, *125*, e2019JC015643.

65. Lazure, P.; Dumas, F. An external-internal mode coupling for a 3D hydrodynamical model for applications at regional scale (MARS). *Adv. Water Resour.* 2008, *31*, 233–250.
66. Roland, A.; Ardhuin, F. On the developments of spectral wave models: Numerics and parameterizations for the coastal ocean. *Ocean Dyn.* 2014, *64*, 833–846.
67. Soulsby, R. *Dynamics of Marine Sands: A Manual for Practical Applications*; Inst of Civil Engineers Pub: London, UK, 1997.
68. Grasso, F.; Verney, R.; Le Hir, P.; Thouvenin, B.; Schulz, E.; Kervella, Y.; Khojasteh Pour Fard, I.; Lemoine, J.P.; Dumas, F.; Garnier, V. Suspended sediment dynamics in the macrotidal seine estuary (France)—Part 1: Numerical modeling of turbidity maximum dynamics. *J. Geophys. Res. Oceans* 2008, *123*, 558–577.
69. Global Fishing Watch. Available online: https://globalfishingwatch.org (accessed on 13 March 2019).
70. Kroodsma, D.A.; Mayorga, J.; Hochberg, T.; Miller, N.A.; Boerder, K.; Ferretti, F.; Wilson, A.; Bergman, B.; White, T.D.; Block, B.A.; et al. Tracking the global footprint of fisheries. *Science* 2018, *359*, 904–908.
71. Clarke, K.R.; Somerfield, P.J.; Gorley, R.N. Testing of null hypotheses in exploratory community analyses: Similarity profiles and biota-environment linkage. *J. Exp. Mar. Biol. Ecol.* 2008, *366*, 56–69.
72. Clarke, K.R. Non-parametric multivariate analyses of changes in community structure. *Aust. J. Ecol.* 1993, *18*, 117–143.
73. Clarke, K.R.; Warwick, R.M. *Change in Marine Communities: An Approach to Statistical Analysis and Interpretation*, 2nd ed.; PRIMER-E: Plymouth, UK, 2001.
74. Lansard, B.; Rabouille, C.; Denis, L.; Grenz, C. Benthic remineralization at the land-ocean interface: A case study of the Rhône River (NW Mediterranean Sea). *Estuar. Coast. Shelf Sci.* 2009, *81*, 544–554.
75. Antonelli, C.; Eyrolle, F.; Rolland, B.; Provansal, M.; Sabatier, F. Suspended sediment and 137Cs fluxes during the exceptional December 2003 flood in the Rhone River, southeast France. *Geomorphology* 2008, *95*, 350–360.
76. Touzani, A.; Giresse, P. The Rhone River prodelta: Short-term (100–103 year) sedimentation patterns and human impact. *J. Coast. Res.* 2002, *18*, 102–117.
77. Marion, C.; Dufois, F.; Arnaud, M.; Vella, C. In situ record of sedimentary processes near the Rhône River mouth during winter events (Gulf of Lions, Mediterranean Sea). *Cont. Shelf Res.* 2010, *30*, 1095–1107.
78. Dufois, F.; Verney, R.; Le Hir, P.; Dumas, F.; Charmasson, S. Impact of winter storms on

sediment erosion in the Rhone River prodelta and fate of sediment in the Gulf of Lions (North Western Mediterranean Sea). *Cont. Shelf Res.* 2014, *72*, 57–72.

79. Calmet, D.; Fernandez, J. Caesium distribution in northwest Mediterranean seawater, suspended particles and sediments. *Cont. Shelf Res.* 1990, *10*, 895–913.
80. Charmasson, S.; Radakovitch, O.; Arnaud, M.; Bouisset, P.; Pruchon, A.S. Long-core profiles of ^{137}Cs, ^{134}Cs, ^{60}Co and ^{210}Pb in sediment near the Rhone River (northwestern Meiterranean Sea). *Estuaries* 1998, *21*, 367–378.
81. Bourgeois, S.; Pruski, A.M.; Sun, M.Y.; Buscail, R.; Lantoine, F.; Kerhervé, P.; Vétion, G.; Rivière, B.; Charles, F. Distribution and lability of land-derived organic matter in the surface sediments of the Rhône prodelta and the adjacent shelf (Mediterranean Sea, France): A multi proxy study. *Biogeosciences* 2011, *8*, 3107–3125.
82. Labrune, C.; Romero-Ramirez, A.; Amouroux, J.M.; Duchêne, J.C.; Desmalades, M.; Escoubeyrou, K.; Buscail, R.; Grémare, A. Comparison of ecological quality indices based on benthic macrofauna and sediment profile images: A case study along an organic enrichment gradient off the Rhône River. *Ecol. Indic.* 2012, *12*, 133–142.
83. Kaiser, M.J.; Clarke, K.R.; Hinz, H.; Austen, M.C.V.; Somerfield, P.J.; Karakassis, I. Global analysis of response and recovery of benthic biota to fishing. *Mar. Ecol. Prog. Ser.* 2006, *311*, 1–14.
84. Sciberras, M.; Geert, J.; Simon, H.; Szostek, C.L.; Hughes, K.M.; Kneafsey, B.; Clarke, L.J.; Ellis, N.; Rijnsdorp, A.D.; McConnaughey, R.A.; et al. Response of benthic fauna to experimental bottom fishing: A global meta-analysis. *Fish Fish.* 2018, *19*, 698–715.
85. Dufois, F.; Garreau, P.; Le Hir, P.; Forget, P. Wave-and current-induced bottom shear stress distribution in the Gulf of Lions. *Cont. Shelf Res.* 2008, *28*, 1920–1934.
86. Kaiser, M.J.; Spencer, B.E. The effects of beam-trawl disturbance on infaunal communities in different habitats. *J. Anim. Ecol.* 1996, *65*, 348–358.
87. Smith, C.J.; Banks, A.C.; Papadopoulou, K.N. Improving the quantitative estimation of trawling impacts from sidescan-sonar and underwater-video imagery. *ICES J. Mar. Sci.* 2007, *64*, 1692–1701.
88. Olsgard, F.; Schaanning, M.T.; Widdicombe, S.; Kendall, M.A.; Austen, M.C. Effects of bottom trawling on ecosystem functioning. *J. Exp. Mar. Biol. Ecol.* 2008, *366*, 123–133.
89. De Juan, S.; Demestre, M.; Sánchez, P. Exploring the degree of trawling disturbance by the analysis of benthic communities ranging from a heavily exploited fishing ground to an undisturbed area in the NW Mediterranean. *Sci. Mar.* 2011, *75*, 507–516.
90. Widdicombe, S.; Austen, M.C. The interaction between physical disturbance and organic enrichment: An important element in structuring benthic communities. *Limnol. Oceanogr.* 2001, *46*, 1720–1733.

91. Selby, I.; Evans, N.C. Origins of mud clasts and suspensions on the seabed in Hong Kong. *Cont. Shelf Res.* 1997, *17*, 57–78.
92. Fettweis, M.; Du Four, I.; Zeelmaekers, E.; Baeteman, C.; Francken, F.; Houziaux, J.-S.; Mathys, M.; Nechad, B.; Pison, V.; Vandenberghe, N.; et al. *Mud Origin, Characterisation and Human Activities (MOCHA): Final Report*; Belgian Science Policy Office: Brussels, Belgium, 2007.
93. Grémare, A.; (Université de Bordeaux, Talence, France). Personal communication, 2020.
94. Nilsson, H.C.; Rosenberg, R. Effects on marine sedimentary habitats of experimental trawling analysed by sediment profile imagery. *J. Exp. Mar. Biol. Ecol.* 2003, *285–286*, 453–463.
95. Smith, C.J.; Rumohr, H.; Karakassis, I.; Papadopoulou, K.N. Analysing the impact of bottom trawls on sedimentary seabeds with sediment profile imagery. *J. Exp. Mar. Biol. Ecol.* 2003, *285–286*, 479–496.
96. Tiano, J.C.; Van Der Reijden, K.J.; O'Flynn, S.; Beauchard, O.; Van Der Ree, S.; Van Der Wees, J.; Ysebaert, T.; Soetaert, K. Experimental bottom trawling finds resilience in large-bodied infauna but vulnerability for epifauna and juveniles in the Frisian Front. *Mar. Environ. Res.* 2020, *159*, 104964.
97. Darnaude, A.M.; Salen-Picard, C.; Harmelin-Vivien, M.L. Depth variation in terrestrial particulate organic matter exploitation by marine coastal benthic communities off the Rhone River delta (NW Mediterranean). *Mar. Ecol. Prog. Ser.* 2004, *275*, 47–57.
98. Tesi, T.; Miserocchi, S.; Goñi, M.A.; Langone, L. Source, transport and fate of terrestrial organic carbon on the western Mediter- ranean Sea, Gulf of Lions, France. *Mar. Chem.* 2007, *105*, 101–117.
99. Cathalot, C.; Rabouille, C.; Tisnérat-Laborde, N.; Toussaint, F.; Kerhervé, P.; Buscail, R.; Loftis, K.; Sun, M.Y.; Tronczynski, J.; Azoury, S.; et al. The fate of river organic carbon in coastal areas: A study in the Rhône River delta using multiple isotopic ($\delta^{13}C$, $\delta^{14}C$) and organic tracers. *Geochim. Cosmochim. Acta* 2013, *118*, 33–55.
100. Fontugne, M.R.; Jouanneau, J.M. Modulation of the particulate organic carbon flux to the ocean by a macrotidal estuary: Evidence from measurements of carbon isotopes in organic matter from the Gironde system. *Estuar. Coast. Shelf Sci.* 1987, *24*, 377–387.]
101. Middelburg, J.J.; Herman, P.M.J. Organic matter processing in tidal estuaries. *Mar. Chem.* 2007, *106*, 127–147.
102. Savoye, N.; David, V.; Morisseau, F.; Etcheber, H.; Abril, G.; Billy, I.; Charlier, K.; Oggian, G.; Derriennic, H.; Sautour, B. Origin and composition of particulate organic matter in a macrotidal turbid estuary: The Gironde Estuary, France. *Estuar. Coast. Shelf Sci.* 2012, *108*, 16–28.

103. Sottolichio, A.; Castaing, P. A synthesis on seasonal dynamics of highly-concentrated structures in the Gironde estuary. *Earth Planet. Sci.* 1999, *329*, 795–800.
104. Jouanneau, J.M.; Latouche, C. *The Gironde Estuary*; Schweizerbart Science Publishers: Stuttgart, Germany, 1981.
105. Etcheber, H.; Taillez, A.; Abril, G.; Garnier, J.; Servais, P.; Moatar, F.; Commarieu, M.V. Particulate organic carbon in the estuarine turbidity maxima of the Gironde, Loire and Seine estuaries: Origin and lability. *Hydrobiologia* 2007, *588*, 245–259.
106. Ulses, C.; Estournel, C.; Durrieu de Madron, X.; Palanques, A. Suspended sediment transport in the Gulf of Lions (NW Mediterranean): Impact of extreme storms and floods. *Cont. Shelf Res.* 2008, *28*, 2048–2070.
107. Mayer, L.M.; Jumars, P.A.; Taghon, G.L.; Macko, S.A.; Trumbore, S. Low-density particles as potential nitrogenous foods for benthos. *J. Mar. Res.* 1993, *51*, 373–389.
108. Abril, G.; Etcheber, H.; Le Hir, P.; Bassoullet, P.; Boutier, B.; Frankignoulle, M. Oxic/anoxic oscillations and organic carbon mineralization in an estuarine maximum turbidity zone (The Gironde, France). *Limnol. Oceanogr.* 1999, *44*, 1304–1315.
109. Abril, G.; Nogueira, M.; Etcheber, H.; Cabeçadas, G.; Lemaire, E.; Brogueira, M.J. Behaviour of organic carbon in nine contrasting European estuaries. *Estuar. Coast. Shelf Sci.* 2002, *54*, 241–262.
110. Lemaire, E.; Abril, G.; De Wit, R.; Etcheber, H. Effect of turbidity on phytoplanktonic pigments degradation in the Gironde Estuary. *Comptes Rendus Geosci.* 2002, *334*, 251–258.
111. Pearson, T.H.; Rosenberg, R. Macrobenthos succession in relation to organic enrichment and pollution of the marine environment. *Oceanogr. Mar. Biol. Annu. Rev.* 1978, *16*, 229–331.
112. Miralles, J.; Arnaud, M.; Radakovitch, O.; Marion, C.; Cagnat, X. Radionuclide deposition in the Rhône River Prodelta (NW Mediterranean sea) in response to the December 2003 extreme flood. *Mar. Geol.* 2006, *234*, 179–189.
113. Salen-Picard, C.; Darnaude, A.M.; Arlhac, D.; Harmelin-Vivien, M.L. Fluctuations of macrobenthic populations: A link between climate-driven river run-off and sole fishery yields in the Gulf of Lions. *Oecologia* 2002, *133*, 380–388.
114. Miralles, J.; Radakovitch, O.; Aloisi, J.C. ^{210}Pb sedimentation rates from the Northwestern Mediterranean margin. *Mar. Geol.* 2005, *216*, 155–167.
115. Zuo, Z.; Eisma, D.; Berger, G.W. Determination of sediment accumulation and mixing rates in the Gulf of Lions, Mediterranean Sea. *Oceanol. Acta* 1991, *14*, 253–262.
116. Dorgan, K.M.; Jumars, P.A.; Johnson, B.D.; Boudreau, B.P. Macrofaunal burrowing: The medium is the message. *Oceanogr. Mar. Biol.* 2006, *44*, 85–121.

117. Lamarque, B.; Deflandre, B.; Galindo Dalto, A.; Schmidt, S.; Romero-Ramirez, A.; Garabetian, F.; Dubosq, N.; Diaz, M.; Grasso, F.; Sottolichio, A.; et al. Spatial Distributions of Surface Sedimentary Organics and Sediment Profile Image Characteristics in a High-Energy Temperate Marine RiOMar: The West Gironde Mud Patch; SEANOE. 2021. Available online: http://b2find.eudat. eu/dataset/e591e5d7-3dbc-57bc-9588-532deed0a3c2 (accessed on 1 February 2021).

Annexe 2

Spatiotemporal dynamics of surface sediment characteristics and benthic macrofauna compositions in a temperate high-energy River-dominated Ocean Margin

Bastien Lamarque[1], Bruno Deflandre[2], Sabine Schmidt[2], Guillaume Bernard[1], Nicolas Dubosq[2], Mélanie Diaz[2], Nicolas Lavesque[1], Frédéric Garabetian[1], Florent Grasso[3], Aldo Sottolichio[2], Sylvain Rigaud[4], Alicia Romero-Ramirez[1], Marie-Ange Cordier[2], Dominique Poirier[2], Martin Danilo[2], Antoine Grémare[1]

[1]UMR EPOC, Université de Bordeaux, CNRS, UMR 5805, Station Marine d'Arcachon, 2 rue du Professeur Jolyet, 33120, Arcachon, France

[2]UMR EPOC, Université de Bordeaux, CNRS, UMR 5805, Bâtiments B18/B18N, Allée Geoffroy Saint-Hilaire, CEDEX, 33615, Pessac, France

[3]IFREMER, DYNECO/DHYSED, Centre de Bretagne, CS 10070, 29280, Plouzané, France

[4]Université de Nîmes, EA 7352 CHROME, rue du Dr Georges Salan, 30021, Nîmes, France

Article publié en 2022 dans la revue *Continental Shelf Research*

Abstract

The benthic compartment of River-dominated Ocean Margins (RiOMar) is largely affected by sedimentary processes, as well as by natural and anthropogenic disturbances. Recent studies have confirmed the major importance of riverine inputs and local hydrodynamics in the spatial structuration of low and high-energy temperate RiOMar, respectively. Differences in the nature of these structuring factors could also affect the temporal dynamics of these two types of systems. The present study is aiming at: (1) quantifying spatiotemporal changes in surface sediment and benthic macrofauna within the West Gironde Mud Patch (WGMP; high-energy system) over both short (2016–2018) and longer (2010/2016–2018) time scales, (2) identifying the main environmental factors explaining those changes, and (3) achieving a comparison with the Rhône River Prodelta (RRP; low-energy system) in view of further characterizing the functioning of the benthic components of these two temperate RiOMar. Surface sediment characteristics (grain size, quantitative and qualitative descriptors of particulate organic matter) and benthic macrofauna compositions were assessed based on 4 seasonal sampling of 5 stations located along a depth gradient within the WGMP. Results highlighted the existence of spatial patterns for both surface sediment and benthic macrofauna, which are both better explained by local hydrodynamics. Most variables presented seasonal changes. Benthic macrofauna compositions also showed pluri-annual changes, which were attributed to a cicatrization process following a major disturbance caused by the 2013–2014 series of severe winter storms, and suggests the major role of local hydrodynamics in explaining 2010/2016–2018 temporal changes in WGMP benthic macrofauna compositions. The comparison with the RRP further highlighted major discrepancies between the two systems in the main processes (i.e., hydrodynamics *versus* river hydrological regime) explaining surface sediment characteristics and benthic macrofauna compositions, which supports current RiOMar typologies.

Keywords: RiOMar, West Gironde Mud Patch, North East Atlantic shelf, particulate organic matter, benthic macrofauna, spatiotemporal changes, hydrodynamics, storms

1. Introduction

Continental margins are key areas for the marine component of major biogeochemical cycles, accounting for the mineralization of 50–80% of continental Particulate Organic Carbon (POC) inputs (Aller, 1998; Blair and Aller, 2012; Burdige, 2005). Continental margins impacted by major river freshwater and sediment discharges are defined as River-dominated Ocean Margins (RiOMar). RiOMar provide a large variety of ecosystem services including provisioning (e.g. fisheries), regulating (e.g. carbon mineralization/burial) and supporting (e.g. nutrients cycling, habitats) ones (e.g. Aller, 1998; Levin et al., 2001; Lansard et al., 2009). Their benthic components constitute the main marine primary depositional areas of riverine particule inputs (Burdige, 2005; McKee et al., 2004) and it is estimated that RiOMar account for 40–50% of continental POC burial in continental margins (Blair and Aller, 2012; Burdige, 2005; Hedges and Keil, 1995). RiOMar benthic biological compartments (e.g. macrofauna) and biogeochemical fluxes (e.g. mineralization) are largely affected by a variety of natural and anthropogenic disturbances (Aller, 1998; Lansard et al., 2009; Lotze et al., 2006; Rhoads et al., 1985; Tesi et al., 2007; Ulses et al., 2008; Worm et al., 2006).

The impact of both sediment discharges and associated organic matter inputs on the structuration of benthic macrofauna communities and biogeochemical functioning of the sediment-water interface has been documented for a large variety of RiOMar (Akoumianaki et al., 2013; Aller and Aller, 1986; Aller and Stupakoff, 1996; Alongi et al., 1992; Bonifácio et al., 2014; Harmelin-Vivien et al., 2009; Rhoads et al., 1985; Wheatcroft, 2006). Mostly based on the analysis of macrofauna vertical distribution within the sediment column and X-ray radiographies, Rhoads et al. (1985) first proposed a conceptual model describing the response of benthic macrofauna and surface sediments to the inputs of major rivers. According to this model, macrofauna spatial distribution is mainly controlled by the interaction between: (1) the physical disturbance induced by intense riverine particles inputs, and (2) Particulate Organic Matter (POM) availability. In proximal (i.e., the closest to the river mouth) parts of RiOMar, high and irregular sedimentation rates induce sedimentary instability, precluding the establishment of mature macrobenthic communities. The high turbidity of river plumes also limits primary production in the water column, resulting in mainly low (refractory) POM concentrations in surface sediments. Accordingly, RiOMar proximal areas are characterized by low bioturbation intensities and low mineralization fluxes. Conversely, in distal (i.e., deeper) parts, moderated sedimentation and enhanced primary production in the water column allow for the establishment of mature macrobenthic communities, high bioturbation intensities and mineralization fluxes.

More recent RiOMar typologies, based on meta-analyses (mostly achieved on tropical and subtropical systems) of geomorphological and biogeochemical processes, highlighted the major effect of local hydrodynamics on RiOMar morphologies and POC mineralization/burial intensities (Blair and Aller, 2012; McKee et al., 2004). This led to a clear distinction between: (1) low-energy systems, with both high sedimentation rates and carbon preservation (later referred as type 1), and (2) high-energy tidal and/or wave systems with both high sediment oxygenation and low carbon preservation rates (later referred as type 2). Lamarque et al. (2021) recently assessed the main environmental factors responsible for the spatial structuration of temperate type 1 and type 2 systems based on the comparison between extensive spatial surveys conducted within the Rhône River Prodelta (RRP; type 1, French Mediterranean coast) and the West Gironde Mud Patch (WGMP; type 2, French Atlantic coast). Their results confirmed the major importance of riverine inputs and local hydrodynamics in the spatial structuration of type 1 and type 2 temperate RiOMar, respectively.

Such a difference in the nature of their main structuring factors could as well affect the spatiotemporal dynamics of these two types of systems. Seasonal changes in both surface sediment characteristics and benthic macrofauna compositions along a depth gradient have already been addressed within the RRP by Bonifácio et al. (2014). Results showed that temporal changes were larger at the most proximal station in relation with changes in river flows. Major changes were observed after a prolonged low-flow period, which allowed for the development of a mature macrobenthic community (otherwise precluded due to high sedimentation rates resulting from POM riverine inputs). Conversely, temporal changes in benthic surface sediment characteristics and benthic macrofauna compositions within the WGMP have only been poorly documented so far. The only available quantitative benthic macrofauna composition data have been collected during a single cruise and at only 3 stations (Massé et al., 2016). Consequently, the explaining factors and the magnitude of spatiotemporal changes in surface sediment characteristics and benthic macrofauna compositions within the WGMP (taken as an example of temperate type 2 RiOMar) are still largely unknown.

The present study is aiming at filling this gap by: (1) quantifying spatiotemporal changes in surface sediment characteristics and benthic macrofauna compositions within the WGMP over both short (2016–2018) and long (2010/2016–2018) time scales, (2) identifying the main environmental factors explaining these changes, and (3) achieving a comparison with the RRP. Main tackled questions were as follows: (1) What are the relative importance of spatial and temporal changes in both WGMP surface sediment characteristics and benthic macrofauna composition? (2) Are the factors better explaining spatial changes in WGMP sediment profile image characteristics and spatio-temporal changes in benthic macrofauna composition similar?

(3) Are the differences between spatiotemporal changes in benthic macrofauna composition in the RRP and the WGMP compatible with their classification as type 1 and type 2 RiOMar?

Abbreviations:

AFDW	Ash-Free Dry Weight
AJD	Annual Julian Days
BSS	Bottom Shear Stress
BSS_{100}	Bottom Shear Stress integrated over 100-day periods
BSS_{365}	Bottom Shear Stress integrated over 365-day periods
Chl-*a*:	Chlorophyll-*a*
CJD	Cumulated Julian Days
$D_{0.5}$	Median diameter of sediment particles
dbRDA	distance-based Redundancy Analysis
DISTLM	DISTance-based Linear Model
DW	Dry Weight
EHAA	Enzymatically Hydrolysable Amino Acids
$Flow_{100}$	River flows integrated over 100-day periods
$Flow_{365}$	River flows integrated over 365-day periods
nMDS	non-Metric Multidimensional Scaling
PCA	Principal Components Analysis
Phaeo-*a*	Phaeophytin-*a*
POC	Particulate Organic Carbon
POM	Particulate Organic Matter
RiOMar	River-dominated Ocean Margin
RRP	Rhône River Prodelta
SIMPROF	SIMilarity PROFile procedure
SSA	Sediment Surface Area
THAA	Total Hydrolysable Amino Acids
WGMP	West Gironde Mud Patch

2. Materials and methods

2.1 WGMP: Sampling area

The West Gironde Mud Patch (WGMP) is a 420 km^2 sedimentary body located in the Bay of Biscay 40 km off the Mouth of the Gironde Estuary, between ca. 30 and 75 m depth (**Figure 7.1**). This relict paleovalley is the primary depocenter (sedimentation rates between less than 1 and 10 mm y^{-1}; Dubosq et al., 2021) of fine particles originating from the Gironde Estuary, which has an annual mean water flow of 944 m^3 s^{-1}(Doxaran et al., 2009) with daily flows up to 7500 m^3 s^{-1} (Constantin et al., 2018). The WGMP is located in a macro-tidal environment with a tidal range from 1.5 to 5 m (Jalón-Rojas et al., 2018). The continental shelf off the Mouth of the Gironde Estuary is periodically submitted to strong swells/waves, which can reach maximal amplitudes of 15 m and periods of 15 s (Cirac et al., 2000; Masselink et al., 2016). The sedimentology of the WGMP has been extensively studied based on stratigraphic sequences, palynological data, X-ray radiographies and radiochronographies (Castaing et al., 1979, 1982; Castaing and Allen, 1981; Gadel et al., 1997; Jouanneau et al., 1989; Lesueur et al., 1991, 1996, 2001, 2002; Lesueur and Tastet, 1994; Longère and Dorel, 1970; Parra et al., 1998; Weber et al., 1991). These surveys have attributed a major role to local hydrodynamics in controlling the spatial structuration of the WGMP. This paradigm was based on both: (1) the segmentation between a proximal and a distal part with no modern persistent sedimentation in the former, and (2) the decreasing frequency of occurrence of vertical erosional sequences within the sediment column with station depth (Jouanneau et al., 1989; Lesueur et al., 1991, 2001, 2002; Lesueur and Tastet, 1994). It was recently further validated by a synoptic survey of the spatial distributions of surface sediment and sediment profile image characteristics (Lamarque et al., 2021).

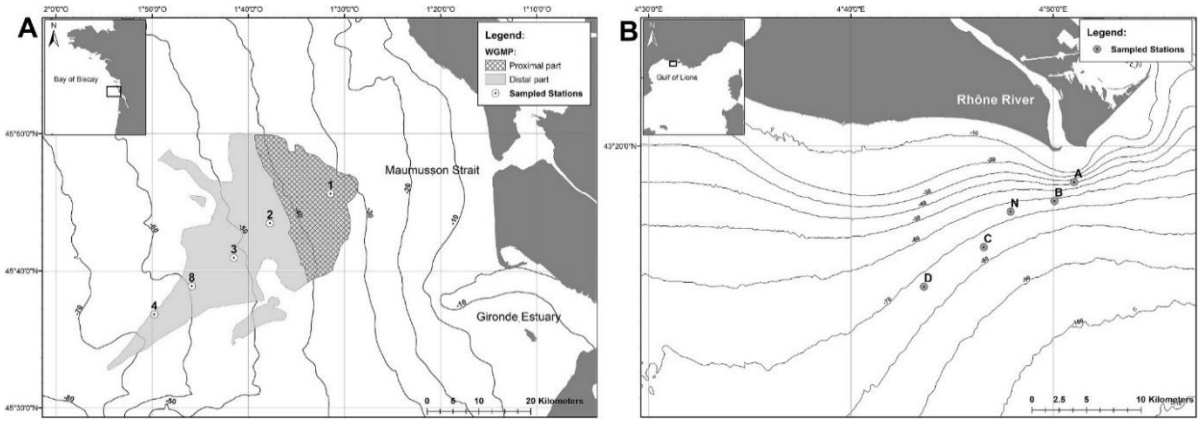

Figure 7.1. Sampling: Map showing the delimitation of: (**A**) the West Gironde Mud Patch (WGMP) along the French Atlantic Coast together with the locations of the 5 sampled stations. Stations 1, 3 and 4 had also been sampled in July 2010 by Massé et al. (2016); and (**B**) the Rhône River Prodelta (RRP) in the Gulf of Lions (NW Mediterranean) together with the locations of the 5 stations sampled by Bonifácio et al. (2014) in April 2007, May and December 2008, and July 2011.

2.2 WGMP: Sampling of surface sediment and benthic macrofauna

Five stations located along a depth gradient (**Figures 7.1A**, **Table 7.1**) were sampled for surface sediment characteristics and benthic macrofauna during 4 cruises, which took place on board of the R/V Côtes de la Manche in October 2016 (Deflandre 2016), August 2017 (Deflandre 2017), February 2018 (Deflandre 2018a) and April 2018 (Deflandre, 2018b). This sampling design was set to document, over the whole WGMP, seasonally contrasted situations in terms of Gironde Estuary river flows and local hydrodynamics. Only 4 stations were sampled in February 2018 due to bad meteorological conditions. During each cruise, 4 sediment cores (10 cm internal diameter) were collected at each station using an Oktopus GmbH® multiple corer. The upper top 0.5 cm of each core was sliced and immediately frozen (-20°C) on board. A single core was used to assess sediment grain size, Sediment Surface Area (SSA; Mayer, 1994b), POC concentrations (hereafter POC) and $\delta^{13}C$. The remaining 3 cores were used to assess chloropigment and amino acid concentrations. Benthic macrofauna was sampled using a 0.25 m^2 Hamon grab (3 replicates), sieved on a 1 mm mesh and fixed with 4% formalin.

2.3 WGMP: Gironde Estuary water flows

Daily water flows of the Gironde Estuary were assessed by summing the flows of the Garonne and Dordogne Rivers. Data were downloaded at http://www.hydro.eaufrance.fr.

2.4 WGMP: Local hydrodynamics

At each of the 5 sampled stations (**Figure 7.1**, **Table 7.1**), daily values of Bottom Shear Stress (BSS) were computed from a tridimensional numerical model (Diaz et al., 2020; Grasso et al., 2018). This model is based on the MARS3D hydrodynamic model (Lazure and Dumas, 2008) and the WAVE WATCH III® wave model (Roland and Ardhuin, 2014) with a resolution

of ca. 0.5 × 0.5 km^2 over the WGMP. The model integrates realistic hydro-meteorological forcing (i.e., wind, tide, surge and river flows). BSS were computed following Soulsby's formulation (Soulsby, 1997). Simulations provided hourly outputs from 2010 to 2018 that were daily compiled and 95^{th} percentiles were used to characterize BSS intensities accounting for intense hydrodynamic events.

Table 7.1: Sampling: Location (WGS84, degrees, and decimal minutes) and depth of the 5 stations (1, 2, 3, 8, 4) sampled in the West Gironde Mud Patch (WGMP) during the present study and of the 5 stations (A, B, N, C, D) sampled in the Rhône River Prodelta (RRP) by Bonifácio et al. (2014). (See text for details).

System	Station	Latitude (N)	Longitude (W)	Depth (m)
WGMP	1	45°45.580′	1°31.489′	37
	2	45°43.511′	1°37.773′	47.8
	3	45°41.007′	1°41.545′	56.5
	8	45°38.873′	1°45.777′	64.5
	4	45°36.924′	1°49.712′	71.5
RRP	A	43°18.690′	04°51.042′	24
	B	43°18.013′	04°50.068′	54
	N	43°17.626′	04°47.896′	67
	C	43°16.343′	04°46.565′	76
	D	43°14.917′	04°43.613′	74

2.5 WGMP: Surface sediment characteristics

Grain sizes were measured on aliquots of unreplicated sediment samples using a Malvern® Master Sizer laser microgranulometer. Almost all particle-size distributions were unimodal and therefore characterized through their median diameter ($D_{0.5}$). SSA was measured on unreplicated freeze-dried sediment samples, previously degassed overnight at 150°C, using a Gemini® VII Surface Area Analyzer (Micromeritics® 2390a model) with the multi-point Brunauer-EmmettTeller method (Mayer, 1994b). POC were assayed using a LECO® CS 200 analyzer, after 2M HCl overnight decarbonatation (Etcheber et al., 1999) of previously freeze-dried unreplicated sediment samples. They were normalized for SSA (i.e., expressed in terms of mass per SSA) since these two parameters were assessed on the same sediment core at each combination of stations*dates.

Total and Enzymatically Hydrolysable Amino Acids (THAA and EHAA) were analyzed on triplicates for each of the 3 sampled cores. THAA were extracted through acid hydrolysis (6M HCl, 100°C, 24h). EHAA were extracted following the biomimetic approach proposed by Mayer et al. (1995). THAA and EHAA were derivatized to form fluorescent amino compounds, which were separated by reverse phase High-Performance Liquid Chromatography (Agilent® 1260 INFINITY) on a Phenomenex® Kinetex 5 µm EVO C18 column and detected using a 338 nm excitation wavelength. Their concentrations (hereafter THAA and EHAA) were expressed in terms of mass per mass of sediment Dry Weight (DW) since SSA were not measured on the same sediment cores.

Chlorophyll-*a* and Phaeophytin-*a* were assayed on unreplicated thawed frozen (-20°C) sediment samples after overnight acetone extraction (90% final concentration) using a PerkinElmer® LS-55 spectrofluorometer following Neveux and Lantoine (1993). Their concentrations (hereafter Chl-*a* and Phaeo-*a*) were expressed in terms of mass per mass of sediment DW since SSA were not measured on the same sediment cores.

Chl-*a*/(Chl-*a* + Phaeo-*a*) ratios (hereafter Chl-*a*/(Chl-*a* + Phaeo-*a*)) were used as a lability index of vegetal biomass (Bonifácio et al., 2014; Pastor et al., 2011) and EHAA/THAA ratios (hereafter EHAA/THAA) were used as a lability index of bulk sedimentary organics (Bonifácio et al., 2014; Grémare et al., 2005; Medernach et al., 2001; Pastor et al., 2011; Wakeham et al., 1997).

For the analysis of POC isotopic ratio, duplicated freeze-dried sediment samples were decarbonated (1M HCl) and later analyzed using a Thermo Scientific® Delta V plus IRMS coupled with a Thermo Scientific® Flash 2000 EA. Raw measurements were converted in usual $\delta^{13}C$ units (Coplen, 2011).

2.6 WGMP: benthic macrofauna

Macrofauna was sorted, identified to the lowest tractable taxonomic level and counted. Species richness was computed on pooled replicates for each combination of stations and dates. Biomasses (Ash-Free Dry Weights, AFDW) were measured for each individual taxon as ignition loss (450°C, 4 h) except for Ophiuridae for which an allometric regression was used to account for arm loss: AFDW = 0.0111 x (disk diameter)$^{2.5268}$ (where AFDW and disk diameter are expressed in g and mm, respectively; N. Lavesque, personal communication). Abundances and biomasses were standardized per m^2.

2.7 WGMP: data analysis

To identify the most pertinent time scales for assessing the structuring role of river flows and local hydrodynamics on spatiotemporal changes in surface sediment characteristics (i.e., mean: SSA, POC/SSA, Chl-*a*, Phaeo-*a*, Chl-*a*/(Chl-*a*+Phaeo-*a*), THAA, EHAA, EHAA/THAA and $\delta^{13}C$) and benthic macrofauna compositions, the Pearson correlation coefficients linking their similarity matrices (Euclidean and Bray-Curtis distances, respectively) with similarity matrices based on either integrated river flows or integrated BSS were computed. This was achieved using R version 3.6.1 (R Core Team, 2019) with the additional packages vegan (Oksanen et al., 2019), BBmisc (Bischl et al., 2017) and Hmisc (Harrell, 2021) for river flows and BSS integrated over 1–365 days before each of the 4 cruises.

For the same surface sediment characteristics as described above, hierarchical clustering (Euclidean distance and average group linking) and Principal Components Analysis (PCA) were used to define groups of stations*sampling dates and to assess relationships between variables. A SIMilarity PROFile procedure (SIMPROF; Clarke et al., 2008) was used to test for the statistical significance of between-group differences. A DISTance-based Linear Model (DISTLM) was established to assess the potential contributions of river flows and BSS to spatiotemporal changes in surface sediment characteristics. This model was built using the Best selection procedure (Anderson et al., 2008) and the AIC selection criterion (Akaike, 1973). It was represented in a multidimensional space through a distance-based Redundancy Analysis (dbRDA; Anderson et al., 2008). All surface sediment analyses were performed on normalized data and river flows and BSS were integrated over both 100(i.e., seasonal) and 365 (i.e., annual) day periods based on results of the above-described correlation analysis. Station depth, Annual Julian Days (i.e., AJD: the number of days since the beginning of the sampling year), and Cumulated Julian Days (i.e., CJD: the number of days since the first day of the October 2016 cruise) were introduced as supplementary variables. The same approach was used for benthic macrofauna abundances (square-root transformed data). However, in this case and because of the use of the Bray-Curtis similarity, a non-Metric Multidimensional Scaling (nMDS) was achieved instead of a PCA. Moreover, an intermediate DISTLM/dbRDA was achieved using macrofauna composition as response variable and normalized surface sediment characteristics as predictor variables. POC, Phaeo-*a* and EHAA were excluded from this last procedure due to their strong correlation with other surface sediment characteristics.

A comparison was achieved with macrofauna abundance data collected in July 2010 at stations 1, 3 and 4 (i.e., station E, C and W in Massé et al., 2016) using exactely the same methodology (sampling gear and design, sorting procedure). Macrofauna identification was achieved at the same taxonomic resolution by the same Research group as well. Nevertheless, to avoid inconsistencies in taxa identification between the two studies, benthic macrofauna data were degraded at the genus level. The comparison was achieved through hierarchical clustering (square-root transformed data, Bray-Curtis distance and average group linking) and nMDS together with the SIMPROF procedure.

All multivariate analyses were computed using the PRIMER® 6 software package (Clarke and Warwick, 2001) with the PERMANOVA + add-on (Anderson et al., 2008).

2.8 Comparison between the WGMP and the RRP

Intra-station temporal variabilities (i.e., among sampling dates considering each station individually) in sediment surface characteristics and benthic macrofauna compositions were compared in the WGMP (4 cruises between 2016 and 2018 as described above) and the RRP. The latter was sampled by Bonifácio et al. (2014), using the same approach and methodology as in the present study. More specifically, 5 stations located along a depth gradient from the mouth of the Rhône River, taking into account the preferential direction of its plume (**Figure 7.1B**; **Table 7.1**), were sampled during 4 cruises carried out in April 2007, May and December 2008, and July 2011 (corresponding to different hydrological regimes of the Rhône River).

These comparisons were based on the information contained in dissimilarity matrices computed using: (1) $D_{0.5}$, POC, Chl-*a*, Phaeo-*a*, Chl-*a*/(Chl-*a*+Phaeo-*a*), THAA, EHAA and EHAA/THAA (i.e., all the surface sediment characteristics measured during both studies), and (2) benthic macrofauna abundances. The sums of squared distances from individual points (i.e., station*sampling date) to their group (i.e., station) centroids were computed for each station (following Anderson, 2001 and Anderson et al., 2008) and used as an indices of intra-station temporal variability after standardization for the number of sampling dates.

3. Results

3.1 WGMP: Water flows and Bottom Shear Stress over the 2010–2018 period

Water flows presented a clear seasonal pattern with winter floods (peaks up to 5590 $m^3 s^{-1}$ on January 23, 2018) and low-flow periods during summer and fall (**Figure 7.2A**). Over the whole 2010–2018 period, major events were the January 2018 and to a slightly lower extent the January 2014 floods. Between October 2016 and April 2018, there were clear inter-annual differences in water flows during the high-flow period as indicated by the moderate values recorded during the 2016–2017 as opposed to 2017–2018 winter. The July 2010 cruise (Massé et al., 2016) was achieved immediately after the end of a high-flow period. The October 2016 and August 2017 cruises were achieved during low-flow periods (112 and 67 days after the end of the preceding high-flow period, respectively). Conversely, both the February 2018 and April 2018 cruises took place during a high-flow period, respectively 5 and 87 days after the January 2018 flood.

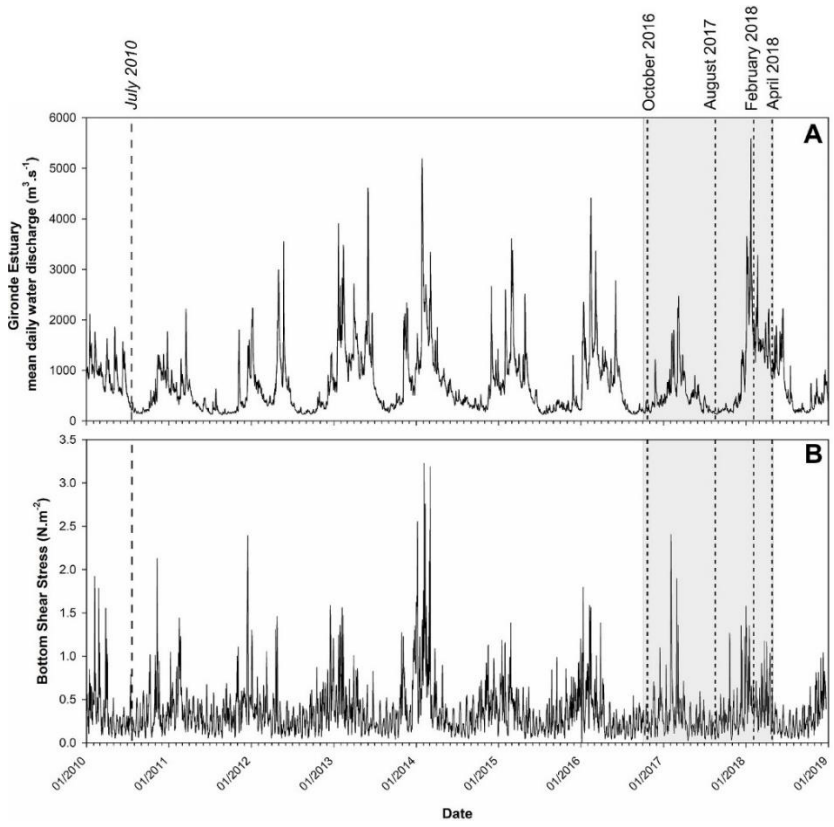

Figure 7.2: *WGMP:* Temporal changes in Gironde Estuary mean daily water flows (**A**) and in the 95th percentile of Bottom Shear Stress at station 3 (**B**) between 2010 and 2018. Short-dashed lines indicate the 4 cruises achieved in 2016–2018 (grey area) and the long-dashed line indicates the July 2010 cruise (Massé et al., 2016).

Although clearly decreasing with depth, Bottom Shear Stress (BSS) showed similar temporal patterns at all 5 stations (Lamarque et al., 2021). Their temporal changes are therefore only presented for station 3. BSS showed a clear seasonal pattern with a succession of peaks induced by winter storms and conversely low values during summer and fall (**Figure 7.2B**). Over the whole 2010–2018 period, the major event was the succession of peaks (i.e., up to 3.23 N m^{-2}) induced by the repetition of strong storms during the 2013–2014 winter. The July 2010 cruise (Massé et al., 2016) was achieved at the end of a low-BSS period. During the 2016–2018 period, there were slight differences between temporal changes in water flows and BSS since: (1) high-BSS periods generally preceded high-flow periods, and (2) highest BSS (up to 2.40 N m^{-2} on February 3, 2017) were recorded during 2016–2017 versus 2018 for highest water flows. Nevertheless, both the October 2016 and August 2017 cruises were conducted during low-BSS periods (i.e., <0.5 N m^{-2}) as opposed to the February 2018 and April 2018 cruises, which both took place during the 2017–2018 high-BSS period.

Table 7.2: *WGMP:* Mean values (± standard deviations for replicated measures) of surface sediment and main univariate benthic macrofauna characteristics during the 4 cruises achieved between 2016 and 2018. $D_{0.5}$: median grain size, SSA: Sediment Surface Area, POC: Particulate Organic Carbon, Chl-*a*: Chlorophyll-*a*, Phaeo-*a*: Phaeophytin-*a*, THAA: Total Hydrolyzable Amino Acids, EHAA: Enzymatically Hydrolyzable Amino Acids, SR: Species Richness and J': Pielou's evenness.

Cruise	Station	$D_{0.5}$ (µm)	SSA (m^2 gDW^{-1})	POC (mg m^{-2} SSA)	Chl-*a* (µg gDW^{-1})	Phaeo-*a* (µg gDW^{-1})	Chl-*a*/(Chl-*a*+Phaeo-*a*) (%)	THAA (mg gDW^{-1})	EHAA (mg gDW^{-1})	EHAA/THAA (%)	$\delta^{13}C$ (‰)	Abundance (ind. m^{-2})	Biomass (mgAFDW m^{-2})	SR (taxa.0.75m^{-2})	J'
October 2016	1	60.0	5.0	0.97	0.36 ± 0.10	2.95 ± 0.27	10.9 ± 2.0	0.69 ± 0.06	0.18 ± 0.05	26.5 ± 4.5	−18.11 ± 0.41	544.0 ± 198.9	1969.2 ± 2260.5	38	0.73
	2	26.0	6.1	1.14	0.90 ± 0.36	8.27 ± 1.05	10.0 ± 4.6	2.13 ± 0.13	0.44 ± 0.06	20.7 ± 1.8	−23.20 ± 0.05	410.7 ± 112.0	4473.4 ± 4494.1	30	0.69
	3	20.0	8.1	1.42	0.94 ± 0.02	8.39 ± 1.11	10.2 ± 1.3	2.77 ± 0.10	0.45 ± 0.02	16.4 ± 1.1	−23.23 ± 0.13	141.3 ± 68.2	474.2 ± 433.1	16	0.89
	8	23.1	7.5	1.43	0.87 ± 0.35	6.75 ± 0.37	11.3 ± 4.2	3.60 ± 0.23	0.53 ± 0.07	14.9 ± 2.6	−23.16 ± 0.08	228.0 ± 28.0	1922.4 ± 890.6	27	0.88
	4	20.1	10.3	1.49	1.39 ± 0.47	9.59 ± 1.69	13.0 ± 5.8	4.49 ± 0.27	0.65 ± 0.12	14.6 ± 3.2	−23.01 ± 0.03	92.0 ± 42.3	796.2 ± 418.2	18	0.92
August 2017	1	75.8	2.5	1.15	0.23 ± 0.09	1.46 ± 0.46	13.4 ± 2.5	0.51 ± 0.18	0.16 ± 0.04	32.2 ± 3.8	−24.44 ± 0.35	784.0 ± 360.6	958.1 ± 552.5	43	0.67
	2	23.8	7.3	1.27	1.15 ± 0.20	6.65 ± 0.88	14.9 ± 2.7	3.23 ± 0.29	0.61 ± 0.02	18.9 ± 1.4	−24.22 ± 0.55	294.7 ± 109.3	1405.8 ± 259.1	26	0.68
	3	21.2	8.4	1.28	0.87 ± 0.05	6.07 ± 1.64	13.1 ± 3.2	3.97 ± 0.07	0.66 ± 0.10	16.5 ± 2.2	−24.46 ± 0.10	218.7 ± 154.6	754.9 ± 189.9	24	0.67
	8	24.4	7.6	1.40	0.77 ± 0.29	5.25 ± 0.57	12.7 ± 4.0	3.55 ± 0.10	0.44 ± 0.01	12.3 ± 0.5	−24.22 ± 0.19	89.3 ± 43.1	1081.0 ± 1147.4	18	0.92
	4	21.9	9.3	1.50	0.91 ± 0.18	6.90 ± 1.28	12.0 ± 4.0	4.10 ± 0.19	0.38 ± 0.02	9.1 ± 0.5	−24.03 ± 0.38	176.0 ± 60.4	2569.4 ± 1698.6	27	0.92
February 2018	1	92.0	1.9	0.89	0.52 ± 0.37	2.53 ± 1.58	16.4 ± 1.8	0.72 ± 0.32	0.29 ± 0.12	41.0 ± 2.0	−25.12 ± 0.23	840.0 ± 342.0	1625.4 ± 541.0	32	0.62
	2	17.5	14.2	1.16	2.09 ± 0.72	9.61 ± 2.47	17.6 ± 1.5	3.10 ± 0.16	0.59 ± 0.14	19.0 ± 4.2	−24.58 ± 0.48	269.3 ± 217.0	1149.6 ± 1093.7	35	0.81
	3	23.7	6.2	1.58	0.96 ± 0.19	6.22 ± 0.63	13.3 ± 1.3	2.87 ± 0.43	0.45 ± 0.06	15.7 ± 0.3	−24.41 ± 0.01	174.7 ± 130.1	1113.3 ± 1190.6	27	0.85
	4	17.4	12.6	1.32	1.12 ± 0.17	9.51 ± 1.86	10.6 ± 1.0	4.32 ± 0.43	0.57 ± 0.07	13.3 ± 3.0	−23.91 ± 0.10	162.7 ± 112.4	1313.4 ± 1035.7	22	0.88
April 2018	1	16.3	12.9	0.93	0.66 ± 0.05	3.67 ± 0.38	15.2 ± 0.5	0.98 ± 0.51	0.26 ± 0.04	29.6 ± 11.0	−24.29 ± 0.002	821.3 ± 615.5	1271.2 ± 175.0	35	0.62
	2	15.8	11.0	1.44	4.54 ± 1.96	18.16 ± 8.17	20.1 ± 0.6	3.94 ± 0.67	0.56 ± 0.07	14.2 ± 1.4	−24.05 ± 0.05	314.7 ± 32.6	1569.5 ± 1071.7	25	0.67
	3	17.9	7.7	1.49	3.48 ± 1.98	15.57 ± 8.18	18.1 ± 0.6	4.65 ± 1.44	0.56 ± 0.11	12.2 ± 1.2	−24.11 ± 0.20	134.7 ± 50.0	306.8 ± 354.9	25	0.84
	8	16.2	10.0	1.48	3.99 ± 1.66	18.37 ± 6.26	17.6 ± 2.1	4.36 ± 0.26	0.61 ± 0.03	14.0 ± 0.9	−23.69 ± 0.18	388.0 ± 69.4	1522.5 ± 1301.5	28	0.62
	4	17.4	8.9	1.79	5.86 ± 0.85	29.35 ± 2.83	16.6 ± 1.3	4.65 ± 0.49	0.72 ± 0.20	15.3 ± 2.8	−23.74 ± 0.31	882.7 ± 202.6	4985.9 ± 5475.4	33	0.45

3.2 WGMP: 2016–2018 spatiotemporal changes in surface sediment characteristics

$D_{0.5}$ of surface sediments were usually larger (60, 76 and 92 μm in October 2016, August 2017 and February 2018, respectively) and much more variable (16 μm in April 2018) at station 1 (**Table 7.2**, **Figure 7.3A**). At all other stations, $D_{0.5}$ were homogeneous (mean values around 20 μm) and temporally stable. Spatiotemporal changes in $\delta^{13}C$ were limited (i.e., between - 25.12 and -23.01‰) with the exception of station 1 in October 2016 (-18.11‰, **Table 7.2**, **Figure 7.3B**). Particulate Organic Carbon (POC) clearly increased with station depth (i.e., from stations 1 to 4), with a maximal value of 1.79 mg m^{-2} of Sediment Surface Area (SSA) at station 4 during April 2018 (**Table 7.2**, **Figure 7.3C**). The only exception to this pattern was February 2018 with a maximal value of 1.58 mg m^{-2} SSA at station 3. At station 4, POC was higher in April 2018 than during the 3 other cruises (mean value of 1.44 mg m^{-2} SSA). Total Hydrolysable Amino Acids concentrations (THAA) also increased with station depth (**Table 7.2**, **Figure 7.3D**). THAA ranged from 0.51 mg gDW^{-1} (station 1 in August 2017) to 4.65 mg gDW^{-1} (stations 3 and 4 in April 2018). Temporal changes in THAA were lower at station 4 (variation coefficient of 5.4% versus a mean of 22.0% at the 4 other stations). Chlorophyll-*a* concentrations (Chl-*a*) at station 1 were low (i.e., between 0.23 and 0.66 μg gDW^{-1} in August 2017 and April 2018, respectively) during all cruises, (**Table 7.2**, **Figure 7.3E**). At all other stations, Chl-*a* were much higher in April 2018 (with a maximal value of 5.86 μg gDW^{-1} at station 4) than during the 3 other cruises (mean value of 1.09 ± 0.37 μg gDW^{-1} for stations 2, 3, 8 and 4). The ratio between Enzymatically and Total Hydrolysable Amino Acids (EHAA/THAA) clearly decreased with station depth (**Table 7.2**, **Figure 7.3F**). EHAA/THAA was maximal (41.0%) at station 1 in February 2018 and minimal (9.1%) at station 4 in August 2017. Temporal changes were larger at stations 4 and 1 (variation coefficient of 21.0 and 19.2%, respectively) than at the 3 other stations (mean variation coefficient of 12.7%).

The Pearson correlation coefficients linking the similarity matrix based on integrated river flows and those based on either surface sediment characteristics or benthic macrofauna compositions are shown in **Figure 7.4A**. When using surface sediment characteristics, correlation coefficients first increased with integration period durations, became significant for a 53-day integration period and reached a maximal value of 0.34 for integration periods between 156 and 222 days. They then decreased constantly down to a value of 0.01 for an integration period of 365 days. When using benthic macrofauna compositions, correlation coefficients remained insignificant over the whole range of river flows integration periods.

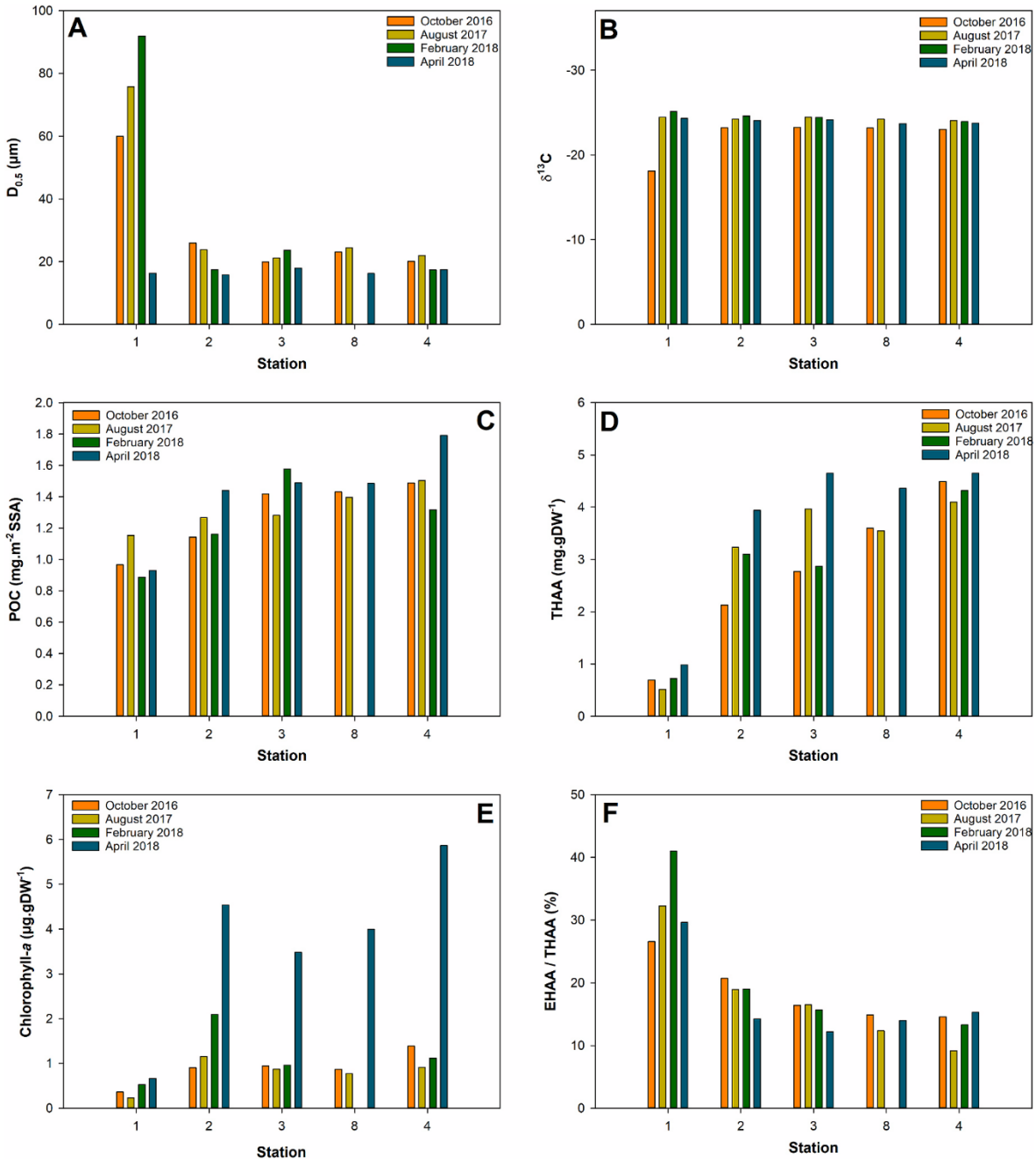

Figure 7.3: *WGMP:* Spatiotemporal changes in the (mean) values of surface sediment characteristics during the 4 cruises achieved between 2016 and 2018: Median grain sizes ($D_{0.5}$; **A**), $\delta^{13}C$ (**B**), Particulate Organic Carbon concentrations normalized by SSA (POC; **C**), Total Hydrolysable Amino Acids concentrations (THAA; **D**), Chlorophyll-*a* concentrations (**E**), and Enzymatically/Total Hydrolysable Amino Acids ratios (EHAA/THAA; F). Stations are ordered according to their depth.

The Pearson correlation coefficients linking the similarity matrix based on integrated BSS and those based on either surface sediment characteristics or benthic macrofauna compositions are shown in **Figure 7.4B.** In both cases, they increased with BSS integration periods and their maximal values were reached around 1-year (i.e., 0.56 and 0.73 at 365 and 351 days for surface sediment characteristics and benthic macrofauna compositions, respectively). However, the patterns of changes with increasing integration periods clearly differed. When using surface

sediment characteristics, correlation coefficients were always significant and almost constant for integration periods between 1 to ca. 250 days. Conversely, when using benthic macrofauna compositions, correlation coefficients were not significant for integration periods shorter than 65 days. They then presented a relative maximum (0.19 for a 90-day integration period) before almost constantly increasing for integration periods longer than 130 days.

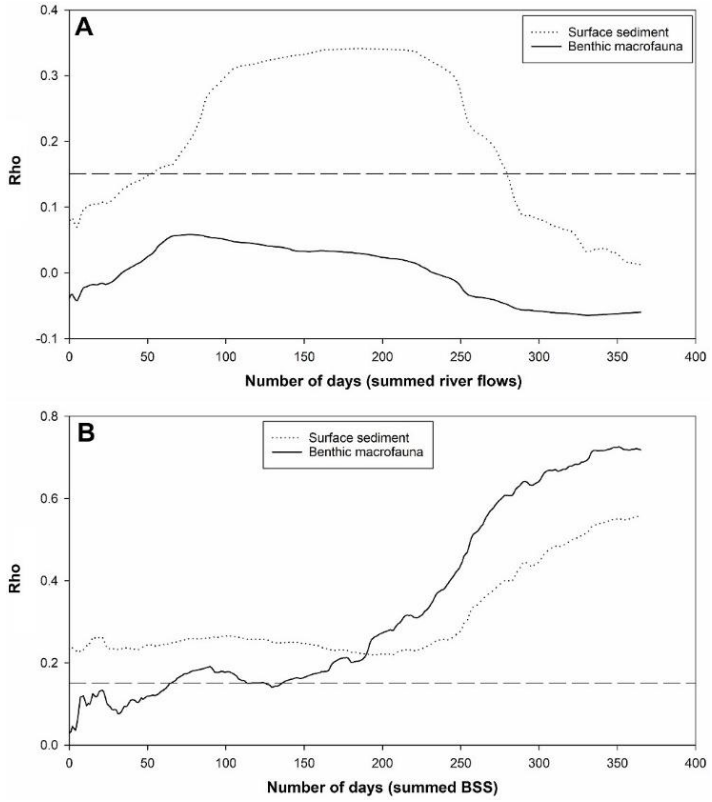

Figure 7.4: *WGMP*: Changes in the Pearson correlation coefficient (Rho) linking the similarity matrices based on either surface sediment characteristics or benthic macrofauna compositions (data collected between 2016 and 2018) with river flows (**A**) and Bottom Shear Stress (**B**) integrated over 1 to 365-day time periods preceding the 4 cruises. Dotted lines represent 5% significance thresholds.

The first two components of the PCA based on surface sediment characteristics accounted for 72.8% (i.e., 55.4% and 17.4%, respectively) of their total variance (**Figure 7.5A**). Hierarchical clustering and the associated SIMPROF procedure resulted in the identification of 3 groups and 2 "isolated" stations*dates (**Figure 7.5A**). "Isolated" stations*dates consisted of station 2 in February 2018 and station 4 in April 2018. Group I was exclusively composed of stations 1 (all sampling dates). Group II was composed of all remaining stations*dates except for the April 2018 cruise. All the stations sampled during this cruise clustered into group III, except stations 1 (Group I) and 4 (isolated). The first principal component was mostly defined by the opposition between the quantitative and qualitative characteristics of surface sedimentary organics with THAA, EHAA, POC, Chl-*a*, Phaeo-*a* and POC concentrations on one side and

EHAA/THAA on the other. The second component was mostly defined by the Chl-*a*/(Chl-*a*+Phaeo-*a*) and to a lesser extent EHAA/THAA (**Figure 7.5B**).

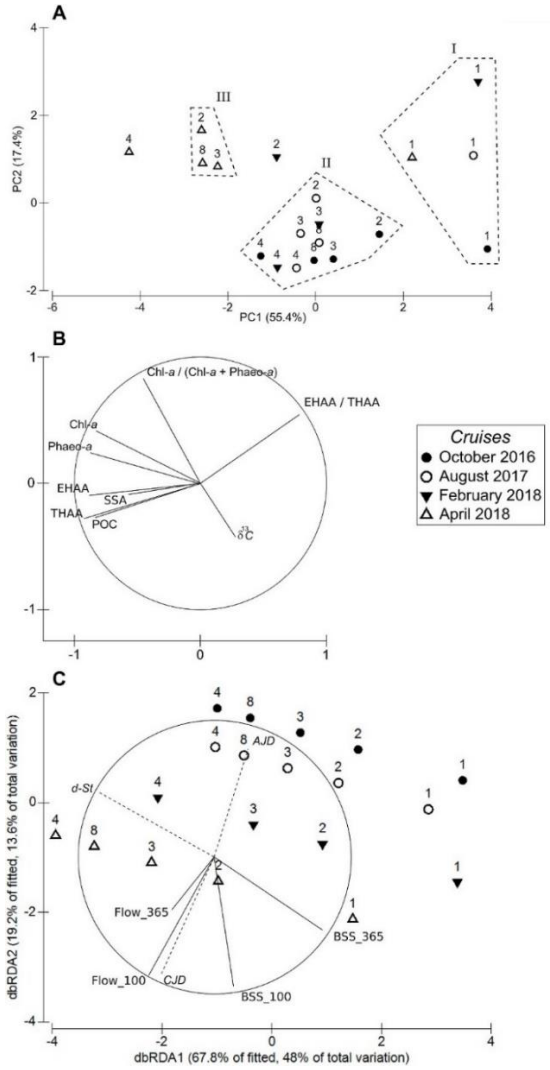

Figure 7.5: *WGMP:* Multivariate analyses of surface sediment characteristics recorded between 2016 and 2018. Projection of stations*cruises on the first plane of a Principal Component Analysis (**A**). Figures refer to stations and symbols to cruises. Dotted lines indicate groups of stations*cruises issued from hierarchical clustering. Correlations of the variables with the first two principal components (**B**). Distance-based Redundancy Analysis based on integrated Bottom Shear Stress and river flows (**C**). Station depth (d-St), Annual Julian Days (AJD) and Cumulated Julian Days (CJD) were used as supplementary variables. SSA: Sediment Surface Area; POC: Particulate Organic Carbon; Chl-*a*: Chlorophyll-*a*; Phaeo-*a*: Phaeophytin-*a*; THAA; Total Hydrolysable Amino Acids; EHAA: Enzymatically Hydrolysable Amino Acids; BSS_100 and BSS_365: integrated Bottom Shear Stress over 100 and 365 days; Flow_100 and Flow_365: integrated river flows over 100 and 365 days. (See text for details).

The DISTLM included river flows and BSS integrated over both 100 and 365-day periods (hereafter $Flow_{100}$, $Flow_{365}$, BSS_{100} and BSS_{365}) as independent variables. It explained 70.7% of the total variance of surface sediment characteristics. Its representation through the first plane of the dbRDA accounted for 61.6% of this total variance and showed two main orientations (**Figure 7.5C**). The first one, mainly along the first component of the dbRDA, corresponded to

the positioning of the stations along the depth gradient and was mainly cued by BSS_{365}. The second one, mainly along the second component of the dbRDA, separated the 4 cruises and was mainly cued by $Flow_{100}$ and to a lesser extent BSS_{100}. Cumulated and Annual Julian Days (CJD and AJD, respectively) correlated significantly ($p < 0.05$) with this second orientation. This correlation was slightly higher for CJD ($r = 0.934$ *versus* $r = 0.822$).

3.3 WGMP: 2016–2018 spatiotemporal changes in benthic macrofauna compositions

Overall, 6391 specimens belonging to 146 taxa were collected and identified (123 taxa after pooling species at the Ampelisca, Glycera and Nephtys genus). Molluscs (mainly abundant at stations 1 and 2) represented 34% of total macrofauna abundance, followed by polychaetes (27.8%), echinoderms (22%) and crustaceans (13.4%).

Species richness did not show any clear spatiotemporal pattern (**Table 7.2**, **Figure 7.6A**). It seemed higher at station 1, with a maximum of 43 taxa in August 2017. It tended to decrease from stations 1 to 3, where a minimal value of 16 taxa was recorded in October 2016. Species richness then seemed to increase from stations 3 to 4 in August 2017 and April 2018. Equitability tended to be lower at stations 1 and 2 than at stations 3, 8 and 4 (**Table 7.2**). It was temporally more stable at stations 1 and 2 than at stations 8 and 4, whose variability resulted from low values in April 2018 caused by the exceptionally high abundances of Ampelisca spp. and Hyala vitrea. Mean macrobenthic abundances were between 882.7 (station 4*April 2018) and 89.3 (station 8*August 2017) individuals per m^2 (**Table 7.2**, **Figure 7.6B**). Abundances were higher at station 1 and tended to decrease with station depth. Only stations 8*April 2018 and 4*April 2018 differed from this general pattern with especially high values due to high abundances of Ampelisca spp. (182.7 and 593.3 individuals per m^2 at station 8 and 4 respectively) and Hyala vitrea (93.3 and 100.0 individuals per m^2 at stations 8 and 4 respectively). Changes in mean macrobenthic biomasses did not show any clear spatiotemporal pattern (**Table 7.2**, **Figure 7.6C**) and were characterized by the occurrence of 3 outliers featuring high values. The high biomass recorded for station 2*October 2016 resulted from the presence of both a single individual of Asterias rubens (2019.0 mgAFDW) and a high biomass of numerous individuals (i.e., 57.3 per m^2) of Abra alba (910.6 mgAFDW $m^{-2)\cdot}$ The high biomasses recorded for station 4*August 2017 and station 4*April 2018 both resulted from the presence of single individuals of Cereus pedunculatus in August 2017 (747.0 mgAFDW) and of Nephrops norvegicus in April 2018 (2379.2 mgAFDW).

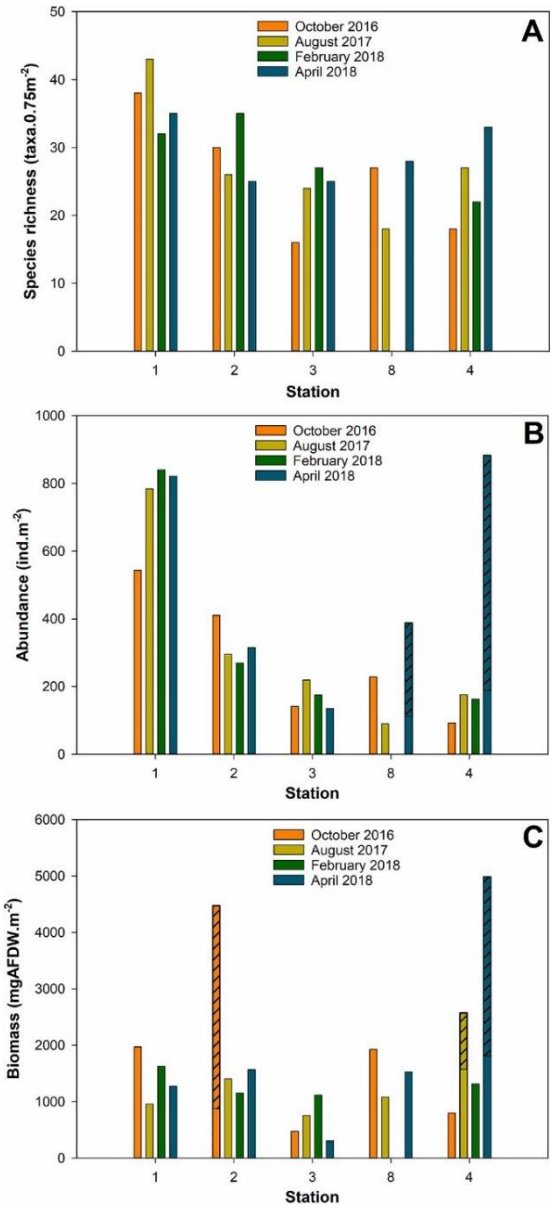

Figure 7.6: *WGMP*: Spatiotemporal changes in the (mean) values of main univariate benthic macrofauna characteristics recorded between 2016 and 2018: species richness (**A**), abundance (**B**), and biomass (**C**). Hatching corresponds to the exceptional presence of: (1) numerous individuals of a single taxon for abundance barplot and (2), high biomass of a single taxon for biomass barplot. Stations are ordered according to their depth.

The nMDS based on 2016–2018 macrofauna abundance data is shown in **Figure 7.7A**. The horizontal dimension of the reduced space corresponded to station depth, reflecting the progressive change in benthic macrofauna compositions along this gradient. Amphiura filiformis and Kurtiella bidentata accounted for 20.6 and 40.9% of total macrofauna abundance at station 1 (43.4 and 10.3% at station 2). Stations 8 and 4 were, conversely, characterized by the presence of burrowing macrofauna (e.g. Callianassa subterranea and Oestergrenia digitata). For all stations, the vertical dimension of the reduced space mostly separated sampling cruises. The dispersion of the different cruises for each station suggests that between-cruises changes in benthic macrofauna compositions were larger at deep (i.e., stations 3, 4 and 8) than at shallow

(i.e., stations 1 and 2) stations. The hierarchical clustering further confirmed this pattern with the identification of 5 groups: (I) station 1 in February and April 2018, (II) station 2 during all cruises, (III) station 3 in February and April 2018, (IV) stations 8 and 4 in October 2016, and (V) stations 8 and 4 in August 2017, February 2018 and April 2018.

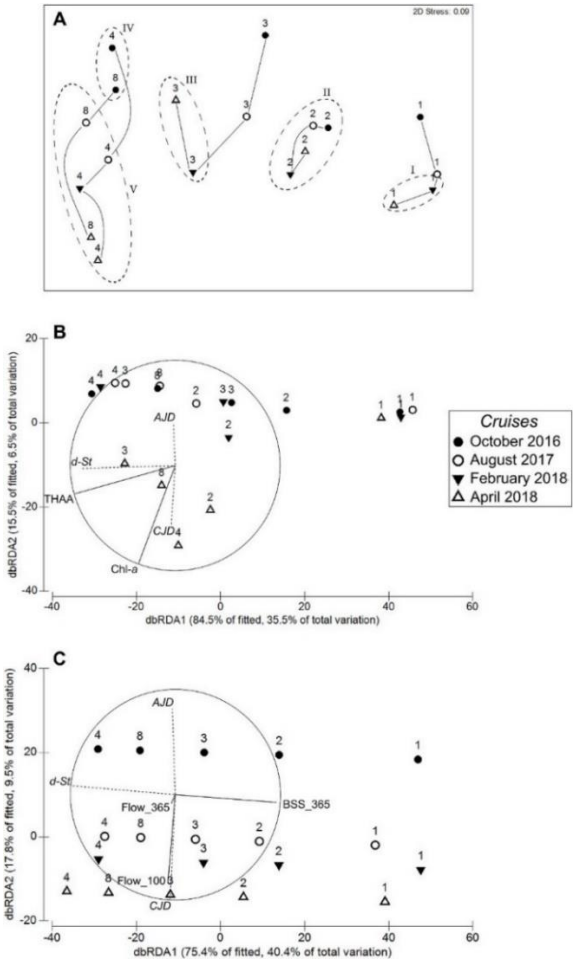

Figure 7.7: *WGMP*: Multivariate analyses of spatiotemporal changes in benthic macrofauna compositions recorded between 2016 and 2018. Non-Metric Multidimensional Scaling of benthic macrofauna compositions data for stations*dates during 2016–2018 cruises (**A**). Figures refer to stations and symbols to cruises. Solid lines represent trajectories of stations over time and dotted lines indicate groups of stations*dates issued from hierarchical clustering. Distance-based Redundancy Analysis based on surface sediment characteristics (**B**). Distance-based Redundancy Analysis based on integrated BSS and river flows (**C**). Station depth (*d-St*), Annual Julian Days (*AJD*) and Cumulated Julian Days (*CJD*) were used as supplementary variables. Chl-*a*: Chlorophyll-*a*; THAA; Total Hydrolysable Amino Acids; BSS_365: integrated Bottom Shear Stress over 365 days; Flow_100 and Flow_365: integrated river flows over 100 and 365 days.

The DISTLM involving surface sediment characteristics as predictory variables included THAA and Chl-*a*. It explained 42.0% of the total variance of benthic macrofauna compositions. Its representation through the first plane of the dbRDA also accounted for 42.0% of this total variance and showed two main orientations (**Figure 7.7B**). The first one, mainly along the first component of the dbRDA, corresponded to station depth and was mainly explained by THAA. The second one, mainly along the second component of the dbRDA, separated stations (except

station 1) sampled during April 2018 from all other stations*dates, and was mainly cued by Chl-*a* concentrations. CJD correlated significantly with this second orientation ($r = 0.560$, $p < 0.05$) but not AJD ($r = 0.393$, $p = 0.07$). The DISTLM involving BSS and river flows included BSS_{365}, $Flow_{100}$ and $Flow_{365}$ as independent variables. It explained 53.5% of the total variance of benthic macrofauna compositions. Its representation through the first plane of a dbRDA accounted for 49.9% of this initial variance and here again showed two main orientations (**Figure 7.7C**). The first one, mainly along the first component of the dbRDA, corresponded to station depth and was mainly explained by BSS_{365}. The second one, mainly along the second component of the dbRDA, separated the 4 cruises, and was mainly cued by $Flow_{100}$. The contribution of $Flow_{365}$ was poorly described by the first plane of the dbRDA. CJD and AJD correlated significantly ($p < 0.05$) with this second orientation. This correlation was slightly higher for CJD ($r = 0.992$ versus $r = 0.820$).

3.4 WGMP: 2010/2016–2018 spatiotemporal changes in benthic macrofauna compositions

The 2010/2016–2018 comparison of univariate benthic macrofauna descriptors highlighted major differences between July 2010 (Massé et al., 2016) and the 2016–2018 cruises. Species richness values were in the same order of magnitude in July 2010 (32, 22 and 21 taxa at stations 1, 3 and 4, respectively) and in 2016–2018 (means of 37, 23 and 25 taxa at stations 1, 3 and 4, respectively). Conversely, abundances were much higher at station 1 in July 2010 than during all 2016–2018 cruises (1628.0 vs 747.3 ± 137.5 ind m^{-2}, respectively). Abundances were also higher at station 3 in July 2010 (328.0 vs 167.4 ± 38.5 ind m^{-2}). They conversely tended to be equivalent at station 4 (118.7 in July 2010 vs155.0 ± 43.4 ind m^{-2} during 2016–2018 cruises) when excluding the numerous Ampelisca spp. and Hyala vitrea individuals present in April 2018. Biomasses were higher at stations 1 and 3 in July 2010 (4696.0 and 3495.7 mgAFDW m^{-2}, respectively) than during the 2016–2018 cruises (means of 1456.0 ± 437.5 and 662.3 ± 353.0 mgAFDW m^{-2}, respectively). They also tended to be equivalent at station 4 between July 2010 (1901.9 mgAFDW m^{-2}) and 2016–2018 cruises (1374.2 ± 436.1 mgAFDW m^{-2}) when excluding the large and rarely present individuals identified at station 4 during August 2017 and April 2018 (*see section 3.3*).

The representation of stations*dates through the nMDS based on macrofauna abundance data from the 2010 and 2016–2018 cruises is shown in **Figure 7.8**. The horizontal dimension accounted for the positioning of stations along the depth gradient, whereas the vertical dimension separated sampling dates and more specifically July 2010 (Massé et al., 2016) from all the 2016–2018 cruises. Hierarchical clustering confirmed this pattern with the identification of 5 clusters. The first 4 were almost identical to those of the analysis conducted on the sole

2016–2018 data (see above) and group V was only constituted by stations 3 and 4 in July 2010. The positioning of stations*dates along the horizontal dimension were similar in 2010 and 2016–2018 as opposed to their positioning along the second dimension, which showed major 2010/2016–2018 changes in benthic macrofauna compositions and suggested that these changes were larger at stations 3 and 4 than at station 1.

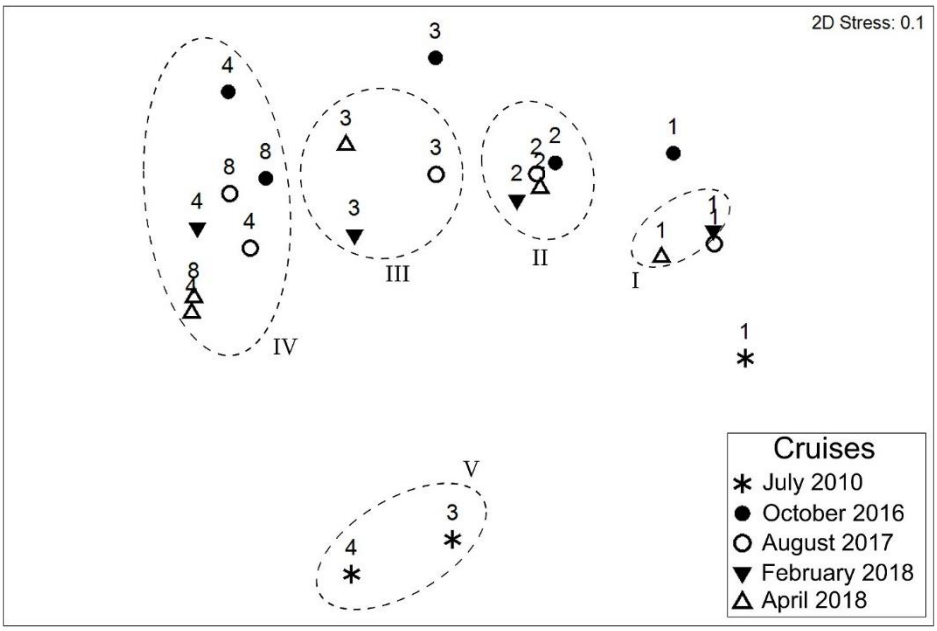

Figure 7.8: *WGMP:* non-Metric Multidimensional Scaling of 2010/2016–2018 spatiotemporal changes in benthic macrofauna compositions. Data for stations*dates have been collected during both the 2010 and 2016–2018 cruises. Figures refer to stations and symbols to cruises. Dotted lines indicate the groups of samples issued from hierarchical clustering.

3.5 Comparison of spatiotemporal changes in surface sediment characteristics and benthic macrofauna compositions within the WGMP and the RRP

The relationships between station depth and intra-station temporal variabilities in surface sediment characteristics (**Figure 7.9A**) and benthic macrofauna compositions (**Figure 7.9B**) both largely differed in the West Gironde Mud Patch (WGMP) and the Rhône River Prodelta (RRP). In both cases, and although caution should clearly be taken when comparing absolute values of WGMP and RRP data, highest intra-station variabilities were associated with the RRP shallowest station. Intrastation temporal variabilities in RRP surface sediment characteristics decreased with station depth. Conversely, they did not show any clear pattern relative to station depth in the WGMP. In the RRP temporal variabilities in benthic macrofauna compositions was much higher at the shallowest station (i.e., station A) than at the 4 other stations, whereas in the WGMP, they were lower at the two shallowest stations.

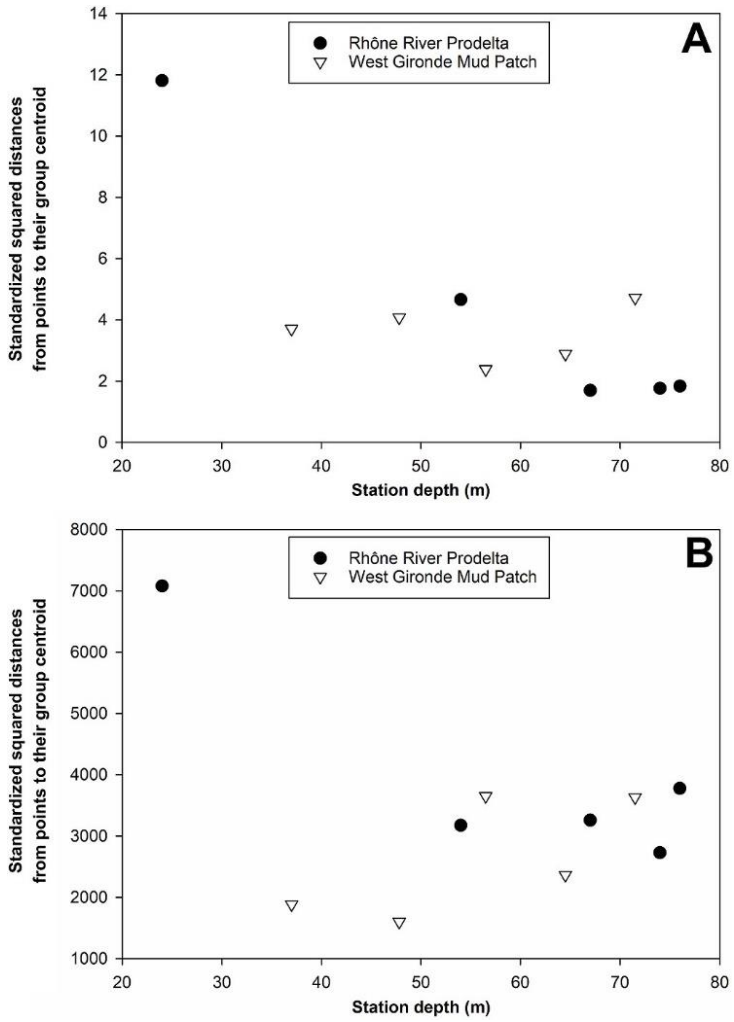

Figure 7.9: Comparison between the West Gironde Mud Patch (WGMP) and the Rhône River Prodelta (RRP): Relationship between station depth and intrastation temporal variabilities (standardized squared distances from points to their group centroid) in sediment surface characteristics (**A**) and benthic macrofauna compositions (**B**) in both the WGMP (data collected between 2016 and 2018) and the RRP (data collected between 2007 and 2011; Bonifácio et al., 2014). (See text for details).

4. Discussion

4.1 WGMP 2016–2018 spatiotemporal changes

4.1.1 Surface sediment characteristics

Spatial changes in surface sediment characteristics were larger than temporal ones. Station 1 was located in the proximal part of the West Gironde Mud Patch (WGMP). It presented coarser surface sediments during 3 cruises (i.e., October 2016, August 2017 and February 2018) than during April 2018. This likely resulted from the transient deposition of coarser sediments during high-energy events (Lesueur et al., 1991, 1996, 2001, 2002; Lesueur and Tastet, 1994). All other 4 stations were located in the distal part. They presented restricted spatial changes in surface sediment granulometry, but conversely a clear increase in bulk organic contents (i.e.,

Particulate Organic Carbon and Total Hydrolysable Amino Acids) with station depth, which supports previous observations by Lamarque et al. (2021) and Massé et al. (2016). Such a pattern is rather uncommon in River-dominated Ocean Margins (RiOMar; e.g., Bonifácio et al., 2014; Cathalot et al., 2013; Goñi et al., 1998; Gordon et al., 2001; Keil et al., 1997) and has been attributed to a particle sieving process cued by particle density (Lamarque et al., 2021) rather than size (Hedges and Keil, 1995; Keil et al., 1998; Mayer, 1994a, b) during the succession of sedimentation/resuspension cycles governing the transfer of particles offshore in RiOMar (Blair and Aller, 2012). The results of the DISTLM/dbRDA analysis support the predominant role of local hydrodynamics as the driving factor of the spatial distribution of surface sediment characteristics in the WGMP as already put forward by Lamarque et al. (2021) based on a synoptic spatial survey. Caution should nevertheless be taken in interpreting this result since river flows did not include any spatial component.

The importance of the seasonal component in driving 2016–2018 temporal changes in surface sediment characteristics is supported by the results of the DISTLM/dbRDA analysis, showing that temporal changes correlate better with river flows, and to a lesser extent hydrodynamics, integrated over a seasonal (i.e., $Flow_{100}$ and BSS_{100}) than a yearly period (i.e., $Flow_{365}$ and BSS_{365}). The most important changes in surface sediment characteristics occurred during spring 2018. A spring increase in chloropigment concentrations has already been reported by Relexans et al. (1992) in the distal part of the WGMP. The seasonality of pelagic primary production in this area of the Bay of Biscay is characterized by the occurrence of a spring phytoplankton bloom (Herbland et al., 1998; Labry et al., 2002). Both fluorescence profiles and satellite image analyses (Copernicus Sentinel data 2018 processed using SNAP software, data available on request to B. Lamarque) confirmed that the period immediately preceding April 2018 was characterized by high Chlorophyll-a (Chl-*a*) concentrations (i.e., ca. 10 mg m^{-3}) in surface waters overlying the WGMP. The high chloropigment concentrations and Chl-*a*/(Chl-*a*+Phaeo-*a*) recorded in surface sediments during April 2018 thus probably resulted from the sedimentation of a spring bloom.

4.1.2. Benthic macrofauna

Our results clearly show the higher importance of spatial relative to 2016–2018 temporal changes in benthic macrofauna composition. Benthic macrofauna compositions changed with station depth. The spatial pattern observed in July 2010 by Massé et al. (2016) was strongly dominated by differences between the proximal (i.e., station 1) and the distal (i.e., stations 3 and 4) parts. During the present study, stations 1 and 2 were dominated by Amphiura filiformis and Kurtiella bidentata, which is consistent with the presence of the A. filiformis-K. bidentata-Abra nitida community in cohesive muddy sands off wave exposed coast (Hiscock, 1984;

Picton et al., 1994). This corresponds to the A5.351 ("Amphiura filiformis, Kurtiella bidentata and Abra nitida in circalittoral sandy mud") habitat of the EUNIS classification (Bajjouk et al., 2015). Stations 8 and 4 were strongly bioturbated (Lamarque et al., 2021 and unpubl. data) and characterized by the presence of: (1) a large variety of polychaetes, (2) seapens (Cavernularia pusilla and Veretillum cynomorium) and (3) Nephrops norvegicus (G. Bernard, personal observation). They therefore can be related with the EUNIS A5.361 ("Seapens and burrowing megafauna in circalittoral fine mud") habitat (Bajjouk et al., 2015). Our results thus confirm that benthic macrofauna compositions clearly differ between the proximal and distal parts of the WGMP. They however also show the occurrence of a depth gradient in these compositions within the sole distal part.

Overall, benthic macrofauna abundances tended to decrease with depth, which is conform to the trend observed by Massé et al. (2016). Such a decreasing pattern is not fully consistent with the results of surveys achieved in other RiOMar, where increasing trends in benthic macrofauna abundances with the distance to the river mouth have been most often observed (Akoumianaki et al., 2013; Aller and Aller, 1986; Alongi et al., 1992; Bonifácio et al., 2014; Rhoads et al., 1985) and interpreted based on the Rhoads et al. (1985) model. According to this model, benthic macrofauna communities at the immediate vicinity of river mouths are limited by the sediment instability induced by riverine inputs. During the present study, spatial changes in benthic macrofauna compositions correlated best with BSS_{365} and not significantly with river flows. Although caution should clearly be taken (see above), this suggests that local hydrodynamics is the main factor explaining benthic macrofauna composition in the WGMP. Its predominance over riverine inputs within the proximal part being further supported by the lack of modern sedimentation (Lesueur et al., 2001, 2002; Lesueur and Tastet, 1994). Along the same line, the importance of local hydrodynamics in explaining spatial changes in sediment profile image characteristics was put forward by Lamarque et al. (2021). According to the current RiOMar typology (Blair and Aller, 2012), the WGMP would therefore correspond to a type 2/high energy "bypassed" (sensu McKee et al., 2004) system where the impact of local hydrodynamics is dominant relative to the one of riverine inputs.

2016–2018 temporal changes in benthic macrofauna compositions tended to be larger at deep stations than at the two shallowest ones, with some evidence that these changes included both a seasonal and an interannual component. There are several rationales for the occurrence of seasonal changes. First, in the reduced space of the nMDS, individual station trajectories tended to "close" when they were defined based on Annual Julian Days (AJD), which can be considered as indicative of within year/seasonal variability. Second, temporal changes correlated best with $Flow_{100}$, which suggests the link between changes in seasonally integrated

river flows and benthic macrofauna compositions. Third, AJD correlated significantly with the second component of the dbRDA, which was indicative of temporal changes. There is some indirect evidence for an inter-annual component to 2016–2018 temporal changes as well since: (1) a common inter-annual trend was observed at stations 1, 8 and 4, and (2) the second component of the dbRDA correlated slightly better with Cumulated Julian Days (CJD; indicative of inter-annual/ cumulated changes) than with AJD.

4.2 WGMP: 2010/2016–2018 comparison of benthic macrofauna compositions

The existence of an inter-annual component to temporal changes in benthic macrofauna compositions became even more obvious when July 2010 (Massé et al., 2016) and 2016–2018 data were compared. Differences between 2010 and 2016–2018 were indeed much larger than differences observed during 2016–2018. At all 3 sampled stations, differences in benthic macrofauna compositions relative to July 2010 were maximal in October 2016 and, for most of them, changes occurring during the 2016–2018 period tended to reduce those differences, which would be indicative of an ongoing cicatrization process following a major disturbance (Pearson and Rosenberg, 1978) that would have taken place between July 2010 and October 2016.

In the WGMP, local hydrodynamics is a key factor structuring the spatial distributions of benthic macrofauna composition and activity (Lamarque et al., 2021 and above). The frequency of sediment disturbances induced by strong hydrodynamic events have been documented based on the analysis of vertical erosional sequences within the sediment column (Lesueur et al., 1991, 2002; Lesueur and Tastet, 1994). It has been estimated that such disturbances occur every ca. 22 years at 35m depth and only every ca. 80 years at 64m depth (Lesueur et al., 2002). The analysis of the 2010–2018 Bottom Shear Stress time series showed higher values during the 2013–2014 winter when the WGMP experienced higher significant wave heights and a longer total storm duration (i.e., 40 and 300%, respectively) than the overall means of the 1948–2015 period. Overall, the 2013–2014 winter has been the most energetic during the 1948–2015 period along most of the European Atlantic coast (Masselink et al., 2016). Storm-induced physical disturbance during this uncommon winter is likely to have affected surface sediments, and also possibly, benthic macrofauna compositions over the whole WGMP. In this context, the increase in 2010/2016–2018 temporal changes in benthic macrofauna compositions with station depth may seem counter-intuitive since the intensity of physical disturbance during strong storms is clearly higher at shallower stations. In “normal” conditions (i.e., not during extreme events), these stations are, however, also experiencing tougher hydrodynamics. Moreover, the frequency of extreme events affecting the sediment column and thus potentially benthic macrofauna compositions (Dobbs and Vozarik, 1983; Glémarec, 1978; Rees et al., 1977) also

decreases with station depth (Lesueur et al., 2002). One can thus assume that resident benthic macrofauna in the WGMP are less tolerant to physical disturbance at deeper than at shallower stations, thereby accounting for larger changes in benthic macrofauna composition at deeper stations. Based on these elements, our current interpretation is that: (1) the repetition of major storms during the 2013–2014 winter has induced strong physical disturbances of benthic habitats and consequently strong changes in benthic macrofauna compositions over the whole WGMP, and (2) since then temporal changes in benthic macrofauna compositions consist in an ongoing (pluri-annual) cicatrization process superimposed to a seasonal dynamics (Cárcamo et al., 2017). It should nevertheless be stressed that this working hypothesis clearly remains to be further tested through an extension of the WGMP observation period.

4.3 Comparison between the WGMP and the RRP

Intra-station temporal variabilities in surface sediment characteristics were much higher at the immediate vicinity of the Rhône River Mouth than in the proximal area of the WGMP. In the shallowest area of the Rhône River Prodelta (RRP), this variability is mainly resulting from high sedimentation during floods (Bonifácio et al., 2014; Cathalot et al., 2010; Pastor et al., 2018). Mostly during autumn and winter, part of deposited sediments are resuspended initiating a series of resuspension/depositions, which results in the displacement of fine particles offshore (Marion et al., 2010; Ulses et al., 2008). During this transfer, particles are sorted relative to their size and the most labile particulate organic matter component is degraded (Bonifácio et al., 2014), which contributes to reduce temporal variabilities in surface sediment characteristics in deeper areas. Conversely, temporal variabilities in surface sediment characteristics tended to be constant all over the WGMP. In the proximal part, temporal variability is mostly linked to granulometry, whereas in the distal part, it mostly resulted from elevated chloropigment concentrations and ratios in April 2018. Dilution/mixing effects between continental and marine Particulate Organic Matter sources are affecting the whole WGMP as indicated by the almost constancy in surface sediment $\delta^{13}C$ and previous water column observations by Fontugne and Jouanneau (1987). Conversely, they clearly increase with the distance to the river mouth (and thus station depth) in the RRP (Bourgeois et al., 2011; Cathalot et al., 2013; Lansard et al., 2009; Tesi et al., 2007). Moreover, due to strong local hydrodynamics, the fine particles originating from the Gironde Estuary do not settle in the proximal part of the WGMP (Lesueur et al., 2001), whereas conversely, high sedimentation rates are taking place at the immediate vicinity of the Rhône River Mouth (Miralles et al., 2005; Zuo et al., 1991). Overall, in the proximal part of the WGMP, this contributes to reduce temporal variabilities in surface sediment characteristics possibly induced by seasonal changes in the hydrological regime of the Gironde Estuary.

Intra-station temporal variabilities in benthic macrofauna compositions showed opposite spatial patterns in the RRP and the WGMP. In the RRP, temporal variabilities were much higher at the immediate vicinity of the Rhône River due to the shift between high and low sedimentation rates during high and low-flow periods, respectively (Bonifácio et al., 2014). This pattern largely conforms to the Rhoads et al. (1985) model, which attributes a major role to sedimentation in controlling benthic macrofauna in RiOMar. Conversely, temporal variabilities in benthic macrofauna compositions within the WGMP tended to be lower at the 2 shallowest stations than at the 3 deepest ones, which could be attributed a better tolerance of benthic macrofauna to wave-induced disturbance in the shallowest part of the WGMP (see above). Here again, this pinpoints to differences in the relative roles of riverine inputs and local hydrodynamics in explaining spatiotemporal changes within the two systems and thereby supports the current RiOMar typologies (Blair and Aller, 2012; McKee et al., 2004).

5. Conclusions

The present assessment of 2016–2018 spatiotemporal changes in West Gironde Mud Patch (WGMP) surface sediment characteristics confirms the existence of: (1) a spatial structuration relative to station depth mainly explained by local hydrodynamics, and (2) seasonal changes mainly resulting from the sedimentation of the spring bloom.

Our results also demonstrate the existence of: (1) differences in benthic macrofauna composition between the proximal and distal parts of the WGMP, and (2) a depth gradient in its distal part. Overall, spatial changes in benthic macrofauna composition were best explained by local hydrodynamics integrated over a 1-year period. Benthic macrofauna compositions presented inter-annual changes superimposed over seasonal ones. The marked shift observed between 2010 and 2016–2018 suggests that a major disturbance occurred between these two periods. Our current working hypothesis is that this disturbance was caused by the series of extremely severe winter storms that took place during 2013–2014.

The comparison between the WGMP and Rhône River Prodelta (RRP) shows major differences in the control of temporal variabilities in both surface sediment characteristics and benthic macrofauna compositions within their proximal parts. In the RRP, these variabilities are associated with changes in sedimentation rates in relation with the Rhône River hydrological regime, whereas in the WGMP they result from transient particle deposition induced by intense hydrodynamic events.

Our results further support the characterization of the WGMP as temperate type 2 (i.e., high-energy system) RiOMar. They highlight the different mechanisms involved in the control of surface sediment characteristics and benthic macrofauna compositions in the WGMP and the

RRP and are in line with current RiOMar typologies derived from meta-analyses mainly achieved on tropical and subtropical systems (Blair and Aller, 2012; McKee et al., 2004).

Author contributions

Conceptualization, B.L., B.D., and A.G.; Data curation, B.L.; Formal analysis, B.L. and A.G.; Funding acquisition, B.D. and A.G.; Investigation, B.L., B.D., S.S., G.B., N.D., and A.G.; Methodology, B.L., B.D., S.S., M.D. (Mélanie Diaz), F.G. (Florent Grasso), A.S. and A.G.; Resources, B. L., B.D., S.S., G.B., N.D., M.D. (Mélanie Diaz), N.L., F.G. (Frédéric Garabetian), F.G. (Florent Grasso), A.S., S.R., A.R.-R., M.-A.C., D.P. and M.D. (Martin Danilo); Validation, B.L., B.D., and A.G.; Visualization, B.L. and A.G.; Writing—original draft, B.L. and A.G.; Writing—review and editing, B.L., B.D., S.S., G.B., N.D., F.G. (Frédéric Garabetian), F.G. (Florent Grasso), S.R., A.R.-R. and A.G. All authors have read and agreed to the published version of the manuscript.

Declaration of competing interest

The authors declare that they have no known competing financial interests or personal relationships that could have appeared to influence the work reported in this paper.

Acknowledgements

This work is part of the PhD thesis of Bastien Lamarque (Bordeaux University). Bastien Lamarque was partly supported by a doctoral grant from the French “Ministère de l’Enseignement Supérieur, de la Recherche et de l’Innovation”. This work was supported by: (1) the JERICO-NEXT project (European Union’s Horizon 2020 Research and Innovation program under grant agreement no. 654410), (2) the VOG project (LEFE-CYBER and EC2CO-PNEC), and (3) the MAGMA project (COTE cluster of Excellence ANR-10-LABX-45). It also benefited from additional fundings allocated by the Conseil Régional NouvelleAquitaine and the Office Français de la Biodiversité. Operations at sea were funded by the French Oceanographic Fleet. The authors wish to thank the crew of the R/V Côtes de la Manche for their help during field sampling, Christophe Fontanier, Marie Claire Perello, Pascal Lebleu and Hervé Derriennic for their help during sampling and analyses.

References

Akaike, H., 1973. Information theory as an extension of the maximum likelihood principle. In: Csaki, F., Petrov, B.N. (Eds.), Proceedings, 2nd International Symposium on Information Theory, pp. 267–281. Budapest.

Akoumianaki, I., Papaspyrou, S., Kormas, K.A., Nicolaidou, A., 2013. Environmental variation and macrofauna response in a coastal area influenced by land runoff. Estuar. Coast Shelf Sci. 132, 34–44. https://doi.org/10.1016/j.ecss.2012.04.009.

Aller, J.Y., Aller, R.C., 1986. General characteristics of benthic faunas on the Amazon inner continental shelf with comparison to the shelf off the Changjiang River, East China Sea. Continent. Shelf Res. 6, 291–310. https://doi.org/10.1016/0278-4343 (86)90065-8.

Aller, J.Y., Stupakoff, I., 1996. The distribution and seasonal characteristics of benthic communities on the Amazon shelf as indicators of physical processes. Continent. Shelf Res. 16, 717–751. https://doi.org/10.1016/0278-4343(96)88778-4.

Aller, R.C., 1998. Mobile deltaic and continental shelf muds as suboxic, fluidized bed reactors. Mar. Chem. 61, 143–155. https://doi.org/10.1016/S0304-4203(98)00024-3.

Alongi, D.M., Christoffersen, P., Tirendi, F., Robertson, A.I., 1992. The influence of freshwater and material export on sedimentary facies and benthic processes within the Fly Delta and adjacent Gulf of Papua (Papua New Guinea). Continent. Shelf Res. 12, 287–326. https://doi.org/10.1016/0278-4343(92)90033-G.

Anderson, M., Gorley, R.N., Clarke, K.R., 2008. PERMANOVA + for PRIMER User

Anderson, M.J., 2001. A new method for non-parametric multivariate analysis of variance. Austral Ecol. 26, 32–46. https://doi.org/10.1111/j.1442-9993.2001.01070.

Bajjouk, T., Guillaumont, B., Michez, N., Thouin, B., Croguennec, C., Populus, J., LouvelGlaser, J., Gaudillat, V., Chevalier, C., Tourolle, J., Hamon, D., 2015. Classification EUNIS, Système d'information européen sur la nature : Traduction française des habitats benthiques des Régions Atlantique et Méditerranée. In: Habitats Subtidaux & Complexes D'habitats, 2. https://archimer.ifremer.fr/doc/00271/38223/.

Bischl, B., Lang, M., Bossek, J., Horn, D., Richter, J., Surmann, D., 2017. BBmisc: Miscellaneous Helper Functions for B. Bischl. R Packag version 1-1-1.

Blair, N.E., Aller, R.C., 2012. The fate of terrestrial organic carbon in the marine environment. Ann. Rev. Mar. Sci 4, 401–423. https://doi.org/10.1146/annurev- marine-120709-142717.

Bonifácio, P., Bourgeois, S., Labrune, C., Amouroux, J.M., Escoubeyrou, K., Buscail, R., Romero-Ramirez, A., Lantoine, F., Vétion, G., Bichon, S., Desmalades, M., Rivière, B., Deflandre, B., Grémare, A., 2014. Spatiotemporal changes in surface sediment characteristics and benthic macrofauna composition off the Rhône River in relation to its hydrological regime. Estuar. Coast Shelf Sci. 151, 196–209. https://doi.org/ 10.1016/j.ecss.2014.10.011.

Bourgeois, S., Pruski, A.M., Sun, M.Y., Buscail, R., Lantoine, F., Kerhervé, P., Vétion, G., Rivière, B., Charles, F., 2011. Distribution and lability of land-derived organic matter

in the surface sediments of the Rhône prodelta and the adjacent shelf (Mediterranean Sea, France): a multi proxy study. Biogeosciences 8, 3107–3125. https://doi.org/ 10.5194/bg-8-3107-2011.

Burdige, D.J., 2005. Burial of terrestrial organic matter in marine sediments: a reassessment. Global Biogeochem. Cycles 19, 1–7. https://doi.org/10.1029/ 2004GB002368.

Cárcamo, P.J., Hernández-Miranda, E., Veas, R., Quiñones, R.A., 2017. Macrofaunal community structure in Bahía Concepcion (Chile) before and after the 8.8 Mw Maule mega-earthquake and tsunami. Mar. Environ. Res. 130, 233–247. https://doi.org/ 10.1016/j.marenvres.2017.07.022.

Castaing, P., Allen, G., Houdart, M., Moign, Y., 1979. Etude par télédétection de la dispersion en mer des eaux estuariennes issues de la Gironde et du Pertuis de Maumusson. Oceanol. Acta 2, 459–468. https://archimer.ifremer.fr/doc/00122/23361/.

Castaing, P., Allen, G.P., 1981. Mechanisms controlling seaward escape of suspended sediment from the Gironde: a macrotidal estuary in France. Mar. Geol. 40, 101–118. https://doi.org/10.1016/0025-3227(81)90045-1.

Castaing, P., Philipps, I., Weber, O., 1982. Répartition et dispersion des suspensions dans les eaux du plateau continental aquitain. Oceanol. Acta 5, 85–96. https://archimer. ifremer.fr/doc/00121/23193/.

Cathalot, C., Rabouille, C., Pastor, L., Deflandre, B., Viollier, E., Buscail, R., Grémare, A., Treignier, C., Pruski, A., 2010. Temporal variability of carbon recycling in coastal sediments influenced by rivers: assessing the impact of flood inputs in the Rhône River prodelta. Biogeosciences 7, 1187–1205. https://doi.org/10.5194/bg-7-1187-2010.

Cathalot, C., Rabouille, C., Tisnérat-Laborde, N., Toussaint, F., Kerhervé, P., Buscail, R., Loftis, K., Sun, M.Y., Tronczynski, J., Azoury, S., Lansard, B., Treignier, C., Pastor, L., Tesi, T., 2013. The fate of river organic carbon in coastal areas: a study in the Rhône River delta using multiple isotopic ($\delta^{13}C$, $\delta^{14}C$) and organic tracers. Geochem. Cosmochim. Acta 118, 33–55. https://doi.org/10.1016/j.gca.2013.05.001.

Cirac, P., Berne, S., Castaing, P., Weber, O., 2000. Processus de mise en place et d'évolution de la couverture sédimentaire superficielle de la plate-forme nordaquitaine. Oceanol. Acta 23, 663–686. https://doi.org/10.1016/s0399-1784(00)00110-9.

Clarke, K.R., Somerfield, P.J., Gorley, R.N., 2008. Testing of null hypotheses in exploratory community analyses: similarity profiles and biota-environment linkage.J. Exp. Mar. Biol. Ecol. 366, 56–69. https://doi.org/10.1016/j.jembe.2008.07.009.

Clarke, K.R., Warwick, R.M., 2001. Change in Marine Communities: an Approach to Statistical Analysis and Interpretation, second ed. PRIMER-E, Plymouth.

Constantin, S., Doxaran, D., Derkacheva, A., Novoa, S., Lavigne, H., 2018. Multitemporal

dynamics of suspended particulate matter in a macro-tidal river Plume (the Gironde) as observed by satellite data. Estuar. Coast Shelf Sci. 202, 172–184. https://doi.org/10.1016/j.ecss.2018.01.004.

Coplen, T.B., 2011. Guidelines and recommended terms for expression of stable isotope ratio and gas-ratio measurement results. Rapid Commun. Mass Spectrom. 25, 2538–2560. https://doi.org/10.1002/rcm.5129.

Deflandre, B., 2018a. JERICOBENT-3 Cruise. RV Côtes De La Manche. https://doi.org/10.17600/18000469.

Deflandre, B., 2018b. JERICOBENT-4 Cruise. RV Côtes De La Manche. https://doi.org/10.17600/18000470.

Deflandre, B., 2017. JERICOBENT-2 Cruise. RV Côtes De La Manche. https://doi.org/10.17600/17011000.

Deflandre, B., 2016. JERICOBENT-1 Cruise. RV Côtes De La Manche. https://doi.org/10.17600/16010400.

Diaz, M., Grasso, F., Le Hir, P., Sottolichio, A., Caillaud, M., Thouvenin, B., 2020. Modeling mud and sand transfers between a macrotidal estuary and the continental shelf: influence of the sediment transport parameterization. J. Geophys. Res. Ocean. 125 https://doi.org/10.1029/2019JC015643.

Dobbs, F.C., Vozarik, J.M., 1983. Immediate effects of a storm on coastal infauna. Mar. Ecol. Prog. Ser. 11, 273–279. https://doi.org/10.3354/meps011273.

Doxaran, D., Froidefond, J.M., Castaing, P., Babin, M., 2009. Dynamics of the turbidity maximum zone in a macrotidal estuary (the Gironde, France): observations from field and MODIS satellite data. Estuar. Coast Shelf Sci. 81, 321–332. https://doi.org/10.1016/j.ecss.2008.11.013.

Dubosq, N., Schmidt, S., Walsh, J.P., Grémare, A., Gillet, H., Lebleu, P., Poirier, D., Perello, M.C., Lamarque, B., Deflandre, B., 2021. A first assessment of organic carbon burial in The West gironde mud patch (Bay of Biscay). Continent. Shelf Res. 221 https://doi.org/10.1016/j.csr.2021.104419.

Etcheber, H., Relexans, J.C., Beliard, M., Weber, O., Buscail, R., Heussner, S., 1999. Distribution and quality of sedimentary organic matter on the Aquitanian margin (Bay of Biscay). Deep. Res. Part II 46, 2249–2288. https://doi.org/10.1016/S0967-0645(99)00062-4.

Fontugne, M.R., Jouanneau, J.M., 1987. Modulation of the particulate organic carbon flux to the ocean by a macrotidal estuary: evidence from measurements of carbon isotopes in organic matter from the Gironde system. Estuar. Coast Shelf Sci. 24, 377–387. https://doi.org/10.1016/0272-7714(87)90057-6.

Gadel, F., Jouanneau, J.M., Weber, O., Serve, L., Comellas, L., 1997. Traceurs organiques dans les dépôts de la vasière Ouest-Gironde (Golfe de Gascogne). Oceanol. Acta 20, 687–695. https://archimer.ifremer.fr/doc/00093/20426/.

Glémarec, M., 1978. Problèmes d'écologie dynamique et de succession en baie de Concarneau. Vie Milieu 1–20.

Goñi, M.A., Ruttenberg, K.C., Eglinton, T.I., 1998. A reassessment of the sources and importance of land-derived organic matter in surface sediments from the Gulf of Mexico. Geochem. Cosmochim. Acta 62, 3055–3075. https://doi.org/10.1016/ S0016-7037(98)00217-8.

Gordon, E.S., Goñi, M.A., Roberts, Q.N., Kineke, G.C., Allison, M.A., 2001. Organic matter distribution and accumulation on the inner Louisiana shelf west of the Atchafalaya River. Continent. Shelf Res. 21, 1691–1721. https://doi.org/10.1016/S0278-4343(01)00021-8.

Grasso, F., Verney, R., Le Hir, P., Thouvenin, B., Schulz, E., Kervella, Y., Khojasteh Pour Fard, I., Lemoine, J.P., Dumas, F., Garnier, V., 2018. Suspended sediment dynamics in the macrotidal seine estuary (France): 1. Numerical modeling of turbidity maximum dynamics. J. Geophys. Res. Ocean. 123, 558–577. https://doi.org/ 10.1002/2017JC013185.

Grémare, A., Gutiérrez, D., Anschutz, P., Amouroux, J.M., Deflandre, B., Vétion, G., 2005. Spatio-temporal changes in totally and enzymatically hydrolyzable amino acids of superficial sediments from three contrasted areas. Prog. Oceanogr. 65, 89–111. https://doi.org/10.1016/j.pocean.2005.02.016.

Harmelin-Vivien, M.L., Bănaru, D., Dierking, J., Hermand, R., Letourneur, Y., Salen-Picard, C., 2009. Linking benthic biodiversity to the functioning of coastal ecosystems subjected to river runoff (NW Mediterranean). Anim. Biodivers. Conserv. 32, 135–145. https://doi.org/10.32800/abc.2009.32.0135.

Harrell, F.E., 2021. Hmisc: Harrell Miscellaneous. R Packag, version 4-5-0.

Hedges, J.I., Keil, R.G., 1995. Sedimentary organic matter preservation: an assessment and speculative synthesis. Mar. Chem. 49, 81–115. https://doi.org/10.1016/0304-4203(95)00008-F.

Herbland, A., Delmas, D., Laborde, P., Sautour, B., Artigas, F., 1998. Phytoplankton spring bloom of the Gironde plume waters in the Bay of Biscay: early phosphorus limitation and food-web consequences. Oceanol. Acta 21, 279–291. https://doi.org/10.1016/S0399-1784(98)80015-7.

Hiscock, K., 1984. Rocky shore surveys of the Isles of Scilly. March 27th to April 1st and July 7th to 15th 1983. Peterbrgh. Nat. Conserv. Counc. CSD Rep. 509.

Jalón-Rojas, I., Sottolichio, A., Hanquiez, V., Fort, A., Schmidt, S., 2018. To what extent multidecadal changes in morphology and fluvial discharge impact tide in a convergent (turbid) tidal river. J. Geophys. Res. Ocean. 123, 3241–3258. https:// doi.org/10.1002/2017JC013466.

Jouanneau, J.M., Weber, O., Latouche, C., Vernet, J.P., Dominik, J., 1989. Erosion, nondeposition and sedimentary processes through a sedimentological and radioisotopic study of surficial deposits from the "Ouest-Gironde vasière" (Bay of Biscay). Continent. Shelf Res. 9, 325–342. https://doi.org/10.1016/0278-4343(89)90037-X.

Keil, R.G., Mayer, L.M., Quay, P.D., Richey, J.E., Hedges, J.I., 1997. Loss of organic matter from riverine particles in deltas. Geochem. Cosmochim. Acta 61, 1507–1511. https://doi.org/10.1016/S0016-7037(97)00044-6.

Keil, R.G., Tsamakis, E., Giddings, J.C., Hedges, J.I., 1998. Biochemical distributions (amino acids, neutral sugars, and lignin phenols) among size-classes of modern marine sediments from the Washington coast. Geochem. Cosmochim. Acta 62, 1347–1364. https://doi.org/10.1016/S0016-7037(98)00080-5.

Labry, C., Herbland, A., Delmas, D., 2002. The role of phosphorus on planktonic production of the Gironde plume waters in the Bay of Biscay. J. Plankton Res. 24, 97–117. https://doi.org/10.1093/plankt/24.2.97.

Lamarque, B., Deflandre, B., Dalto, A.G., Schmidt, S., Romero-Ramirez, A., Garabetian, F., Dubosq, N., Diaz, M., Grasso, F., Sottolichio, A., Bernard, G., Gillet, H., Cordier, M.A., Poirier, D., Lebleu, P., Derriennic, H., Danilo, M., Tenório, M.M.B., Grémare, A., 2021. Spatial distributions of surface sedimentary organics and sediment profile image characteristics in a high-energy temperate marine riomar: the west gironde mud patch. J. Mar. Sci. Eng. 9, 242. https://doi. org/10.3390/jmse9030242.

Lansard, B., Rabouille, C., Denis, L., Grenz, C., 2009. Benthic remineralization at the land-ocean interface: a case study of the Rhône River (NW Mediterranean Sea). Estuar. Coast Shelf Sci. 81, 544–554. https://doi.org/10.1016/j.ecss.2008.11.025.

Lazure, P., Dumas, F., 2008. An external-internal mode coupling for a 3D hydrodynamical model for applications at regional scale (MARS). Adv. Water Resour. 31, 233–250. https://doi.org/10.1016/j.advwatres.2007.06.010.

Lesueur, P., Jouanneau, J.M., Boust, D., Tastet, J.P., Weber, O., 2001. Sedimentation rates and fluxes in the continental shelf mud fields in the Bay of Biscay (France). Continent. Shelf Res. 21, 1383–1401. https://doi.org/10.1016/S0278-4343(01)00004-8.

Lesueur, P., Tastet, J.P., Weber, O., Sinko, J.A., 1991. Modèle faciologique d'un corps sédimentaire pélitique de plate-forme la vasière Ouest-Gironde (France). Oceanol. Acta 11, 143–153. https://archimer.ifremer.fr/doc/00267/37871/.

Lesueur, P., Tastet, J.P., 1994. Facies, internal structures and sequences of modern Gironde-derived muds on the Aquitaine inner shelf. France. Mar. Geol. 120, 267–290. https://doi.org/10.1016/0025-3227(94)90062-0.

Lesueur, P., Tastet, J.P., Marambat, L., 1996. Shelf mud fields formation within historical times: examples from offshore the Gironde estuary, France. Continent. Shelf Res. 16, 1849–1870. https://doi.org/10.1016/0278-4343(96)00013-1.

Lesueur, P., Tastet, J.P., Weber, O., 2002. Origin and morphosedimentary evolution of fine-grained modern continental shelf deposits: the Gironde mud fields (Bay of Biscay, France). Sedimentology 49, 1299–1320. https://doi.org/10.1046/j.1365-3091.2002.00498.x.

Levin, L.A., Boesch, D.F., Covich, A., Dahm, C., Erséus, C., Ewel, K.C., Kneib, R.T., Moldenke, A., Palmer, M.A., Snelgrove, P., Strayer, D., Weslawski, J.M., 2001. The function of marine critical transition zones and the importance of sediment biodiversity. Ecosystems 4, 430–451. https://doi.org/10.1007/s10021-001-0021-4.

Longère, P., Dorel, D., 1970. Etude des sédiments meubles de la vasière de la Gironde et des régions avoisinantes. Rev. des Trav. l'Institut des Pêches Marit. 34, 233–256.

Lotze, H.K., Lenihan, H.S., Bourque, B.J., Bradbury, R.H., Cooke, R.G., Kay, M.C., Kidwell, S.M., Kirby, M.X., Peterson, C.H., Jackson, J.B.C., 2006. Depletion, degradation, and recovery potential of estuaries and coastal seas. Science 312, 1806–1809. https://doi.org/10.1126/science.1128035.

Marion, C., Dufois, F., Arnaud, M., Vella, C., 2010. In situ record of sedimentary processes near the Rhône River mouth during winter events (Gulf of Lions, Mediterranean Sea). Continent. Shelf Res. 30, 1095–1107. https://doi.org/10.1016/ j.csr.2010.02.015.

Massé, C., Meisterhans, G., Deflandre, B., Bachelet, G., Bourasseau, L., Bichon, S., Ciutat, A., Jude-Lemeilleur, F., Lavesque, N., Raymond, N., Grémare, A., Garabetian, F., 2016. Bacterial and macrofaunal communities in the sediments of The West gironde mud patch, Bay of Biscay (France). Estuar. Coast Shelf Sci. 179, 189–200. https://doi.org/10.1016/j.ecss.2016.01.011.

Masselink, G., Castelle, B., Scott, T., Dodet, G., Suanez, S., Jackson, D., Floc'h, F., 2016. Extreme wave activity during 2013/2014 winter and morphological impacts along the Atlantic coast of Europe. Geophys. Res. Lett. 43, 2135–2143. https://doi.org/ 10.1002/2015GL067492.Received.

Mayer, L.M., 1994a. Relationships between mineral surfaces and organic carbon concentrations in soils and sediments. Chem. Geol. 114, 347–363. https://doi.org/ 10.1016/0009-2541(94)90063-9.

Mayer, L.M., 1994b. Surface area control of organic carbon accumulation in continental shelf

sediments. Geochem. Cosmochim. Acta 58, 1271–1284. https://doi.org/ 10.1016/0016-7037(94)90381-6.

Mayer, L.M., Linda, L.S., Sawyer, T., Plante, C.J., Jumars, P.A., Sel, R.L., 1995. Bioavailable amino acids in sediments: a biomimetic, kinetics based approach. Limnol. Oceanogr. 40, 511–520. https://doi.org/10.4319/lo.1995.40.3.0511.

McKee, B.A., Aller, R.C., Allison, M.A., Bianchi, T.S., Kineke, G.C., 2004. Transport and transformation of dissolved and particulate materials on continental margins influenced by major rivers: benthic boundary layer and seabed processes. Continent. Shelf Res. 24, 899–926. https://doi.org10.1016/j.csr.2004.02.009.

Medernach, L., Grémare, A., Amoureux, J.M., Colomines, J.C., Vétion, G., 2001. Temporal changes in the amino acid contents of particulate organic matter sedimenting in the Bay of Banyuls-sur-Mer (northwestern Mediterranean). Mar. Ecol. Prog. Ser. 214, 55–65. https://doi.org/10.3354/meps214055.

Miralles, J., Radakovitch, O., Aloisi, J.C., 2005. ^{210}Pb sedimentation rates from the Northwestern Mediterranean margin. Mar. Geol. 216, 155–167. https://doi.org/ 10.1016/j.margeo.2005.02.020.

Neveux, J., Lantoine, F., 1993. Spectrofluorometric assay of chlorophylls and phaeopigments using the least squares approximation technique. Deep. Res. Part I 40, 1747–1765. https://doi.org/10.1016/0967-0637(93)90030-7.

Oksanen, J., Blanchet, F.G., Friendly, M., Kindt, R., Legendre, P., McGlinn, D., Minchin, P.R., O'Hara, R.B., Simpson, G.L., Solymos, P., Stevens, M.H.H., Szoecs, E., Wagner, H., 2019. Vegan: Community Ecology Package. R Packag. Version 2-5-6.

Parra, M., Castaing, P., Jouanneau, J.M., Grousset, F., Latouche, C., 1998. Nd-Sr isotopic composition of present-day sediments from the Gironde Estuary, its draining basins and the West Gironde mud patch (SW France). Continent. Shelf Res. 19, 135–150. https://doi.org/10.1016/S0278-4343(98)00083-1.

Pastor, L., Deflandre, B., Viollier, E., Cathalot, C., Metzger, E., Rabouille, C., Escoubeyrou, K., Lloret, E., Pruski, A.M., Vétion, G., Desmalades, M., Buscail, R., Grémare, A., 2011. Influence of the organic matter composition on benthic oxygen demand in the Rhône River prodelta (NW Mediterranean Sea). Continent. Shelf Res. 31, 1008–1019. https://doi.org/10.1016/j.csr.2011.03.007.

Pastor, L., Rabouille, C., Metzger, E., Thibault de Chanvalon, A., Viollier, E., Deflandre, B., 2018. Transient early diagenetic processes in Rhône prodelta sediments revealed in contrasting flood events. Continent. Shelf Res. 166, 65–76. https://doi.org/10.1016/j.csr.2018.07.005.

Pearson, T.H., Rosenberg, R., 1978. Macrobenthos succession in relation to organic enrichment

and pollution of the marine environment. Oceanogr. Mar. Biol. Annu. Rev. 16, 229–331.

Picton, B.E., Emblow, C.S., Morrow, C.C., Sides, E.M., Costello, M.J., 1994. Marine communities of the Mulroy Bay and Lough Swill area, north-west Ireland, with an assessment of their nature conservation importance. Environ. Sci. Unit, Trinity Coll. (f. Surv. Report).

R Core Team, 2019. R: A Language and Environment for Statistical Computing. R Foundation for Statistical Computing, Vienna, Austria. https://www.R-project.org/.

Rees, E.I.S., Nicholaidou, A., Laskaridou, P., 1977. The effects of storms on the dynamics of shallow water benthic associations. Biol. Benthic Org. 465–474. https://doi.org/10.1016/b978-0-08-021378-1.50052-x.

Relexans, J.C., Lin, R.G., Castel, J., Etcheber, H., Laborde, P., 1992. Response of biota to sedimentary organic matter quality of the west Gironde mud patch, Bay of Biscay (France). Oceanol. Acta 15, 639–649. https://archimer.ifremer.fr/doc/00101/21231/.

Rhoads, D.C., Boesch, D.F., Zhican, T., Fengshan, X., Liqiang, H., Nilsen, K.J., 1985. Macrobenthos and sedimentary facies on the Changjiang delta platform and adjacent continental shelf, East China Sea. Continent. Shelf Res. 4, 189–213. https://doi.org/10.1016/0278-4343(85)90029-9.

Roland, A., Ardhuin, F., 2014. On the developments of spectral wave models: numerics and parameterizations for the coastal ocean. Ocean Dynam. 64, 833–846. https://doi.org/10.1007/s10236-014-0711-z.

Soulsby, R., 1997. Dynamics of Marine Sands: A Manual for Practical Applications. Thomas Tel.

Tesi, T., Miserocchi, S., Goñi, M.A., Langone, L., 2007. Source, transport and fate of terrestrial organic carbon on the western Mediterranean Sea, Gulf of Lions. France. Mar. Chem. 105, 101–117. https://doi.org/10.1016/j.marchem.2007.01.005.

Ulses, C., Estournel, C., Durrieu de Madron, X., Palanques, A., 2008. Suspended sediment transport in the Gulf of Lions (NW Mediterranean): impact of extreme storms and floods. Continent. Shelf Res. 28, 2048–2070. https://doi.org/10.1016/j. csr.2008.01.015.

Wakeham, S.G., Lee, C., Hedges, J.I., Hernes, P.J., Peterson, M.L., 1997. Molecular indicators of diagenetic status in marine organic matter. Geochem. Cosmochim. Acta 61, 5363–5369. https://doi.org/10.5833/jjgs.33.70.

Weber, O., Jouanneau, J.M., Ruch, P., Mirmand, M., 1991. Grain-size relationship between suspended matter originating in the Gironde estuary and shelf mud-patch deposits. Mar. Geol. 96, 159–165. https://doi.org/10.1016/0025-3227(91)90213-N.

Wheatcroft, R.A., 2006. Time-series measurements of macrobenthos abundance and sediment

bioturbation intensity on a flood-dominated shelf. Prog. Oceanogr. 71,88–122. https://doi.org/10.1016/j.pocean.2006.06.002.

Worm, B., Barbier, E.B., Beaumont, N., Duffy, J.E., Folke, C., Halpern, B.S., Jackson, J.B. C., Lotze, H.K., Micheli, F., Palumbi, S.R., Sala, E., Selkoe, K.A., Stachowicz, J.J., Watson, R., 2006. Impacts of biodiversity loss on ocean ecosystem services. Science 314, 787–790. https://doi.org/10.1126/science.1132294.

Zuo, Z., Eisma, D., Berger, G.W., 1991. Determination of sediment accumulation and mixing rates in the Gulf of Lions, Mediterranean Sea. Oceanol. Acta 14, 253–262. https://archimer.ifremer.fr/doc/00101/21255/.

Annexe 3

Table 8.1: Summary of the sampling stations and associated measured parameters in the water column of the West Gironde Mud Patch for each cruise.

Cruise	Station	Date	Temperature	Salinity	Dissolved Oxygen	Chl-*a*	Turbidity	pH
JERICObent-1	1	25/10/2016	X	X	X	X		
JERICObent-1	2	26/10/2016	X	X	X	X		
JERICObent-1	3	27/10/2016	X	X	X	X		
JERICObent-1	8	29/10/2016	X	X	X	X		
JERICObent-1	4	28/10/2016	X	X	X	X		
JERICObent-2	1	15/08/2017	X	X	X	X		
JERICObent-2	2	16/08/2017	X	X	X	X		
JERICObent-2	3	21/08/2017	X	X	X	X		
JERICObent-2	8	20/08/2017	X	X	X	X		
JERICObent-2	4	17/08/2017	X	X	X	X		
JERICObent-3	1	28/01/2018	X	X	X	X		
JERICObent-3	2	31/01/2018	X	X	X	X		
JERICObent-3	3	03/02/2018	X	X	X	X		
JERICObent-3	4	08/02/2018	X	X	X	X		
JERICObent-3	Transect (st. 0 to W)	28/01/2018	X	X	X	X	X	
JERICObent-4	2	23/04/2018	X	X	X	X		
JERICObent-4	3	22/04/2018	X	X	X	X		
JERICObent-4	8	25/04/2018	X	X	X	X		
JERICObent-4	4	26/04/2018	X	X	X	X		
JERICObent-4	4	29/04/2018	X	X	X	X		
JERICObent-4	Transect (st. 0 to W)	20/04/2018	X	X	X	X	X	
JERICObent-4	Transect (st. 0 to W)	21/04/2018	X	X	X	X	X	
JERICObent-7	1	12/07/2019	X	X	X	X	X	
JERICObent-7	2	14/07/2019	X	X	X	X	X	
JERICObent-7	3	11/07/2019	X	X	X	X	X	
JERICObent-7	4	13/07/2019	X	X	X	X	X	
MAGMA-1	1	12/04/2021	X	X	X			
MAGMA-1	10	21/04/2021	X	X	X			
MAGMA-1	2	19/04/2021	X	X	X			
MAGMA-1	3	13/04/2021	X	X	X			
MAGMA-1	8	20/04/2021	X	X	X			
MAGMA-1	4	17/04/2021	X	X	X			
MAGMA-1	Transect (st. 0 to 12)	22/04/2021	X	X	X			
MAGMA-2	1	17/10/2021	X	X	X		X	X
MAGMA-2	10	28/10/2021	X	X	X		X	X
MAGMA-2	2	18/10/2021	X	X	X		X	X
MAGMA-2	3	24/10/2021	X	X	X		X	X
MAGMA-2	8	27/10/2021	X	X	X		X	X
MAGMA-2	4	23/10/2021	X	X	X		X	X
MAGMA-2	Transect (st. 0 to 12)	19/10/2021	X	X	X		X	X

Table 8.2: Monthly averages of Gironde flows, Sea Surface Temperaure (SST) and surface Chl-*a* concentrations ([Chl-*a*]) in the proximal and distal areas of the West Gironde Mud Patch.

				Proximal area						Distal area					
Month	Mean Gironde Flows (m^3 s^{-1})	SD	*n*=	Mean SST (°C)	SD	*n*=	Mean [Chl-*a*] (µg/L)	SD	*n*=	Mean SST (°C)	SD	*n*=	Mean [Chl-*a*] (µg/L)	SD	*n*=
January 2016	1180	605	31	11.9	0.8	5	2.7	0.0	1	13.0	0.5	5	2.3	0.0	1
February 2016	1841	986	29	10.6	0.8	8	3.1	0.1	3	11.4	0.8	6	3.5	0.4	2
March 2016	1492	632	31	10.5	0.4	13	3.8	0.5	6	10.6	0.4	13	3.4	1.7	8
April 2016	1110	151	30	12.5	0.8	16	3.7	1.8	14	12.6	0.8	14	2.0	0.9	11
May 2016	810	71	31	14.9	1.9	10	3.1	0.9	5	15.3	1.6	11	1.3	0.4	6
June 2016	1124	522	30	18.8	1.1	9	3.9	0.8	3	18.7	1.2	7	5.3	4.2	3
July 2016	319	93	31	21.0	0.8	20	1.5	0.7	10	21.5	0.8	17	1.1	0.5	10
August 2016	161	22	31	20.3	1.1	22	1.3	0.4	17	20.9	0.9	19	0.7	0.1	16
September 2016	208	48	30	20.3	1.0	18	1.1	0.6	16	20.3	1.0	17	0.8	0.7	12
October 2016	227	61	31	17.3	1.5	14	1.6	0.4	15	17.5	1.3	15	0.7	0.1	12
November 2016	419	294	30	14.2	1.0	11	2.0	0.6	3	14.4	14.4	13	1.1	0.3	5
December 2016	392	80	31	12.6	0.5	11	1.9	0.2	5	13.5	0.4	10	1.1	0.5	4
January 2017	564	170	31	10.5	1.1	14	2.1	0.2	9	12.0	1.0	13	1.1	0.6	4
February 2017	983	426	28	9.7	0.5	9	2.3	0.3	4	10.7	0.5	8	2.3	NA	1
March 2017	1217	547	31	11.4	1.0	9	2.4	0.3	6	11.7	1.1	8	2.4	0.7	5
April 2017	554	216	30	13.8	0.9	25	2.5	1.4	22	14.0	1.0	23	2.2	0.9	21
May 2017	523	106	31	15.7	2.3	16	2.4	1.4	13	15.9	2.2	15	1.2	0.2	13
June 2017	366	175	30	19.9	1.6	16	1.5	1.0	8	20.6	1.8	15	1.3	0.7	9
July 2017	273	95	31	21.1	0.9	15	1.1	0.4	6	20.9	0.9	12	1.0	0.8	6
August 2017	160	22	31	21.0	1.0	12	0.9	0.3	7	21.2	0.8	16	0.6	0.1	7
September 2017	207	28	30	18.9	1.0	10	1.3	0.5	7	19.3	0.7	10	0.7	0.0	4
October 2017	220	42	31	18.4	0.6	15	1.4	0.5	6	18.6	0.7	14	0.8	0.3	5
November 2017	322	93	30	14.7	1.0	11	2.0	0.2	6	15.7	1.0	9	1.3	0.6	4
December 2017	844	345	31	11.8	0.4	4	NA	NA	0	13.3	0.3	3	NA	NA	0
January 2018	2777	970	31	10.8	0.6	6	3.1	1.0	3	11.7	0.6	5	2.7	1.0	2
February 2018	1787	457	28	9.4	0.7	12	2.9	0.6	9	9.6	0.6	14	2.2	0.4	7
March 2018	1481	190	31	9.4	0.6	11	2.2	0.6	7	10.0	0.3	11	2.0	0.5	10
April 2018	1302	407	30	14.8	2.2	9	2.3	0.3	7	14.0	2.2	11	1.2	0.2	8
May 2018	1189	276	31	14.8	1.5	16	2.8	1.7	10	15.3	1.6	17	1.6	0.3	9
June 2018	1195	511	30	19.9	1.3	17	4.7	2.3	10	20.1	1.4	17	2.7	1.2	8
July 2018	436	162	31	22.2	0.9	19	3.5	1.0	13	22.4	0.8	19	2.7	1.1	14
August 2018	200	24	31	21.1	1.1	22	1.7	0.7	18	21.6	0.7	21	1.0	0.4	15
September 2018	211	45	30	18.6	1.2	22	1.1	0.4	18	19.0	1.5	21	1.0	0.4	19
October 2018	270	147	31	15.7	1.2	17	1.9	1.2	14	16.0	0.9	16	1.2	0.6	12
November 2018	439	112	30	13.2	0.4	14	2.1	0.5	7	13.5	0.3	13	1.6	0.7	7
December 2018	584	188	31	12.1	0.4	3	NA	NA	0	13.0	0.2	3	NA	NA	0
January 2019	526	314	31	10.5	0.6	6	1.6	0.5	3	11.5	1.2	8	1.2	0.1	2
February 2019	1231	750	28	10.7	0.7	16	2.6	0.3	13	11.4	0.5	15	1.3	0.4	10
March 2019	589	79	31	12.2	0.8	17	2.2	0.7	13	12.3	0.7	17	1.7	0.4	11
April 2019	541	102	30	12.9	1.1	14	2.6	0.9	11	13.0	1.0	14	1.4	0.5	10
May 2019	575	180	31	15.0	1.2	15	2.2	1.5	10	15.2	1.4	12	1.6	0.4	9
June 2019	384	106	30	18.6	2.0	11	2.7	1.1	4	18.2	1.6	10	2.2	1.6	6
July 2019	163	33	31	21.0	1.0	19	1.7	1.2	12	21.6	1.0	18	1.0	0.5	11
August 2019	151	43	31	21.0	1.0	16	1.5	0.9	12	21.2	1.1	17	0.7	0.2	11
September 2019	138	13	30	18.0	1.4	20	3.3	1.9	16	19.1	1.0	20	1.1	0.5	18
October 2019	318	310	31	18.1	0.4	7	1.0	0.4	4	17.7	0.5	10	0.7	0.3	6
November 2019	1415	403	30	13.5	0.8	2	2.5	NA	1	16.1	1.2	4	NA	NA	0
December 2019	2589	1447	31	12.6	0.8	10	NA	NA	0	14.1	0.6	9	NA	NA	0
January 2020	1028	258	31	11.2	1.1	9	3.0	0.6	4	12.5	0.7	8	2.6	0.3	4
February 2020	886	272	29	11.1	0.4	8	2.5	0.6	5	11.8	0.6	11	1.6	0.1	3
March 2020	1640	946	31	11.8	0.8	16	3.9	1.4	8	11.8	0.8	14	2.1	0.5	7
April 2020	651	230	30	14.0	1.8	16	2.0	0.6	14	13.9	1.6	16	1.6	0.5	14
May 2020	1009	491	31	17.2	1.5	20	5.6	2.4	15	16.9	1.6	21	5.1	2.4	16
June 2020	542	240	30	18.6	1.7	15	4.2	2.6	7	18.8	1.9	13	2.6	2.1	9
July 2020	207	62	31	20.6	0.8	21	1.6	0.8	14	20.9	0.7	23	1.0	0.4	15
August 2020	156	15	31	21.7	1.0	14	1.6	0.8	12	22.2	0.9	14	0.6	0.2	9
September 2020	224	81	30	20.9	0.9	17	1.4	0.5	15	21.1	1.1	19	0.6	0.2	13
October 2020	651	152	31	17.2	0.4	10	1.4	0.5	6	17.2	0.7	10	0.7	0.2	7
November 2020	498	109	30	15.6	0.5	15	2.3	0.1	9	16.0	0.5	16	1.3	0.5	10
December 2020	1460	873	31	12.9	0.9	9	NA	NA	0	13.7	0.8	5	NA	NA	0
January 2021	1925	891	31	9.3	9.3	7	2.8	0.6	3	10.2	1.2	8	2.2	0.3	2
February 2021	2729	1837	28	11.1	0.8	7	3.0	0.5	7	11.3	0.9	9	1.8	0.4	7
March 2021	788	162	31	11.3	0.7	20	1.5	0.6	8	11.7	0.7	17	1.4	0.2	8
April 2021	426	83	30	13.1	1.1	20	1.3	0.6	16	13.1	0.9	20	0.8	0.5	17
May 2021	585	197	31	14.8	1.4	14	1.7	0.3	9	14.7	1.3	12	0.8	0.2	8
June 2021	445	112	30	19.8	1.3	19	1.6	0.6	12	20.1	1.3	20	0.8	0.1	12
July 2021	493	177	31	20.4	1.1	15	2.4	1.1	8	20.3	1.3	14	0.8	0.3	8
August 2021	237	58	31	20.5	0.6	19	1.0	0.4	13	20.7	0.5	21	0.6	0.1	14
September 2021	377	157	30	19.9	1.3	20	1.3	0.6	16	20.4	1.2	19	0.8	0.4	16
October 2021	322	110	23	17.3	0.6	21	1.8	0.4	16	17.2	0.6	21	1.0	0.2	19
November 2021	489	133	30	14.9	0.7	12	2.1	0.8	6	15.3	0.5	10	1.0	0.4	4
December 2021	1389	862	31	11.3	0.8	7	2.4	0.1	2	12.6	0.3	8	1.1	0.1	2

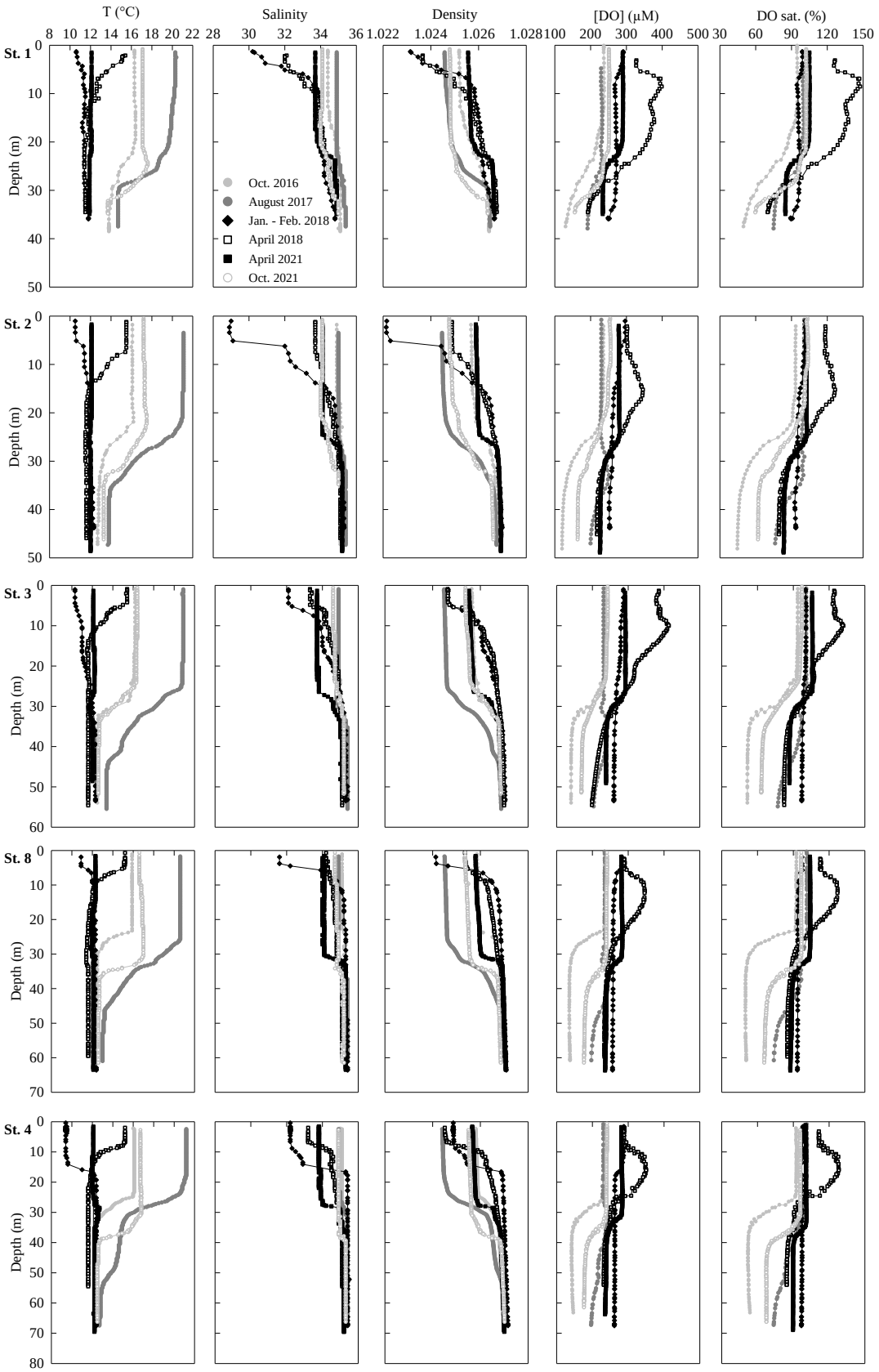

Figure 8.1: Profiles of temperature, salinity, density, dissolved oxygen (DO) concentrations and saturations performed in the water column of the WGMP at stations 1, 2, 3, 8 and 4 in October 2016, August 2017, January - February and April 2018, April and October 2021.

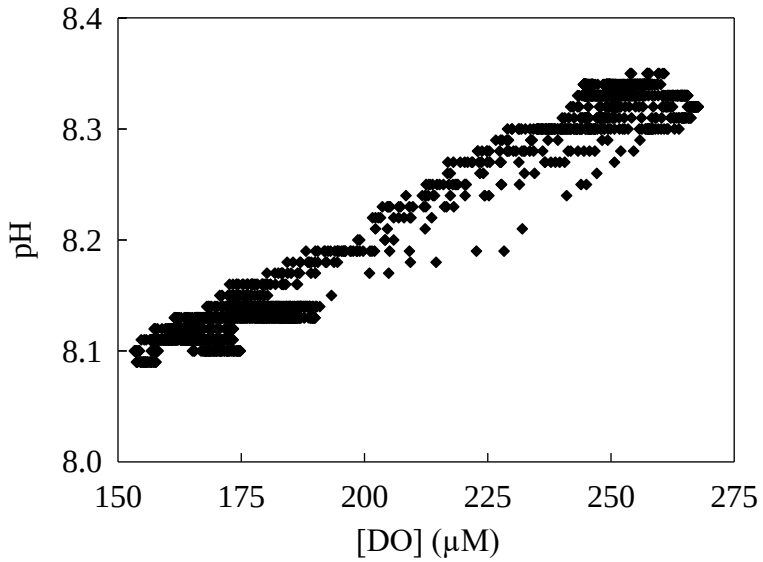

Figure 8.2: Relationship of dissolved oxygen (DO) concentrations (µM) and pH measured simultaneously in October 2021 with a WiMo Plus multiparameter probe (*NKE Instrumentation*) by profiling in the water column of the continental shelf off the Gironde (13 profiles). The significance of the correlation was confirmed by a Spearman rank correlation ($p<0.01$, $n=2351$).

Annexe 4

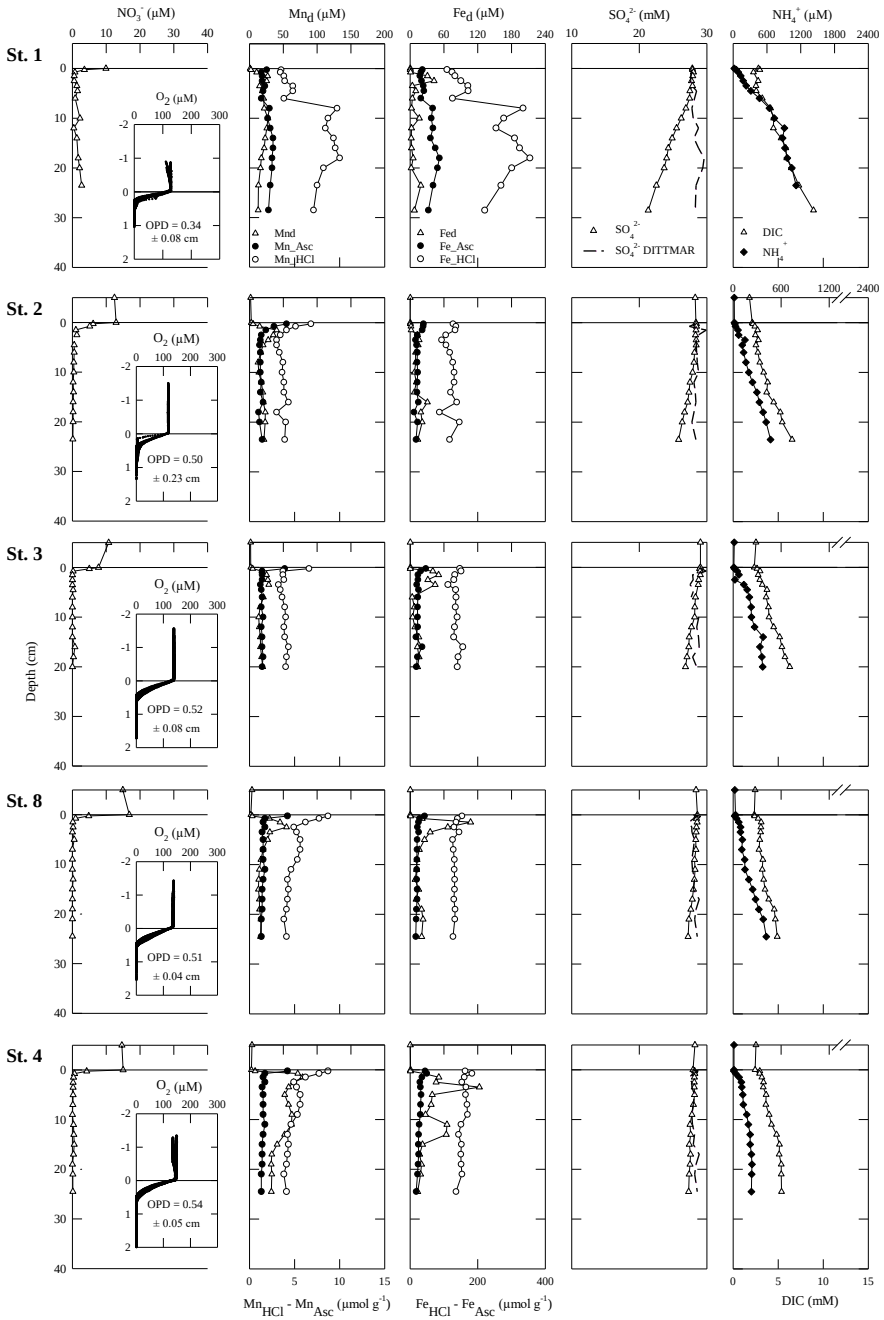

Figure 9.1: Depth profiles of dissolved oxygen (O_2), nitrate (NO_3^-), dissolved (Mn_d) and particulate ($Mn_{Asc,}$ Mn_{HCl}) manganese, dissolved (Fe_d) and particulate ($Fe_{Asc,}$ Fe_{HCl}) iron, sulfate (SO_4^{2-}), dissolved inorganic carbon (DIC) and ammonium (NH_4^+) in sediments and oxygen penetration depth (OPD) at the six stations sampled in October 2016. The dash line represents theoretical sulfate concentrations calculated from chloride concentrations using the DITTMAR ratios.

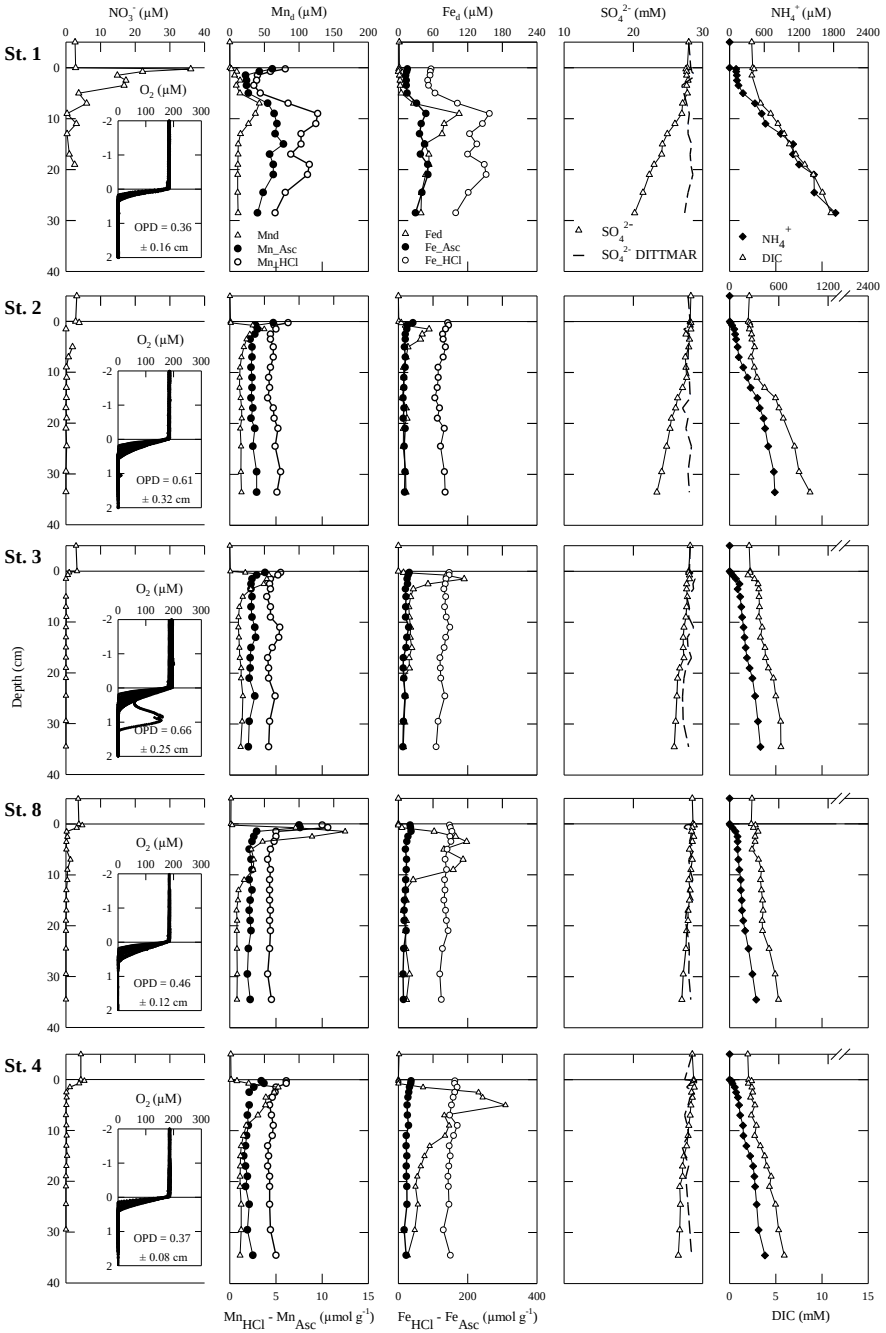

Figure 9.2: Depth profiles of dissolved oxygen (O_2), nitrate (NO_3^-), dissolved (Mn_d) and particulate ($Mn_{Asc,}$ Mn_{HCl}) manganese, dissolved (Fe_d) and particulate ($Fe_{Asc,}$ Fe_{HCl}) iron, sulfate (SO_4^{2-}), dissolved inorganic carbon (DIC) and ammonium (NH_4^+) in sediments and oxygen penetration depth (OPD) at the six stations sampled in August 2017. The dash line represents theoretical sulfate concentrations calculated from chloride concentrations using the DITTMAR ratios.

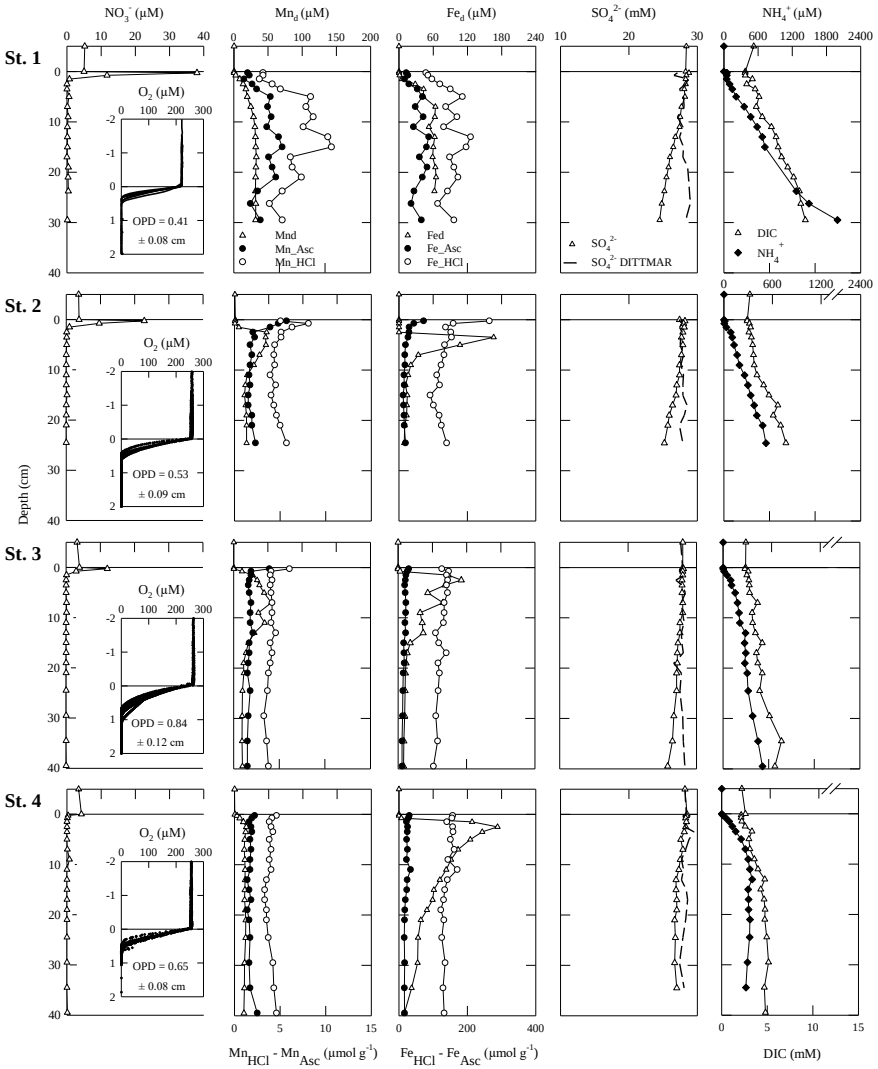

Figure 9.3: Depth profiles of dissolved oxygen (O_2), nitrate (NO_3^-), dissolved (Mn_d) and particulate ($Mn_{Asc,}$ Mn_{HCl}) manganese, dissolved (Fe_d) and particulate ($Fe_{Asc,}$ Fe_{HCl}) iron, sulfate (SO_4^{2-}), dissolved inorganic carbon (DIC) and ammonium (NH_4^+) in sediments and oxygen penetration depth (OPD) at the six stations sampled in January - February 2018. The dash line represents theoretical sulfate concentrations calculated from chloride concentrations using the DITTMAR ratios.

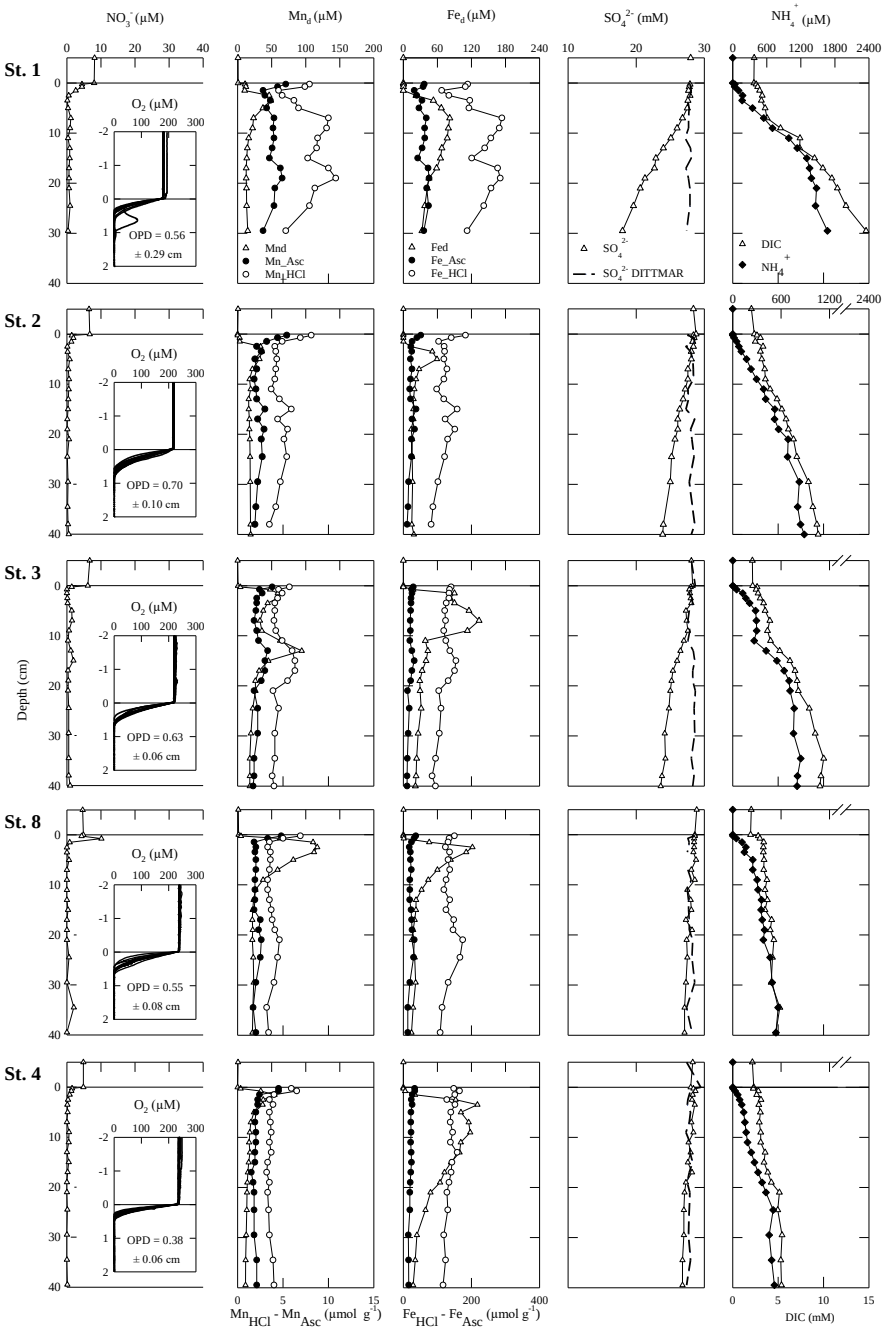

Figure 9.4: Depth profiles of dissolved oxygen (O_2), nitrate (NO_3^-), dissolved (Mn_d) and particulate ($Mn_{Asc,}$ Mn_{HCl}) manganese, dissolved (Fe_d) and particulate ($Fe_{Asc,}$ Fe_{HCl}) iron, sulfate (SO_4^{2-}), dissolved inorganic carbon (DIC) and ammonium (NH_4^+) in sediments and oxygen penetration depth (OPD) at the six stations sampled in April 2018. The dash line represents theoretical sulfate concentrations calculated from chloride concentrations using the DITTMAR ratios.

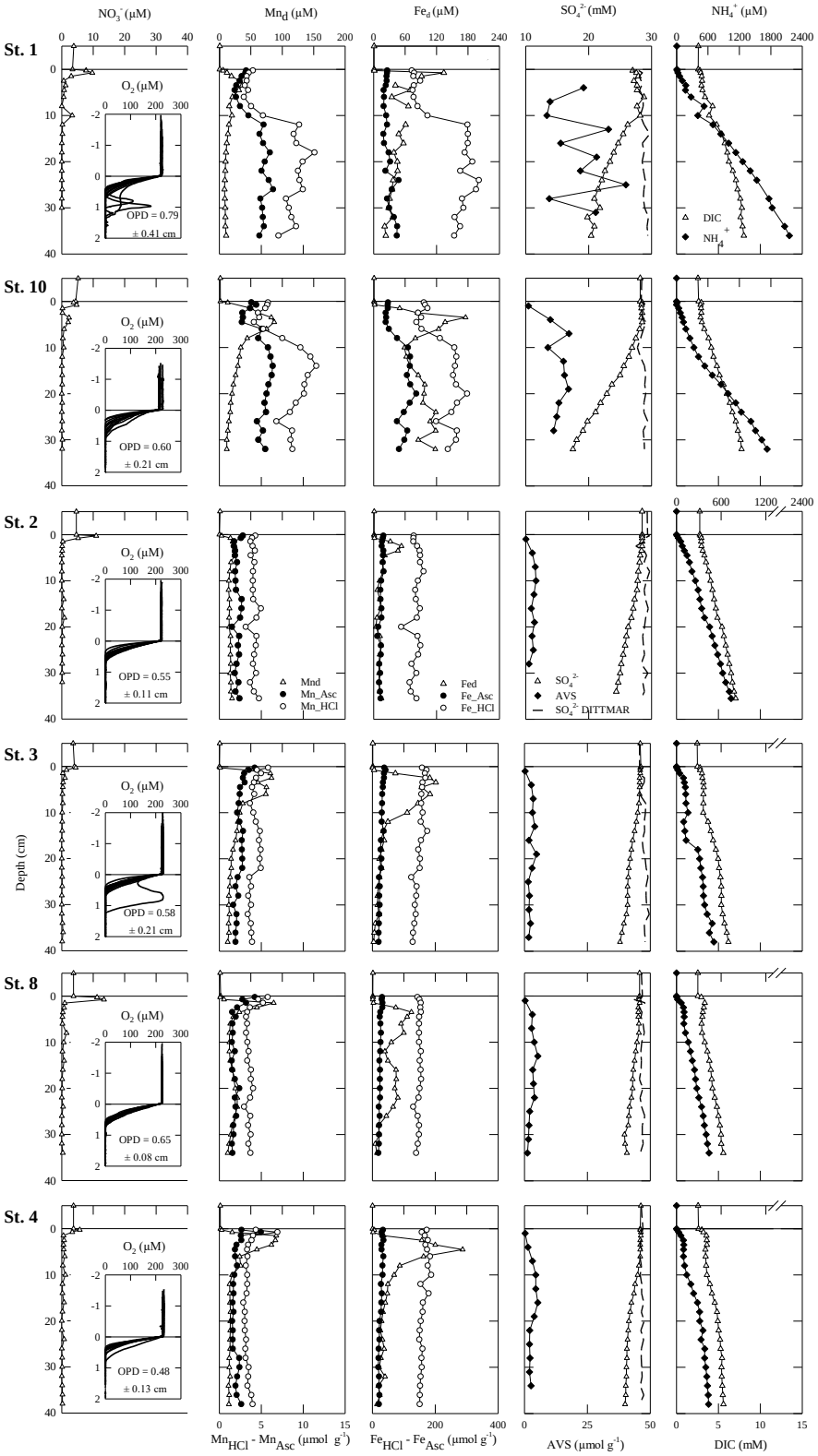

Figure 9.5: Depth profiles of dissolved oxygen (O_2), nitrate (NO_3^-), dissolved (Mn_d) and particulate ($Mn_{Asc,}$ Mn_{HCl}) manganese, dissolved (Fe_d) and particulate ($Fe_{Asc,}$ Fe_{HCl}) iron, sulfate (SO_4^{2-}), dissolved inorganic carbon (DIC) and ammonium (NH_4^+) in sediments and oxygen penetration depth (OPD) at the six stations sampled in April 2021. The dash line represents theoretical sulfate concentrations calculated from chloride concentrations using the DITTMAR ratios.